IN VIVO INVESTIGATION OF MUSCLE BEHAVIOUR DURING VOLUNTARY AND ELECTRICALLY INDUCED MUSCLE CONTRACTION USING B-MODE ULTRASOUND IMAGING

Margaret Armentano, MEng

Submitted in fulfilment of the requirements for the degree of Doctor of Philosophy (PhD)

School of Engineering
College of Science and Engineering
University of Glasgow

January 2017

Abstract

Musculoskeletal Ultrasound Imaging (USI) is a growing field in literature. It has been proven to be a useful tool for investigating the properties of the muscle. There is growing interest in ultrasound imaging techniques for the description of skeletal muscle function, and different algorithms have been developed for this purpose. The majority of studies limit their focus on a particular area of the muscle, such as the aponeuroses, or on architectural parameters such as fiber length and pennation angle. The investigation of the entire muscle visualised on the ultrasound image may help elucidate the muscle function under normal conditions or when external factors compromise or alter the muscle function.

Functional electrical stimulation (FES) is a technique based on the use of electrical current to activate skeletal muscles and facilitate their contraction. It is commonly used for strength training or in rehabilitation to accelerate or enhance the recovery of skeletal muscle's function. The ability of this technique to improve muscle performance in both healthy and diseased muscles has been demonstrated in research and in clinical practice. However the artificial nature of the muscle activation during FES leads to some important differences from the voluntary muscle contraction. Ultrasound Imaging (USI) is a potential tool that could provide objective measurements of the muscle's response during electrical stimulation, thus helping to describe and understand these differences.

The aim of this study is to develop techniques based on USI that helps to elucidate the muscle function during electrical stimulation and allow comparison with voluntary contractions.

Ultrasound videos were collected from healthy participants during experimental procedures involving voluntary and electrically induced muscle contractions. The videos were analysed using software algorithms for the tracking of features in US images. The resulting parameters were used as the basis for characterisation methods to describe the muscle contraction, both globally and locally.

The effectiveness of the USI analysis techniques was tested and methods for extraction of

physiological information from the video analysis were implemented.

The regional distribution of muscle displacement during the tasks was analysed. Larger displacements were observed at deeper portions of the muscle in both the voluntary and the electrically induced contractions. Differential displacements across muscle depths were observed to differ during voluntary and FES contractions. The electric currents applied induce a uniform muscle contraction across different depths, most likely influenced by the way the electric field recruits muscle fibers.

Muscle displacement was correlated to the force exerted by the muscle. Areas close to the deep aponeurosis have higher correlation with torque exerted and a second order polynomial can be used to define the relationship between displacement and torque. The relationship between the whole muscle displacement at different depths and the torque exerted was described using a polynomial surface fitting.

Mechanical strain was used to map the muscle activation. Middle areas of the muscle undergo higher positive vertical strain (i.e. the muscle thickens) while deeper portions of the muscle are the most affected by shortening horizontal strain (i.e. the muscle shortens) in both voluntary and FES contractions. The muscle contractility was analysed through strain rate. A time-frequency analysis of the strain rate was performed. More frequency components and higher bandwidths were observed in FES induced contractions when compared to the voluntary. The frequency components might reflect the motor unit activation, suggesting that during FES all the motor units, firing at different rates, are recruited.

In this project, USI was used as a tool to characterise the muscle behaviour locally. Regional muscle displacement and strain distribution have been used to elucidate the muscle function and quantify how different muscle areas are mechanically involved in the contraction. Strain rate was correlated with the muscle contractility and hypotheses regarding the correlation with motor units firing rate have been proposed.

In conclusion a number of techniques were developed with the purpose to investigate the muscle function in normal conditions and when external factors, such as electrical stimulation, alter the natural muscle behaviour.

Acknowledgements

I am finally here writing my acknowledgements. During these 4 years many people have made me feel at home and I will never forget this.

I would first like to thank my supervisor, Dr. Henrik Gollee who has always been supportive during any problems both in my PhD and in my personal life. He has not only been a supervisor but a person I could rely on. I would like to acknowledge also my second supervisor Prof. Ian Loram who has also contributed to the achievements of this project. Thanks to Dr. P.Harding, Dr. E.Hodson-Tole and Dr. R.J. Cunningham for their advice on ultrasound image analysis. Thank you to Jennifer Miller for proof reading my thesis, I wish her all the best for her PhD.

To all the volunteers who took part in the study, I would like to extend my thanks. Special thanks to all the wonderful people I have met in Glasgow: Jenni, Patricia Agi, Hiba, Cristiano, Ross, Davide, Mehemed, Ceasar. Thank you to my friend Sofia for keeping in contact with me every day, I wish her a lot of happiness. I can't forget all the people who shared their daily activities with me. Many thanks to Dr. Aleksandra Vuckovic for being like a mother for the lab. To Adamantia who was my first friend at University I hope I will see her again soon. To the Iraqi colleagues, Salim, Mohammed, Manaf and Aso, who showed me a side of their country and their religion that the newspapers want to hide, I wish you and your families all the best. Thank you to my friends and colleagues Finda, Ania, Linda, Sarah and Lin for sharing with me happy moments and bringing color to my days in the university. Thank you to Bethel, for all the discussions, all the marking, all the chips and all the amazing moment shared, lot of luck for you my dear friend. I am extremely grateful to Alberto for being supportive every day and encouraging me to always be the best version of myself. Without you I would not be writing my acknowledgment at this moment. Thank you to Lucio and Divinia I wish you a bright future. Thank you to my mom for supporting my choice to come to Glasgow, I hope we will be living closer soon.

Author's Declaration

I declare that, except where explicit reference is made to the contribution of others, this thesis is the result of my own work and has not been submitted for any other degree at the University of Glasgow or any other institution.

All of the analysis and data collection techniques presented in this thesis were created by the author.

M. Armentano

January 2017

Publications

Conference Proceedings

M. Armentano, I.D. Loram, H. Gollee, "Quantification of muscle displacement during isometric contraction using B-mode ultrasound", *In proceedings of 9th IEEE EMBS UK & Republic of Ireland Postgraduate Conference on Biomedical Engineering and Medical Physics, Liverpool, UK 2015*

M. Armentano, I.D. Loram, H. Gollee, "Regional muscle displacement during isometric contraction using B-Mode ultrasound", *In proceedings of 37th IEEE EMBS Conference on Biomedical Engineering and Medical Physics, Milano, IT 2015*

Contents

List of Tables

List of Figures

Chapter 1

Introduction

1.1 Summary

In this first chapter, the basic concepts and terms used throughout the thesis are defined. The chapter introduces the principles of ultrasound, some definitions of physiology and describes functional electrical stimulation. It highlights the way neural stimulus activates muscles and how muscle activation can be artificially evoked using electrical stimulation.

1.2 Ultrasound, history and working principles

An introduction about diagnostic ultrasound is given in the following sections. The aims and objectives of this PhD are presented and the outline of the thesis given.

1.2.1 Principles of diagnostic Ultrasound

Ultrasound imaging uses the interaction of sound waves with living tissue to produce an image of the tissue, or to determine the velocity of moving tissue and fluids (Doppler-based modes) [1–3].

An ultrasound imaging system uses a transducer probe to generate and receive sound waves. The probe is consists of piezoelectric crystals which, when a current is applied, start vibrating and generate sound waves. As acoustic waves travel through the body, they are transmitted, reflected, attenuated and absorbed. These effects occur every time the wave is at the interface between tissues with different acoustic impedance. The acoustic impedance is an intrinsic physical property of the tissue and can be thought of the resistance of a tissue to the passage of acoustic waves [1].

In diagnostic ultrasound systems, when an incident ultrasound pulse encounters a large, smooth interface of two body tissues with different acoustic impedances, the sound energy is reflected back to the transducer By examining the amplitude of the wave that returns back, the time taken and the position where the wave came from it is possible to reconstruct the image of the tissue [1]. There are different ways, called *modes*, of displaying the electrical signal representing the ultrasound echo which returns from the tissue. The most common modes are:

- A-mode, or Amplitude Mode, displays amplitude of the returned echo along a single line (Amplitude vs depth).
- B-Mode, or Brightness Mode, displays a 2D map where the amplitude of the returned echo is represented as grey levels, the higher the amplitude the brighter the point on the map

(Grey Levels vs depth).

- M-Mode, or Motion Mode, displays in grey levels the amplitude of the echo returned back by analysing a single line of the object changing over time (Grey levels line vs time) [4, 5].

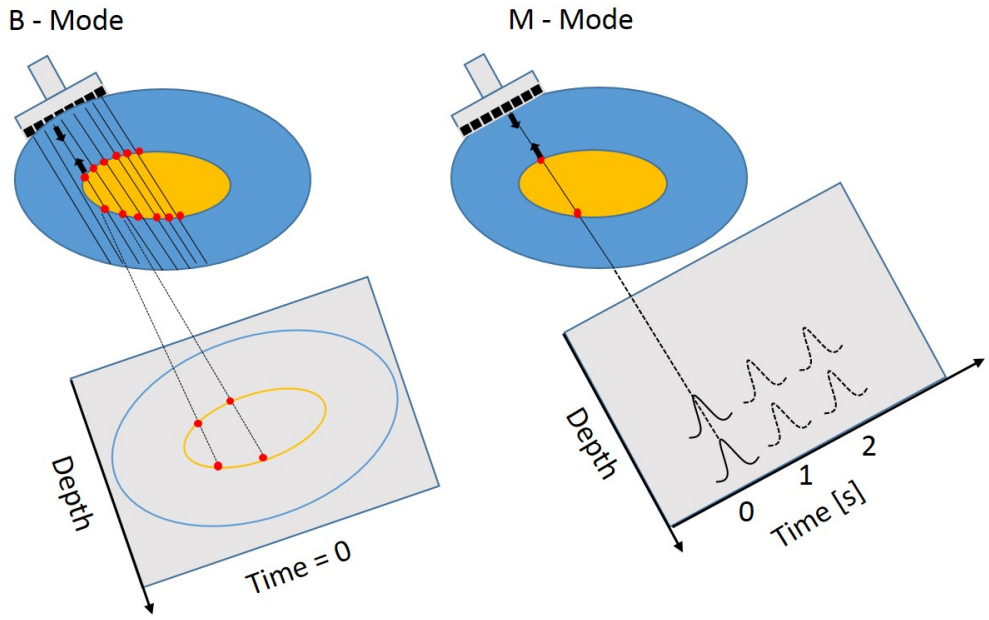

(a) Construction of the image

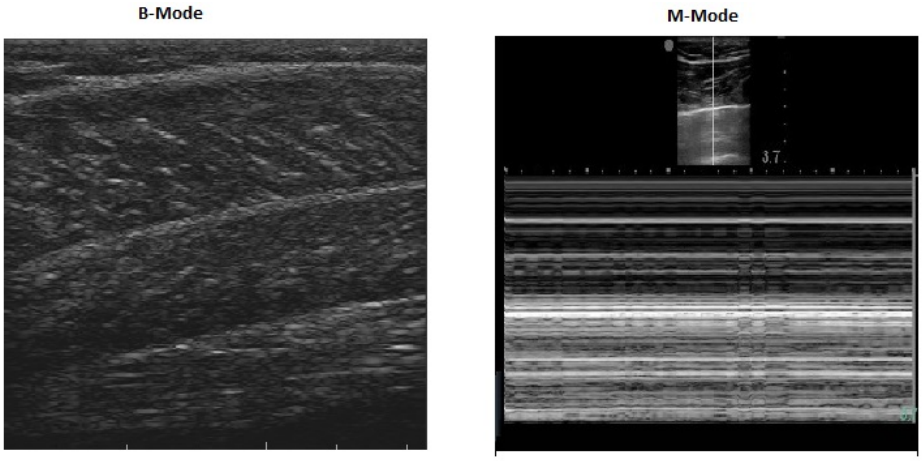

(b) Example of the image

Figure 1.1: Examples of how the ultrasound image is built (a) and of real ultrasound images (b) in B-mode (left) and M-mode (right).

1.2.2 Skeletal muscle ultrasound

In the1980s ultrasound was used for the first time to discriminate between healthy and diseased muscle [6]. The sonographic appearance of muscle can be distinguished from the surrounding tissue because, since it has low echo intensity, it appears relatively black; the boundaries of the

muscle, such as the epimysium, the aponeurosis or tendons appear bright [7]. If the transducer image plane is properly aligned with the muscle fascicles, it is possible to distinguish the orientation of the fascicles relative to the transducer (pennation angle). In the1990s the first studies to examine pennation angle changes during muscle contraction and passive joint movements were performed [8, 9]. By using ultrasound imaging it is possible to analyse muscles features such as thickness, fascicle pennation angle, and fascicle length during static and dynamic conditions.

1.3 The Nervous System

The Nervous System (NS) is a network of billions of highly organised cells that are able to transmit informations within the body. The Nervous System can be divided into two parts:

- **Central Nervous System (CNS)**: includes the brain and the spinal cord
- **Peripheral Nervous System (PNS)**: includes the nerve connections that lie outside the CNS. Its main function is to connect the CNS to the limbs, organs and peripheral body parts.

The spinal cord is the principal conduit for a two-way flow of information from the skin, joints and muscles to the brain. The communication between the CNS and the rest of the body is provided via the *spinal nerves* which compose the PNS. The nerves of the PNS are arranged in bundle of axons. The PNS consists of 12 pairs of cranial nerves and 31 pairs of spinal nerves. Some of these are exclusively sensory cells (which detect information such as smell and vision), others are exclusively motor cells (which control movement).

The nerves exit the spinal cord through small openings. Each spinal nerve connects to the spinal cord with two branches, the dorsal root (afferent or sensory pathway) and the ventral root (efferent or motor pathway) [10]. See Figure 1.2.

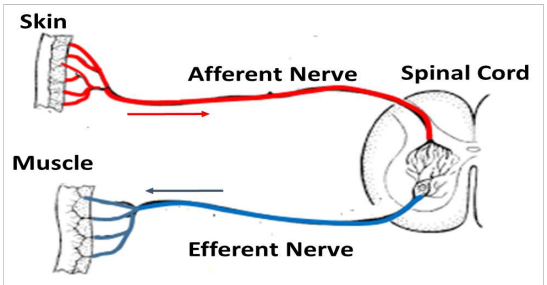

Figure 1.2: An example of part of the nervous system.The image shows the spinal cord and the motor (or efferent) and sensory (or afferent) nerves that connect to the muscle and the skin respectively.

The cells of the CNS are called **neurons** which are the fundamental units for the production and exchange of informations. Neurons transmit both afferent and efferent signals to and from the CNS respectively . Within the NS a number of specialised neurons exists:

- Sensory Neurons: respond to stimuli such as sound or light perceived in the sensory organs and send this information to the CNS.
- Motor Neurons: receive signals from the CNS and cause muscle contraction.
- Interneurons: connect neurons within the same region of the CNS.

The **neurons** have a specif structure, three main parts can be distinguished:

soma : is the nerve cell which is the control center of the neuron.

dentrites : are short branched extensions of a nerve cell whose main function is to receive signals from other cells and transfer them to a processing region of the neuron. The simplest neurons have one dentrite, however, more commonly, neurons have more than one dentrite.

axon : is a long, slender projection of the neuron which conducts electrical impulses away from the neurons' cell body. The majority of the neurons have one single axon which originates from the soma. At the distal extremity of the axon the electrical signal is transduced into a chemical message. Axons' terminals which end close to blood vessels release neurohormones while those which end close to a muscle or to other neurons releases neurotransmitters. At the level of the synapse, the neuron that releases the neurotransmitters is considered *presynaptic* while the one that receives it is defined as *postsynaptic*.

Some axons are surrounded by a fatty substance called myelin which forms an electrically insulating layer. The main purpose of the myelin sheath is to increase the speed at which impulses propagate along the axon. The velocity of propagation of the action potential of the mammalian's neurons depends on the diameter of the neurons and the resistance of the membrane to currents dispersion. The higher the diameter of the axon, the higher the resistance to the currents dispersion and the faster the action potential travels.

[11, 12]

Resuming, the signal is received from the dentritic branches, it is then sent to a specific region of the soma which process the information and generates a new signal which is transmitted along the axon. At the end of the axon the electrical signal is converted into a chemical signal that is transferred through a synapse to another neuron, to a fiber cell or to the blood.

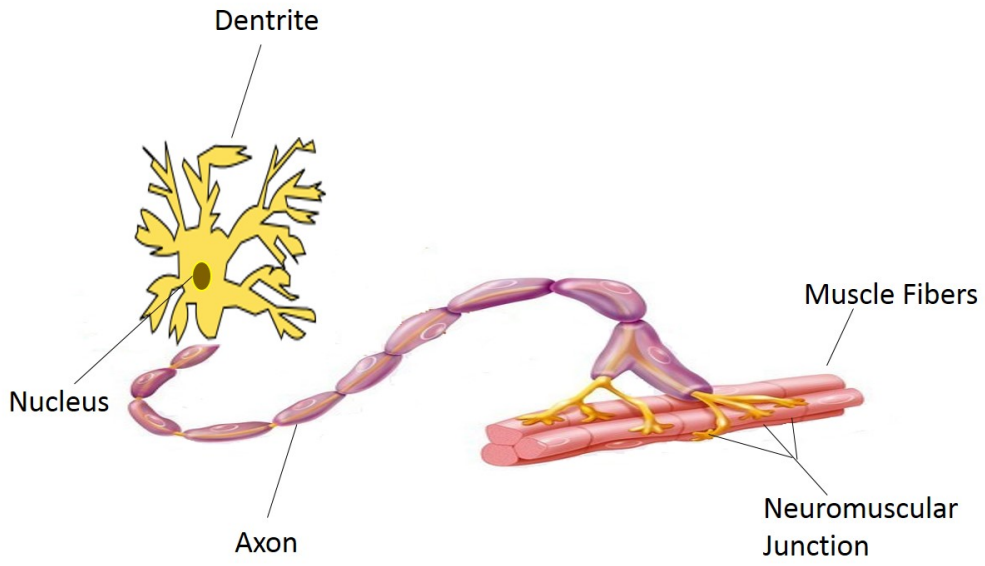

Figure 1.3: In figure it is possible to distinguish the parts composing the neuron and the fibers innervation. The dentrite receives the information which is processed within the nucleus. An action potential is generated and transmitted along the axon up to the neuromuscular junction. The synapse constituting the neuromuscular junction release neurotransmitters that trigger the action potential in the fibers.

1.3.1 Nerve supply to muscle

The functional unit of muscle contraction is called a **Motor Unit** (MU). A MU consists of a motor neuron and the specific muscle cells (fibers) it innervates. The motor neurons controlling the skeletal muscle are known as *alpha* (α) or *anterior* motor neurons. The α motor neurons enable the transmission of an electrochemical impulse from the spinal cord to the muscle. A motor neuron innervates many muscle fibers because the terminal end of an axon has many branches. Muscle contraction results from the combined action of many motor units. The group of motor neurons that innervate a single muscle is called the **motor neuron pool**.

The exchange of information between the nerve cell and the muscle fiber happens through a chemical synapse which releases neurotransmitter from the end of the axons to the fiber. The interface between these two is called the **neuromuscular junction** (**NMJ**) or **motor endplate**. Its function is to transmit the nerve impulse to initiate the muscle action. Each muscle fiber has only one NMJ. See Figure 1.3.

A motor unit contains only one specific muscle fiber type. In addition, motor units are classified based on the physiological and mechanical properties of the fiber they innervate. Three main characteristic can be distinguished among motor units: twitch, tension and fatigability. Three main categories of MU are observed:

- Fast twitch, high force and fast fatigue (type IIb)
- Fast twitch, moderate force and fatigue resistant (type IIa)
- Slow twitch, low tension and fatigue resistant (type I)

Generally, large motor neurons have fast conduction velocity and activate fast twitch fibers. The fast-fatigable (FF) and fast-fatigue-resistant (FR) motor units develop higher force and are faster than the slow-twitch (S) motor units, however the slow-twitch are more fatigue resistant [10].

1.3.2 Force development during muscle contraction

When an action potential is triggered in the motor neuron it propagates up to the NMJ activating all the fibers of the motor units synchronously. A motor unit does not activate gradually, it either activates or not. This is known as the **all-or-none** principle.

The force gradation within the skeletal muscle is regulated via two mechanisms:

1. Increasing the number of motor units recruited.
2. Increasing the frequency of discharge (the firing rate) of the motor units.

[13].

A muscle generates considerable force upon the activation of more motor units. In addition, repetitive stimuli which reach the muscle before it relaxes increase the total tension. A low-force muscle contraction is generated by few motor units and a progressive recruitment of motor units determines an increment in force. As muscle force increases, motor units with progressively larger axons are recruited. This is known as the **size principle** which indicates an orderly recruitment and results in a smooth muscle contraction [14].

The motor units within the same motor neuron pool do not all fire at the same time, in fact they activate asynchronously. A different strategy would not allow a fine control of force output. The selective recruitment and the firing pattern of fast and slow twitch motor units provide the control mechanism to produce the desired response.

Recent studies observed that the size principle does not always hold true. Slow-twitch motor units are activated during light-to-moderate efforts, however during more rapid, powerful contractions fast-twitch motor units can be activated without prior activation of slow twitch motor units [15].

The mechanism of force generation can be compromised by many factors which impact the contraction. Repeated stimulations can result in a decline in muscle tension. The phenomenon is known as *neuromuscular fatigue*. The origin of fatigue is still a matter of debate and is related to an interruption in the chain between the CNS, PNS, neuromuscular junction and muscle fiber. As muscle function deteriorates as a result of the fatigue, additional motor units are recruited in order to maintain the desired output force [10].

1.4 The Skeletal Muscle

In mammals, all activities that involve movement depend on muscles. The human body is constituted of three types of muscles: skeletal, cardiac and smooth. They have various purposes: locomotion, upright posture, balancing on two legs, support of internal organs, controlling valves and body openings and movement of materials along internal tubes. Skeletal muscles provide strength and protection for the skeleton, enable bones to move and maintain body posture against gravity. Skeletal muscles attach to the bones through a connective tissue called **tendon**. When the attachment is at a joint the muscle contraction results in movement.

The structural unit of skeletal muscles is a multinucleated cylindrical cell known as a **fiber**. Individual fiber length varies from a few millimeters to nearly 30 mm, with a width of up to 0.15 mm [10]. A fine layer of connective tissue, the endomysium, wraps each muscle fiber and separates it from neighbouring fibers. Another layer of connective tissue, the perimysium, surrounds a bundle of up to 150 fibers called fasciculus. Finally the epimysium, a fascia of fibrous connective tissue, surrounds the entire muscle. It tapers at its distal and proximal ends and blends with intramuscular tissue sheaths to the aponeuroses and then to the tendons [10,12].

The arrangement of muscle fibers varies among muscles, significantly affecting the muscles capacity to generate force and power. **Fusiform** fibers run parallel along the muscle's long axis. In this case the long axis is defined as an imaginary line between the origin and the insertion of the muscle and the muscle is defined as *non-pennate*. On the other side **pennate** fibers lie at an oblique angle relative to the force-generating axis. This angle is known as the **angle of pennation**. The pennate arrangement permits a larger number of fibers to be packed n the same cross-sectional-area, however there is a loss in the force transmitted to the tendons [16,17].

The arrangement of muscle fibers within a muscle relative to the axis of force generation [18] is defined as *muscle architecture*. The amount of force that a muscle can exert depends on the number of active fibers and on the fibers arrangement according to the formula in Equation (1.1). An example of a different kind of arrangement is shown in Figure 1.4 where it is possible

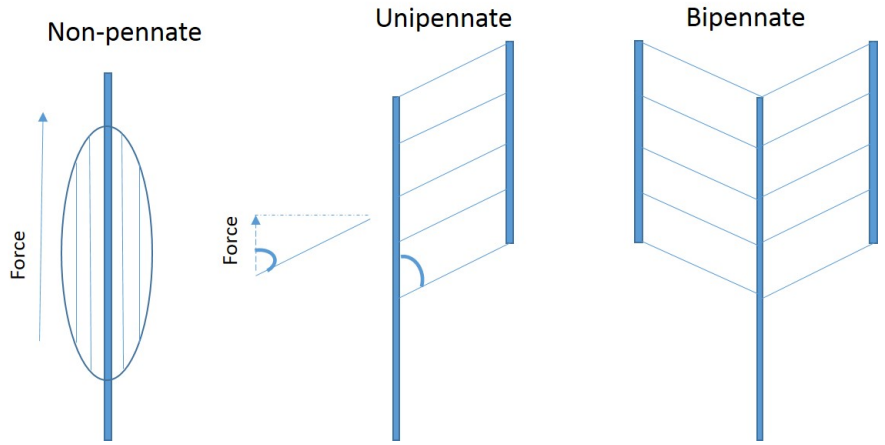

Figure 1.4: In order left to right: fusiform non pennate arrangement, unipennate and bipennate arrangement. The force is directed along the long axis of the fiber and it depends on the pennation of the fiber.

to distinguish a non-pennate a unipennate and a bi-pennate muscles' configuration.

$$F_{tendon} = F_{fascicle} \times cos\theta \tag{1.1}$$

Where θ is the angle of pennation. Note that $\theta = 0$ in non-pennate muscles.

1.4.1 Skeletal Muscle contraction

The muscle fiber contractile structure is called a **myofibril**. Each fiber contains million of myofibrils. A myofibril is composed of different proteins; among these are the contractile proteins *myosin* and *actin*. Each molecule of myosin is made of two protein chains which twist forming a thick spiral spiral. In contrast, actin forms thin filaments. The myosin heads connect to two actin filaments constituting what is called a **sarcomere**. Within a myofibril many repetitions of sarcomeres are observed. The muscle contraction is explained with the *sliding filament theory* proved by Huxley in 1954 [19]. The contraction is caused by a series of molecular events known as the cross- bridge cycle which makes the heads of myosin slide over the actin filaments. It is important to notice that each filament does not change length but overlaps each other causing a shortening of the sarcomeres [10, 11].

1.4.2 Muscle Action Forms

Following neural stimulation (action potential propagation up to the muscle), the contractile elements of the fibers attempt to shorten along the longitudinal axis. Three different cases of

muscle action can be observed:

- **Isometric**: when a muscle generates force and attempts to shorten but cannot overcome external resistance. From a physics standpoint, the isometric contraction does not produce external work. Despite the lack of external visible movement, considerable forces are generated and the muscle contracts. Isometric contraction literally means no change in muscle length, however it has been proven that there is still shortening of the muscle fibers and of the muscle. What is intended for isometric is therefore the length of the total muscle-tendon complex [8].
- **Concentric**: when the muscle shortens resulting in joint movement and development of tension. An example is lifting a weight.
- **Eccentric**: when external resistance exceeds the muscle force and the muscle lengthens while developing tension.

1.5 Functional Electrical Stimulation

Neuromuscular Electrical Stimulation (NMES) is the application of a train of intermittent electrical stimuli to superficial skeletal muscles with the purpose of triggering the muscle contraction through intramuscular nerve branches [20–22]. NMES is adopted as rehabilitation or training method in both research and clinical settings. Depending on the needs NMES can be used to: prevent muscle wasting during prolonged periods of immobilisation, recover muscle function resulting from immobilisation and improve muscle function in healthy population [21]. The application of NMES in a particular sequence with the purpose of performing a functional task is known as Functional Electrical Stimulation (FES) and was first proposed by Liberson et al. in 1961 [23] for the treatment of foot drop. Within the category of NMES there is also the Transcutaneous Electrical Nerve Stimulation (TENS) which differs from the FES in terms of its final outcome. Unlike FES, TENS is used as a therapeutic treatment for pain relief.

1.5.1 Principles of FES

People affected by paralysis due to damage at the level of the spinal cord are not able to voluntarily control their actions resulting in a inability to perform a functional task. In this condition the pathways connecting the spinal cord to the peripheral nerves are still intact, preserving its ability to trigger muscle contraction. FES can be used to provide the electrical

stimulus to the nerve to initiate the action potential that results in the contraction of those paralysed muscles. It is important to highlight that FES triggers the contraction through the nerve rather than through the muscle fiber itself because the former has a significantly lower threshold for the initiation of an action potential [21].

The achievement of muscle contraction of a paralysed muscle has great benefit in terms of reducing muscle wasting and improving its strength. Although there is evidence of FES being beneficial for people who are not able bodied, such as those with spinal cord injury, many clinicians are still reluctant about its use. The main reason is because there is scarce knowledge of the physiological and methodological way of achieving a non- voluntary electrically induced muscle contraction [24, 25]. Examples are the lack of evidence on how the motor units are activated [26, 27] or the settings of the current values and electrodes placement often done on an empirical basis [24, 25].

It is believed that FES leads to a 'reverse recruitment order' of the motor units where motor units with larger axons, related to the Type II Fast Fatigant fibers, are activated first. This goes against the *size principle* of fiber recruitment explained in Section 1.3.1. On the other side, Bickel *et al.* [27] argues that the motor unit recruitment is random and that the belief of the 'reverse order recruitment' is based on the fact that it explains the early onset of fatigue. More details about this topic are given in Section 2.3.1. Whether motor units are recruited in reverse order or random, during FES increased levels of muscle fatigue are observed. For instance, the repeated activation of the same motor units and the more frequent recruitment of fast-fatigant Type II fibers are the main difference between FES and voluntary muscle activation. The faster fatigability of the muscle during FES results in the need to increase the stimulation charge to maintain a constant muscle contraction when using FES for an extended period of time.

1.5.1.1 Electrodes placement

FES is delivered via electrodes that can be placed in three different ways: i) on the skin (transcutaneous or surface stimulation), ii) inserted through the skin (percutaneous stimulation) iii) implanted into the body and placed around or in close proximity to the nerve (implanted devices) [28].

Transcutaneous stimulation has as main advantage the fact that it is non-invasive, but it is less precise in terms of the muscle or zone of the muscle being targeted. Pecutaneous stimulation allows a greater selectivity of the correct motor point but problems are related to the fact that needle electrodes are prone to failure [29]. Implanted device are for long term use and require a

surgical procedure for the implantation. The electrodes can be implanted on the target muscle (epimysial electrodes), penetrate the nerve (intraneural electrodes) or surround the nerve (cuff electrodes) [30].

Two kinds of electrode configurations are used for the transcutaneous stimulation: monopolar and bipolar. In a monopolar configuration the active electrode is placed on the target nerve and the reference electrode on a remote location This arrangement provides a rather general stimulation pattern because the current has more variance in the pathways. It is therefore more common when using an electrode arrays with one common reference. In bipolar configuration both cathode (negative) and anode (positive) electrodes are placed on the treatment area in relative proximity to each other. This arrangement provides for rather specific stimulation of structures with few variations in responses [30].

1.5.1.2 Stimulation Parameters

The effect of the FES on the muscle contraction depends on the type and location of electrodes and on the setting of the stimulating current. Each electrical pulse is characterised by its pulsewidth, current amplitude, waveform and frequency [31]. Pulsewidth is the duration of a pulse, it is usually in the range between 100 and 500 μs. The amplitude is the intensity of the current and, during transcutanous stimulation, is usually in the range of 10 to 100 mA.

The total charge, Q delivered to the muscle is the product between the amplitude, I, and the pulsewidth, PW (see Equation (1.2)), and is measured in Coulombs. The electric field produced is the electric force per unit of charge and its unit is $[N \times C^{-1}]$ or $[V \times m^{-1}]$

$$Q = I \times PW \quad [C] \tag{1.2}$$

$$\vec{E} = \frac{\vec{F}}{Q} \quad [N \times C^{-1}] \quad or \quad [V \times m^{-1}] \tag{1.3}$$

A higher amount of charge is therefore delivered at higher amplitude and higher pulsewidth. Increase in charge results in an increasing electric field which spreads within the muscle, resulting in more fiber recruitment and greater force exertion. An example of how the electric field spread within the muscle is shown in Figure 1.5

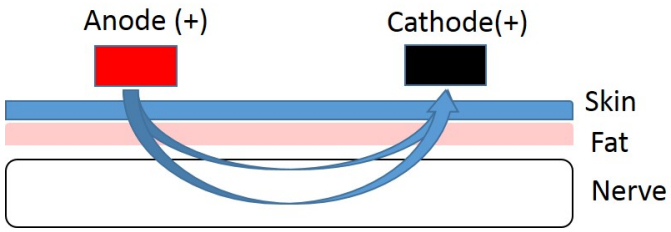

Figure 1.5: The electric field is produced among the electrodes and it spread with open lines in the surrounding of the application point. The higher the current, the deeper the field penetrates.

Regarding the waveform, different shapes can be used such as biphasic or monophasic. A monophasic waveform applies only positive or negative charges. A biphasic waveform applies a positive followed by a negative charge. It is usually regarded as safer because balances the polarity of the charge entering the body. For the monophasic waveform the balance of charges is usually obtained by applying monophasic waveforms of opposite direction resulting in an overall neutral charge. An example of the FES stimulation in terms of parameters is shown in Figure 1.6.

The frequency of the stimulation influences the contraction producing either a tetanic (constant) contraction or a twitch (intermittent) [28]. The greater the stimulation, the stronger the force generated but with faster muscle contraction which results in fast fatigue.

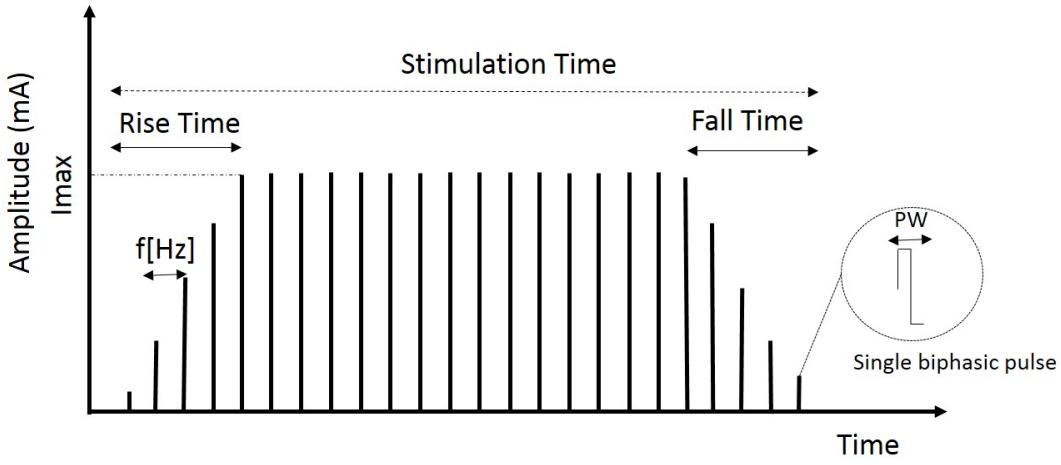

Figure 1.6: The graph shows the main parameters that characterise the FES stimulation: the frequency, the pulsewidth and the amplitude. Usually FES is delivered with a ramping pattern (rise and fall times) in order to allow the subject to get used to the stimulation.

1.6 Aims and Objectives

USI is a good method to visualise the muscle contraction, including regional variation. FES provides artificial contraction but differs significantly from voluntary contraction in the force produced and in the fatigue resistance. The open question is why FES is less effective than the voluntary contraction. Can USI be used to elucidate this?

The main aim of this PhD is to give further insight in to the way the muscle contracts when FES is applied. The novelty of the PhD exists in the use of USI for analysing regional muscle activation. In previous works USI was used to describe the muscle contraction by analysing architectural parameters of the muscle such as fascicle length, pennation angle or muscle thickness. To our knowledge, this study is the first to investigate the mechanical activation of a whole portion of the muscle during voluntary and electrically induced muscle contractions. The objectives are:

i) Interpretation of the information extracted from USI

ii) Identification of significant parameters for the description of the muscle contraction

iii) Comparison between voluntary and electrically induced muscle contraction

iv) Evaluation of muscle contraction in relation to torque exerted

1.6.1 Thesis Outline

Chapter 2: A review of studies investigating ultrasound imaging for muscle function and the benefits and limitations of functional electrical stimulation. Ultrasound Imaging has been widely used to investigate the muscle architecture and algorithms for automatic tracking of architectural muscle parameters have been proposed. The FES has been used to enhance muscle function and perform muscle training in people affected by neuromuscular diseases, however the fiber recruitment during FES differs from the Voluntary contraction making it inefficient and prone to develop early muscle fatigue.

Chapter 3: The experimental methods used throughout the thesis are presented in this chapter. This includes the description of the software for tracking persistent features in the ultrasound images of the muscle and the way they are processed for extracting functional information. An overview of general methodology for statistical analysis and signal processing is also given.

Chapter 4: This chapter is divided into two parts. In the first part the ultrasound information will be explored. The information will be presented in terms of muscle displacement as a function

of time and against the torque exerted during the task. The experimental setup for a feasibility study will be presented as well. The second part investigates the feasibility of using ultrasound imaging to detect the muscle function information. The quality of the ultrasound image depends on the device used therefore three different devices and different FES protocol will be compared. In addition, the consistency of the ultrasound features detection will be analysed with two different software.

Chapter 5: This chapter compares the ultrasound outcome of the voluntary muscle contraction with electrically induced contraction. Electrical stimulation is delivered in two ways: transcutaneous on the gastrocnemious muscle belly and transcutaneous on the tibial nerve. The ultrasound information will be used to map muscle activation during both voluntary and electrically elicited contractions. The displacement information at different muscle depths and the strain distribution over the muscle will be presented. In addition a time-frequency analysis of the strain rate is performed and the frequency components for the voluntary and electrically induced muscle contractions will be investigated.

Chapter 6: In this chapter the relationship between torque exerted and ultrasound information is evaluated using polynomial fitting . The consistency of the polynomial among different subjects is evaluated in terms of the order of the polynomial. The coefficients characterising the polynomial obtained for each subject are evaluated for the voluntary and the electrically induced contraction.

Chapter 7: In this chapter the main results are discussed.

Chapter 8: The main conclusions of this thesis are summarised in this chapter. Suggestions for future work are given as well.

1.7 Contributions

- In this thesis a unique technique based on analysis of US images for the investigation of muscle activation during electrically induced muscle contraction was implemented and developed. It is shown that USI can potentially answer open questions about the way the electrical stimulation activates the muscle. Demonstration of the feasibility and effectiveness of the technology and protocols is a necessary step towards the implementation of USI as an assistive method for improving the Functional Electrical Stimulation (FES) technique. As such, a key of this thesis is proof of feasibility.

- USI has been used for the first time to investigate the activity of a whole muscle during

voluntary and electrically induced contractions. Parameters characterising the muscle contraction were identified and their physiological meaning was extrapolated.

- Neuromuscular Electrical Stimulation was investigated using both transcutaneous stimulation and nerve stimulation and was compared to the voluntary activation. The relative muscle displacement across depths was more similar between the voluntary and the electrically induced contraction through the nerve rather than the transuctaneous stimulation. The result suggests that, unlike the nerve stimulation and the voluntary contraction, transcutaneous electrical stimulation recruits muscle fibers through a peripheral pathways resulting in less variable fiber activation which could be related to the early onset of muscle fatigue.

- USI was used to explore the regional activity of the muscle contraction by visualising changes in local strain. Higher vertical strain is observed in the middle portion of the muscle while negative horizontal strain affects deeper regions. Horizontal strain becomes more negative while vertical strain increases with strength of contraction or intensity of the stimulation. The map of the stimulation can be useful to detect the amount of muscle activated during electrical stimulation.

- Local changes in strain rate were analysed as well and related to the muscle's contractility. A time-frequency analysis of the strain rate indicated activity at the onset and offeset of the contraction. More frequency components and higher power are observed with increasing the strength of the contraction or the intensity of the stimulation. What mainly differentiates the the electrically induced contraction from the voluntary contraction is a much higher activity at the onset of the contraction when electrical stimulation is applied. This phenomenon can be related to the different firing rate in the motor units recruitment that could explain the early onset of fatigue during electrical stimulation.

- The relationship between the torque exerted and global muscle displacement was analysed in a group of eleven healthy subjects. A unique curve was observed to characterise the relationship across the subjects. A polynomial was used to model the relationship and it was validated using cross-validation. A different relationship could be observed in cases where the status of the muscle is compromised, among these neuromuscular diseases and spinal cord injury.

- In this thesis the feasibility of using USI to estimate the torque exerted by the gastrocnemius medialis muscle was investigated. The study indicated that the displacement at deeper areas of the muscle is more suitable for torque prediction when using polynomial curve fitting.

Chapter 2

Literature Review

2.1 Summary

Musculoskeletal Ultrasound Imaging has proven to be a useful tool to understand the muscle architecture which can reveal information on the muscles' mechanical properties. Ultrasonography has detected differences in muscle architecture and appearance across age, sex, status and health of the muscle. The potential of its applications has pushed researchers to develop automatic algorithms for tracking muscle changes or to analyse muscle contraction. Ultrasound imaging is also a useful tool to describe the muscle activation resulting from a voluntary movement or artificially achieved through electrical stimulation.

In this chapter the main findings from the past studies are discussed.

2.2 Ultrasound Imaging (USI)

Diagnostic Ultrasound Imaging (USI) appears in medicine in the 1950's following the work of Professor Ian Donal from University of Glasgow who firstly used an ultrasound flow detector for diagnosis of carcinoma and ovarian cysts [32]. Not much later the first report of musculoskeletal ultrasonography was published, and the ability of discriminating between soft tissues, tendon and skin was shown [33,34]. A picture representing the prototype built by Professor Donald and his group is shown in Figure 2.1.

Figure 2.1: Diagnostic ultrasound built by Professors Donald, MacVicar and Brown. It is now held at the Hunterian Museum of University of Glasgow. Taken from http://www.gla.ac.uk/news/archiveofnews

The B-mode US scan was introduced in 1972 [35] and its first application on skeletal muscle dates back to 1980 when a research group from Oxford investigated the loss of mass of the quadriceps following immobilisation [36]. In the study they demonstrated that the anthropometric estimates of the cross-sectional area of the thigh obtained with the measuring tape were underestimating the mass wasting when compared with the measurements obtained with the

ultrasound [36]. Several studies followed investigating changes in cross-sectional area produced by strength-training and related to age [37, 38].

In the 90s, advances in the technology of ultrasound in terms of quality of the image made the applications on skeletal muscle quite widespread and becoming a promising technique [39].

USI on skeletal muscles provides the possibility to measure static and dynamic parameters of the muscle. Static parameters are related to muscle morphology, such as muscle size, shape (e.g. thickness and length) and structure (e.g. organisation of muscle fascicles) [40, 41]. To visualise the movement of muscle during activity (i.e. in dynamic conditions) it is possible to either record a video of ultrasound imaging of the muscle for offline analysis, or to use image analysis on the real-time video stream. Both the off-line and the real-time analysis of the ultrasound videos allow dynamic measurement of the muscle including changes in muscle fascicle length, pennation angle and muscle shape and provide an indication of muscle activity (e.g. muscle lengthening or shortening). These dynamic measures are dependent on factors such as type of contraction (isometric, concentric, eccentric) [42], extensibility of the tendon or activity of adjacent muscles [43]. The most useful feature of ultrasound videos analysis is that movement of anatomical structures can be observed as it actually occurs.

Following the great interest shown in literature in the use of USI as feedback for muscular imaging, the term Rehabilitative Ultrasound Imaging (RUSI) was coined in 2006 to indicate the procedure used by physical therapists to evaluate muscle and soft tissues related morphology and behaviour during physical tasks [43]. The purpose of this technique is to provide feedback to the patient and therapist to improve outcomes. It is important to notice that RUSI is not a treatment but a tool to aid motor learning and improve neuromuscular function.

2.2.1 Skeletal Muscle Architecture with USI

Skeletal muscle architecture is defined as the arrangement of muscle fibers within a muscle relative to the muscle's line of action [18, 44]. All the muscles are made of similar contractile elements (sarcomeres) but their arrangement change across muscles influencing their contractile properties [17, 18]. The clinical significance of skeletal muscle architecture has been widely investigated over the years and its role in muscle function has been shown to be associated with sport injuries, motor control and surgical restoration [16, 17, 45].

Until a few years ago, morphological and architectural information of the skeletal muscle were obtained from *in vitro* measurements of cadavers. Pioneering works from Gans Bock and de Vriee [46, 47] developed precise methodologies based on dissection to evaluate parameters such

as muscle length, fascicle length, pennation angle and cross-sectional area. These parameters have been used to describe the mechanical properties of active muscles with the assumption that the change in length of the muscle was not affecting the results [9]. It is nowadays clear that this approach is questionable because dead fibers and muscles are shorter than the live ones and because the architectural parameters depend on the muscle length at rest [9].

The recent development in non-invasive image analysis techniques, such as magnetic resonance and ultrasound, made *in vivo* evaluation of the muscle architecture and morphology possible [9,42,48–51]. What is mainly remarkable is that USI allows the estimation of muscle parameters both at rest and in dynamic conditions while performing a task.

Parameters such as pennation angle, fascicle length and muscle thickness were successfully estimated at rest in healthy people and for a variety of muscles [52]. Pennation angles vary from 0° (for non-pennate muscles) to 30°, while the fascicle length has a higher range of measurements. For instance they are about $5cm$ on the gastrocnemius and 40 cm on the sartorius [53].

Pennate muscles are the most studied because the fascicle's span can be fully visualised on the ultrasound image and because both fascicle length and pennation angle undergo remarkable changes during contraction. Several studies demonstrated that during isometric muscle contraction, independently from the joint angle, the pennation angle increases while the fibers shorten and rotate [9,44,50,54]. During isokinetic concentric contractions a curvilinear increase in fascicle length and a curvilinear decrease in pennation angle was observed, while in eccentric contraction a quasi-isometric behaviour of fascicle length was shown [42].

Both fascicle length and pennation angles have on average higher values in tensed muscles when compared to muscles in relaxed state [50, 54–56]. It is important to notice that the muscle's tensed or relaxed states depend on the joint angle. It was shown that architectural parameters change with joint angle [50, 54, 57]. The architectural properties and their relationship with the joint angles are specific to the individual muscle [56]. For example the triceps surae muscles (gastrocnemius medialis, gastrocnemius lateralis and soleus) are synergistic for the plantarflexion but have different muscle and fascicle lengths and pennation angles.

The skeletal muscle architecture plays a fundamental role in the development of force. Different studies have investigated the relationship between architectural parameters and force exerted observing a curvilinear relationship [8, 50, 51]. Hodges explains the phenomenon looking at the whole muscle-tendon complex: at low forces, tendon stiffness is low and small changes in force produce large changes in muscles fascicle length; when the force increase the stiffness increase too and changes in muscle fascicle length become progressively smaller [51]. The curvilinear

relationship means that at low forces the muscle undergos big architectural changes while with increased force very little changes are observed. This highlights the fact that architectural parameters measured with the ultrasound imaging can be used to discriminate between low levels of contraction but are less suitable for strong contractions.

2.2.2 Muscle ultrasound in neuromuscular disorders

Soon after the first applications of USI on healthy muscles, the potentiality of muscle USI was exploited in diseased muscle. The first study to report differences between US images of healthy and diseased muscle was made by Heckmatt et al. who compared a group of 10 children affected by muscular dystrophy with 40 healthy controls [6]. They observed that pathological muscle was characterised by reflecting surfaces. The phenomenon was attributed to infiltration of fat and connective tissues and suggested that visual analysis of the US image was a way to evaluate the status of the muscle. In addition they observed different degrees of changes in US images associated with different levels of pathological involvement of the muscle [6]. Not much later, Heckmatt and his group correlated average values of muscle thickness to age of children between 0 and 12 years old [58].

Following these studies the potential for USI to discriminate between healthy and diseased muscle was widely investigated (see Review [59]). Different studies showed that neuromuscular disorders lead to an increase in echo intensity because of the replacement of muscle tissue with fat and fibrosis [59,60], however the echo intensity is not suitable for detection of muscle changes at early stages of the disease if performed visually [59]. Pillen et al. investigated the importance of a quantitative method to assess the gray-scale of muscle echo intensity in terms of sensitivity and independent of the operator [61].

Different diseases involving the skeletal muscle are characterised by increased values of architectural parameters such as pennation angles and fascicle length [62, 63].

2.2.3 Muscoloskeletal USI during electrical stimulation

Few studies have used the USI technique to investigated the mechanisms of force transmission within the muscle. As explained in Section 1.4 the axis of force transmission is along the aponeuroses which connects it to the tendon. USI can be used to describe the movement of the aponeuroses.

Muscle shortening results in the displacement of the aponeuroses, however differences between

the superficial and deeper aponeuroses were oberved. Studies showed that during voluntary contraction the displacement of the superficial aponeurosis is smaller than that of those deeper and in the opposite direction [64, 65]. The phenomenon was explained concluding that the architectural muscle arrangement facilitates the displacement at deeper area [65]. In addition the work of Shin et al. identified local differences along each aponeurosis, being greater at the muscle's distal areas.

Bojsen-Moller et al. analysed the displacement of the aponeuroses during both voluntary and electrically induced muscle contraction [66]. The purpose of using the electrical stimulation was to isolate the muscle function from the effect of other synergistic muscles. The study reported the tissue displacement of the gastrocnemius medialis (GM) during voluntary isometric contraction and during electrically elicited contraction [66]. It showed that during voluntary isometric contraction the muscle displacement in proximity of the GM deeper aponeurosis was comparable to the muscle displacement at the superficial part of the soleus (>0.8 mm). The muscle displacement at the surface of the GM was much lower (>0.3 mm). Conversely, during electrically elicited contraction, the GM appeared to have a statistically different range of movement than the soleus (SOL). Thus they suggested that intermuscular force transmission occurring within the triceps surae muscles influenced the displacement of the deeper aponeurosis in order to relieve the muscle and the Achilles tendon from stress concentration. Other studies investigating the superficial and deeper aponeurosis of the GM showed that the displacement of the superficial aponeurosis is smaller than the movement of the deeper muscles structures [67, 68]. Shin at al. suggested that this happens because the fascicular strain is translated into proximodistal movement of the deep aponeurosis whereas the superficial aponeurosis remains approximately stationary [67].

2.2.4 Automatic analysis of muscle USI

The most common approach for the estimation of architectural parameters is based on manual identification of the information frame-by-frame. It is easy to understand that the technique is operator-dependent and time consuming. This has led research groups to develop automated tracking approaches.

A variety of algorithms have been developed which include cross-correlation [64] or optical flow analysis [69–71]. Since the ultrasound image only provides a single slice into the muscle structure, features can appear and disappear out of this plane, making simple feature tracking algorithms unsuitable.

Loram et al. proposed a technique based on cross correlation for tracking features in US images of the gastrocnemius muscle [64]. The algorithm allows the tracking of the changes in relative movement of markers placed at the proximal and distal aponeuroses. Those changes are not the same as changes in fascicle length because they do not consider the pennation angle but they can still be associated to changes in contractile length [64]. The technique has the limitation that only regions of interest which are visible throughout the whole sequence can be tracked.

Techniques based on optical flow can overcome the problem because the global movement of visible muscle can be determine from one frame to the next one. In addition the optical flow can cope with the physiological characteristic that the fascicles both shorten and rotate during contraction [72].

Magnusson et al. used the Lukas-Kanade optical flow algorithm to track strain distribution along the free tendon and the aponeurosis. The study identified a 5 times higher strain in the tendon compared to the aponeurosis suggesting a different functional role in the force transmission [69]. In a subsequent study they used the same algorithm to evaluate the displacement of the superficial and deeper aponeuroses of the gastrocnemius medialis (GM) and soleus (SOL) during voluntary and electrically induced isometric ramp plantarflexion. They observed the displacement in the proximal direction (i.e. toward the knee) and higher displacement for the deeper aponeuroses of both the gastrocnemius medialis (GM) and the soleus (SOL) [73].

Changes in fascicle length and pennation angle were also successfully tracked with automatic tracking algorithms based on optical flow [70–72].

2.2.5 Measuring Muscle Contractility

When a neural stimulus reaches the muscle-fiber, the contractile portion responds to the stimulation by shortening [64]. On the other side, when the stretch is caused by external factors, the contractile portion lengthens [64].

If we regard the muscle- tendon unit as a series of contractile element (muscle) and a series of elastic element (tendon, series aponeurosis) the changes in length of segments of muscle tissue correspond to the contractile portion of the muscle [64]. This means that changes in fascicle length are related to changes in length of the contractile portion.

Contractile properties of the muscle have been studied with a sonomicrometry technique [74, 75]. The sonomicrometry utilises piezoelectric crystals that are able to measure the transmitted wave within a medium and estimate the distance. It is quite accurate however it is invasive and

requires the piezoelectric element to be implanted.

The USI techniques proposed and introduced in the previous section, are able to track changes in fascicle length but only referring to one fascicle. They do not allow the analysis of a portion of the muscle and limit the analysis to measurements at the extremity of the fascicle leaving the activation in middle portions unclear .

Traditionally physiologists and biomechanics have studied the mechanisms, the activity, and the function of muscles in relation to the neural stimulation using surface electromyogram (sEMG) signals. The change in contractile length is the mechanical consequence of the neural stimulus and it therefore provides complementary information to the sEMG. Different techniques have been developed to analyse the sEMG recording and excellent outcomes were obtained, however some technical limitations remain. In particular the sEMG cannot access deep muscles and it is affected by cross-talk coming from adjacent muscles [51].

In the previous sections the significance of the muscle architecture was highlighted. It is clear that muscle architecture is useful for understanding the force transmission within the muscle-tendon complex which has implication in sport injuries, surgical decisions and control of movement or to asses the status of the muscle in neuromuscular disorders. However, the architectural parameters describe the muscle function at a macroscopic scale and cannot be associated with regional contractility. Previous studies reported regional fiber distribution and selective activation of muscle regions for different motor tasks [76–78]. The sEMG is able to detect differences in electrical activation evaluating the changes in sEMG along the proximal-distal area [77], however the technique is not able to exploit a whole muscle portion from the surface to the deeper area.

Darby et al. proposed an algorithm for the tracking of persistent features covering the whole portion of the muscle visualised in the US video frames [79]. The main advantage of the technique is that it is able to evaluate regional changes in muscle activity which can give insights into the explanation of physiological properties.

2.2.6 Strain and Strain Rate measurements with US

Thanks to its contractile properties the muscle tissue responds with shortening or lengthening to the neural stimulation. Therefore, the contractile mechanism is accompanied by tissue deformation. The tissue deformation can be quantified through the parameter strain which expresses the percentage of shortening or lengthening compared do the rest state [80]. The relation between contraction and deformation makes the strain a measure of the contractility function. Another parameter closely related to the strain is the strain rate, which is obtained from the derivative

of the strain. Therefore, the strain rate reflects how fast the shortening or lengthening activity is [80]. However, studies made on the myocardium tissue show the evidence that the strain is load dependent while the strain rate is less load-dependent and is a better measure of the contractility [81].

The most common way the strain and strain rates are estimated is related to the fascicle deformation [15, 82]. The studies show that faster motor units are better suited for developing force rapidly resulting in fiber shortening at higher strain rates. Lower strain rates characterises tasks such as maintenance of posture which involve, usually, slow fibers. These results are easily justified if we consider that the mechanical properties of the muscle depends on its fiber type composition [15, 83].

Lindberg et al. analyse the strain distribution from M-mode ultrasound images of the biceps brachii. The study highlights a non linear correlation between strain distribution and force expressed as percentage of the Maximum Voluntary Contraction (MVC). In addition differences in strain were observed between the ascending and descending periods of a ramping task [84].

It is important to clarify that the strain and the strain rate described in this section refer to the deformation resulting from the neural stimulation. Another technique commonly used in literature is known as **elastrography** which aims to assess the mechanical properties of the tissues by applying stress externally to the muscle and detecting the tissue displacement using ultrasound [85]. This technique is useful to detect changes in the elastic properties which results from muscle anomalies caused by diseases or injury [86, 87].

2.3 Muscle training in neuromuscular diseases using FES

A wide range of conditions or pathologies, such as Multiple Sclerosis, Stroke, Duchenne Syndrome and Spinal Cord Injury, can lead to neuromuscular disorders. The disability associated with neuromuscular disorders depends on the specific type of disease. Neuromuscular diseases impact on daily activities such as communication, mobility, independence and result in comorbidities involving different parts of the body. Regarding the skeletal muscle, changes in morphological and contractile properties occur [88, 89]. In both able bodied and disabled people, exercise is essential to maintain and improve strength, improve function and resistance to fatigue, and enhance quality of life. It has been shown that aerobic training provides positive health benefits in terms of improved cardiopulmonary status, increased body mass reduced adiposity and improved sense of well-being [88, 89]. In neuromuscular diseases exercise is therefore used

to enhance musculoskeletal performance, decrease the risk of comorbidities and accelerate rehabilitation and return to activity [90]. The level and the kind of training depends on the type, stage and severity of the disease [88, 89].

Nevertheless, some conditions such as Spinal Cord Injury result in muscle paralysis with consequent failure in carrying out voluntary physical exercise [91]. In this case, an established way to induce muscle contraction in order to perform a task involves the application of low current pulses by means of electrodes placed on the muscle [92, 93]; this technique is called functional electrical stimulation (FES).

FES of skeletal muscle is successfully used in rehabilitation to enhance or to re-establish muscle function. The ability of the technique to improve muscle performance in both healthy and diseased muscles has been demonstrated in research and clinical practice [94].

FES of paralyzed muscle is a common technique used to perform strength-training and aerobic exercises in patients affected by SCI. Examples of training assisted by FES include cycling, rowing, standing and more. In quadriplegics and paraplegic, the training of the lower limbs can be more effective than upper limbs in generating the cardiovascular stress required for gaining in fitness [95]. It has been shown that FES-cycling produces benefits in the cardiorespiratory system (i.e. reduce blood pressure and heart rate, improve ventilation) and improves muscle strength and endurance [96, 97].

2.3.1 Voluntary versus FES contractions

Despite its potential applications, FES has not gained widespread clinical use due to the rapid fatigability of skeletal muscle during FES training [93]. Muscle fatigue results in a reduction or inability to generate force or power output with consequent inability to sustain the task [98]. The rapid onset of fatigue during FES training is a consequence of the fact that muscle contraction resulting from FES differs from voluntary muscle activation. Different studies were conducted to give insights into the differences between voluntary and electrically evoked contractions. These differences are usually associated with three phenomena [93]:

i Reverse order recruitment of motor unit (motor unit with large axon are recruited first)

ii Synchronous activation of motor units [99]

iii Muscle paralysis induces loss of fatigue-resistant fiber types and reduction of capillary density

The Henneman's 'size principle' of voluntary muscle activation describes a progressive recruitment of small, typically slow, followed by larger, fast, motor units in order of increasing size [14]. This strategy, associated with an asynchronous activation of motor units, allows the modulation of the force exerted and limits fatigue. On the other hand, during FES induced contraction, the motor units recruitment is synchronous and faster, larger motor units are activated first. Motor units with larger axons are less resistant to the current and conduct action potentials at faster rates, this causes the fast fatiguing fibers to be recruited first. In addition, the activation is spatially limited and non-variable, which means that the same motorneurons will be stimulated again and again [94]. Gregory et al. suggested that the fatigue during electrical stimulation is mainly determined by the inability to alter the recruitment pattern or to modulate the firing frequency, or both [94].

It is generally accepted that larger motor-units are activated first during electrical stimulation. However some studies indicate that this finding might not always hold truth. Kim et al. measured the energy consumption through blood sample and the intramuscular pressure, through implanted catheters, during both voluntary and electrical induced muscle contractions [100]. Their findings suggested that during electrically elicited contractions both type I and type II fibers were engaged in the exercise resulting in an increased metabolic response compared to the voluntary. Therefore they concluded that the reverse order recruitment is applicable for direct stimulation of the motor nerve but not for cutaneous stimulation because of the peripheral nerve orientation [94, 100].

Similarly, Feiereisen et al. compared the recruitment order of 302 motor-units during voluntary and electrically induced contractions [101]. During voluntary contraction, in 94% of the cases, the size principle was respected. On the other side during electrical stimulation at the motor point, reverse recruitment was observed in 30% of the cases. Evidence to reject the reverse recruitment order was found also by Knaflitz and colleagues who suggested that the location of motor units branches is the the primary factor to determine the fiber activations via transcutaneous electrical stimulation [102].

The studies discussed, even if they do not agree on the order of the recruitment of the motor-units, bring the spotlight to a common problem: the lack of control of the muscle activation during electrical stimulation. The insufficient knowledge on the physiological aspect related to the FES cuts drastically its potentiality due to the rapid onset of muscle fatigue observed during the FES-training.

2.3.2 Minimising muscle fatigue during FES

The effect of fatigue can be partially mitigated by choosing optimised stimulation parameters or electrode configurations. In the last few years, researchers have been investigating stimulation methods that could mimic the natural physiology of muscle activation [93,99,103]. Attention was given to modulation of stimulation parameters (frequency, pulse-width, amplitude) or electrodes placement and configuration (see Review [31]). Approaches based on multichannel electrodes and irregular stimulation patterns are the most common.

Classical methods involve the use of two electrodes to perform synchronous muscle activation [99,104], however studies involving multichannel electrodes appear to be more robust to the onset of fatigue. Multichannel electrodes allow an asynchronous activation of motor units, the main purpose is to activate different portions of a muscle sequentially so that successive portions of the muscle are activated before the preceding portions are completely relaxed. Binder-Macleod et al. have demonstrated that synchronous activation produces greater force than asynchronous [104] however, asynchronous activation results in better resistance to muscle fatigue of paralyzed muscle and in a longer capacity in sustain the exercise [99, 105].

Similarly, Popovic and Maleevic compared a multi-electrode (asynchronous activation of 4 pads at 16 Hz) with a two electrode stimulation (synchronous activation of 2 pads at 40 Hz) [105]. They showed that asynchronous low frequency activation of multi-pad electrodes results in better resistance to muscle fatigue of paralyzed muscle and muscle force is the summation of the forces produced by all stimulated muscle units. Decker et al. analysed the efficiency of cycling comparing the classic co-activation stimulation protocol that involves the use of 2 surface electrodes placed on the anterior thigh, with an alternation-protocol that involves the application of 6 electrodes and an interchange of stimulation among them [99]. Although in their study no significant difference between the two stimulation strategies was found, the total ride time and the virtual distance were on average longer in the alternation protocol (2.36 min longer and 0.4 miles further). Moreover, FES-cycling with the co-activation protocol required greater stimulation intensity to hold the same velocity than in the alternation pattern [99].

The classic way of delivering FES for therapy and training involves the use of a stimulus pulse between 15 to 400 us and frequencies between 15 to 50 Hz. Recently, a research group from Canada has been investigating the effect of using wide pulses and high frequency on the torque exerted [106–108]. In their study they demonstrated that stimulating pulses of $1ms$ and frequency of 80-100 Hz are able to activate motor units through both motor and sensory pathways. The latter results in a contribution of the Central Nervous System which recruit motor units in

an asynchronous way. The total effect of the wide pulse stimulation is a higher torque. Moreover, they suggest that the central mechanism involved in this way of applying FES might be helpful to delay the onset of fatigue.

2.3.3 Mapping voluntary and electrically induced muscle contractions

From what has been discussed so far it is clear that the optimisation of the execution of the FES is a key topic to enhance the potentiality and the efficiency of this technique. While many groups focus their attention on the placement and number of the electrodes, the setting of current amplitude and frequency of the stimulation or on the recruitment order of the motor units, few studies have addressed the problem of understanding the muscle activation pattern resulting from the application of the FES [109,110]. Knowledge of the way the muscle is activated during FES as a function of stimulation or electrode placement can help the optimisation process and can give further knowledge into the physiology of the muscle contraction.

For a long time it has been assumed that FES activates primarily the superficial areas of the muscle being closer to the electrodes where the electric field is generated [111]. Pioneering works from Adams, Hillegas and Dudley attempted the mapping of muscle activation by extracting information from Magnetic Resonance (MRI) images obtained just after voluntary and electrically induced contractions [109, 110].

In order to better understand the work it is worthwhile to emphasise the physiological basis of the muscle function in MRI images. It should be clear that MRI does not measure neither the electrical activity nor the mechanical function of the muscle; but it rather depicts the muscle cell metabolism and fluid uptake that results in changes in contrast in MRI images [112]. In fact when the cellular energy metabolism rate increases, the water content and the blood oxygenation increase and the pH of the cell decreases. Those factors produce changes in contrast properties that are visualised on the MRI images [113].

Adams et al. investigated the muscle activation analysing images of the muscle obtained from magnetic resonance (MRI) scans [109, 110]. The study showed that the pattern of stimulation is not exclusively superficial but rather dispersed and variable among subjects, suggesting that the stimulation of a given region of the muscle cannot be taken for granted [109, 110]. When comparing the contrast of the images obtained with electrical stimulation with the voluntary contractions, differences are observed suggesting that the voluntary task is performed at lower metabolic rate [109].

Hillegass and Dudley investigated the muscle activation region of the quadriceps in both healthy

and spinal cord injured subjects demonstrating in both cases the spatial dependency of activation on electrodes placement and current intensity. The main focus of the study was to explain the limited torque exerted by SCI even if the MRI images had similar pattern as the one found in able bodied. The outcome of the study identified atrophy and fatigue as being mainly responsible for the reduction in force [110].

Kinugasa et al. [68] analysed MRI images of the GM muscle during voluntary contraction. They demonstrated that areas in the muscle are differently activated and non- uniformly distributed concluding that compartmentalisation of muscle activation during physical tasks occurs. Evidence of selective activation of muscle fibers was observed in the sEMG, as discussed in section 2.4.

These studies showed that MRI imaging is a useful tool to extract information on muscle activation. However the technique has the main limitations that it is expensive and the images cannot be acquired in real time during the execution of the task, in fact typically acquired several minutes after the task.

2.3.4 Nerve vs cutaneous stimulation

Neuromuscular Electrical Stimulation (NMES) is usually applied through electrodes placed on the skin located over the peripheral nerve trunk or the muscle belly. For instance, the stimulation over the nerve is used to restore the dorsiflexion of the foot during walking, while the stimulation over the muscle belly is used to facilitate functions such as walking, rowing, cycling. Both locations generate contraction by depolarising axons beneath the electrodes resulting in an action potential that propagates up to the fibers producing contraction. The difference is the contribution made by the *peripheral* and *central pathways* to the motor units recruitment.

The depolarisation of motor axons produces action potentials traveling through the peripheral pathway with no involvement of the Central Nervous System [107]. The motor units recruited through the peripheral pathway discharge synchronously and their activity is expressed in the M-wave of the electromyographic (EMG) signal which generates at each stimulation pulse [107,108]. On the other hand, when sensory axons are activated, the motor units are recruited through the central pathway in two different ways. One from the reflex pathway which produces an H wave on the EMG signal whose pacing is controlled by the stimulation pulses. The other results in asynchronous motor unit discharge probably caused by persistent inward currents in spinal neurons [107]. Both forms of central recruitment are likely to follow the Henneman's size principle typical of the voluntary muscle activation. It has been shown that when both the

central and peripheral mechanism recruit motor units, higher torque is exerted when compared to the only peripheral pathway [107].

Bergquist et al. compared the contribution made by the central and peripheral pathways to the motor unit recruitment when applying NMES over the tibial nerve and over the triceps surae muscle [114]. The study showed that when a stimulation at frequency 20 Hz was delivered over the nerve trunk the contribution of the central pathway was visible through the H-reflexes. While when applying the stimulation at 20 Hz over the muscle belly, the M-wave was visualised indicating a peripheral activation. The difference between the nerve trunk and muscle belly stimulation was diminishing at higher frequencies (50-100 Hz) [107,114]. The cause of the differences observed was identified in the axons distribution. Sensory and motor axons are bundled together in proximity of the nerve trunk and the recruitment is a combination of axon diameter and distance from the stimulating electrode. A different effect is obtained when stimulating over the muscle belly. Within the muscle belly, the axon branches are diffuse throughout the muscle. In addition the use of large electrodes activate axons over a wide spatial distribution resulting in a less synchronous sensory volley reaching the motor neuron [114]. The study clearly recruited fibers through a central pathway during nerve trunk stimulation and through peripheral pathway during muscle belly stimulation. The central pathway has the advantage of following the Henneman's size principle and the asynchronous motor unit recruitment, and therefore may lead to contractions that are more fatigue-resistant and may help to optimise the therapies based on NMES for rehabilitation.

2.4 Motor unit recruitment and fiber activation

Muscle force is generated by the Central Nervous System (CNS) by varying the activity and number of motor units within the muscle [115]. The modulation of the force is achieved by changing the firing rate and the number of active motor units [13]. Henneman demonstrated that the recruitment of the motor units is ordered according to the *size principle*. The *size principle* states that smaller, slower and more fatigue resistant motor units are recruited first followed by the faster motor units [14]. The effect of the size principle has been investigated *in vivo* using electromyography (EMG), however the most recent studies show evidence that the size principle do not always hold true [15, 82]. A study from Burke suggests that faster motor units are recruited when it is necessary to develop force rapidly [116].

Muscle fibers belonging to a single motor unit have similar biochemical and contractile properties resulting in specific physiological and mechanical properties. This suggests that muscle fibers

are specialised to perform distinct functional tasks [117]. Studies based on multichannel EMG revealed spatial inhomogeneous activation of muscle fibers at different force levels [118, 119]. This means that different parts of the muscle are dominantly active as a function of the force level and can vary over time with sustained contraction [119]. The inhomogeneities observed in muscle activation are related to the fact that fiber types are organised according to their histochemical composition.

Spatial muscle activation inhomogeneities were also observed in images obtained from magnetic resonance. In addition a significant correlation between the MRI images and the multi-channel EMG was obtained. The advantage of the imaging technique is based on the ability to visualise deep lying musculature [68].

2.5 Force transmission

During muscle contraction, mechanical tension is generated so that the tendon connections produce movement of the locomotor system or maintain a static position (in isometric recruitment) [120]. It is well known that the force exerted by a muscle is generated in the sarcomeres of the fibres and is transmitted to the bone via the tendons [121, 122]. Recent studies showed that the force generated through the contraction converges in the intramuscular connective tissue making it clear that the anatomical structure of the muscle and the fibers arrangement plays a fundamental role in the tension produced and transmitted to the tendons [120, 123, 124].

In the classic view of skeletal muscle, the force exerted by a muscle is generated in the sarcomeres and transmitted to tendons via the specialised myotendinous junctions. The myotendinous junctions are defined as the site where muscle fibers connect to the tendons or aponeurosis. The junctions are arranged in series with fibers that serve as sites of force transmission. The force transmission along the fiber axis to the tendon at the myotendinous junctions is called myodendinous or longitudinal force transmission [52]. Recent studies suggest that the direction of the force is not only along the longitudinal line, thus from the aponeurosis of origin to the aponeurosis of insertion, but also via adjacent structures (myofascial and epimuscular force transmission) [125–127]. The epimuscular myofascial force transmission pathways are either intermuscular, between neighbouring muscles via the connective tissue at their interface, or extramuscular, between the muscle and adjacent non muscular structures. The proof of the epimuscular myofascial force transmission is identified in the difference in force exerted at the origin (proximal) and at the insertion (distal) of the muscle [124]. It is accepted today that the force transmission is due to both the myodendinous and myofascial force transmission.

When the fiber contracts the length of individual sarcomeres change. The amount of changes is variable across sarcomeres and their properties depend on their proximity to the motor endplate. Both spatial and temporal distribution of the sarcomeres' strain is not uniform [122]. Fiber shortening is accompanied by fiber rotation with increase in pennation angle. The fiber rotation is induced by a moment force acting on the fiber. It is not clear whether this moment is active, contributing to the force acting on the tendon, or passive, a consequence of tendon shortening [128].

In pennate muscles, fibers are oriented at an angle which during shortening undergo rotation making the force be transmitted to the tendon along the muscle's line of action. Therefore, the force transmitted depends on the force produced within the fascicle and on the pennation angle according to the formula expressed in Equation 1.1 on page 9. Subsequently the muscle's shortening velocity along its line of action can be greater than the fibers' shortening velocity. The ratio between the shortening velocity of the whole muscle and of the fiber is known as Architectural Gear Ration (AGR) [44]. Azizi et al. showed that the magnitude of the AGR depends on the muscle shape. In its turn, the muscle shape is related to the force output. Assuming that the volume of the muscle remains constant during contraction, changes in shape are identified in two main ways: *thickness* as distance between the two aponeuroses and *width* measured orthogonally to the plane of the measurement of the thickness. As a result, the AGR varies with the load shifting from high gear during rapid contractions to low gear during forceful contractions. Therefore the variable AGR in pennate muscles modulate the performance according to the function [44].

2.6 Conclusions

Ultrasonography has been shown to be useful in the investigation of musculoskeletal architecture and pathologies. The advances in quality of the image, together with its relatively low cost, made it a potential tool for assisting diagnosis and for monitoring soft tissues changes. Recently, different techniques have been developed for an automatic analysis of ultrasound images enlarging its potential applications. Ultrasound imaging has also been used during electrical muscle stimulation to track the displacement of the aponeuroses but it was not used for tracking the activation of a whole muscle.

FES is used to train muscles in neuromuscular diseases. Uncertainty regarding the way the FES activates the muscle and the early onset of fatigue during the FES limit its applications . A majority of studies focus their attention on the stimulation parameter and electrodes positions.

Some studies investigated the muscle activation pattern resulting from the FES from a physiological point of view using MRI images. MRI images show the metabolic consumption of the fiber cells and was used to investigate the areas of the muscle more active during FES. They showed a compartmentalisation of muscle activation and debunked the myth that muscle areas close to the electrodes are more active because they are immersed in higher electric field. However MRI does not offer the possibility to perform the analysis of the muscle metabolism during the actual application of the FES.

Ultrasound is a potential tool to track muscle mechanical activation during a task. However the literature does not present studies that map the muscle activation during the application of the FES which is the main focus of the research in this PhD.

Chapter 3

Experimental Methods

3.1 Summary

This chapter introduces the methods used throughout this work. The algorithm used for the identification of features in the ultrasound images will be explained. Following this, the main methods used to analyse the information extracted from the ultrasound analysis will be presented. General information on the experimental setup will then be given.

3.2 Methods for Ultrasound analysis

During the PhD two software algorithms for the tracking of information in an US video of the muscle were used. Although they have some differences in the implementation, the common algorithm is based on two main methods: the Active Shape Model (ASM) for the image segmentation, and the Kanade-Lucas-Tomasi (KLT) feature tracker for tracking movements. Once persistent features are identified by the KLT within the relevant image segment selected by the ASM, their movement can be tracked over time and can be related to the muscle movement.

The software algorithms were developed within the Institute for Biomedical Research into Human Movement and Health (IRM) of Manchester Metropolitan University under the direction of Professor Ian Loram. The two algorithms were part of a post-doctoral position and a Ph.D work [129, 130].

3.2.1 Algorithm description

The first part of the algorithm performs a segmentation of the image into three regions: upper aponeurosis, muscle, lower aponeurosis. For the segmentation an Active Shape Model (ASM) is used. The ASM is a widely used algorithm for shape detection, it is a statistical model of the shape of the object that iteratively deforms to fit to a new image of the object [131]. The shapes are constrained by a Point Distribution Model (PDM) that is created by manually placing some markers on the main shape of the image.

To capture shape variations undergone during a muscle movement, the technique of Point Distribution Models (PDM) was used. The PDM can be created for each video by manually labeling a certain number of frames. A general model representing a particular muscle can be created by labeling frames from different subjects. The more subjects included, the more variance the model has in order to recognise a new subject automatically without prior labeling. With the second approach the attempt is to define a general model that represents a particular muscle.

The labelling consists of marking up the contours of the three regions mentioned above in order to define their shape.

To allow a probabilistic search of known shapes in new images an Active Shape Model (ASM) is applied. The fitting task of the ASM aims to adjust the set of landmarks in the PDM to describe the shape in every image. Using a principal component analysis it is possible to define a model of the shape variation from the dataset. This allows an estimation of any data point spanned by the training set. The fitting process is initialised with the mean shape. Each landmark is then permitted to move along a fixed, straight line extending 3 pixels to each side and running perpendicular to its neighbours. Landmarks are moved pixel by pixel along this line and new intensity samples are drawn to determine their most likely location. The likelihood is evaluated according to the Mahalanobis distance. When the Mahalonobis distance is minimised for each landmark, the new shape is projected in the PDM and the nearest plausible shape is found. The comparison process is repeated 10 times at each image scale, moving from the lowest-resolution to the original high-resolution images.

The second part of the algorithm focuses on the tracking of features. Features in the image are identified according to Shi and Tomasis algorithm that allows the identification of corners and edges in the images by minimising the eigenvalues of the matrix of intensity [132]. Features identified are later tracked by the Lucas-Kanade- Tomasi feature tracking algorithm (KLT). The KLT aligns a feature template with the new image by minimising some measures of the difference between two regions. When updating the KLT features, a set of displacement fields are estimated by finite differencing the locations of all the templates that have persisted from the previous frame [129].

The features in the US images can appear or disappear according to the reflected wave. To make the tracking robust to these changes, some test points, called **probes**, are placed along the image. The probes are placed in an automatic way according to the information contained in the ASM segmentation; 4 points are calculated from the shape information and the others are placed by performing a linear interpolation between the extreme points.

A total of 80 probes (10x8) are placed on the first frame. In every frame a triangular interpolation (Voronoi or Delaunay) is applied on the KLT features and the probe position is updated by averaging the vertices of the polygon defined in the triangulation.

The main steps characterising the algorithm are shown in Figure 3.1.

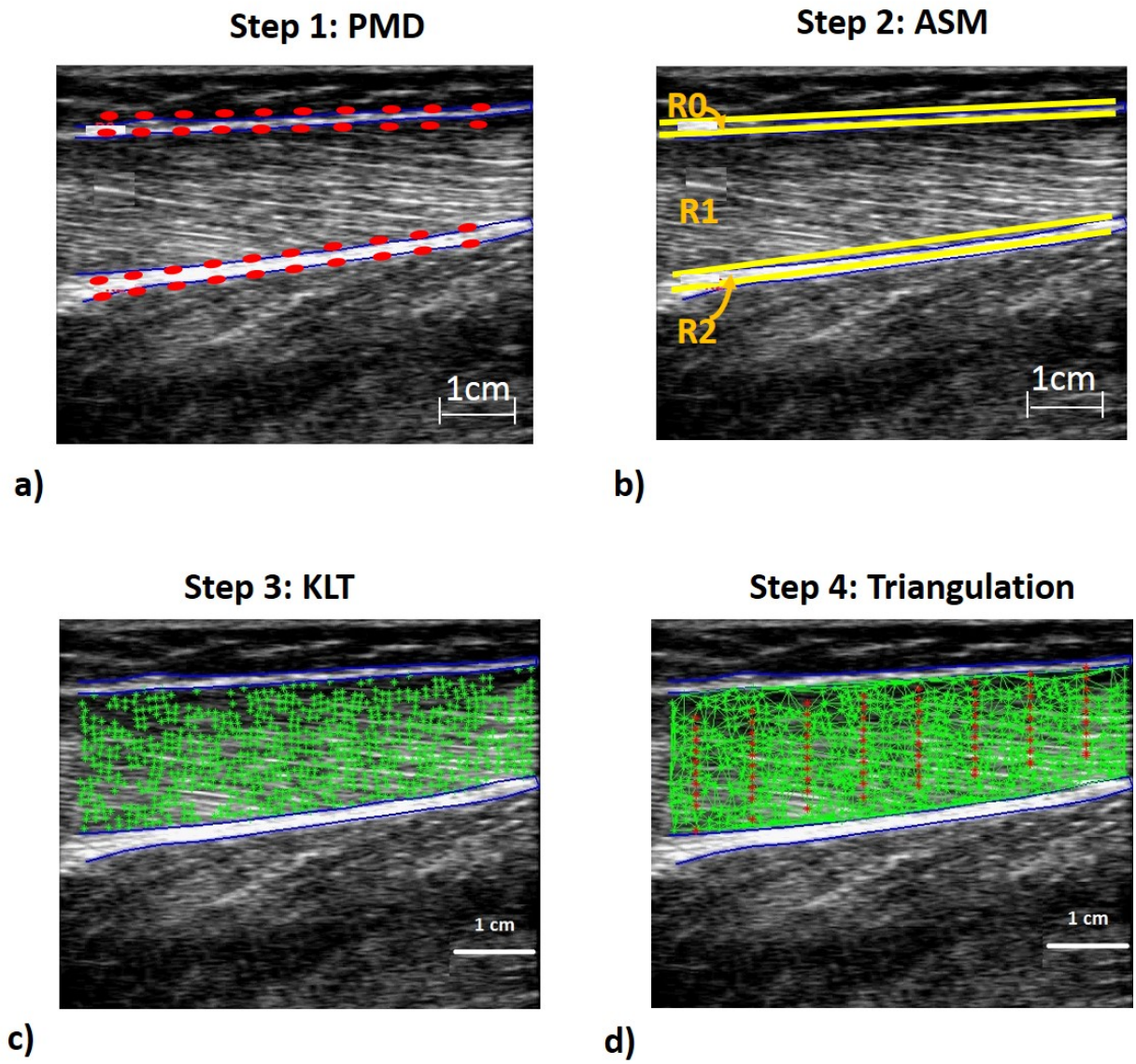

Figure 3.1: The figure summarises the algorithm. Figure a) shows the PMD. The red dots indicate the marks that are manually placed over the image. In figure b) following the ASM the three regions are identified: the upper aponeurosis (indicated as R0), the muscle (R1) and the lower aponeurosis(R2). Figure c) represent the KLT. In figure d) the triangulation of probes is shown (the red dots represent the probes, the green grid is the Delaunay triangulation.)

An example of the US image of the Gastrocnemius Medialis is shown in Figure 3.2 where it is possible to identify the distribution of the probes (the green dots). In the figure the way the probes move during plantarflexion is also indicated. In particular, a probe movement in proximal direction (toward the knee) is indicated as positive x, and a movement towards the deeper areas, positive y. Throughout the thesis this convention will be used to express the probe movements.

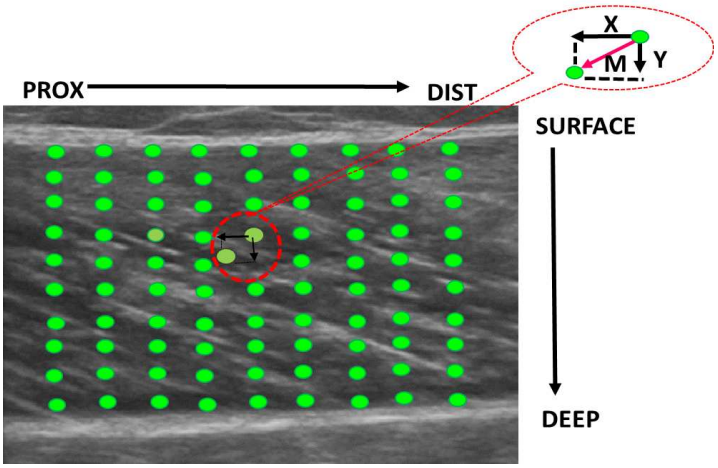

Figure 3.2: Description of a probe movement. During the isometric plantar flexion the muscle contracts and the probe moves in the X direction towards the knee and in the Y direction towards the deeper aponeurosis. In the image, a zooming movement of one probe is shown; the coordinates of the updated position of the probe are indicated by X and Y components and their Magnitude M

As mentioned above two different software implementations were available for the tracking, which will be referred to as SW1 and SW2. Both software algorithms are implemented in Matlab and integrate the ASM and the KLT steps outlined above. Differences are summarised below:

SW1 : This software has a database of data on the GM muscle from different subjects that makes it completely automatic. An initialisation is necessary only if the shape of a new muscle is not found in the database. Interpolation among the KLT points allows the tracking of the probes [133].

SW2 : A pre-model for the ASM is integrated but some parameters such as distance between the two aponeuoroses or the zone of interest must be inserted. The software does not use any interpolation algorithm, the probes are placed by averaging a region of KLT points [130].

3.2.2 Arrangement of probes

The way the probes are placed over the image is shown in Figure 3.2. To analyse the information a particular order of the probes was considered. The probes were labeled according to rows and columns as shown in Figure 3.3.

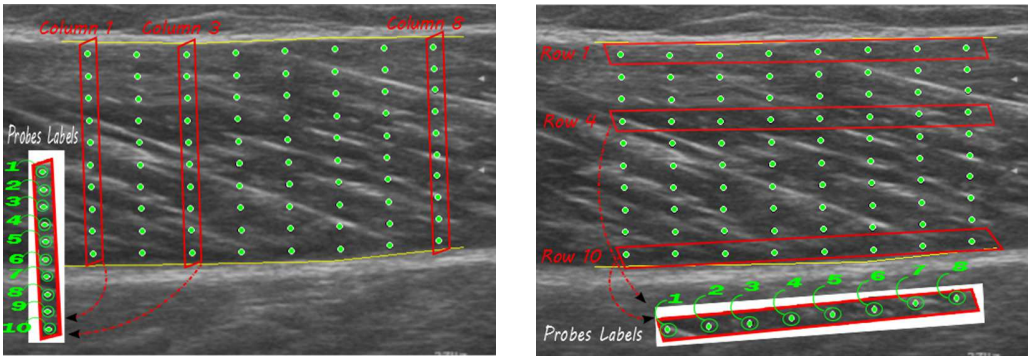

A B

Figure 3.3: Figure A shows the probes grouping in 8 columns, in each column the probes are identified with the numbers from 1 to 10. In Figure B the probes are grouped in 10 rows. In each row, the probes are identified with numbers from 1 to 8.

The way the results are presented is based on the analysis of groups of probes. The probes are organised according to rows or columns, as shown in Figure 3.3. Ten rows are identified, each row is composed of a total of 8 probes. Similarly, 8 coloumns are idetified and each coloumn is composed of 10 probes. The movement of the probe is described by its x- and y-components, and by the total movement magnitude. The magnitude of the movement of a probe is calculated by summing vectorially the x and y components. For better understanding of how the variables move in the US video, refer to Figure 3.2. In Figure 3.2 the direction of the probe's movement during a task is shown. In particular during an isometric plantarflexion the probes move towards the proximal part of the muscle (i.e towards the knee), in this case the x-direction is considered positive. During the relaxation phase the probes move back towards the original position.

A description of the variables used for studying the probes movement is presented in Chapter 4.3.

3.3 Strain Measurements

In this section the estimation of the strain distribution starting from the *probes* movement is presented. First, general definitions are given and later the application on USI is shown.

3.3.1 Definition of Strain and Strain Rate

When a force is applied to a material it develops stress that causes a deformation of the material itself. The way the object deforms depends on how the force is applied and it can either elongate or compress. The equation for the strain is defined as follows:

$$\varepsilon = \frac{L - L_0}{L_0} = \frac{\Delta L}{L_0} \tag{3.1}$$

Where L_0 is the initial length and L is the final length [134]. Thus, strain is a dimensionless quantity and represents the fractional or percentage change in dimension [80]. In macroscopic terms, the *strain* is a measure of deformation representing the displacement between particles in the object relative to a reference length. The velocity of the deformation is called the *strain rate* and is expressed as:

$$\dot{\varepsilon} = \frac{\partial \varepsilon}{\partial t} \tag{3.2}$$

The concept of strain in physiology was introduced in 1973 to facilitate the understanding of elastic stiffness in the heart [135]. In this case strain represents the regional deformation of the tissue from an applied force. Negative strain indicates compression or shortening; positive strain implies lengthening or expansion [136]. In muscle tissues, the deformation is caused by the fiber contraction, which is a result of the contraction of the sarcomeres. Thus in physiology strain and strain rate are indicative of the contractile properties of the tissue [80].

3.3.2 Strain and Strain Rate measurements in USI

USI allows the visualisation of an entire portion of the muscle. The tracking technique introduced in 3.2 can identify the location of the probes at each frame during a muscle contraction. Local measurement of strain and strain rate can therefore be performed in order to map the contractile activity of the muscle. In order to measure the local strain the procedure presented below was used.

The local strain can be calculated as the differential motion between two points corrected to their initial separation [136]. The strain rate is the first derivative of the strain, thus it represents the differential velocity between two adjoining points. In this analysis we refer to the arrangement of the probes according to Figure 3.3, where a total of 80 (10×8) probes are tracked over the video. Thus, the local strain is calculated by differentiating the instantaneous location between two probes and normalising it to their initial distance.

The strain can be estimated in horizontal or vertical directions. Horizontal strain is obtained if the change in length is calculated between two consecutive probes in the same row, this can be visualised in Figure 3.4 a). Conversely vertical strain is estimated from change in length between two consecutive probes in the same coloumn, see Figure 3.4 b).

If the local strain at each probe is given, the information would be very detailed but difficult

to interpret and to summarise the outcome. For this reason average local strain measurements were considered. The average strain was calculated by averaging according to rows of the matrix of probes, see Figure 3.4 a.1) and b.1), or according to coloumns, see Figure 3.4 a.2) and b.2).

When strain is averaged according to different rows, the strain at different depths is obtained. In contrast, averaging according to coloumns, the strain in the proximal-distal direction is obtained.

The mathematical notation is given below. We remind that the probes are arranged in a matrix $N \times M$, where $N = 10$ and $M = 8$. Referring to Figure 3.4 a), the local strain for the vertical direction is defined as:

$$\text{vertical local strain at } n, m: \quad \varepsilon_{nm} = \frac{d_{nm} - d_{nm_0}}{d_{nm_0}} = \frac{\Delta d}{d_{nm_0}} \tag{3.3}$$

Where n indicates the row and m the column of the matrix arrangement of the probes. The strain at different depth and at different proximal-distal locations are respectively defined as:

$$\begin{aligned} \text{where the average strain at depth n is:} \quad & \bar{\varepsilon}_n = \sum_{m=1}^{M} \frac{\varepsilon_{nm}}{M} \\ \text{and the average strain at coloumn m is:} \quad & \bar{\varepsilon}_m = \sum_{n=1}^{N} \frac{\varepsilon_{nm}}{N} \end{aligned} \tag{3.4}$$

Similarly, the strain in horizontal direction, see Figure 3.4 b) can be calculated as:

$$\text{horizontal local strain at } n, m: \quad \varepsilon_{nm} = \frac{l_{nm} - l_{nm_0}}{l_{nm_0}} = \frac{\Delta l}{l_{nm_0}} \tag{3.5}$$

Also in this case, the average strain for different depths and proximal-distal locations are defined as in Equation (3.4).

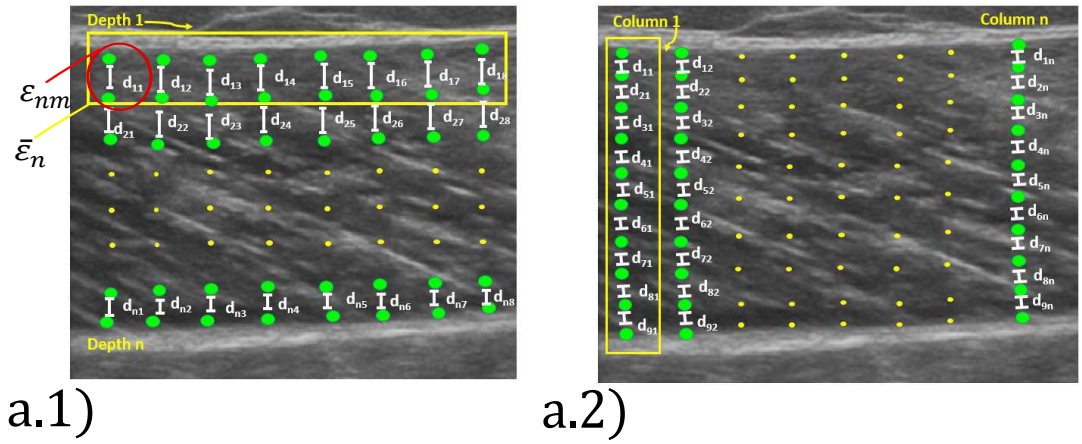

(a) Local Vertical Strain

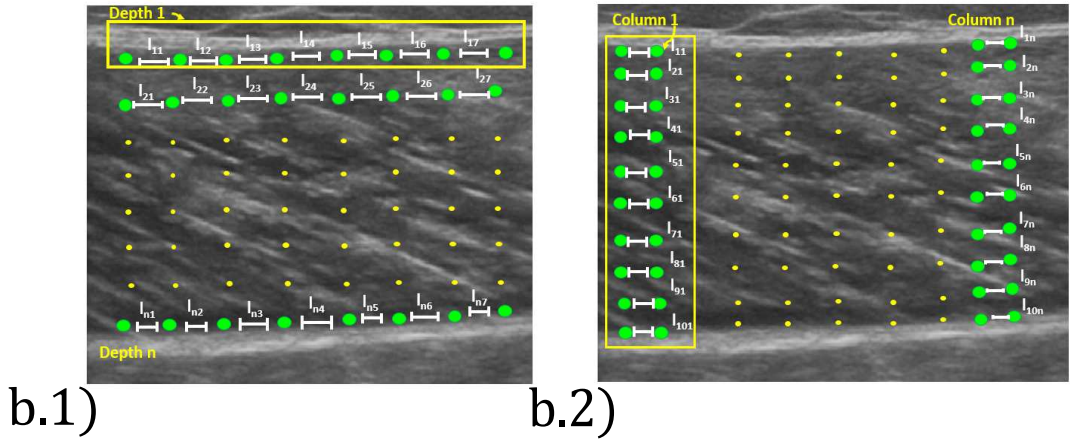

(b) Local Horizontal Strain

Figure 3.4: The figure shows how the local strain was calculated in vertical, 3.3.2, and horizontal, 3.3.2, directions. For the vertical strain, the average strain was calculated per each coloumn. Conversely, for the horizontal strain, it was average according to rows

The strain rate was calculated as the first derivative of the local strain ε as follows:

$$\dot{\varepsilon}_{nm} = \frac{\partial \varepsilon_{nm}}{\partial t} \tag{3.6}$$

The average strain rate was defined as:

$$\begin{aligned} \text{at depth } n \text{ is:} \quad & \dot{\varepsilon}_{avg_n} = \sum_{m=1}^{M} \frac{\dot{\varepsilon}_{nm}}{M} \\ \text{at coloumn } m \text{ is:} \quad & \dot{\varepsilon}_{avg_m} = \sum_{n=1}^{N} \frac{\dot{\varepsilon}_{nm}}{N} \end{aligned} \tag{3.7}$$

3.4 FES application

Functional Electrical Stimulation (FES) was applied in order to induce muscle contraction. The FES involves setting of parameters such as:

- Electrodes placement
- Current Amplitude
- Pulsewidth
- Frequency of the stimulation

Bi-phasice current controlled stimulation pulse trains were generated by a neuromuscular stimulator (Rehastim v1, Hasomed GmbH, Germany). The parameters were adjusted from a PC in real time via a USB interface using the ScienceStim protocol . Throughout the thesis two electrode configurations were used:

i) on the muscle belly, Surface Stimulation (SS)

ii) on the nerve, Nerve Stimulation (NS)

See Figures 3.5 and 3.6 respectively for SS and NS.

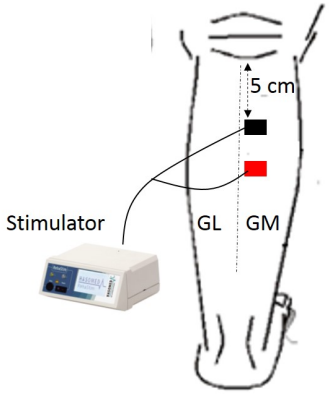

Figure 3.5: Surface Stimulation. Both the electrodes are placed on the muscle belly of the Gastrocnemius Medialis (GM) muscle.

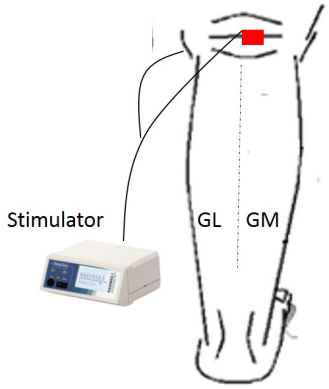

Figure 3.6: Nerve Stimulation. One electrode is placed on the tibial nerve, behind the knee and the reference electrode on the thigh just above the knee

Different ways of setting the amplitude and the pulsewidth of the current were used throughout the PhD project, details will be given within each chapter. The stimulation was always applied

with ramping configuration in order to limit discomfort to the participants, cf. Section 1.5.1.2. Frequency at 50 Hz was used for the experiment described in Chapter 4 and a frequency of 33 Hz for Chapters 5 and 6.

3.5 Linear Mixed Effects Model

In this thesis, the Linear Mixed Effects Models (LME) are used to find dependency on specific variables, such as SW version, ultrasound device and FES vs voluntary. A statistical analysis was performed by the *linear mixed-effects models*.

Linear Models are commonly used to describe and analyse data in biological science. A mixed model is a statistical model useful in case of repeated measurements. Linear mixed-effects models describe the relationship between a response variable and independent variables, with coefficients that can vary with respect to one or more grouping of variables [137].

A mixed-effects model consists of two parts: *fixed effects* and *random effects*. The fixed-effects terms are the conventional terms used in the linear regression, they represent the observed quantities in terms of explanatory variables. In conventional statistical models, the fixed effects are non-random quantities. In the linear mixed-effects models, the fixed-effects are treated as if they arise from random causes. The random effects are associated with individual experiment units drawn at random from a population. Mixed models are widely applied in biological and social sciences because the variability of the measurements related to subjects can be taken into account as a random effect [138].

The standard form for a linear-mixed-effects is expressed as follows:

$$y = X\beta + Z\gamma + \epsilon \tag{3.8}$$

where:

y is the response vector

X is the fixed-effects design matrix of known constants.

β is the fixed-effects vector.

Z is the random-effects design matrix of known constants.

γ is the random-effects vector, with mean $E(\gamma) = 0$ and covariance matrix $Cov(\gamma) = G$

ϵ is the observation error vector, with mean $E(\epsilon) = 0$ and covariance matrix $Cov(\epsilon) = R$

Because the model includes both fixed and random effects (in addition to the random errors), it is called a mixed-effects model. A key assumption in this analysis is that γ and ϵ are normally distributed. The equation for the mixed models can then be solved as:

$$\begin{pmatrix} X'R^{-1}X & X'R^{-1}Z \\ Z'R^{-1}X & Z'R^{-1}Z + G \end{pmatrix} \begin{pmatrix} \hat{\beta} \\ \hat{\gamma} \end{pmatrix} = \begin{pmatrix} X'R^{-1}\mathbf{y} \\ Z'R^{-1}\mathbf{y} \end{pmatrix}$$

The solutions to the model, $\hat{\beta}$ and $\hat{\gamma}$ are the best linear unbiased estimates predictors for β and γ .

3.5.1 Understanding the LME: a study on simulated data

The LME is a powerful tool to evaluate the effect of one or more variables on the overall model or to evaluate the difference between groups within a model. To extract the correct information it is important to define the right model. For this purpose some tests based on synthetic data were performed.

3.5.1.1 Generating simulated data

For the purpose of reproducing the experimental setup, simulated data was built based on the US information measured for the trials. The experimental data was collected from tests where the subjects were asked to perform isometric contraction at different strength (different trials) during both voluntary and electrically induced muscle contraction. During the test, the ultrasound video and the torque exerted were recorded. Each subject repeated the test in three sessions where different US machines were used to record the video of the muscle contraction. Each video was then analysed offline with the different algorithms.

Thus, the simulated data took into consideration the fact that different trials are performed at different strengths, and that different algorithms are used to extract the information from the US videos.

To simulate the behaviour of the US information for one probe and one algorithm, a signal *sim_probes* was generated as follows :

- A Gaussian function between -2 and 2 with mean 0 and variance 1 is generated; this simulates 1 trial of the task.
- Random noise is added to the data that simulates each trial.

- A vector of numbers between 1 and 10 was randomly generated to simulate differences in amplitude among different trials.
- 10 trials at different baselines are generated by multiplying the single test for the different amplitudes.

The process is also shown in Figure 3.7.

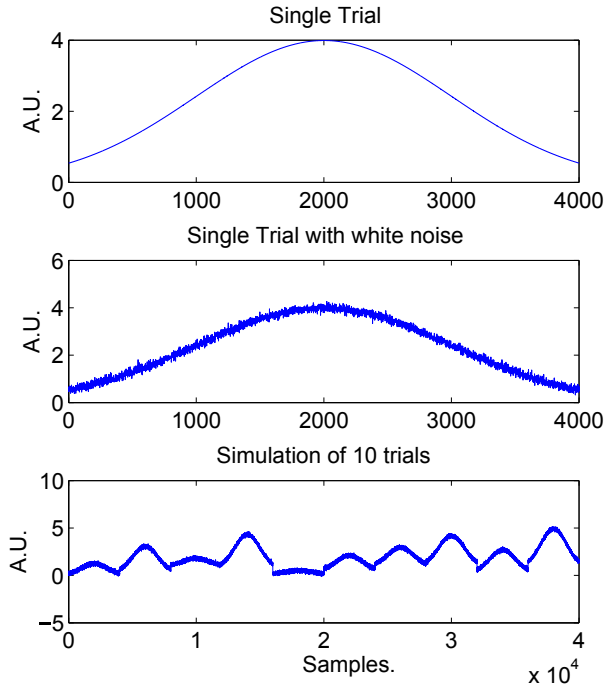

Figure 3.7: Simulation of Probes behaviour with one software. Single trial (top), single trial with noise (middle); whole test with 10 trials at different baselines.

3.5.1.2 Evaluation of signal with different amplitudes

Here we evaluate how different two signals, *sim_probes1* and *sim_probes2*, are which are obtained respectively from two different software algorithms and correspond to 10 trials for one subject.

Three different conditions are analysed where $sim\_probes1 = sim\_probes$ and $sim\_probes2$ varies according to the following cases:

(i) $sim\_probes2 = sim\_probes1$, i.e. both cases are identical

(ii) $sim\_probes2 = 0.1 * rand(1) * sim\_probes1 + sim\_probes1$, i.e. the second case is slightly different from the first

(iii) $sim\_probes2 = rand(1) * sim\_probes1 + sim\_probes1$, i.e. the second case is very different from the first.

Where *rand(1)* is a uniformly distributed random number between 0 and 1, it was used to randomly generate a number for the current trial of the test. Different trials were performed, in this section the case of $rand(1) = 0.48$ is reported. *rand(1)* multiplies the amplitude of *sim_probes2* changing, therefore, its amplitude and mean. The three conditions are represented in Figure 3.8.

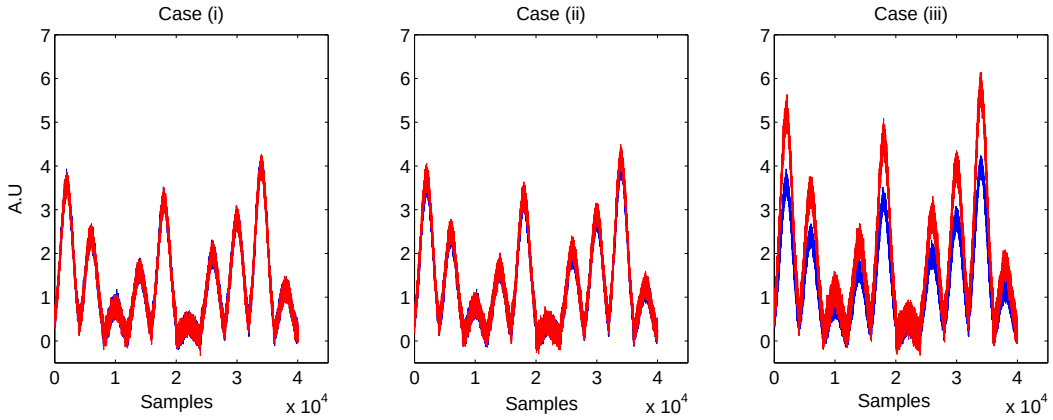

Figure 3.8: Simulation of Probes behaviour for *sim_probes1* (in blue) and *sim_probes2* (in red). In the figure $rand(1) = 0.48$. Each subplot represents a different condition where *sim_probes1* does not change and *sim_probes2* changes according to the cases stated above.

To classify the two signals using the LME, the formula representing the relationship must be indicated.

The aim of the analysis is to evaluate two groups *sim_probes1* and *sim_probes2*. The formula in Equation 3.9 evaluates the relationship between *sim_probes1* and *sim_probes2*.

$$Probes \sim Group \tag{3.9}$$

However in our experiment, every time a new trial is performed, the muscle could assume a different position which would result in a different location of the probes tracked. Therefore, in the model it is necessary to take into account this variability. This can be done by considering a random effect. The formula is expressed in Equation 3.10:

$$\text{Model1: } Probes \sim Group + (1|trials) \tag{3.10}$$

Where:

Probes: is the dataset that simulates the probes beahviour, it is composed of *sim_probes1* and *sim_probes2*

Group: the dataset is composed of two groups to simulate the behaviour of SW1 and SW2

trials: 10 trials per group are considered

The formula in Equation 3.10 expresses the relationship between the probes belonging to two groups (this represents the *fixed effect*) and takes into account that these probes come from repeated measures from different trials (*random effect*). The term $(1|trials)$ assumes that there will be multiple responses for different trials.

Different baseline-levels are considered in the random effect term *trials*, however different responses can be caused by the fact that the probes are obtained from different softwares. Then the formula should be modified as follows:

$$\text{Model2: } Probes \sim Group + (1 + Group|trials) \tag{3.11}$$

A good interpretation of the random effect is important otherwise the model can give a wrong interpretation. An example is shown in Table 3.1. Table 3.1 shows the outcome of *Model1* when equation 3.9 is used and of *Model2* when equation 3.11 is used, applied on case (i) where the two signals composing the groups are the same.

Table 3.1: Case(i)

	Name	Estimate	SE	tStat	Df	p
Model 1	**Intercept**	1.9302	0.22695	8.5047	80018	1.39E-09
	Group_2	-0.10086	0.00509	1.08E-12	80018	1.80E-80
Model 2	**Intercept**	1.9302	0.22695	8.5047	80018	1.39E-09
	Group_2	-0.10086	0.12914	-0.78097	80018	0.43482

To understand the table an explanation is necessary. The single parameters can be interpreted as follows:

Intercept: refers to the portion of the analysis of one of the two groups, in this case to *sim_probes1*. Accordingly *Group_2* refers to the analysis for the other group *sim_probes2*.

Estimate: corresponds, in the case of the intercept, to the mean value, in the case of *Group_2* to the difference between the mean value of *sim_probes1* and *sim_probes2*.

SE: is the standard error

tStat: is the t statistic test for evaluating the difference between the mean values of the groups, the higher it is the more the groups are different

Df: : degree of freedom for the dataset

p: : expresses the probability that the two groups belong to the same population

If we focus the attention to the p value we can observe that *Model 1* recognises *sim_probes1* different than *sim_probes2*. While *Model 2* does not recognises any statistical difference between *sim_probes1* and *sim_probes2*. We know that in this case *sim_probes1* and *sim_probes2* are exactly the same. The problem is caused by the fact that each trial has a different baseline and this must be taken into account in order to have a correct interpretation of the data. *Model 2* takes into consideration the offset across trials in the *random effect* through the term $(1 + Group|trials)$ which indicated that each trial can have different baseline across trials and groups.

It is now clear that the best formula for our purpose is expressed in the *Model 2* as expressed in Equation (3.11).

In Tables 3.2 and 3.3 we can observe the outcome of *Model 2* in the other cases.

Table 3.2: Case(ii)

Name	Estimate	SE	tStat	Df	p
Intercept	1.6227	0.22871	7.0951	80018	3.70E-11
Group_2	0.27334	0.099844	2.7377	80018	0.062

Table 3.3: Case(iii)

Name	Estimate	SE	tStat	Df	p
Intercept	1.7903	0.26128	6.8521	80018	7.33E-12
Group_2	0.60441	0.13968	4.327	80018	1.51E-05

The **p** values in tables 3.2 shows no statistical significant difference between the two groups while statistical significant difference is shown in Table 3.3. We know that a small difference between the two groups characterises the case ii while case iii has a larger difference. We can then conclude that Model 2 is able to interpret the dataset in a correct way.

3.6 Polynomial regression

To analyse the relationship between the muscle displacement and the torque produced we used a polynomial approach. In particular we considered the case of a curve fitting between torque and muscle displacement near the deep aponeurosis and a surface fitting between torque, displacement and depth information.

3.6.1 Curve fitting

The relationship between two datasets, U and Y, is described by the function which represents the static dependency between the variables [139]. A common approach to solve the polynomial representative of the relationship is based on the Least Squares method [139].
The Least Squares problem can be defined as follow:

Given a set of n data points $u_1 \dots x_n$ with corresponding $y_1 \dots y_n$ and degree p, find a polynomial of degree p that fits the data with a minimal error in the least squares sense.

The polynomial is of the form specified in equation (3.12); the degree of the polynomial is p and has to be determined empirically [139].

$$y = a_1 + a_2 u + ...a_{p+1} u^p \tag{3.12}$$

The polynomial that fits the data is the one with a minimal error, where the error can be defined as the difference between the estimated values and the actual values given in the dataset (u_i, y_i)

The relationship can be written in the form:

$$\mathbf{U\ a} = \hat{y} \tag{3.13}$$

Where the vector **a** represents the coefficients to be estimated, when having a certain number of observations of U and Y. To find **a** the least square method is used which consists of minimising the relationship $J = \sum y - \hat{y}$. If the system is over determined there are more equations than unknowns and the design matrix X is not square but is an m by n with $m > n$. To solve this problems there are mainly two approaches which are illustrated.

The first method involves multiplying both sides of the equation by the U^T, reducing the system to a square, $n \times n$ normal equations:

$$\begin{aligned} U^T U a &= U^T y \\ \text{Thus} \quad a &= \left(U^T U\right)^{-1} U^T y \end{aligned} \tag{3.14}$$

With finite precision or in the case U is rank deficient (has more columns than rows) the square matrix $(U^T U)^{-1}$ is singular thus non-existent. This would mean that there are fewer measurements than the actual order of the polynomial. An alternative to this approach is known

as *QR Factorization* which is privileged in some algorithms such the one used in Matlab.

The *QR Factorization* state that any matrix with dimension $m \times n$ can be decomposed into an orthogonal matrix **Q** of dimensions $m \times m$ and an upper triangular matrix **R** of with same dimensions as **U**. Using this factorisation the matrix **U** can be written as:

$$\begin{aligned} Ua = y \longrightarrow QRa = y \\ \text{Since} \quad Q^TQ = QQ^T = I \\ \text{Then} \quad Q^TQRa = Q^Ty \\ Ra = Q^Ty = c \end{aligned} \tag{3.15}$$

To solve the system we have to look for a solution of the kind:

$$\begin{cases} Qc = y \\ Ra = c \end{cases}$$

where the unknown variable is a. At this point it is possible to express the polynomial relationship between the variables U and Y, as expressed in Equation (3.13), which is the curve that best fits the datasets.

When modeling the relationship between three datasets, U_1, U_2 and Y the polynomial defines the surface that best fits the datasets. In this case the dependent variable Y is expressed as a function of U_1 and U_2. So if you think of the input U as a combination of U_1 and U_2, the approach is the same as the one presented above and the same mathematical approach can be applied.

3.7 The cross-validation

If a model (presented in the previous section) is obtained from all data available, then the data might be overfitted. To overcome this you need to split the data set into training and an independent test data set. Generalising this leads to the k-fold.

The cross-validation is a method for assessing the accuracy and the validity of a statistical model and for comparing learning algorithms [140]. The observed data is divided into two groups one used to train the model, *training dataset*, and one to validate the model, *testing dataset* [140]. To estimate the model only the *training dataset* is used. The model estimated is then used

to predict data in the *test dataset*. In typical cross-validation the training and the validation sets should cross-over in consecutive rounds in order to validate each data point. The standard form of cross-validation is called *k-fold* cross-validation. The *k-fold* cross-validation consists of partitioning the datased into k equal (or nearly equal) large groups. A total of K iterations of training and validation are sequentially performed so that in each iteration a different fold of the data is held-out for validation while the remaining *k-1* folds are used for training.

For each k iteration a model is estimated on the training dataset and is used to make a prediction on the test dataset.

The performance of each model can be analysed using metrics such as the *Error*, the *Root Mean Square Error (RMSE)*, *Normalised Root Mean Squared Error (NRMSE)*, the *coefficient of determination* R^2 and the *adjusted coefficient of determination* R^2_{adj} . Those metrics are defined as follows.

The *Error* is defined as the difference between the real value and the estimated value.

$$Error_i = y_i - \hat{y}_i \tag{3.16}$$

where $\hat{y}_i$ is the model output and y_i is the measured output.

The *RMSE* gives the spread of the y values around their average. It expresses the distance, on average, of a data point from the fitted line measured along a vertical line. The vertical distance between the data points and the fitted line is called the *residuals* when the calculations are performed over the data sample that was used for estimation, and are called *prediction errors* when computed on the validation set. RMSE is a measure of accuracy, but only to compare forecasting errors of different models for a particular variable and not between variables, as it is scale-dependent. Normalizing the RMSE facilitates the comparison between datasets or models with different scales. The NRMSE is obtained by dividing the RMSE by the range of the measured data defined as the maximum value minus the minimum value. The RMSE and the NRMSE are, then, coefficients related to the error of the fitting.

$$RMSE = \sqrt{\frac{\sum_{i=1}^{n} (y_i - \hat{y}_i)^2}{n}} \tag{3.17}$$

$$NRMSE = \frac{RMSE}{y_{max} - y_{min}} \tag{3.18}$$

Information about how well the model fits the data is given by the R^2 and the R^2_{adj} terms. R^2 expresses the percentage of explained variation as if all the independent variables in the model affect the dependent variable. Basically it is the ratio of the explained variation to the total variation and represents the percentage of the data that is the closest to the line of best fit.

$$R^2 = 1 - \frac{SS_{res}}{SS_{tot}} \tag{3.19}$$

$$\text{Where:} \quad SS_{tot} = \sum_{i=1}^{n} (y_i - \bar{y_i})^2 \text{ And} \quad SS_{res} = \sum_{i=1}^{n} (y_i - \hat{y_i})^2 \tag{3.20}$$

with $\bar{y_i}$ indicating the mean of the measured data.

The SS_{tot} is called the total sum of squares and it is defined as the sum, over all observations, of the squared differences of each observation from the overall mean. The SS_{res} is called the residual sum of squares and it expresses the amount of the difference between data and an estimation model.

The R^2_{adj} expresses the percentage of variation explained by only those independent variables that affect the dependent variable.

$$R^2_{adj} = 1 - \left[\frac{\left(1 - R^2\right)(n-1)}{n-q-1} \right] \tag{3.21}$$

Where n is the sample size and q is the number of independent variables in the regression equation.

The difference in explaining the variation between R^2 and R^2_{adj} makes R^2 less indicative of the overfitting of the data. In fact R^2 increases for every predictor added to the model while R^2_{adj} compensates for the addition of variables and only increases if the new term enhances the model. When a model incurs overfitting, an incorrect high value of R^2 leads to a false prediciton ability. This does not happen with R^2_{adj}.

3.8 Summary

In this chapter the experimental methods used throughout the thesis were presented. Two algorithms were used to analyse the US videos and were both developed at Manchester Metropolitan University. The software algorithms track persistent features in an US videos stream. The organisation of the information obtained from the algorithms was developed in this PhD project. The post processing analysis and the way the features are organised is presented in this chapter. In addition the main mathematical approaches used during the project are presented. Among these is the polynomial fitting which find a polynomial for the description of the relationship between input and output variables. The cross-validation analysis which is used to validate a model and exclude overfitting of the data. The linear mixed effects model is used to analyse the statistical difference among groups of data.

Chapter 4

Ultrasound imaging to characterise muscle contraction, a feasibility study

4.1 Summary

This chapter presents a feasibility study for investigating the potential of the USI technique to improve understanding of the physiological behavior of the muscle. The chapter introduces the tools and procedure used for the extraction of the information from the US video and compares the analysis of US videos obtained with different devices and analysed with different software implementations.

Despite the growth of interest observed in literature about US analysis of muscle, no standard parameters have been identified to describe a whole portion of the muscle. Previous studies identify that useful information can be obtained from muscle architectural parameters such as pennation angle, cross-sectional area or fascicle length.

The work of this thesis is based on the use of a software described in Section 3.2.1 which was developed for the tracking of persistent features in US videos. The information generated by the analysis software has been analysed in this chapter and significant parameters are identified. The generated information was evaluated according to different arrangement.

Previous studies showed that the muscle architectural parameters change according to the task performed [42, 43]. This indicates that it is important to validate the measurements according to the particular task performed. In this study, the tasks were performed at different velocities and the measurements were compared.

In addition, the tracking of features in US video is challenging because features are not always persistent over time: a feature can appear and disappear according to the reflected wave. In this study, three US machines of different quality and price range were used in order to investigate the differences in the measurements obtained. The main purpose is to evaluate weather a low cost US machine and high cost US machines offers comparable outcomes.

4.2 Introduction

Ultrasound Imaging (USI) is a tool that can potentially provide objective measures of the functional status of the muscle and its changes during and after acute rehabilitation for individuals with SCI. In the last few years the literature has shown a great interest in US imaging for the description of muscle activity. Different approaches have been applied in vivo to extract information such as muscle size, shape (e.g. thickness and length) and structure (e.g. organisation of muscle fascicles). The majority of the studies rely on the manual measurements

of morphological parameters on frames of the videos recorded. Approaches based on manual identification are time consuming, operator dependent and have, mostly, poor accuracy and repeatability. To overcome these problems, research groups have been focusing their attention on the development of automatic algorithms for the identification or tracking of muscle information [64,70,133,141]. Methods proposed successfully extracted static and dynamic parameters such as the cross-section area, pennation angle, fascicle length or stiffness or shearing of the aponeuroses [64, 67, 70, 133, 142].These algorithms, mainly allowed the tracking and the recognition of a specific parameter of the muscle rather than an entire portion of the muscle.

Loram and colleagues at Manchester Metropolitan University (MMU) have recently developed a software algorithm allowing automatic tracking of features in ultrasound images of a muscle portion [129]. Access to this software was possible within this project as part of a collaboration with MMU, providing an important, verified tool for accurate and automatic exploration of muscle function [129].

Despite the growing interest, the musculoskeletal muscle US still lacks standard techniques in terms of algorithm for information extraction and identification of parameters. In this study the algorithm for detection of US muscle information developed in MMU is used to track features of US videos of a whole portion of the gastrocnemius medialis muscle. The outcome of the software is the pixel location of each feature over time.

When analysing ultrasound videos for functional studies of skeletal muscles, the validity of the investigation must be tested according to the experimental setup, the processing algorithm and the physical limitation of the device itself. Thus, several issues must be considered. First, whether the intrinsic accuracy and resolution of the ultrasound scanner affect the processing algorithm. This means if we repeat the same task when using different ultrasound devices, do the same algorithms produce repeatable measurements? Second, the ultrasound video analysis depends on the frame rate of the video recorded, this limits the analysis of tasks at faster contraction's speed. During electrically elicited contractions fast movements are usually generated, therefore to deduce information on the muscle activation during FES it is important to evaluate the operating range of the ultrasound and associated analysis as a tool for describing muscle behavior. Third the biological meaning: are features extracted from the ultrasound videos related in meaning to other biomechanical factors such as the torque exerted?

This chapter aims at investigating the US information focusing the attention on two points:

i) propose an approach to extract functional and physiological information from the features tracked in US videos. Different parameters are identified and their significance is explored.

ii) establish whether external factors such as the quality of the image produced by the ultrasound device affects the interpretation of the the muscle function. The repeatability of the measurements is studied using three different ultrasound scanners and two software implementations for the automatic tracking of features in the videos recorded. In addition different protocol setups were used to test how the velocity of the movement affects the US measurements.

4.3 Methods

The methods used for data collection and analysis will be presented in this section. Information about the software used for the analysis can be found in Section 3.2.

4.3.1 Setup

The setup used for the data collection involved:

- three ultrasound devices: Echo Blaster 128 LV7.5/60/128Z-2 (Telemed, Lithuania) , MyLab 70 (Esaote, Italy), Aloka SSD 400 (Hitachi, USA). The tests were repeated in three different sessions. In each session, a different US device was used: Echo Blaster 128 LV7.5/60/128Z-2 (Telemed, Lithuania) , MyLab 70 LA523E (Esaote, Italy), Aloka SSD 400 UST-5710 (Hitachi, USA). The ultrasound videos were recorded with a frame rate of 25 Hz.
- Stimulator for FES: Stimulator (Rehastim Hasomed, Germany) and electrodes (Pals Platinum size 3.3x5.3 cm, Axelgaard, USA).
- Dynamometer: Cybex Norm (Germany) screen for visual feedback

In each sessions:

- The subject was lying in prone position with the dominant leg fully extended and with the foot fixed on the footplate of a dynamometer.
- An US probe and two electrodes for FES were placed on the gastrocnemius medialis (GM) muscle and the US video was recorded. See Figure 4.1 which shows the electrodes and the US probe placement.
- The torque signal was recorded from the platform and displayed on a screen as visual feedback.

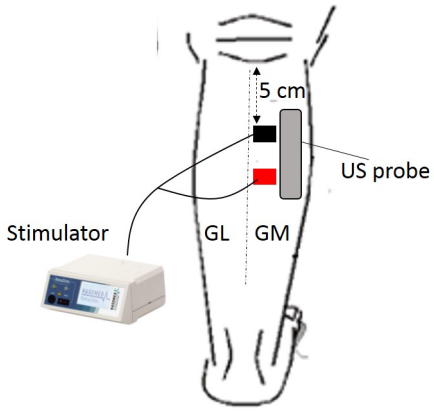

Figure 4.1: Configuration of electrodes and US probe placement. The electrodes were placed on the Gastrocnemius Medialis (GM) muscle next to the US probe at a distance of about $5cm$ from the popliteal fossa.

Two tests were performed: one involving electrical stimulation and one involving voluntary contraction.

During the FES test, electrical stimulation was applied and the torque exerted was recorded. During the voluntary test, the subjects was asked to perform isometric contraction against the dynamometer trying to replicate a signal shown on the screen. Figure 4.2 shows the setup.

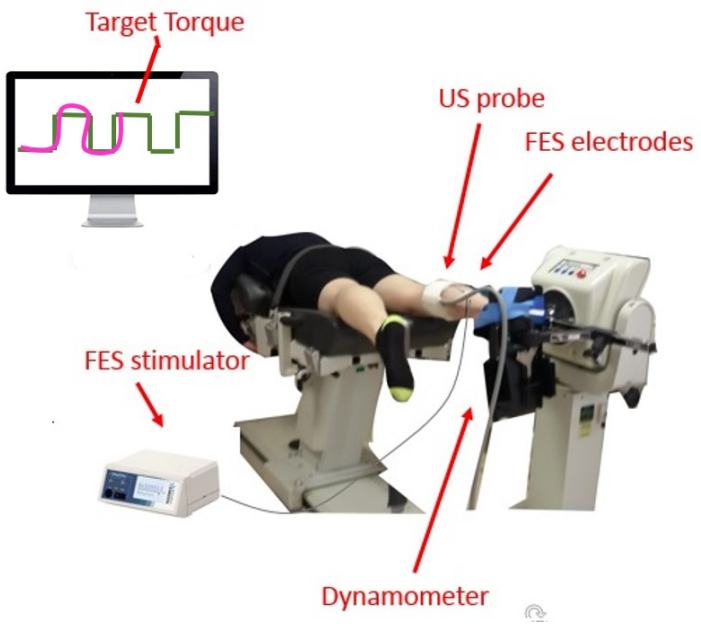

Figure 4.2: Setup. The subject lies in prone position on the chair of a dynamometer (Cybex). An US probe is placed on the dominant leg which is fixed to the footplate of the dynamometer. Electrodes for FES are placed on the muscle belly next to the US probe. Visual feedback of the torque exerted is given on a screen, indicated with a pink line. The subject is asked to push against the platform in order to align the pink line to the green line shown on the screen.

Data was synchronously recorded using custom written Matlab code and Simulink scripts running in a real-time environment (Real Time Windows Target toolbox).

4.3.2 Protocol

Three healthy subjects, age 22, 32 and 25 years, volunteered to participate in the study. The study was approved by the Ethics committee and all the participants gave written informed consent.

Two tests were performed, when:

(i) FES is applied on the medial gastrocnemius

(ii) muscle contraction is achieved voluntarly

At the beginning of each session, the maximum current amplitude for the FES was set according to the capability of the subject to tolerate the stimulation without much discomfort, and in order to get a visible contraction in the US image. The pulse-width and the frequency were fixed respectively at 200 μs and 50 Hz for all subjects. During the FES test the subject was asked to relax while the torque signal and the US videos were recorded.

The voluntary test consisted of recording the torque signal and the US video of the GM muscle when the subject was performing isometric contractions against the footplate of a dynamometer following a target displayed on a screen.

During the FES test, 30 ramp signals were randomly produced; these were composed of 10 different amplitudes, 3 different rise times (2.5, 5 and 7 seconds in a random order) and a constant period of 5 seconds. The ramp signals were used to generate the current profile for the FES. The minimum FES current amplitude was set at 70% of the maximum amplitude and the maximum at 100%. The order was then randomised. The FES test was performed first and the maximum torque value achieved was used to set the maximum torque target for the voluntary test. A break of 5 seconds between each contraction was applied. An example of the signal recorded during an FES test is shown in Figure 4.3.

During the voluntary task, the target torque was displayed on a screen and the subject was asked to reproduce this when performing the voluntary isometric contraction. Thus, the subject was asked to isometrically push his foot against the footplate trying to follow the 30 ramp signals displayed on the screen of the oscilloscope. In the voluntary test, the ramp amplitudes were chosen considering 10 values on a logarithmic scale between the 100% and the 10% of the

maximum torque measured in the FES test.

In Figure 4.4 and Figure 4.3, the 30 ramp signals and the 30 torque signals are shown for the voluntary and FES tests.

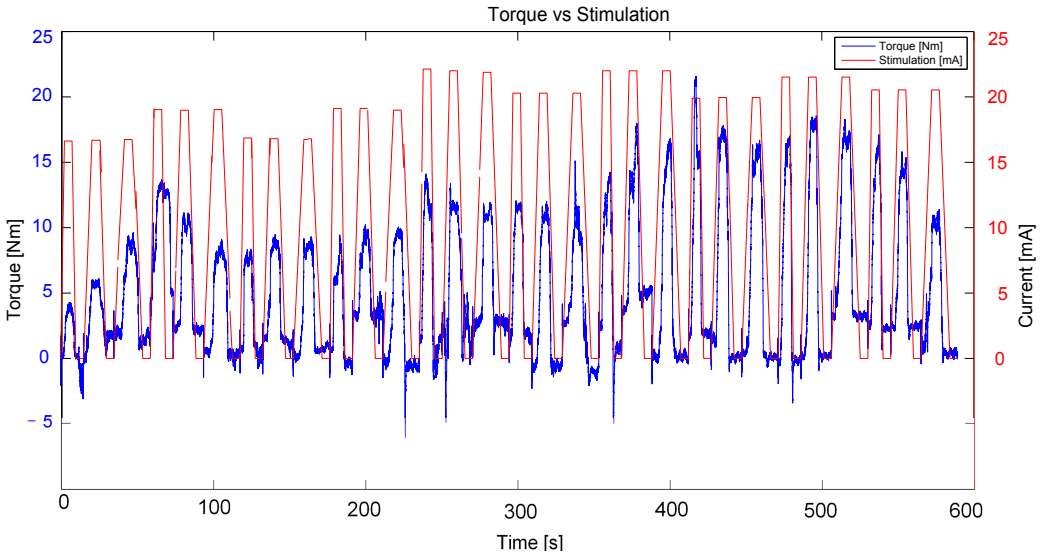

Figure 4.3: 30 FES ramps at 10 different amplitudes (between 15 mA and 23 mA) and at different rise times (red) and thirty torque signals obtained when stimulating the calf muscle

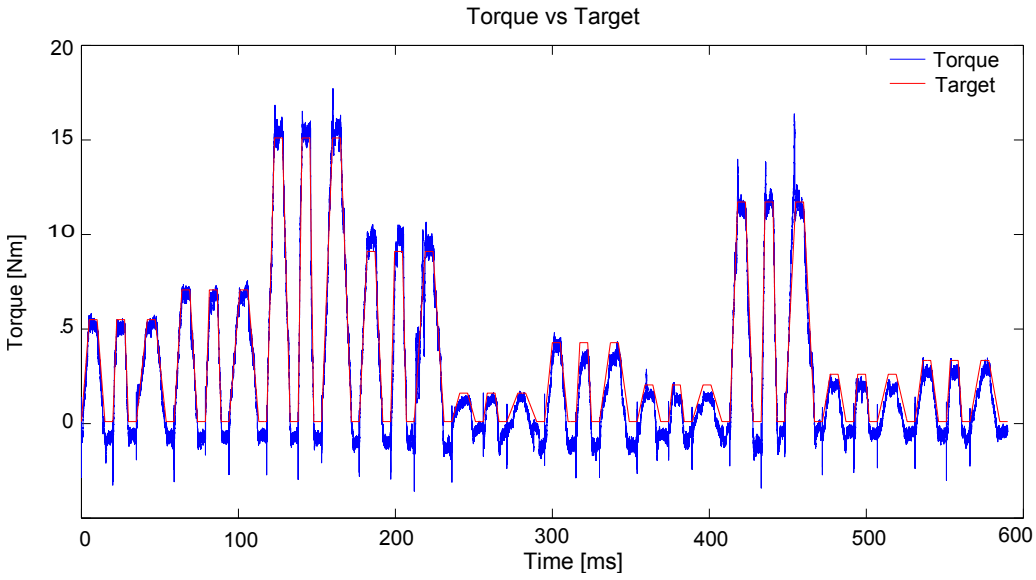

Figure 4.4: 30 ramp targets (red) at 10 Amplitudes and at 3 ramping times 2.5, 5 and 7 seconds, and 30 torque signals (blue)

In Figure 4.5 an example of three trials at 7, 5 and 2.5 seconds rise time respectively, for both Voluntary and FES tests.

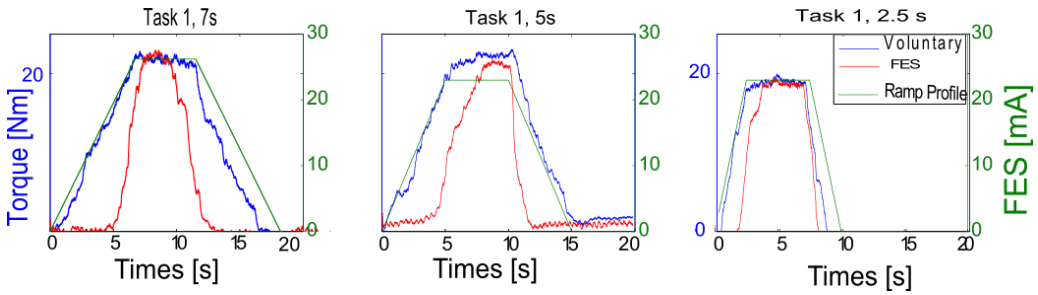

Figure 4.5: Example of one trial FES and Voluntary.Torque measured during the FES test (red) and during its correspondent Voluntary test (blue). In green the stimulation applied during the FES test is shown.

The isometric ramp task involves a phase of activation, where the force exerted increases, a plateau state where the force exerted is constant, and a de-activation phase where the force exerted decreases and the muscle returns to a relaxed state. These three phases are related to different physiological conditions. During the activation phase, the muscle fibers are recruited while during de-activation the fibers are released. In order to discriminate between the recruitment and derecruitment phases of the isometric ramp task, three phases were distinguished. They are indicated as *rise*, *constant* and *fall* as shown in Figure 4.6.

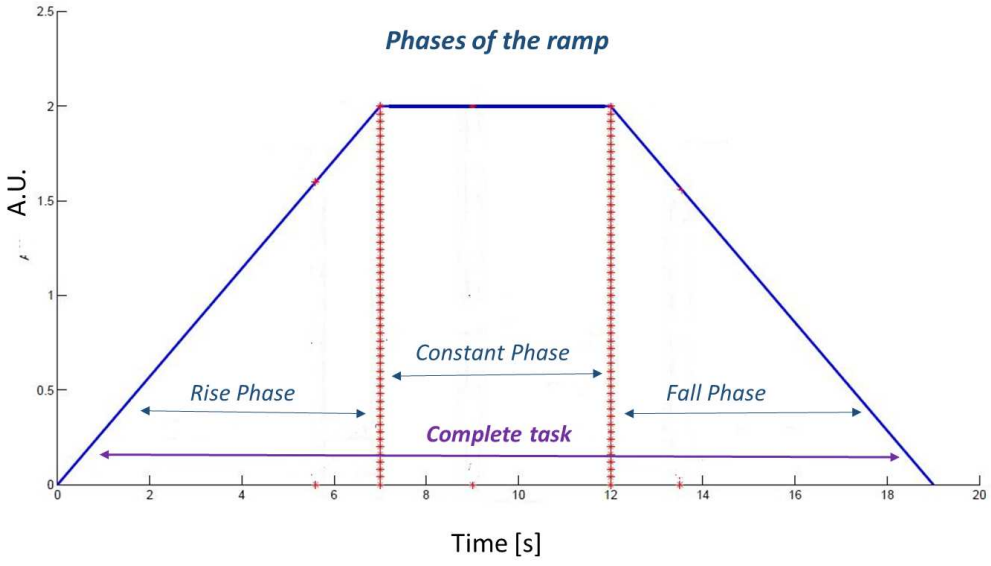

Figure 4.6: Phases discrimination; phases are distinguished, it is possible to distinguish the rise, the constant and the fall phases

4.3.3 Analysis of US video

The US videos were processed with two software algorithms (SW1 and SW2 described in Section 3.2.1). In total a matrix of 10 x 8 *probes* are tracked over the video. The *probes* are the test points tracked at each frame of the US video. For detailed information about the tracking algorithm and the *probes* arrangement see Section 3.2.

4.3.4 Analysis of US information

As a first step, it is necessary to visualise the kind of information obtained from the tracking of the probes on the US video.

Referring to Figure 3.3 on page 40 the tracking over time of each probe is described in x and y directions or according to the magnitude of the movement. As a reminder, the *probe* represents the points on the image tracked by the software algorithm. The information from the *probes* can be grouped according to rows and coloumns. The outcome of the software gives the pixel information of the *probes* at each frame. The pixel information can be converted to millimeters using the conversion factor which depends on characteristics of the ultrasound probe used. In Figure 4.7 an example of the conversion for the device MyLab is shown, the formula applied in this case:

$$x_{mm} = \frac{x_{px} \times 69mm}{690px} \quad y_{mm} = \frac{y_{px} \times 50mm}{520px} \tag{4.1}$$

Where 69 mm corresponds to the length of the US probe and 50 mm is the field of view of the US image. For the other machines, see table below:

Table 4.1: Conversion factors

	Probe Length	Pixels Image	
		x	y
Telemed	59 mm	580	680
Aloka	65 mm	650	750

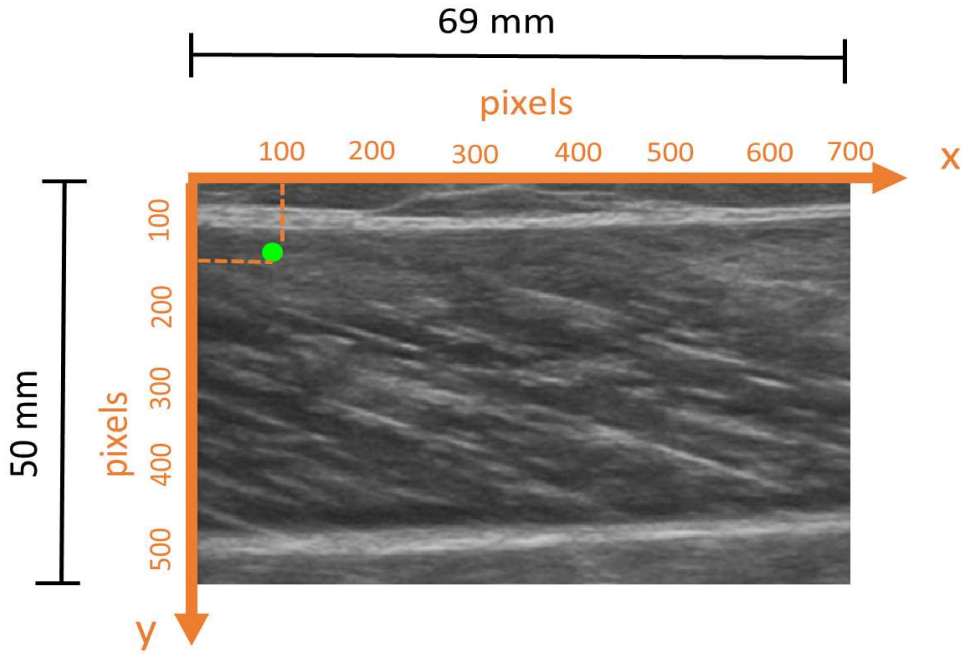

Figure 4.7: Conversion px to mm for My Lab machine. The pixel location of each *probe* can be converted into millimeters considering the conversion factors of the manufacturer. In the example, the *probe* is at pixel 100 on x and 150 mm on y axis. When converting to millimeters using the formula in 4.1 it is 10 mm on the x axis and 14.4 mm on the y axis.

To describe the probes movement, the parameter of *displacement* was used. The *displacement* was calculated normalising the location of the probe at each frame to the correspondent *probes* in the first frame. Therefore at frame 1 of the video, each *probe* has displacement equal to zero. The displacement of each *probe* can be evaluated on its x, y or magnitude components.

The *velocity* of each *probe* was estimated as the variation of the displacement between two frames.

Results obtained are presented in the next section.

4.4 Results

Data was collected from three subjects and with three US devices. A total of 180 (90 Voluntary and 90 FES) videos per subject were analysed with SW1 and SW2. The results of the pilot analysis performed and the evaluation of the technology used is presented in this section.

4.4.1 Evaluation of probes displacement

In the following graphs the results of the *probes displacement* is presented for both the voluntary task and the task performed with FES. The purpose is to give representative results to familiarise with the information obtained from the analysis.

For the figures presented in this section, the following conventions apply:

- The figures refer to a single representative participant and one US device (Telemed) and the analysis with one software algorithm (SW1).
- In each figure the graphs obtained for one amplitude level and the three ramp times (7s, 5s, and 2.5s) are presented. Both voluntary and FES tests have the same torque level (the corresponding stimulation level is given for the FES test).
- The green lines on the figures represent the beginning of the ramp, the start of the constant level, the end of the constant level and the end of the ramp respectively. For reference see Figure 4.6.
- The colors of the graph are in a scale from red to blue, where red refers to the most proximal probes and blue to the most distal.

The displacement of each probe can be evaluated in the X and Y direction or according to its magnitude. In addition probes organisation according to row or columns can be distinguished. For an overview, refer to Figure 3.3 on page 40. The results of the analysis are given below.

4.4.1.1 Displacement, arrangement according to rows, X and Y direction

Figures 4.8 (voluntary) and 4.9 (FES) show the trend of the probes when they are arranged according to rows for the movement in the X direction. The three columns group the data according to the ramp times of 7 seconds, 5 seconds and 2.5 seconds respectively. Each of them is composed of 10 subplots that refer to the 10 rows. In each subplot 8 lines are drawn and they represent the 8 probes that compose each row, cf. Figure 3.3.

From the graph it emerges that no main differences are observed in the size of displacement observed at different ramp times in both the voluntary and the FES induced contraction. In fact, in all the three cases the maximum displacement reached is similar in all the conditions (3 rise time, voluntary and FES induced contraction). In addition comparable displacement is observed during the voluntary(Figure 4.8) and the FES (Figure 4.9) contractions. However

the probes composing one row appear to be moving more uniformly during the voluntary test than during the FES test, especially at deeper rows, where the FES test shows a wide spread of movements for different columns (lines). This indicates more variability across different areas of the muscle during the FES test. In addition, the amount of displacement varies across different depths: superficial areas of the muscle moves less than the deeper areas.

The analysis of the displacement in the Y direction is shown in Figures 4.10 and 4.11. The y-direction is characterised by a lower range of displacement when compared to x-direction. In accordance to the results obtained for the x-direction, the displacement has comparable range across different depths. No difference in the amount of displacement is observed when performing the task at different ramp times. Contrary from the results obtained for the x-direction, in the y-direction the amount of displacement does not remarkably vary across different depths. From the results it is possible to observe that the main movement of the probes is in x-direction, and that the amount of displacement depends on the torque exerted. In fact at lower torque levels, lower range of displacement is observed in both the x and y directions.

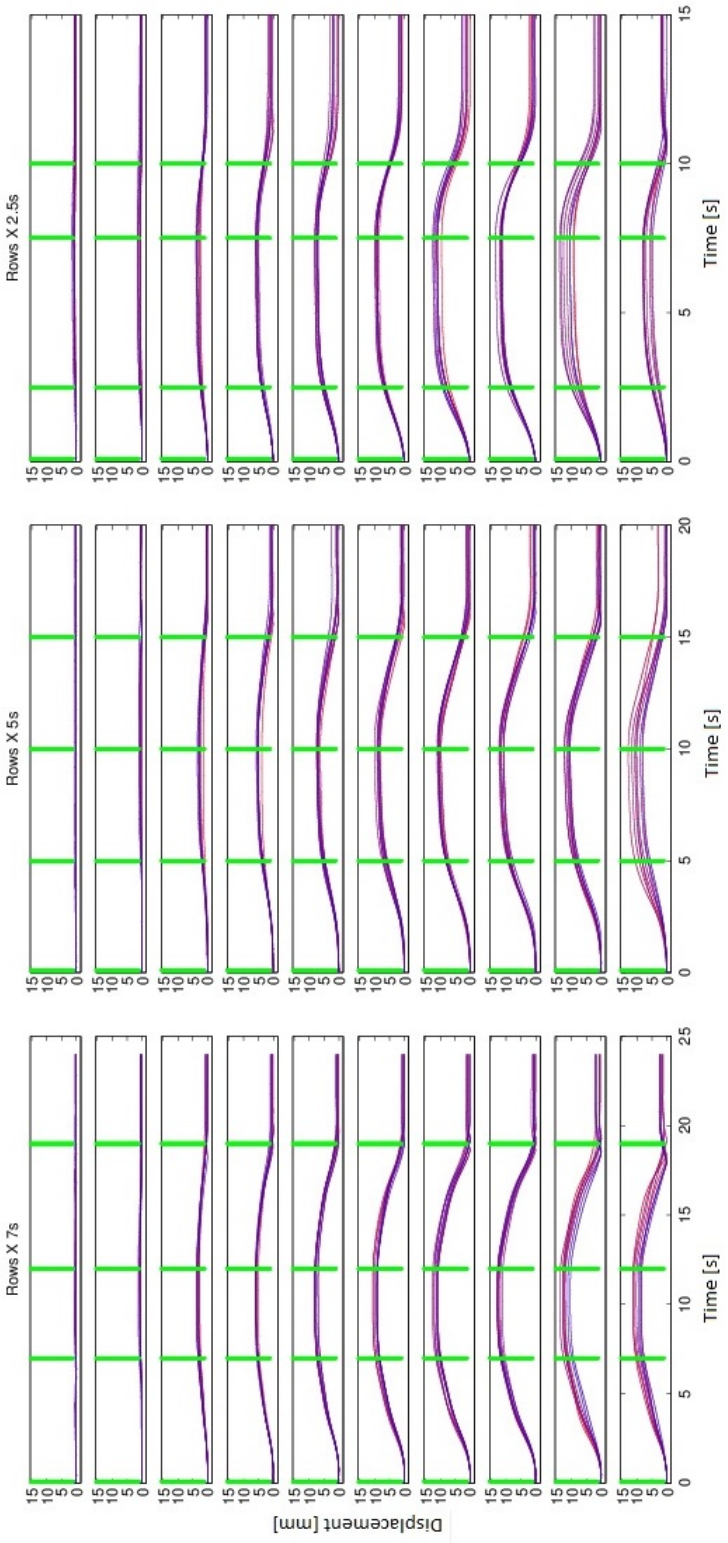

Figure 4.8: X direction. Probes distribution according to rows for voluntary contraction when the maximum torque reached is 20 Nm. The three plots represent the task at the 3 rise times, 7 s, 5 s, 2.5 s. Each subplot of the column represents one row and it displays with lines of different intensity of red the probes trend of the 8 probes of each row. The green vertical lines represent the event of the target ramp: the start, the reach of the beginning of the constant period, the end of the constant period and the end of the ramp.

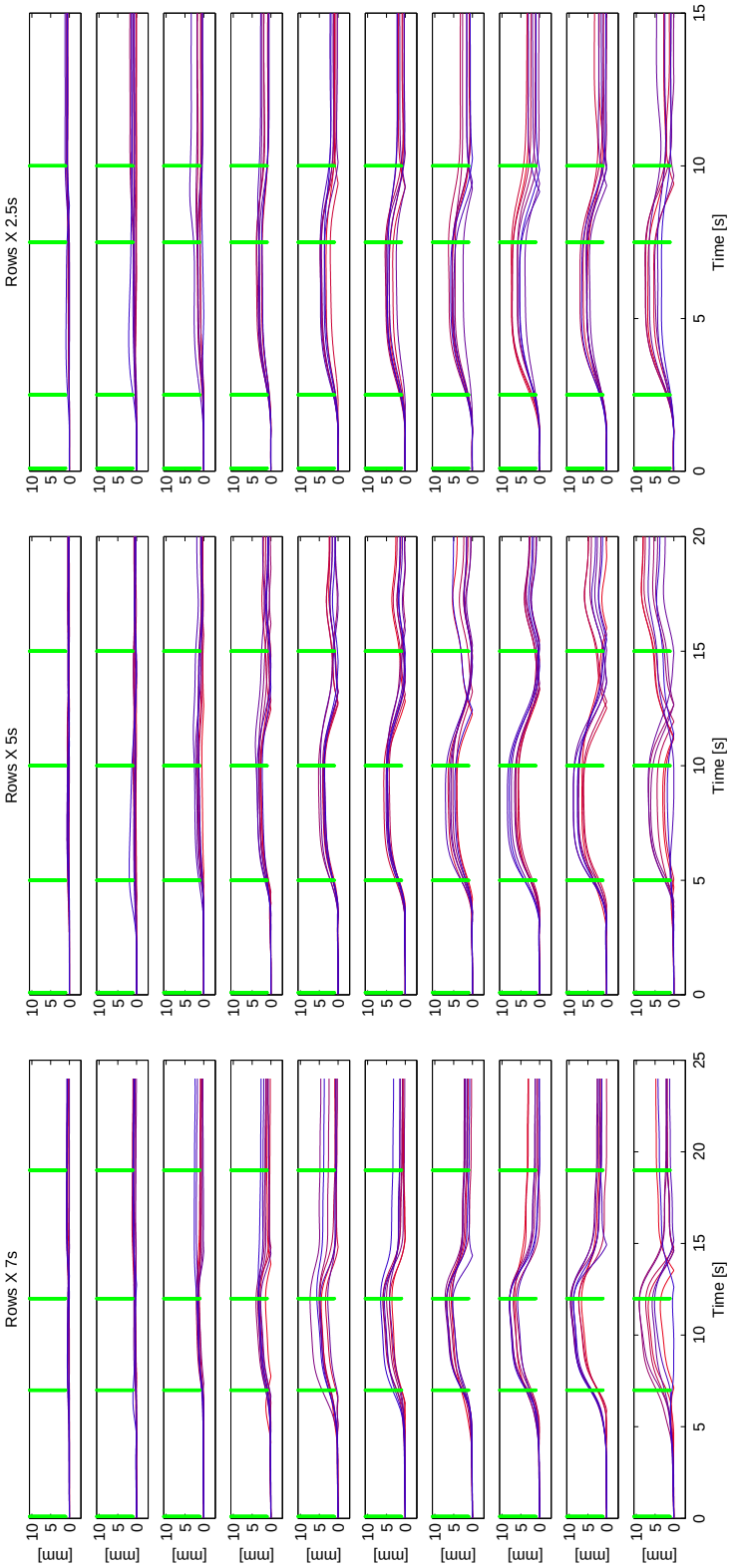

Figure 4.9: X direction. Probes distribution according to rows for FES induced contraction when the maximum torque reached is 20 Nm. The FES current applied is 20 mA, pulsewidth 200 us and the frequency 50 Hz. The three columns represent the task at the 3 rise times, 7 s, 5 s, 2.5 s. Each subplot of the column represents one row and it displays with lines of different intensity of red the probes trend of the 8 probes of each row.The green vertical lines represent the event of the stimulation ramp: the start, the reach of the beginning of the constant period, the end of the constant period and the end of the ramp

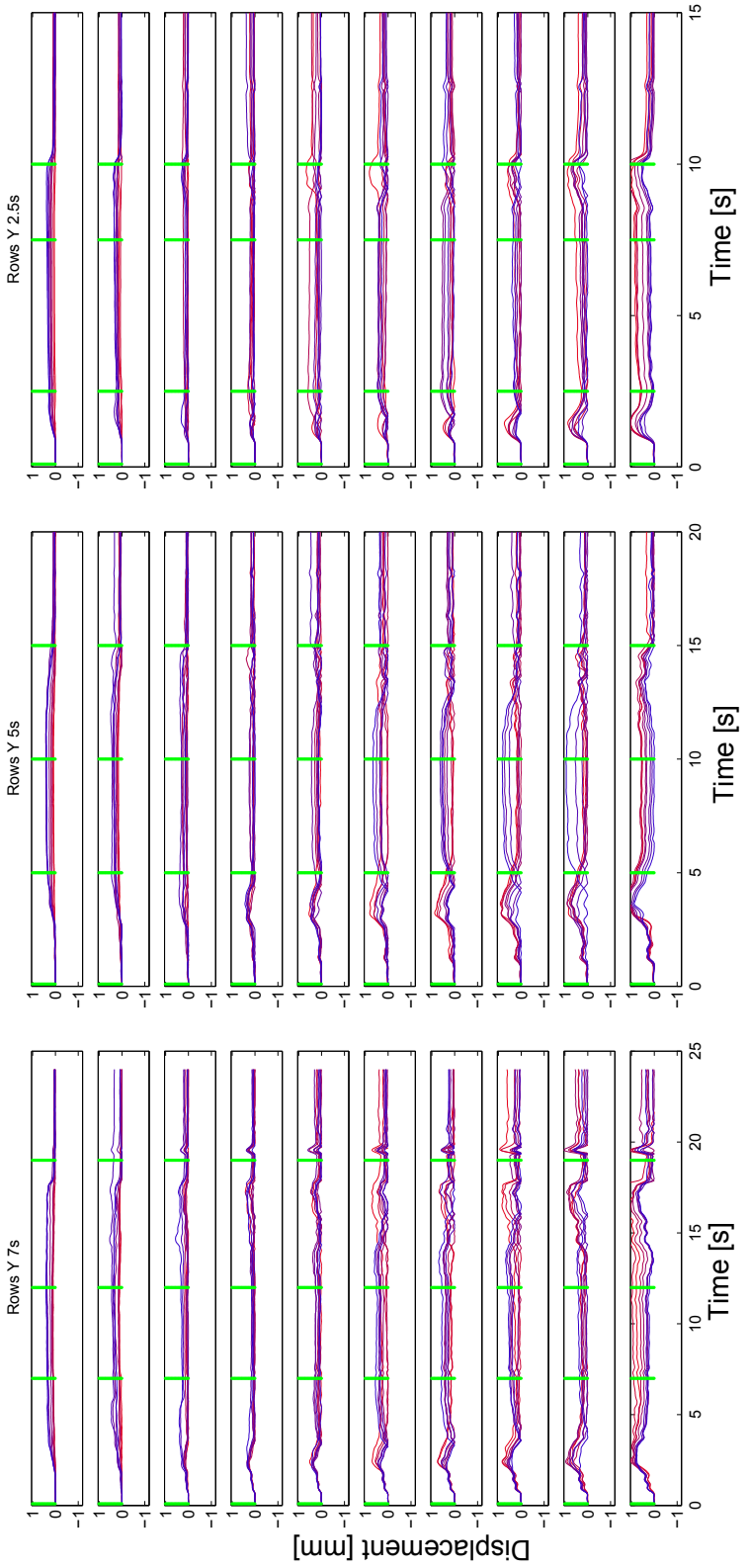

Figure 4.10: Y direction. Probes distribution according to rows for voluntary contraction when the maximum torque reached is 20 Nm. The three plots represent the task at the 3 rise times, 7 s , 5 s , 2.5 s. Each subplot of the column represents one row, and with lines of different intensity of red the probes trend of the 8 probes of each row is displayed

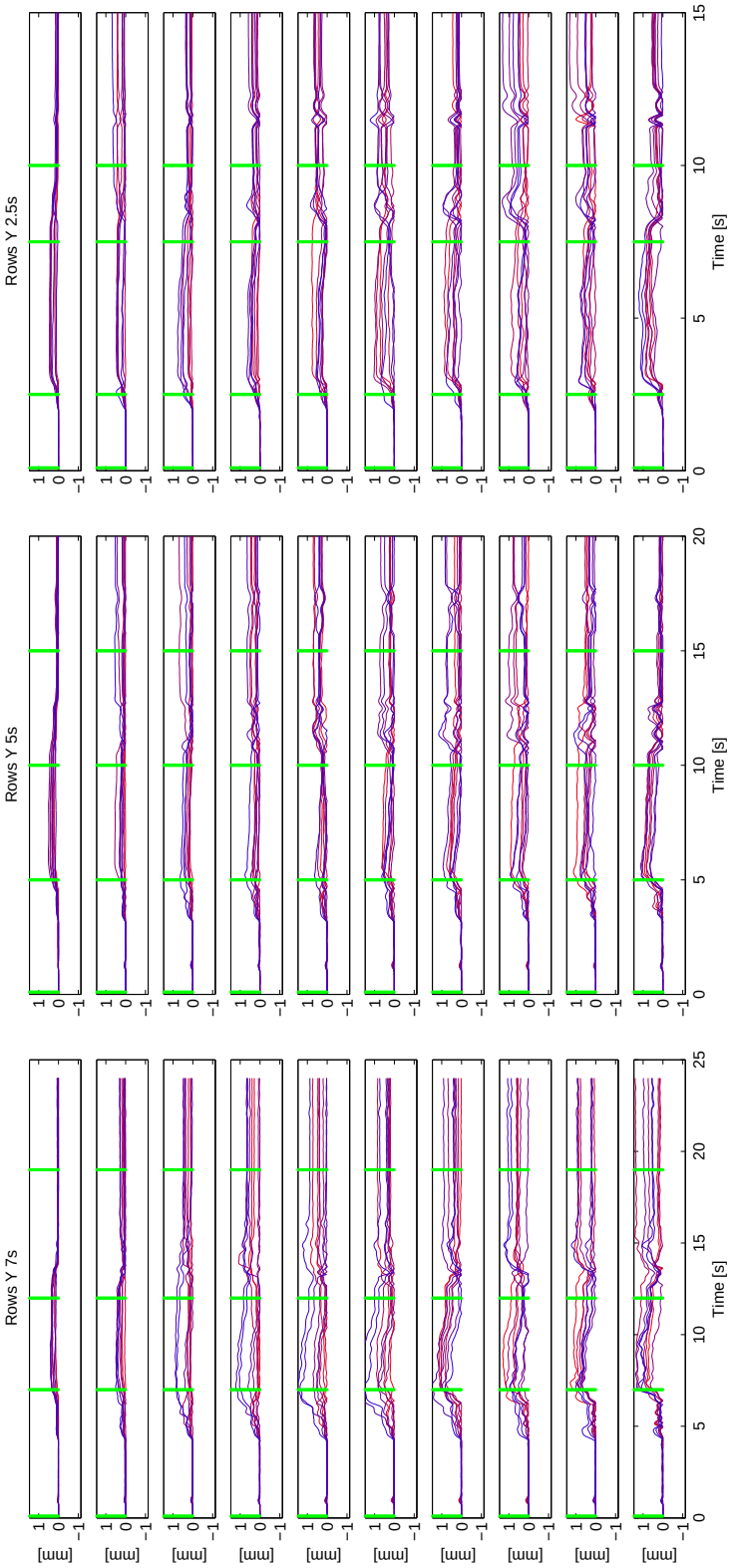

Figure 4.11: Y direction. Probes distribution according to rows for FES induced contraction when the maximum torque reached is 20 Nm. The FES current applied is 23 mA, pulsewidth 200 us and the frequency 50 Hz. The three columns represent the task at the 3 rise times, 7 s, 5 s , 2.5 s . Each subplot of the column represents one row and it displays with lines of different intensity of red the probes trend of the 8 probes of each row.

4.4.1.2 Displacement, arrangement according to columns, X and Y directions

The displacement of the probes can be shown by arranging the results according to columns, cf. Figure 3.3 A. In this case the changes in muscle displacement are evaluated in the proximal-distal direction. The data is the same as that previously shown in Figures 4.8 to 4.11 but it is just displayed differently. Figures 4.12 and 4.13 respectively show the displacement of the probes in x-direction during one trial of voluntary and one of FES induced contractions. Since Figures 4.9 - 4.11 have shown that the displacement in y-direction is much smaller, these are not shown for this arrangement.

The displacement increases with depth, (red to blue lines correspond to superficial to deeper rows). The important information to extract from the graphs is that different columns have a comparable range of values of displacement in both the voluntary and the FES cases. Unlike the voluntary task, during FES the probes do not return to their original position just after the end of the stimulation, which can be observed in Figure 4.13. The phenomenon might depend on force concentration to the tendon which is more difficultly released during FES induced contraction. A return to initial displacement during FES contraction is probably observable in a longer time.

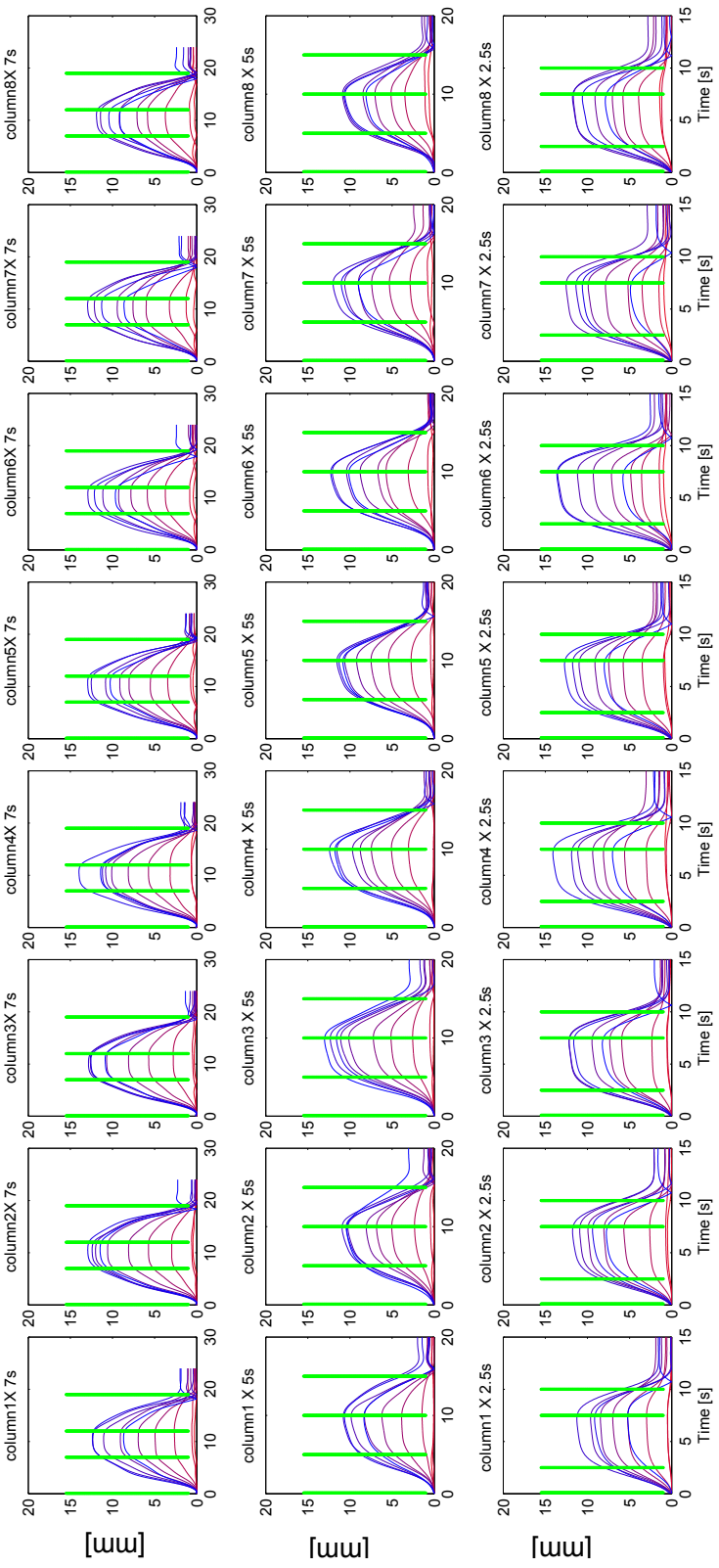

Figure 4.12: X direction. Probes distribution according to columns for voluntary contraction when the maximum torque reached is 20 Nm. The three rows represent the task at the 3 rise times, 7 s , 5 s , 2.5 s . Each supblot of the this row represents one column of probes and it displays with lines of different intensity of red the probes trend of the 10 probes of each column.

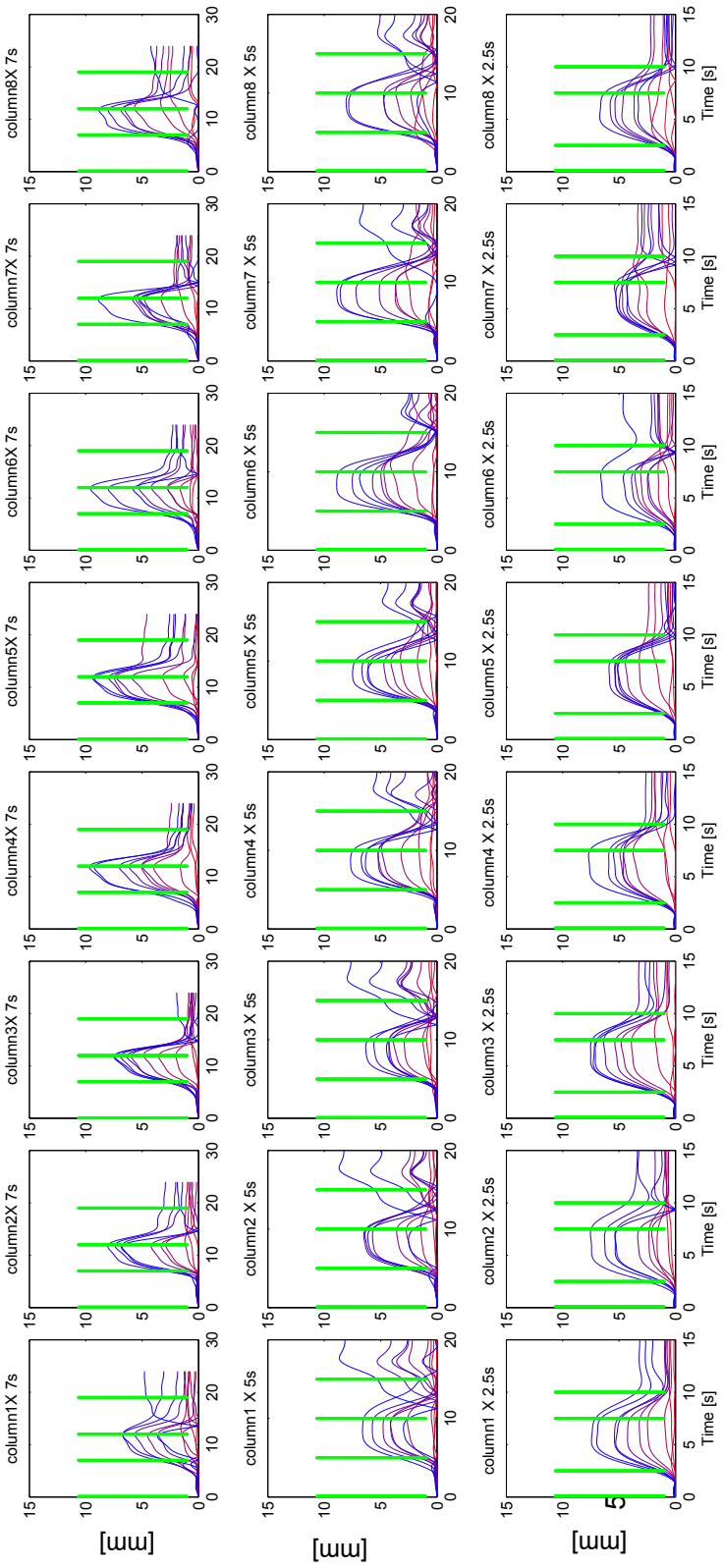

Figure 4.13: X direction. Probes distribution according to columns for FES contraction when the maximum torque reached is 20 Nm. The FES current applied is 23 mA, pulsewidth 200 us and the frequency 50 Hz. The three rows represent the task at the 3 rise times, 7 s, 5 s , 2.5 s. Each subplot of the this row represents one column of probes and it displays with lines of different intensity of red the probes trend of the 10 probes of each column.

4.4.2 Torque vs Displacement relationship

Figures 4.8 to 4.11 show that the displacement is mainly in the x-direction. Since the y-direction component of the displacement is relatively small, the probes movement can be studied either considering only the x-direction or considering the magnitude of the total displacement. In addition, the probes displacement within each row is averaged, cf. Figure 3.3. The next sections show the results of the information in x-direction when averaging across the probes displacement belonging to each row.

To understand how the displacement changes with torque, the torque-displacement relationship was investigated. Figures 4.14 and 4.15 show an example of the torque-displacement relationship obtained for one participant during one voluntary and one FES trial at three ramp times. In each subplot three curves can be distinguished. The red continuous curve refers to the task performed when the ramp time was set at 7 seconds, the green dotted line refers to 5 seconds ramp time and the blue line to the task performed at 2.5 seconds ramp time. In each of the three voluntary trials the subject was asked to reach the same torque value. As previously noted the difference in displacement at different depths (row 1 to row 10 can be measured). The three curves representing the trial at different ramp times have similar behaviour and the ramp time does not seem to influence the relationship.

4.4.2.1 Torque-Displacement linear fitting

In this section, a linear fit describing the relation of displacement as a function of torque will be considered. In all cases a hysteretic curve is observed, i.e. the behaviour during the portion of the curve corresponding to increase torque is different from that during torque decrease. Similar behavior is observed across ramp times. The representative results in Figures 4.14 and 4.15 indicate quite a large hysteretic curve, with an almost linear relationship during the *rise* phase and a slightly curved relation during the *fall phase*. This means that if performing a linear fitting on the whole curve large residuals and error would be obtained. In order to avoid this, the linear fitting was performed separately for each of the three phases *rise*, *constant*,*fall*.

The same trend was observed for each test performed by all the subjects and it was also repeatable for three devices and for both the voluntary and the FES tests.

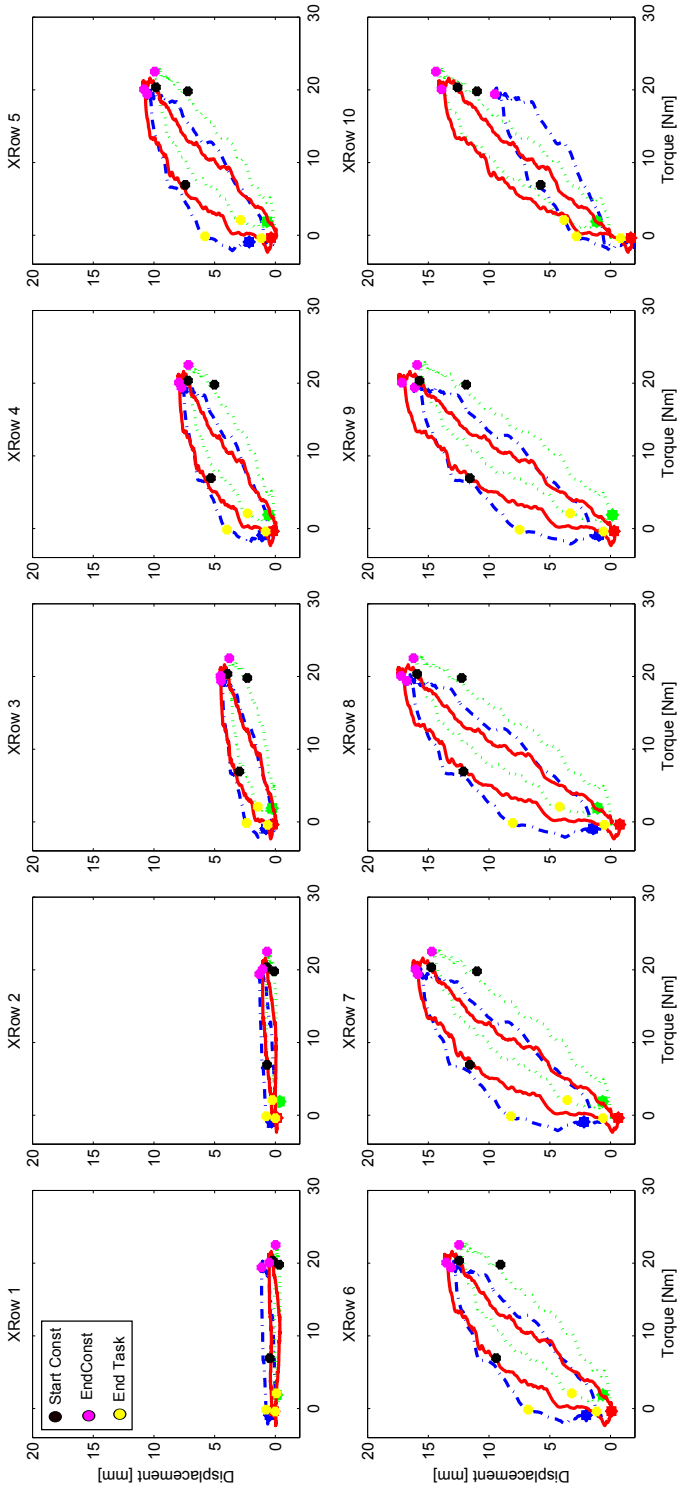

Figure 4.14: Relationship torque vs displacement in X direction per each of the 10 row of probes considered (10 depths), where row 1 is the most superficial part and row 10 is the deepest part of the muscle. Per each subplot three curves are identified, they refer to the trials of the three ramp time 2.5 s (blue), 5 s (green) and 7 s (red) when producing the same torque output. The plots refer to a voluntary test performed with the device Aloka

.

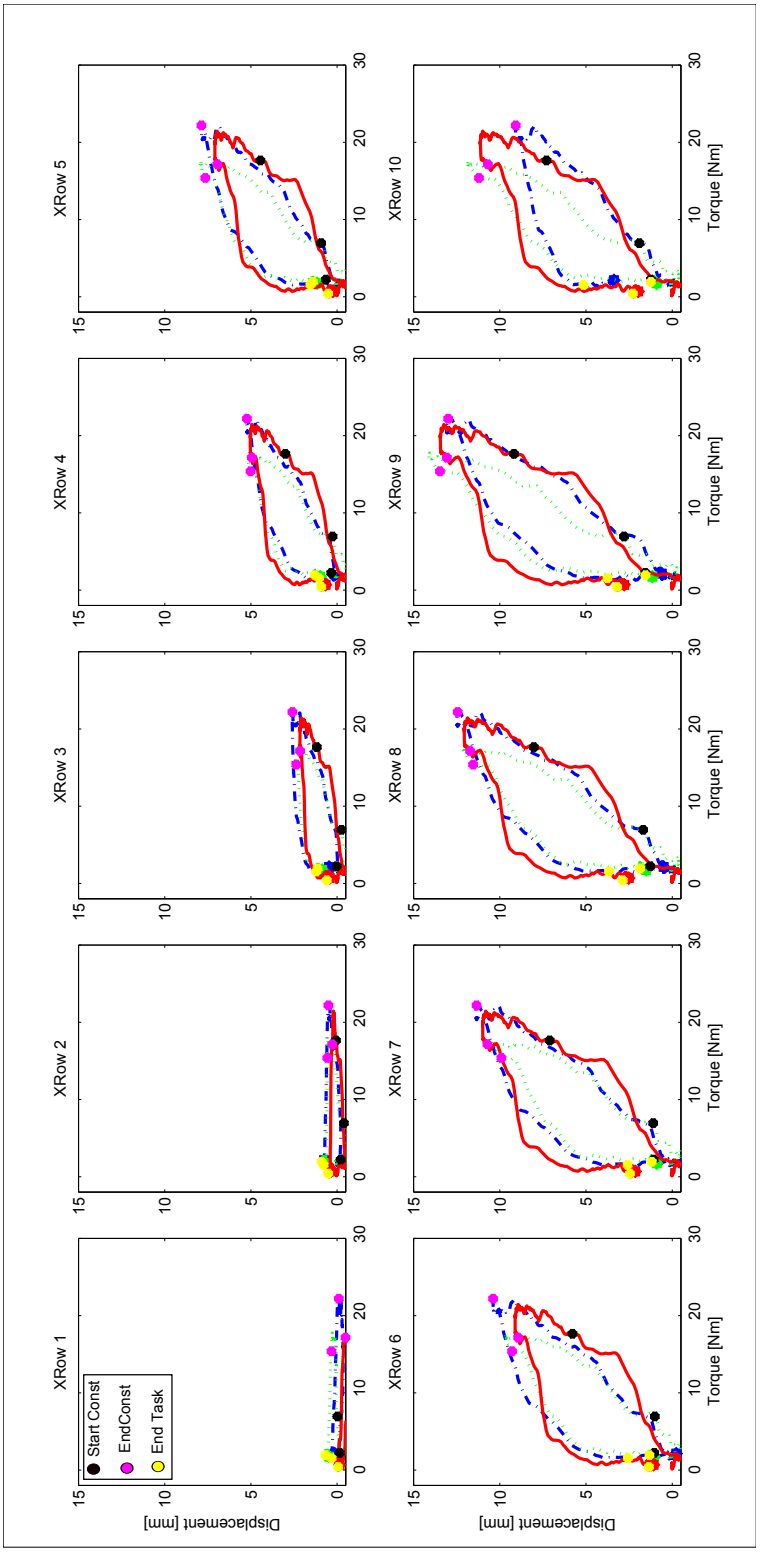

Figure 4.15: Relationship torque vs displacement in X direction per each of the 10 row of probes considered (10 depths), where row 1 is the most superficial part and row 10 is the deepest part of the muscle. Per each subplot three curves are identified, they refer to the trials of the three ramp time 2.5 s (blue), 5 s (green) and 7 s (red) which, when applying the same current amplitude result in the same amount of torque exerted. The plots refer to a FES test performed with the device Aloka

.

The line fitted was of order 1 as expressed in Equation 4.2:

$$d(\tau) = \beta * \tau + q \quad \text{For Rise and Constant phases}$$
$$d(\tau) = \beta * \sqrt{\tau} + q \quad \text{For Fall phase} \tag{4.2}$$

The polynomial $d(\tau)$ fitted the data τ ($Torque$) to $d(\tau)$ ($Displacement$) for the phases Rise and Constant. For the phase Fall $d(\tau)$ fitted the data $\sqrt{\tau}$ ($\sqrt{Torque}$) to $d(\tau)$. In the latter case, $\sqrt{Torque}$ was used because the relationship appeared to be slightly curved and the square root helps to linearise the relationship.

The goodness of the linear fitting was evaluated using the coefficient of determination R^2 which is indicative of how well the line fits the data (cf. Section3.7). The coefficients of determination obtained for the linear fitting for all subjects, all trials and for one device are shown in Figure 4.16 for the voluntary and in 4.17 for the FES tests in the form of a boxplot distribution. No difference is observed across different ramp times in both the voluntary and the FES cases. In all the cases the boxes are aligned at the same height (overlap) withing each subplot, indicating no difference among the groups. This means that the R^2 values obtained across different depths are similar. Analysing in details, during the voluntary task we can observe:

- The Rise phase has 95% of its distribution around $R^2 = 0.8$, in addition it has short boxes indicating small variance across data. This indicates a strong linearity between torque and displacement at all the depths.
- The Constant phase has 95% of distribution around $R^2 = 0.4$, this was expected because during the constant phase the torque is maintained at a constant level and this cannot give a linear relationship.
- The Fall phase has 95% of its distribution around $R^2 = 0.8$ with data skewed R^2 ; also in this case the linearity relationship can be considered as strong.

During the FES task the following is observed:

- The Rise phase has 95% of its distribution around $R^2 = 0.7$ for rows deeper than 3, superficial depths are less linear.
- The Constant phase is strongly linear with 95% of its distribution around $R^2 = 0.8$
- The Fall phase does not show linearity with 95% of its distribution around $R^2 = 0.6$

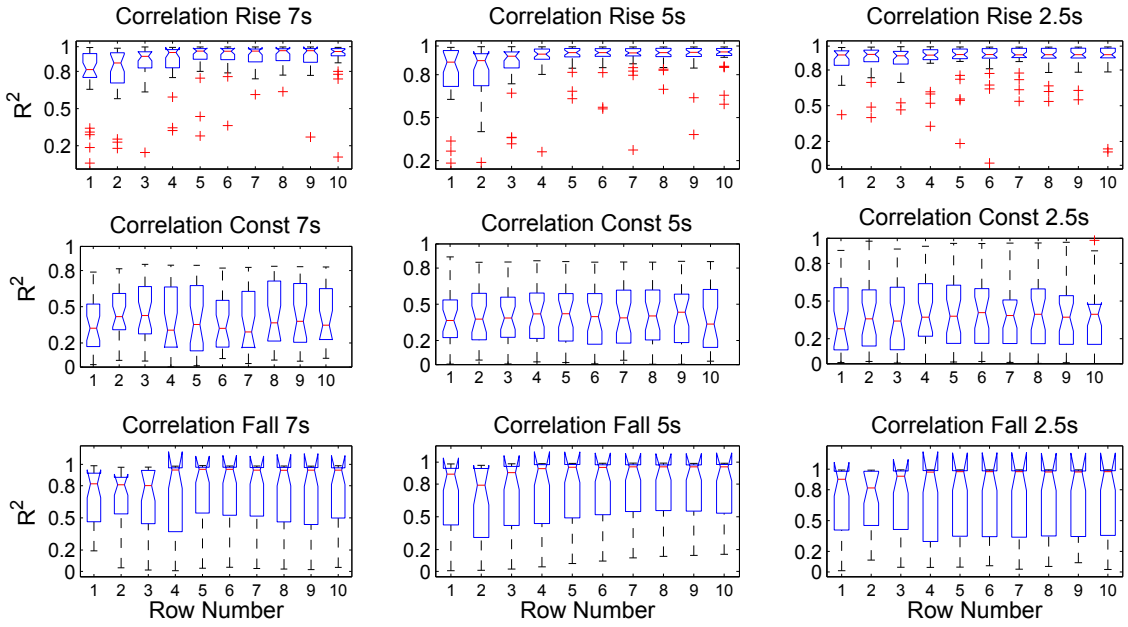

Figure 4.16: The graphs show in boxplots the distribution of the coefficients of determination R^2 obtained for all the trials for all the participant during the voluntary test with the device Telemed. The coefficients of determination are given for each phase and for each ramp time. Rise and Fall phases are characterised by higher values of coefficients of determination. No difference is observed across different rows.

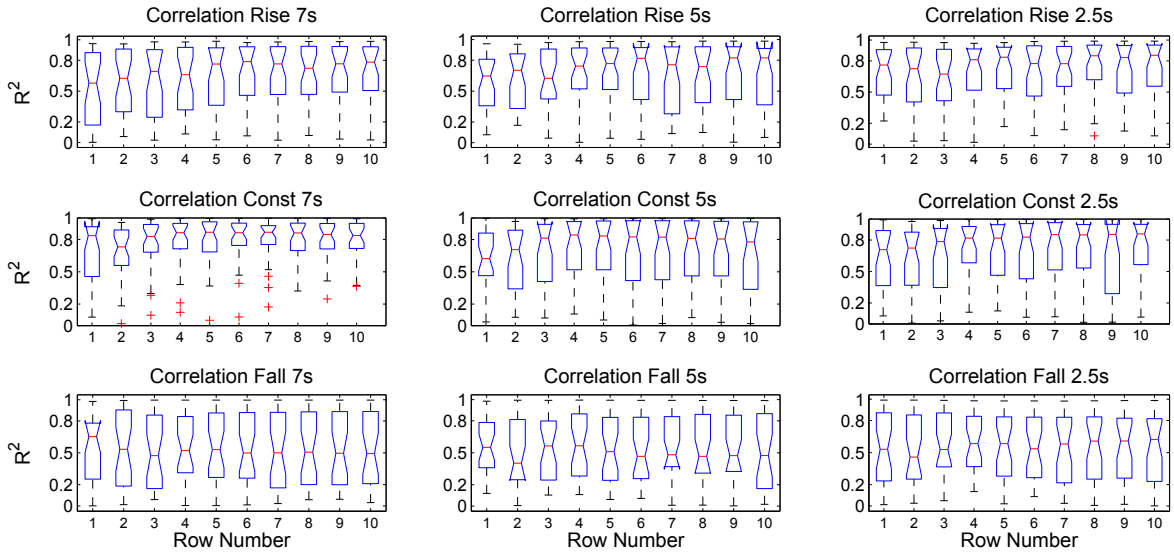

Figure 4.17: The graphs show in boxplots the distribution of the coefficients of determination R^2 obtained for all the trials for all the participant during the FES test with the device Telemed. The coefficients of determination are given for each phase and for each ramp time. Constant phase is characterised by higher values of coefficients of determination, lower values are observed for the Rise and Fall phases.

The values obtained for the slope are presented in Figure 4.18 (a) and (b). Note that a non linear relationship is observed during the Constant Phase for the voluntary test and during the Fall phase for the FES test. The figures show the mean and the standard error of the slope obtained across different trials, for one device and for all subjects. Deeper rows have higher slopes in all the cases. Small standard error are observed for the voluntary task and for the Rise phase of FES. A larger range of standard error are obtained for the Constant Phase of the FES suggesting more variability in this case.

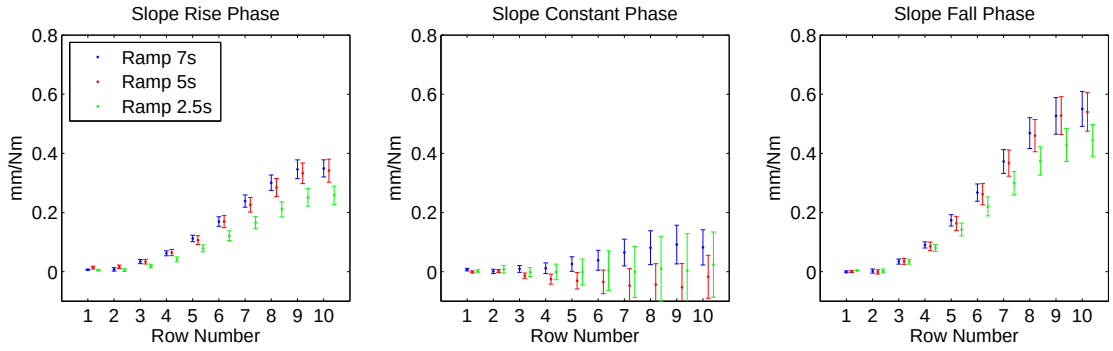

(a) Voluntary Task

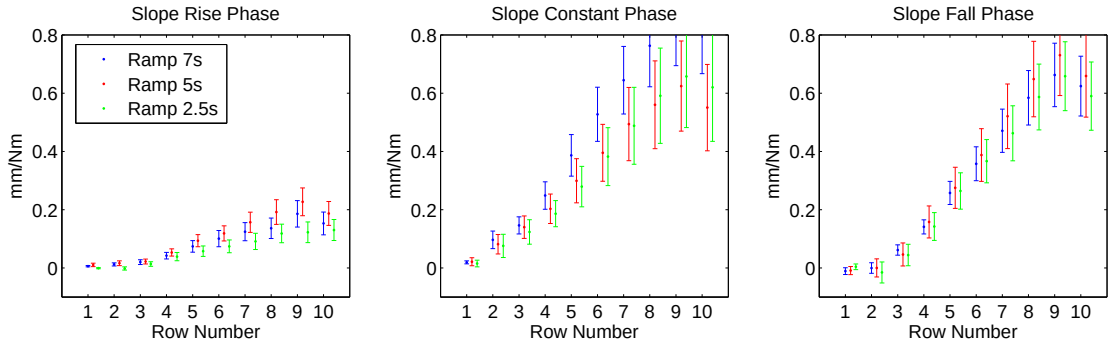

(b) FES Task

Figure 4.18: Mean and Standard error for the values of slope for the linear regression obtained for the Voluntary task (a) and for the FES task(b) during the Rise, Constant and Fall Phases

4.4.3 Evaluation of equipment and protocol setup

The data was collected using three US machines and analysed with two different software with the purpose to evaluate the influence of the quality of the US image on the data analysis and to evaluate the repeatability of the measurements. In this section, we evaluate whether the measurements obtained depend on any of these factors.

A statistical analysis was performed using a *linear mixed-effects model* (LME) in order to take into account the repeated measures. Details about the LME approach can be found in Section 3.5.

The US videos recorded were processed with the two software available and the results were compared using the LME test.

4.4.3.1 Differences between software

The LME model for analysing the difference between software was built considering displacement of probes as a dependent variable, the software group information (SW) as fixed effect values and the subjects and the trials group as random effects. The formula used is the following:

$$Displacement \sim SW + (1 + SW|trials) + (1 + SW|subjects) \tag{4.3}$$

The formula 4.3 means that each value of the vector *Displacement* is associated with a group expressed in the vector SW and is weighted with the vectors *trials* and *subjects* which take into account the variability due to different subjects and the fact that each subject performs more than one trial. The outcome of the probes displacement is estimated by the two software and for different ramp times is shown in Figure 4.19. Figure 4.19 shows the results of the LME relative to Formula 4.3. The mean values and the confidence intervals are shown for each ramp time and for the Voluntary and the FES test. The p values obtained for the FES test are $\mathbf{p} > 0.05$ for all the devices and all the phases indicating no difference between SW1 and SW2. However for the Voluntary test statistical significant differences are observed for the device Telemed during *constant* and *fall* phases and for the Aloka device for the *rise* and fall phases.

4.4.3.2 Differences between ramp times

An LME model was also used for analysing the influence of the ramp times on the displacement-torque relationship. The model considered the ratio *displacement/torque* as a dependent variable, the ramp time information as a fixed value and the trials and subjects as random effects. The formula used is the following:

$$(Displacement/Torque) \sim Ramp + (1 + Ramp|trials) + (1 + Ramp|subjects) \tag{4.4}$$

The results are shown in Figure 4.19 where it can be observed that in both the voluntary and the FES tests and in all three phases there is no significant difference among the three ramp times ($p>0.05$).

4.4.3.3 Differences between devices

In order to evaluate the influence of the quality of the image obtained from different devices on the probes displacement the LME analysis was performed for the voluntary and the FES tests as expressed in the following formula:

$$(Displacement/Torque) \sim Device + (1 + Device|trials) + (1 + Device|subjects) \tag{4.5}$$

No difference between Aloka and MyLab devices was found in any of the cases ($p >0.05$). On the contrary the Telemed device has statistically different values than MyLab and Aloka in the *fall* phase during voluntary test and in the *constant* part during the FES test. In Tables 4.2 to 4.7 the mean values, the confidence intervals and the standard errors are stated for each device and each phase.

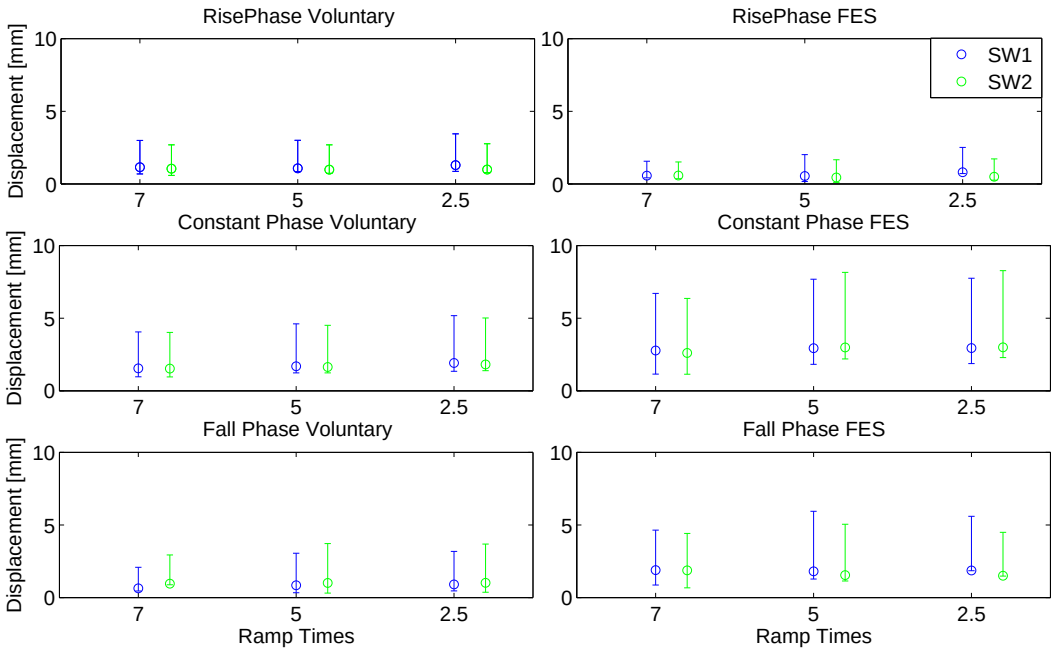

Figure 4.19: Results of the linear mixed models for the ramp comparison in the case of analysis with SW1 (blue) and SW2 (green). The circle represents the mean estimated value and the bars the confidence intervals. In each subplot it can be observed that the mean and confidence intervals of the probes displacement for the three ramp times have a similar range for both SW1 and SW2 and when analysing the three phases separately

.

Table 4.2: LME for device analysis rise phase voluntary

Name	*Estimate*	*SE*	*Lower*	*Upper*	*p*
Aloka	0.826	0.232	0.371	1.282	0.000
MyLab	0.167	0.331	-0.482	0.817	0.613
Telemed	-0.019	0.126	-0.266	0.227	0.877

Table 4.3: LME for device analysis constant phase voluntary

Name	*Estimate*	*SE*	*Lower*	*Upper*	*p*
Aloka	1.714	0.471	0.790	2.638	0.000
MyLab	0.981	1.002	-0.983	2.945	0.327
Telemed	0.311	0.382	-0.437	1.059	0.415

Table 4.4: LME for device analysis fall phase voluntary

Name	*Estimate*	*SE*	*Lower*	*Upper*	*p*
Aloka	0.622	0.218	0.195	1.049	0.004
MyLab	0.507	0.325	-0.130	1.144	0.119
Telemed	0.680	0.232	0.225	1.135	0.003

Table 4.5: LME for device analysis rise phase FES

Name	*Estimate*	*SE*	*Lower*	*Upper*	*p*
Aloka	0.400	0.183	0.042	0.759	0.029
MyLab	-0.169	0.149	0.461	0.123	0.257
Telemed	-0.361	0.165	-0.683	-0.038	0.058

Table 4.6: LME for device analysis constant phase FES

Name	*Estimate*	*SE*	*Lower*	*Upper*	*p*
Aloka	3.650	1.010	1.670	5.630	0.000
MyLab	-0.928	0.372	-1.658	-0.199	0.013
Telemed	-2.495	0.741	-3.947	-1.042	0.001

Table 4.7: LME for device analysis fall phase FES

Name	*Estimate*	*SE*	*Lower*	*Upper*	*p*
Aloka	1.098	0.263	0.582	1.614	0.000
MyLab	-0.338	0.134	-0.601	-0.075	0.012
Telemed	-0.459	0.258	-0.965	0.046	0.075

Notes: Aloka correspond to the intercept.

4.5 Discussion

4.5.1 Considerations about displacement

Studies in literature have demonstrated that US imaging is a potential tool for investigating muscle characteristics and behavior. Although muscle US is an expanding field no previous studies have attempted a description of the whole muscle in vivo under voluntary and electrically induced contraction conditions. [40,41]. This pilot study was performed to identify an approach for extracting the information from the tracking software. In this chapter the US information obtained from the application of two tracking algorithms to data recorded with three different devices was investigated and an approach for the analysis was proposed.

Both the tracking softwares give as an output the pixel location of the 80 *probes* at each frame in x and y direction. This information was grouped according to rows and columns and the displacement over time of each *probe* was evaluated.

Comparing the movement of the *probes* in the X and Y direction, larger displacements are observed in the X direction (range of 10 to 15 mm) and smaller displacement in the Y direction (1 to 2 mm). Moreover, during contraction, the *probe* moves in X direction toward proximal areas (the knee) and in Y direction toward the inner part of the body. This is in agreement with previous studies that demonstrated that during plantar flexion the muscle is pulled toward the knee [64, 143]. Movements in the Y directions represents changes in muscle thickness. The difference in the range of movement between the X and Y directions was expected because different studies have shown that the muscle size mainly changes in longitudinal direction [44, 144].

The muscle displacement is lower at superficial zones and larger at deeper zones. Previous studies showed that the displacement of the superficial aponeurosis is lower than the deeper aponeurosis and in the opposite direction [64, 65]. The cause for this was identified in the architectural muscle arrangement which facilitates the displacement at deeper area [65]. Bojsen-Moller et al. investigated the tissue displacement of the gastrocnemius medialis (GM) during voluntary isometric contraction and during electrically elicited contraction [66]. The study analysed the muscle displacement of the superficial and deeper aponeuroses of the GM and of the superficial aponeurosis of the Soleus. The superficial aponeurosis of the GM was observed to be relatively static during both voluntary and electrically induced muscle contraction. Other studies observed differences in displacement between the superficial and deeper aponeurosis of the GM being the displacement of the superficial aponeurosis smaller than the movement of the

deeper muscles structures [67,68]. Shin at al. suggested that this happens because the fascicular strain is translated into proximodistal movement of the deep aponeurosis whereas the superficial aponeurosis remains approximately stationary [67].

The comparison of the displacement between voluntary (Figure 4.8) and FES contraction (Figure 4.9) showed that the displacement of the probes within the same depth was uniform for the voluntary task but more variable during the FES task suggesting higher variability in muscle activation during the FES task. This is probably related to the way the current spreads within the muscle and the location of the electrodes.

4.5.2 Hysteretic behaviour of torque-displacement curve

In the study, the relationship between the torque produced and *probe displacement* for three ramp times was shown. When examining the graphs, hysteretic behavior can be observed. This behavior was found to be similar in shape and direction (counterclockwise direction) was found at depths (row levels) and in both the voluntary and the FES test.

The presence of hysteresis during isometric ramp contraction was also found by Lindberg et al. when analysing M-mode ultrasound video frames of the biceps brachii [84].

Hysteresis is a characteristic of many biological materials and represents a viscoelastic response to loading and unloading [145]. In physiology it is defined as a system which fails to follow identical paths upon application and withdrawal of forcing agents [146].

At present the analysis of literature does not show agreement upon the explanation of hysteresis on the muscles. Ruch and Pattorn attributed the phenomenon to factor such as tissue elasticity and stress relaxation [146]. Other studies looked for causes of hysteresis at the level of cross-bridge [147, 148].

4.5.3 Influence of ultrasound image quality

In our study we investigated how the quality of the ultrasound image affects the tracking of features when using two software for the video analysis. Different technical and physical factors may influence the image quality by impairing the detection capability of the anatomical structures. Factors such as gray levels or spatial resolution can be manually set, respectively, using the time gain compensation (TGC) or the dynamic focus available in the ultrasound scanners. The appearance of tissue boundaries depends on step changes in acoustic impedance (which is

characteristic of the tissues), distance from and angle relative to the transducer, these parameters can also be controlled. Contrast resolution is altered by compression of the range of reflected ultrasound amplitudes, number of layers of bits per pixel, and the use of contrast agents. On the other hand a global degradation in image quality arises from the beam-forming process which is a characteristic of the transducer. In conventional phased array technologies, beam-forming is accomplished by assuming a constant acoustic velocity and a uniform propagation path and by delaying the appropriate transmission and receiving channels. Aberrations of the acoustic wavefronts due to nonuniform acoustic velocity leads to reduction of spatial and contrast resolutions due to beam broadening and increased magnitude of side-lobes.

Factors such as joint position or location of the transducer can influence the reproducibility of the measurements. In our experiment attention was given to the problem and both the transducer and the position of the leg were controlled as much as possible by using anatomical references. The repeatability of the software to track features on an ultrasound video recorded by the same machine was previously tested in Darby et al. when performing the task at different strengths [129]. In Darby et al. the mean displacement and the standard deviation are shown for one subject for the deeper region of the muscle nearby the deep aponeurosis when performing an oscillatory isometric contraction was about $0.48 \pm 0.1mm$ [129].

In this study, we repeated the tests with three different devices whose image quality was appearing different. Similar results were obtained with the three devices in terms of mean values and confidence intervals, however statistical differences were observed. No significant difference was found between Aloka and MyLab devices in any of the cases of the voluntary tests. Statistically significant differences were observed between Aloka and MyLab devices for the FES tests in the *constant* and *fall* phases. The Telemed devices showed statistically significant differences in the *fall* phase of the voluntary test and in the *constant* phase of the FES test compared to the Aloka and MyLab devices .

It is important to keep in mind that the videos being analysed were recorded during different sessions. Therefore factors such as status of the muscle, location of the US probe or performance of the test make it difficult to interpret the significance of the statistical analysis. The main outcome of these experiments is that a similar range of values are observed.

4.5.4 Influence of ramp times

When analysing ultrasound videos, the validity of the study must be tested according to the experimental setup.

When using the FES for inducing muscle contraction, the way the electric pulses are sent influences the muscle activation differently. An impulsive FES activation (from off to on as quickly as possible) induces a fast muscle contraction which may be difficult to track with the ultrasound due to limitations of the video frame rate. On the other hand, a slower ramping train of pulses produces a smooth contraction.

The purpose of the experiment was to check whether different ramp times have different effects on the muscle activation. The analysis showed that the different ramp times (e.g 2.5, 5 and 7 seconds) do not influence the probes displacement in both the voluntary and the FES test. This indicates that the ultrasound videos and the software tracking are not dependent on the three velocities used to perform the task.

4.5.5 Differences between software

The US images recorded were analysed with two different software algorithms, which were based on the same underlying approach. The accuracy of SW1 was previously analysed with a methodology explained in Darby et al. [133]. SW2 offers a faster analysis than SW1 but its accuracy was not formally tested. The purpose of the analysis was to test whether SW2 offers the same results as SW1.

Similar results were obtained for both software algorithms. The difference was statistically tested using the LME. No statistical significance difference was found between the two algorithms during the FES. However statistically significant differences were observed for the device Telemed and Aloka in *fall* phase of the voluntary test. SW1 and SW2 were processing exactly the same video, therefore it was not expected to be different in any cases. The differences obtained were caused by the fact that SW1 and SW2 analyses the tracked images differently. SW2 averages the tracked points using a squared window of variable size which can include many features. On the other hand, SW1 always averages the position on three points using the mean of a triangular interpolation. The voluntary contraction is characterised by more variability in fiber activation (remember that the recruitment is asynchronous) when compared to the FES induced contraction (where the fibers are synchronously recruited). This phenomenon can add errors to SW2 for the tracking of muscle activation.

4.6 Conclusions

4.6.1 Conclusions on US information

The experiments and analysis described in this chapter provide the basis for the analysis of the information extracted from the tracking of persistent features recognised on US images of the calf muscle. An evaluation of different conditions and different ways to read the information made allows the following conclusions:

- Similar behaviour is observed between Voluntary and FES tasks.
- The *probes* displacement appears to inform the description of the mechanical muscle activation and correlates with the torque exerted mainly during the recruitment phase of the muscle contraction (*rise*).
- The muscle displacement is mainly in the longitudinal direction. This is observed in the *probes* displacement which is larger in the X direction than in the Y direction.
- The amount of displacement produced is independent from the velocity of contraction (dictated by the ramp times).
- Differences in the amount of displacement are observed between most superficial and deeper areas.
- Small proximal distal difference in displacement is observed.
- The arrangement of the probes according to row appears to be more significant because more variability is observed between superficial and deeper areas than in proximal-distal.
- Hysteretic muscle displacement characterises the contraction.
- Differences in linearity are observed between the rise and the fall phases (corresponding to recruitment and de-recruitment of the fibers): the relationship for the Rise phase was modeled with a curve of order 1 while the fall phase with order 2.

4.6.2 Conclusion on the technique used

This work set the basis for the methodologies used for experiments at a larger scale which are presented in the next chapters. The following conclusions can be drawn:

(i) **Device**

- Similar range of displacement values were obtained across the three devices. The results of the statistical analysis should be interpreted with caution because the videos were recorded in different conditions and differences are therefore expected.

(ii) **Software**

- SW1 and SW2 gave statistically different results with data obtained from the Telemed device and for the voluntary test. No difference in the other cases.
- SW1 and SW2 were not statistically different for the FES test

(iii) **Muscle behavior**

- The three ramp times considered (2.5, 5 and 7 seconds) do not produce statistically different results in both the voluntary and the FES tests.

To summarise, with this study we aimed to:

- Establish the operating range of ultrasound and associated analysis, as a tool for description of muscle behavior during the application of FES. In particular, different US machines and different software for image analysis were compared when applying different FES stimulation protocols.
- Evaluate the ability of the technique to track movement performed at different speed.
- Explore possible outcomes and define the next protocol setup.

It is possible to conclude that quality of the image produced by the US probes does not change the tracking of features during the FES task. Comparable values of displacement across devices were obtained. Therefore the choice of using Telemed device as a device for experiment is acceptable The two software showed some statistical differences indicating SW1 as the best choice because its accuracy has been previously proven. The two software and the three US machines used were able to track faster and slower movements and to detect differences in muscle displacement when performing the task at different velocities (the three different ramps) and at different levels of torque. A ramp time of 5 second was therefore selected for the follow-on experiments.

Chapter 5

Mapping muscle displacement during voluntary and electrically induced contractions using USI

5.1 Summary

In this chapter an investigation of muscle contraction during electrical stimulation and during voluntary contraction will be presented . The novelty is the use of Ultrasound video analysis for the description of the muscle activation. USI has great potential for analysing muscle contraction because it allows the visualisation of portions of the muscle.

In this study, the electrical stimulation was applied in two modalities:

- Surface Stimulation (SS)
- Nerve Stimulation (NS)

These two stimulations modalities were chosen because the pathway of the current spreading within the body might induce the contraction differently. For example, during SS, the current field is produced at the surface and spreads within the muscle as fields lines. During NS, on the contrary, the current spread is limited to the nerve and the nerve branches.

In this chapter the muscle activation during contractions obtained voluntarily, with Surface Stimulation and with Nerve Stimulation will be presented. The study involves analysis of local muscle displacement, strain and strain rate measurements. Zones of higher activation were identified in the middle portion of the muscle. Both displacement and strain were influenced by intensity of the stimulation during electrically induced contraction and by the strength of the voluntary contraction. Strain Rate measurements were analysed in the time-frequency domain indicating peaks in power spectrum in correspondence with onset and offset of muscle contraction. Higher values in the power spectrum were observed at the offset time compared to the onset. The voluntary contraction showed low values in the power spectrum at the onset time compared to the electrically stimulated contraction. Conversely both SS and NS had a peak in the power spectrum at the onset time. Frequency components were identified within a bandwidth of 0.5 - 18 Hz. With intensitiy of the current, higher power across more frequencies is observed.

5.2 Introduction

Functional Electrical Stimulation(FES) of skeletal muscle is successfully used in rehabilitation to enhance or re-establish muscle function. The ability of the technique to improve muscle performance in both healthy and diseased muscles has been shown in research and clinical

practice [26]. However the artificial nature of the muscle activation during FES makes it different from the voluntary muscle contraction. Hence, FES has been mainly used without a clear understanding of which muscle regions are activated during the stimulation.

FES is usually applied through surface electrodes placed on the muscle belly. For a long time it has been assumed that FES activates primarily the superficial areas of the muscle, since they are closer to the electrodes where the electric field is generated [111]. The distribution of muscle activation resulting from FES was investigated by Adams, Hillegas and Dudely using magnetic resonance imaging indicating that the stimulation activates areas that are not primarly superficial [109, 110]. Their work was pioneering in giving insights into the regional muscle activity. However the identification of the regions active during muscle contraction does not completely describe the status of the muscle itself. In fact, it is well known that the muscle is made of different fiber types with different contractile properties, whose shortening and lengthening rates vary during muscle activation and deactivation, respectively [149]. Thus, a more complete description of the muscle activation should include both the identification of active regions and the velocity of the changes observed. Because of the fiber shortening during contraction, the zones of the muscle activation during contraction can be identified where changes in length are observed.

When the muscle is active, it deforms. Deformation of an object is generally expressed using a parameter called ***strain***, ε. The strain represents the change in dimension from a resting state to the one achieved following application of force. The rate of the deformation is identified by the ***strain rate***, $\dot{\varepsilon}$, cf. Section 3.3.

Advances in medical imaging technology have made use of imaging in research to explain different functions of human body widespread. In the last few years USI is finding increased interests among research groups which are investigating its use for different applications. Among these, USI of skeletal muscle has shown great potentiality in supporting the understanding of muscle function. Similarly to MRI, USI is non invasive and completely safe but it offers the advantage of performing the scanning quickly, with minimal preparation and during the execution of the task.

The aim of the study is to investigate the potential of Ultrasound video analysis in mapping the muscle activation during voluntary and electrical induced muscle contractions. Three main parameters were identified to be significant for describing the muscle activation: the displacement, the strain and the strain rate. In the chapter the following questions will be addressed:

- Is the muscle displacement uniform over the muscle depths?
- How do strain and strain rate distributions change within the muscle during contractions?

- Are there differences in strain and strain rate during voluntary and electrically induced muscle contraction?
- Are there differences between voluntary, SS and NS

The study will be carried out on the GM muscle during isometric contractions.

5.3 Methodology

5.3.1 Setup

In this section, the setup used for the data collection is described. An ultrasound linear probe (5.9 cm, 5MHz, 40 fps, Echo Blaster 128 LV7.5/60/128Z-2, Telemed) and a pair of electrodes (Pals Platinum size 3.3x5.3 cm, Axelgaard, USA) for functional electrical stimulation (FES) were placed on the muscle belly of the GM muscle. The subject was lying in prone position on the chair of a dynamometer (System 4 Pro, Biodex Germany) with the right foot attached at the force plate while ramping stimulation intensities were applied (Rehastim, Hasomed, Germany).

The ultrasound videos were processed offline using SW1, cf. Section 3.2.1.

The electrical stimulation was delivered according to two configurations as shown in Figures 3.5 and 3.6. During the Surface Stimulation (SS) both the electrodes for FES were placed on the muscle belly, next to the US probe. During Nerve Stimulation (NS) one electrode was placed on the popliteal fossa (behind the knee), the reference electrode just above the knee and the US probe on the muscle belly. Two sessions were performed on different days by each participant.

- Session 1: one voluntary test and one SS test.
- Session2 : one voluntary test and one NS test.

An example of the setup is shown in Figure 5.1.

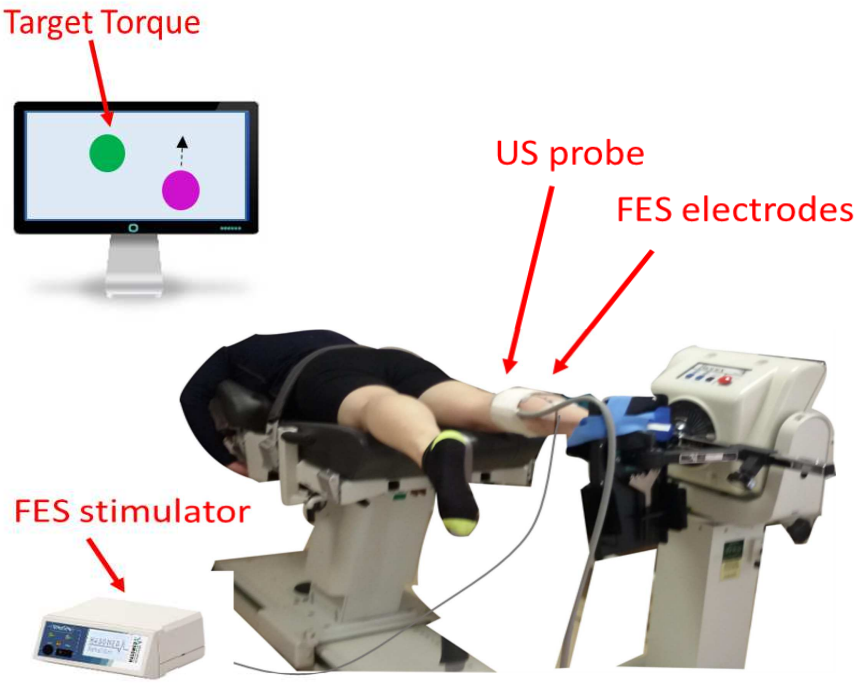

Figure 5.1: Setup. The subject lies in prone position on the chair of a dynamometer (Biodex). An US probe is placed on the dominant leg which is fixed to the footplate of the dynamometer. Electrodes for FES are placed on the muscle belly or behind the knee, respectively during Session 1 and Session 2. The US probe was placed on the muscle belly during both sessions. Visual feedback of the torque exerted is given on a screen, indicated with a pink ball. The subject is asked to push against the platform in order to align the pink ball to the green ball shown on the screen.

The FES test (SS during Session1 and NS during Session2) was performed first. During the FES test the subject was asked to relax while the stimulation train was applied and the torque exerted and the US video were recorded. A total of eleven tasks corresponding to the eleven stimulations were performed.

The torque levels measured during the FES test at three different stimulation intensities were used as visual feedback for the voluntary test. During the voluntary test the subject was asked to push his/her foot against the footplate following a signal displayed on a screen. The signal on the screen corresponded to the visual feedback previously mentioned. The voluntary test was composed of a total of three tasks for each subject.

The torque was recorded with 16 bit resolution at 1 kHz while the US video was recorded at a frequency of 40 fps.

5.3.2 Protocol

Eleven healthy adults, seven females and 4 males age 29.4 ± 6.8, volunteered to participate in the study. No participant had history of neuromuscular disorders. The study was approved by the University Ethics Committee and all the subjects gave written informed consent.

A flow chart summarising the protocol for both the FES and voluntary test is shown in Figure 5.2.

To run the FES test, the current, the pulsewidth and the frequency of the stimulation must be set. The frequency was fixed at *33Hz* for the whole experiment. The parameters of current and pulsewidth of the stimulation were customised for each subject according to an activation curve test which was performed at the beginning of each session. The activation curve test consisted of two parts:

- current selection
- pulsewidth selection

In order to set a value for the current, different values of current were tested and their effect was evaluated through the recruitment curve obtained. The recruitment curve shows how the torque changes as a function of the electrical stimulation applied and it is proportional to the amount of muscle fibers recruited. For each current a pulsewidth increasing from 0 to 300 μs over a time of 10 s, was applied and the torque output was evaluated. The current chosen was the one which produced a curve that increased slowly and reached a plateau, while not inducing a significant increasing in torque compared to the previous value of current tested. An example of current selection by the evaluation of the recruitment curve is shown in Figure 5.3.

After the selection of the current, a minimum pulsewidth value $PWmin$ was chosen as the pulsewidth that produces a value of torque of 5 Nm. Starting from the value, $PWmin$, ten other values at increment of 10 μs were considered.

For the FES test a total of eleven different stimulations patterns were applied in a random order. During all stimulation patterns, the current was fixed at the value identified in the previous step of current selection while the pulsewidth was varied between the minimum value, $PWmin$, to the maximum value, $PWmin{+}10 \times 10$ μs. An example of the pulsewidth train used for an FES test is shown in Figure 5.4.

Each stimulation pattern was applied with a ramp profile composed of three phases of $5s$ each: a rising phase, a constant phase and falling; see Figure 4.6 in Chapter 4.6.2. Each of these

phases correspond, respectively, to a specific stage of the muscle contraction: the recruitment, the isometric contraction and the de-recruitment.

The torque measured during the stimulations at intensities $PWmin$+20 μs, $PWmin$+60 μs, $PWmin$+100 μs was used as a visual feedback for the voluntary test. The torque signal was associated with the movement of a ball on a screen. The participant was asked to push his foot against the plate of the dynamometer and the torque measured was used to guide the movement of a second ball on the screen. The instruction to the participant was to align the two balls. The voluntary test was composed of a total of three tasks.

Throughout these sections the eleven stimulation tasks obtained applying different pulsewidths from $PWmin$ to $PWmin$+10 $\times$ 10 μs will be referred as *Intesity 1* to *Intesity 11* respectively. While the three voluntary tasks as *Torque Level 1*, *Torque Level 2* and *Torque Level 3* which had comparable torque with the torque measured during the stimulation test at Intensity3, Intensity7 and Intensity11.

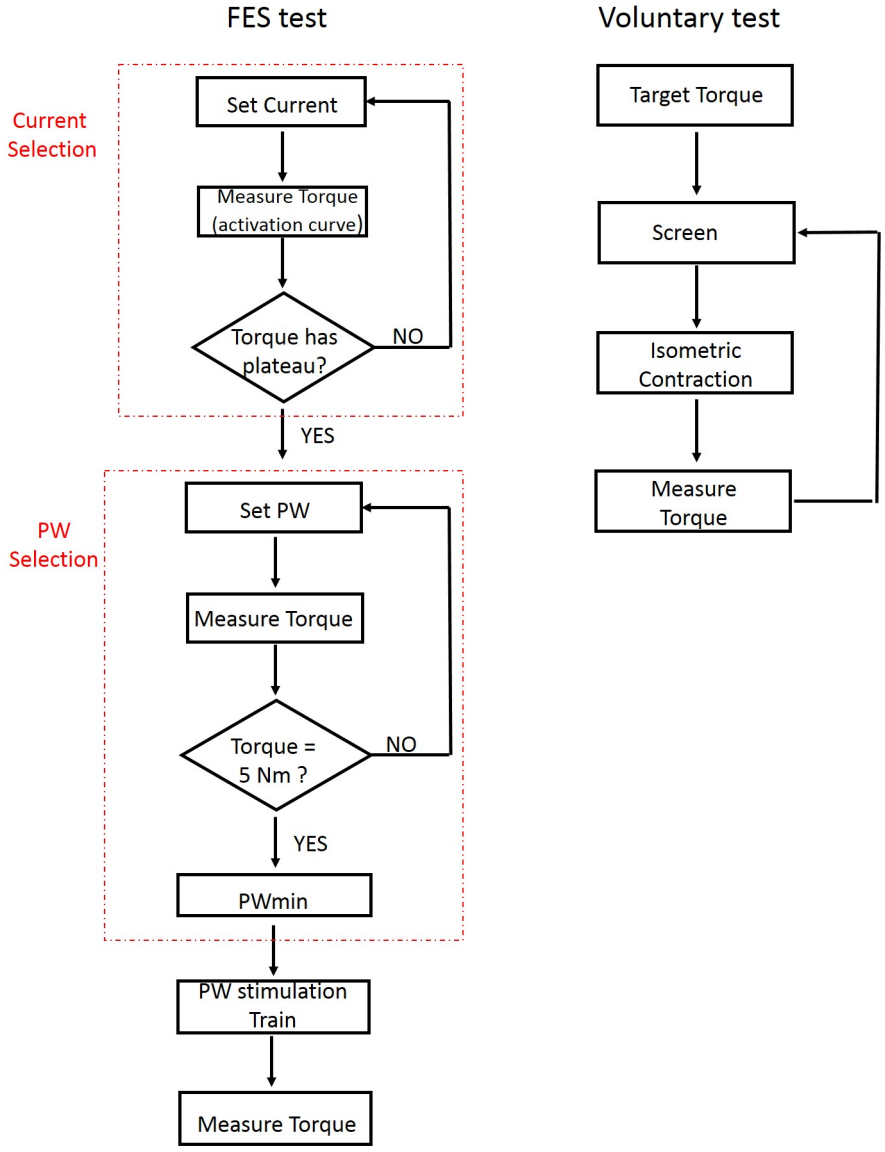

Figure 5.2: The figure shows the protocol used for the FES and the voluntary tests. The FES test includes the setting of the parameters for the stimulation (current and PW selection) and performing the task (the application of a stimulation train). The voluntary test involves the recording of the torque exerted during isometric contraction performed by a subject who is asked to follow a target on a screen.

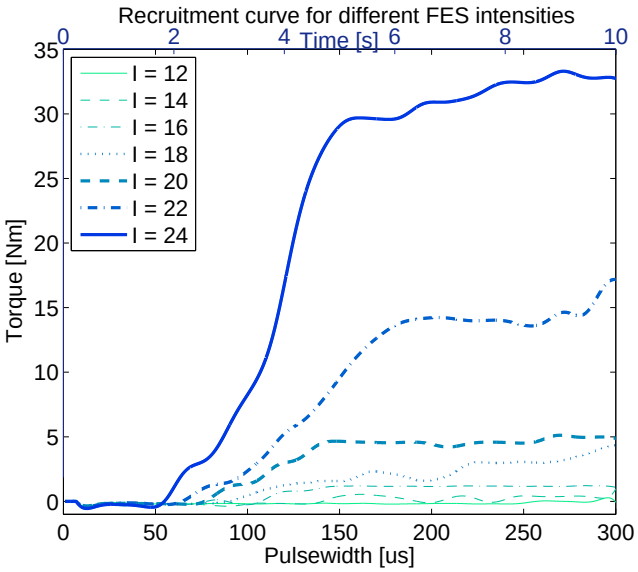

Figure 5.3: The figure shows the recruitment curve at different current intensities. Each line represents a test where the current is fixed and the pulsewidth increases form 0 to 300 μs in a time of 10 s. In the graph, it is possible to observe how the torque increases when changing the amplitude of the current form 12 mA to 24 mA. At 12 mA no significant torque is produced. At 20 mA about 5 Nm of torque are exerted. At 24 mA the torque reaches a plateau at a time between 8 and 10 s; this value is therefore chosen for the test

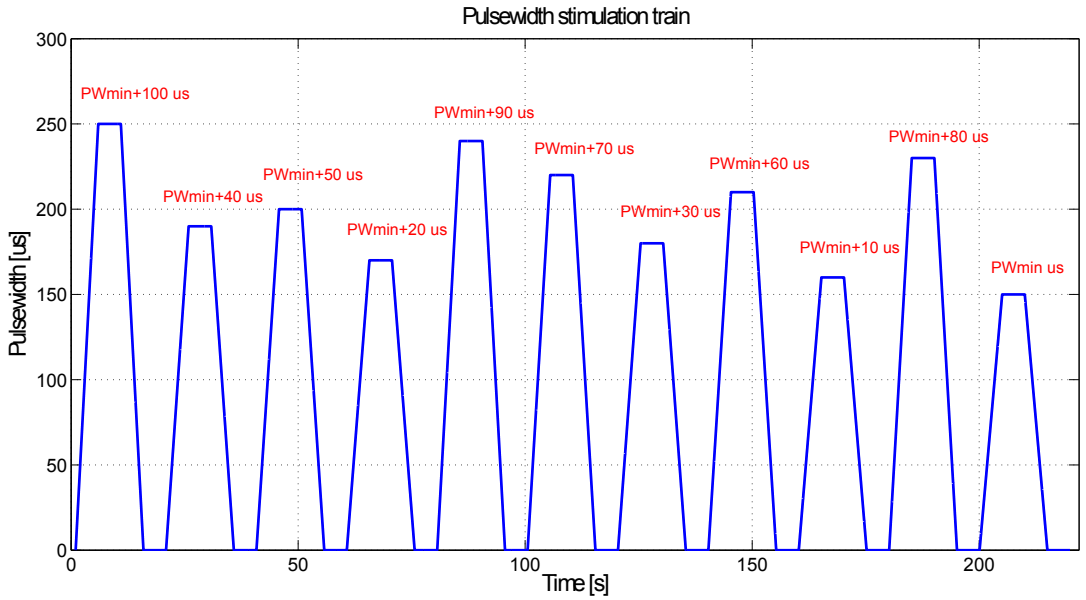

Figure 5.4: Eleven different intensities were used for the FES test. The current was fixed at the value selected using the recruitment curve in Figure 5.3 and the frequency was fixed at 33 Hz. The parameter of pulsewidth varied from a minimum value, *PWmin*, to a maximum value, *PWmin+100 μs* , as shown in the graph.

5.4 Results

The main findings of the study will be discussed in these sections.

5.4.1 Muscle displacement measurements

The first step consisted of visualising the muscle displacement during the SS, NS and voluntary contraction indicated as Vol. For each probe of the tracking software, the displacement over time was calculated.

The displacement was given at each depth; an example for one trial is shown in Figure 5.5 during voluntary contraction, SS and NS. Each subplot of the figure shows 8 lines corresponding to the displacement of the 8 probes composing each row and indicated in a scale of red from light red (row 1) to dark red (row 8), cf. Figure 3.3. The lines are more homogeneous and less spread during voluntary contraction than during SS and NS suggesting less proximal-distal differences in muscle displacement during voluntary contraction and more during SS and NS. In all three cases the deeper regions of the muscle move more than the superficial ones, indicating that the muscle displacement increases with depth.

The graphs in Figure 5.5 correspond to the results obtained for only one trial, which means one stimulation intensity in the cases of SS and NS and one voluntary torque level. The graph is similar to the displacement graphs shown in Figure 4.8, but in this case the ramp time is 5 seconds. Therefore the phases are: rise 0 to 5 seconds, constant 5 to 10 seconds, and fall 10 to 15 seconds But what happens when the intensity of the current or the torque level increases? Figure 5.6 shows example data across different intensities and it can be seen the amount of displacement depends on the intensity of the stimulation in both SS and NS. Similarly in the case of voluntary contraction higher displacement is observed at higher torque levels.

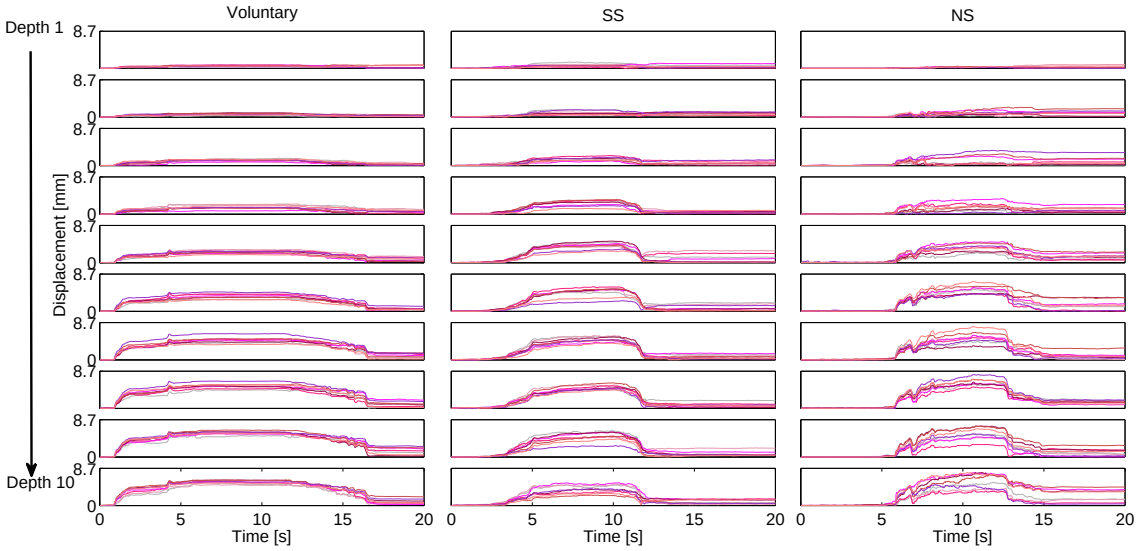

Figure 5.5: Example of muscle displacement estimated with USI during voluntary, SS and NS for one subject and one trial. In each subplot the displacement of the eight probes composing the correspondent row is shown. The displacement within the same row, is obtained at the same at the same depth. The Voluntary task displays more homogeneous displacement (i.e lines less spread) along the depth than the SS and NS. The displacement increases with depth in all three cases showing superficial regions almost stationary during the task.

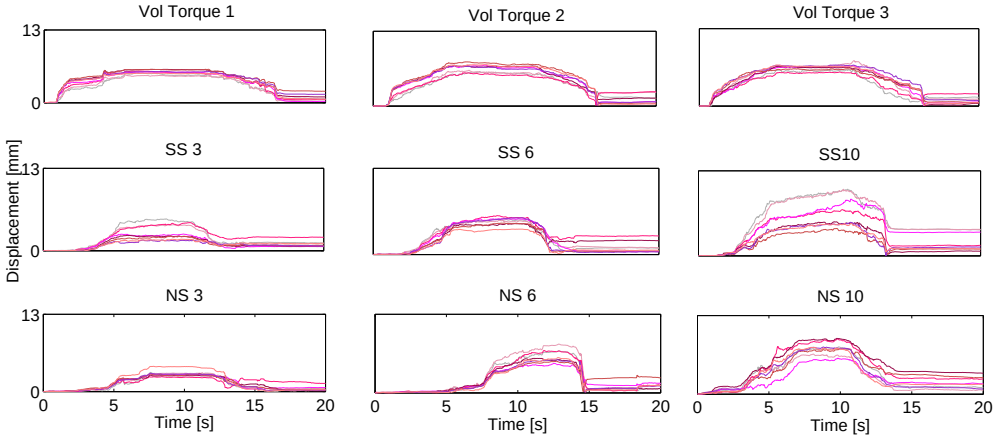

Figure 5.6: Example of muscle displacement for one subject during three trials of voluntary, SS and NS contraction. Reading form left to right, each trial has increasing current intensity for the SS and NS tests and increasing torque for the voluntary test.

As shown above, the results indicate that more displacement is observed at stronger contractions. Thus we can hypothesise that the displacement is proportional to the strength of the contraction in both the cases of voluntary and electrically stimulated muscle activations.

Figure 5.7 shows the mean displacements for all the subjects at three representative depths for the SS, NS and Vol tests.

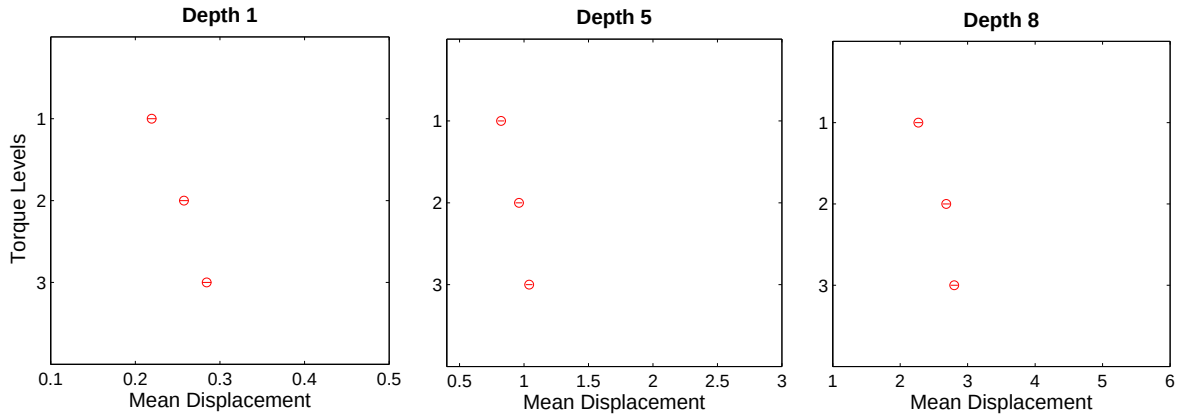

(a) Voluntary

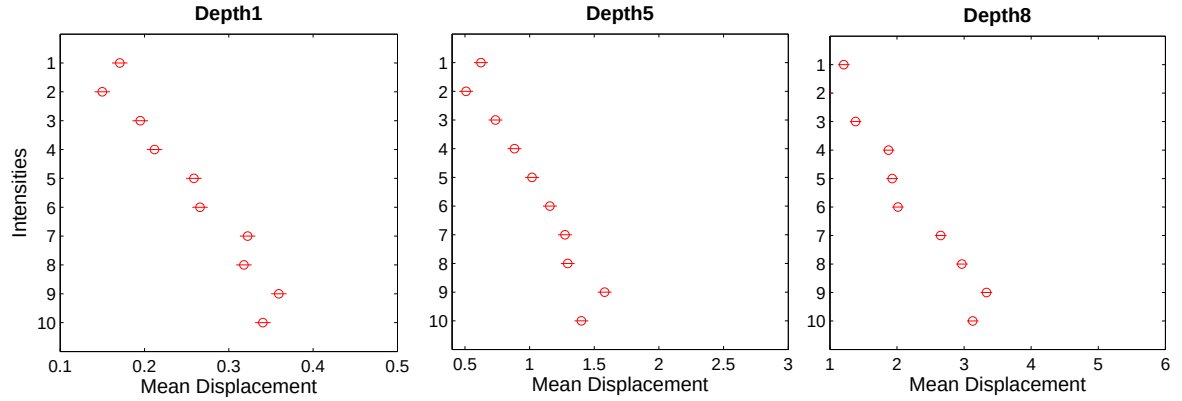

(b) Surface Stimulation

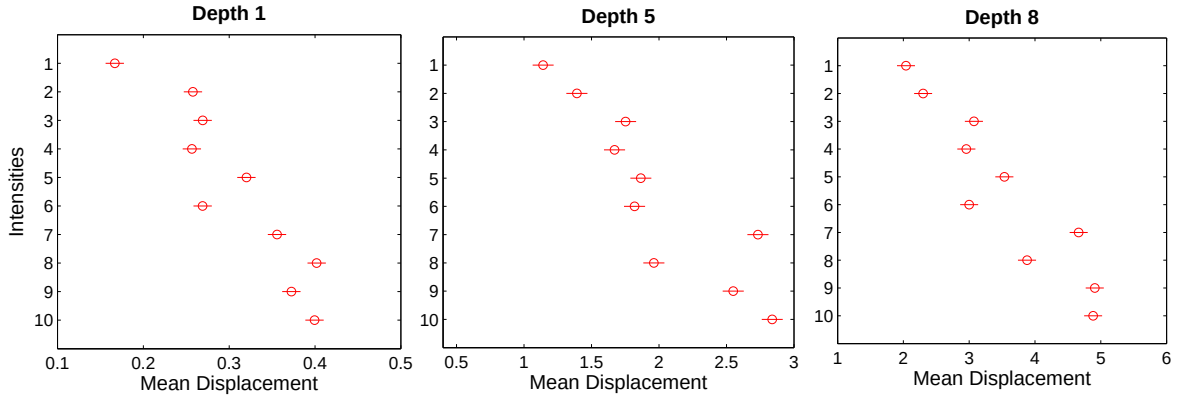

(c) Nerve Stimulation

Figure 5.7: The figure shows the mean displacement obtained for all the subjects during the voluntary, the SS and the NS tests. Each subplot refers to a particular depth, respectively Depth1, Depth 5 and Depth 8.

5.4.1.1 Muscle displacement curve as function of depth

In the previous sections it was shown that the muscle displacement changes over different depths. Thus, the next question is: can a characteristic curve for the muscle displacement at different

depths be identified? And, is the increment in displacement between adjacent depths constant?

The following graphs are obtained from the mean displacement obtained by averaging all the probes composing one row. In this section, representative data from individual participants and the average across all participants will be discussed To identify the increment in displacement between two consecutive depths, the relative mean displacements were calculated, where the relative displacement was obtained as the difference between the mean displacement at one depth minus the mean displacement at the previous depth. The estimation of relative displacement is important to exclude the effect of passive displacement due to the muscle architecture.

In Figure 5.8 the mean displacement and the relative mean displacement obtained across different trials during session 1 (Figure 5.8 a.1) and a.2)) and during session 2 (Figure 5.8 a.3) and a.4)) for Participant 2. In Figure 5.8 a.1) and a.2) the results for Voluntary and SS tests can be compared. The displacement increases with depth in both the Voluntary and the SS cases, but the SS curves are shifted to the left (lower depth) compared to the voluntary curves. During the Voluntary test depths 1, 2 and 3 have low values of relative displacement ($\sim$ 0.5 mm) while higher values of relative displacement ($\sim$1 mm) are seen at depths 4 , 5 and 6, then decreasing to negative values. The SS test has low values of relative displacement at Depth 1 ($\sim$ 0); starting from depth 2 an increase in relative displacement is observed ($\sim$ 1 mm). In Figure 5.8 a.3) and a.4) the Voluntary and the NS tests are compared. In contrast to the SS stimulation, the trends of the absolute and relative displacement are very similar.

Consistent results between session 1 and session 2 of the voluntary are observed. The voluntary is characterised by regional peaks around the middle portion of the muscle (Depth 5).

The cases presented in Figure 5.8 a) refers to a task where the electrical stimulation was efficiently set and where the torque measured had effectively increasing values between one intensity and the next. However few cases where the parameters of the electrical stimulation were not set properly, either because of the current chosen or the location of the electrodes, were identified trough the evaluation of the torque exerted. In these cases both the graphs of displacement and relative displacement were analysed. Examples are shown in Figure 5.8 b.1) to b.4), where Figure 5.8 b.1) and b.2) show the results obtained for Participant 7 during session 1 (Vol - SS). In both cases, a clear difference in muscle activation between the electrically induced contraction and the voluntary task can be observed. Even if the torque reached during the voluntary task was identical to the torque during the electrically induced contraction, the absolute and the relative muscle displacement observed are higher during voluntary contraction than during the electrically induced contraction. In these cases the torque values measured were not showing much difference across the trials and had relatively low values ($\sim$ 10% MVC).

From graphs shown in this section the voluntary contraction appears to be characterised by a curve with a sigmoid shape. The electrically induced contraction in both the cases of SS and NS has a characteristic sigmoid shape only when the current intensity and the location of the electrodes are optimised.

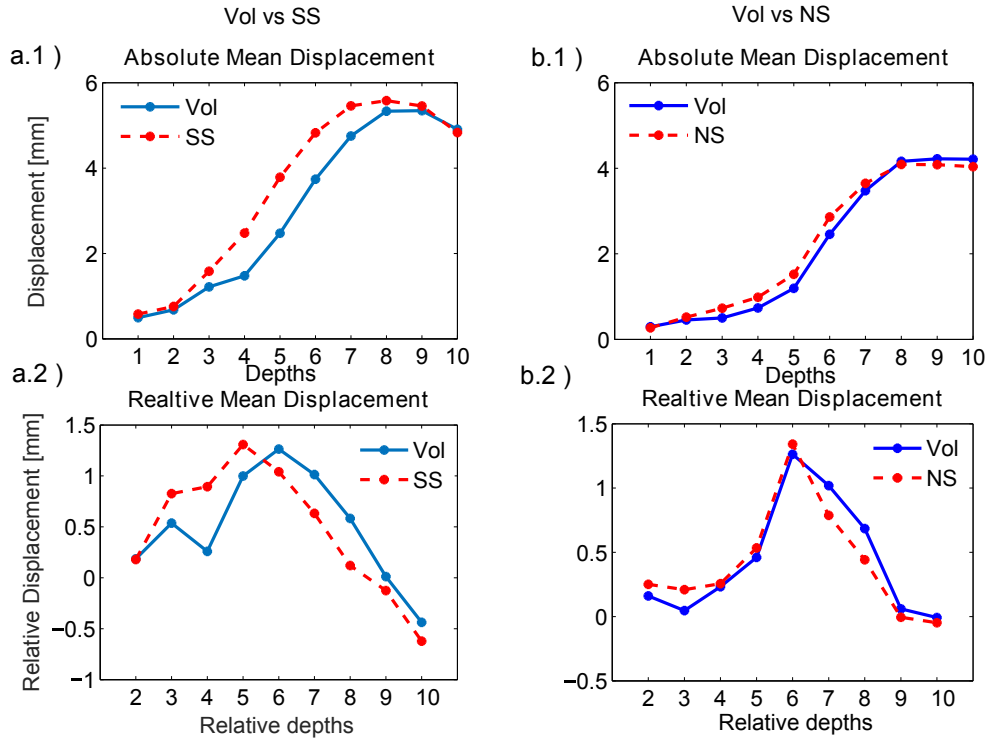

(a) Example of Efficient stimulation

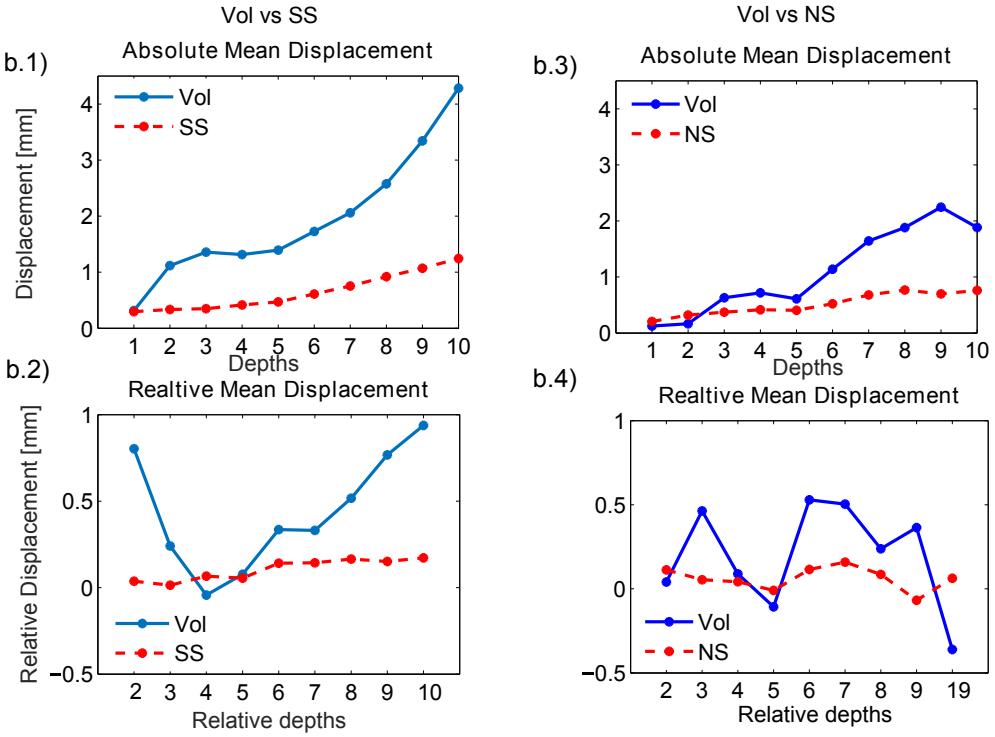

(b) Example of inefficient stimulation

Figure 5.8: In figures a.1) to a.4) Mean displacement and relative mean displacement for Participant 2 during an efficient stimulation. Inefficient stimulation is shown in Figure b). Where Figure b.1) and b.2) refers Session 1 of Participant 7 and Figure b.3) and b.4) refers to Session 2 for Participant 1

The overall behaviour is evaluated by averaging the displacement across subjects. To show whether the intensity of the current influences the shape of the curve, the muscle behaviour when stimulating the muscle with different intensities was observed. Figure 5.9 represents the mean displacement and the mean relative displacement obtained for all the subjects across different trials (different intensities) during Session 1 and Session 2. It shows how the displacement curve changes across different current intensities. During SS, Figure 5.9 a), the displacement curve has a linear behaviour at low current intensities. Increasing the current, the curve assumes a sigmoid shape. Likewise, the relative displacement during SS has a smooth uniform curve which appears flat at low intensities and more concave at higher intensities. In particular, at higher intensities the middle portion of the muscle (relative depth 3 to 7) is almost uniform and the extremities of the curve (relative depths 1, 2 for the surface of the muscle and relative depths 8 and 9 for the deeper muscle) have lower values of relative displacement.

During NS, the displacement curve increases with the intensity applied, see Figure 5.9 b). Regarding the relative mean displacement, the current intensity still influences the trend of the curve that has lower relative displacement at low intensities. However a non smooth curve can be identified across the different intensities with more variability across the relative depths at higher intensities. The behaviour at relative depth 1 is quite unexpected because it shows an increasing in amount of relative displacement with the current intensity

The voluntary contraction, which is performed in the same way during both Session 1 and Session 2, shows a displacement curve with a sigmoid shape and an uneven relative displacement curve at the different torque levels. The relative displacement curve is characterised by a curve which increases form relative depths 4 to 6 and decreases from relative depths 6 to 8. Relative depths 1 and 2 are almost similar while depth 3 has lower values.

In all cases, SS, NS and Vol the depth 10 has less displacement than the previous depth causing a negative relative displacement at relative depth 9.

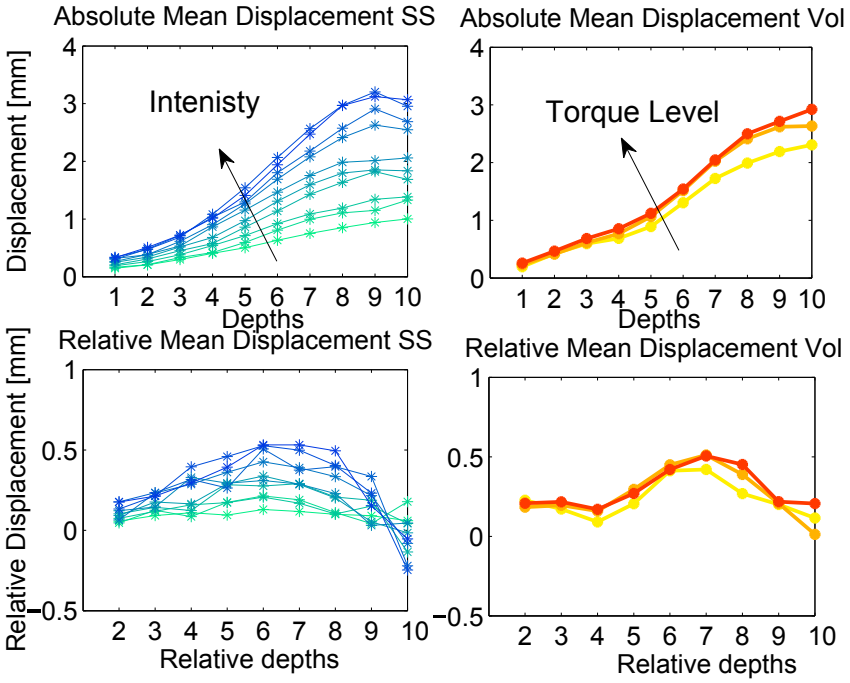

(a) Session 1

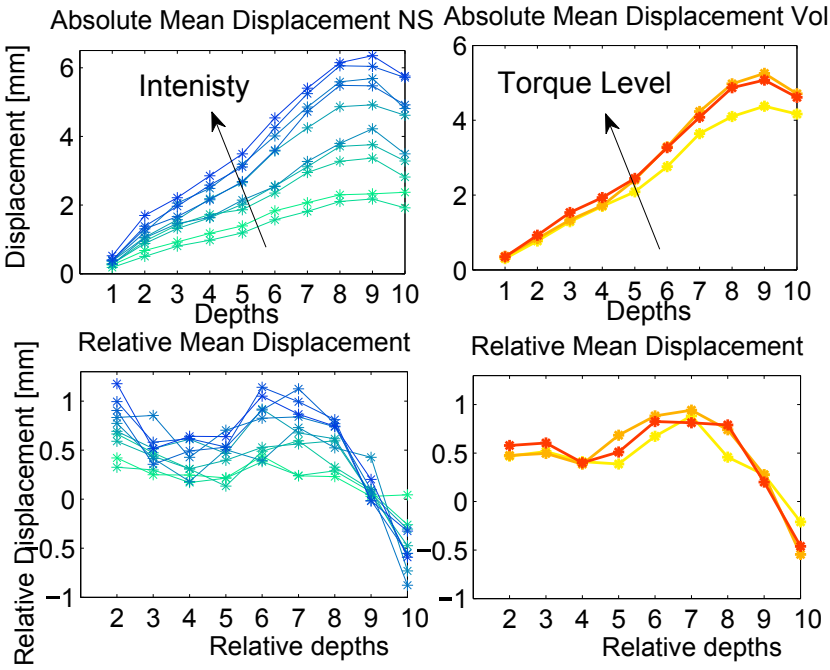

(b) Session 2

Figure 5.9: Figure a) and b) show how the displacement changes across the depths and when applying different intensities or performing the task at different torque levels during session 1 and session 2. The graphs are obtained by averaging across all the participants.

5.4.2 Analysis of Strain and Strain Rate Distribution

In this section, the *strain* and the *strain rate* of the muscle are analysed during the different contractions. The strain represents the change in dimension from a resting state to the one achieved following application of force, while the strain rate represents the rate of the deformation. Thus the analysis of the strain distribution gives information on the regional deformation of the muscle.

The measurements of strain were calculated in both vertical and horizontal directions and by averaging the measurements across different rows (depths, cf. Figure 3.4 a.1) and b.1)) and different columns (proximal-distal, cf. Figure 3.4 a.2) and b.2)), as described in Section 3.3.2. However, in both the vertical and the horizontal strain, no major differences were observed when averaging according to rows or columns. Therefore in this thesis only the results related to the arrangement according to rows for both the vertical and horizontal strain will be presented and discussed.

Figure 5.10 shows the torque, vertical strain, strain rate and rectified strain rate evaluated during a task for one subject during the voluntary test. The figure is a clear example of how small changes in torque are caused by changes in muscle contractions. When no torque is produced the strain is at a zero value. When the torque increases, the strain increases too indicating that the muscle structure is expanding. When the torque is at a plateau state the strain is stable and when the torque decreases the strain returns to zero. In figure 5.10 the Strain Rate and the rectified Strain Rate are shown as well. The Strain Rate is related to changes in strain. When small fluctuations of torque are observed, changes in Strain Rate are visible as well. The rectified strain rate is obtained from the absolute value of the strain rate. It clearly shows the activation and deactivation times.

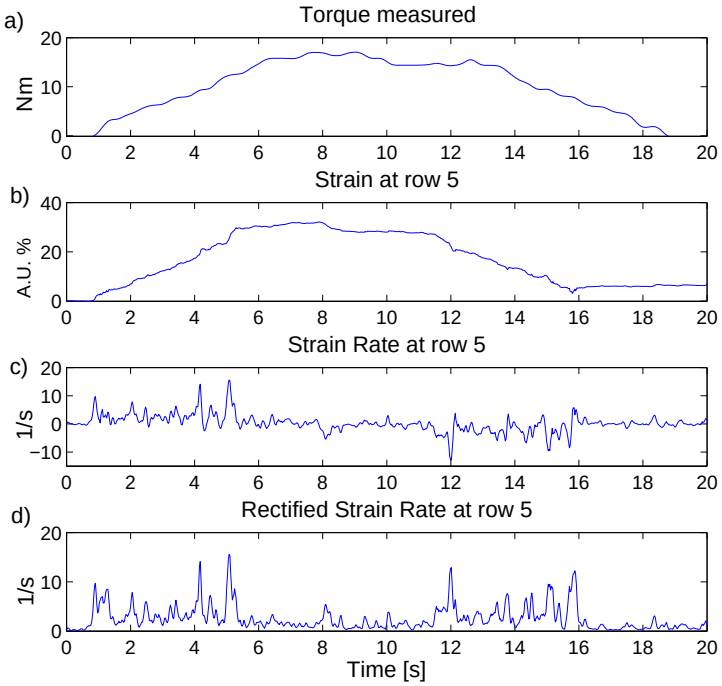

Figure 5.10: In subfigure a) the torque measured during one trial of the voluntary test for one subject is shown. Subfigure b) represents its correspondent strain evaluated at depth 6. The strain increases when torque is produced and goes back to zero when the torque decreases. In Figure c) the strain rate is shown. The strain rate, being the derivative of the strain, is an indication of variation in strain and, consequently of torque. Subfigure d) shows the Strain Rate rectified. Small fluctuations in torque correspond to variations in Strain Rate which are visible in both graphs c) and d).

Figure 5.11 shows the frequency content of the Strain Rate in the frequency domain. The figure shows respectively the Strain Rate in the time domain (Figure 5.11 a)), in the frequency domain (Figure 5.11 b)), and the power spectral density of the Strain Rate (Figure 5.11 c)). Following the Nyquist-Shannon theorem, the bandwidth is comprised between 0 and 20 Hz which is related to the sampling rate of the video (40 Hz).

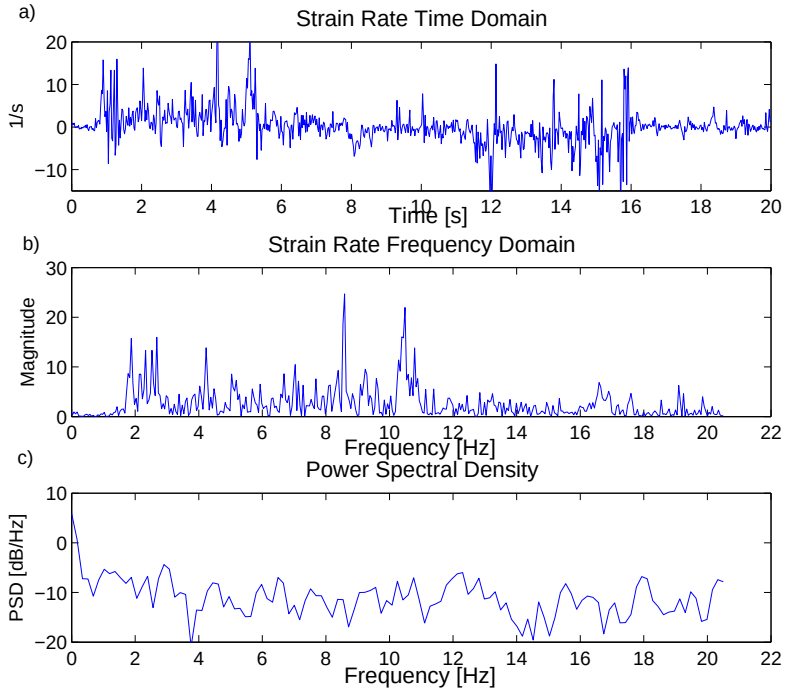

Figure 5.11: In this figure,the Strain Rate in time (a)) and frequency (b)) domain for one participant and one trial of the voluntary test and are shown. The power spectral density is shown in figure c)

5.4.2.1 Analysis of Strain and Strain Rate Distribution, average behaviour

Figure 5.12 shows the strain estimated at different depths in the vertical direction, figures a) and b), and in horizontal direction, figures c) and d), obtained during session 1 averaged across all trials and all subjects.

Figure 5.12 a) shows the strain at different depths during the voluntary test. The strain undergoes big changes between time 2 to 16 seconds, which correspond to events of the task. At time 2 seconds the task involves increasing contraction and the strain increases for depths 1 to 8 and decreases at depths 9 and 10. At time 16 seconds the contraction is released and the strain reaches a stable condition remaining positive.

In Figure 5.12 b) the results obtained during SS can be observed. During SS the strain is positive at all the depths. Higher strain ($\tilde{5}\%$) is observed at deeper depths (7 to 10), while depths 1 to 6 have strains between 2 and 8 %. Also in this case the changes in strain correspond to the events of the stimulation being applied. The strain rapidly increases from about 3 to 5 seconds and then increases slowly between 5 and 15 seconds. The time 15 seconds corresponds to the end of the stimulation and to the return of strain to a stable positive state.

Figure 5.12 c) and d) represent the horizontal strain averaged across different trials of session 1

for all the subjects. For the voluntary test negative strain is observed at all depths with higher percentage of strain at deeper areas (depths 5 to 10). Similar behaviour is observed for the SS test with exception of depth 10 which shows a positive peak at time 5 seconds. Also in these cases the changes in strain correspond to events of the muscle contraction.

The evaluation of both the vertical and horizontal strain indicate that the muscle expands in the vertical direction (thickness increases) but compresses in the horizontal direction at deeper areas (it shortens).

Similar results were obtained for session 2. They are not shown to avoid redundancy.

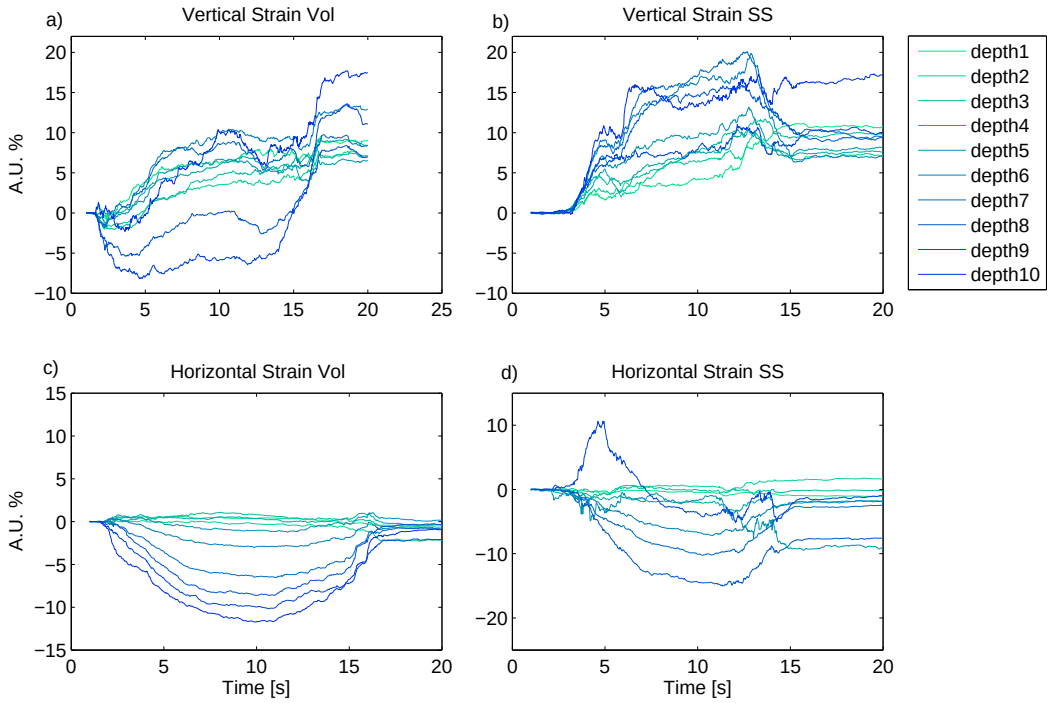

Figure 5.12: The figure shows the strain obtained for different depths in both vertical and horizontal directions averaged among all trials of session 1 and for all the subjects. In Figure a) and b), and c) and d) the strain at different depths is depicted respectively for the cases of voluntary and surface stimulation.Differences in strain distribution are observed at different depths. Vertical strain indicates expansion of the muscle while horizontal strain compression mainly at deeper areas.

5.4.2.2 Strain and Strain Rate distribution across contractions

In order to visualise the strain distribution across different portions of the muscle and over time, a bi-dimensional colormap was used.

In Figures 5.13 (a) to (c) the colormap plots of the strain averaged among subjects and for session 1 and session 2 are shown.

Figure 5.13 (a) shows the average strain obtained for the voluntary task of session 1. Null strain is indicated in figure by the color green. This is visible at all the depths at the beginning of the task (before time 2 seconds) and at the end of the task (after time 15 seconds).

During the task (between 5 and 15 seconds) a positive strain of about 5% is observed in the middle portion of the muscle. At torque level 1 positive strain is mainly identified at depths 5 to 7. Increasing the torque level, the area at high strain enlarges involving more superficial zones, i.e.depths 3 to 7 for torque level 3. The strain increases with torque reaching 15 to 20% strain at torque level 3. Negative strain is observed at deeper rows such as 9 and 10 for torque level1. It reduces its area at higher torque. At the end of the contraction high positive strain is observed. The phenomenon could depend on a failure of the algorithm to track the return of the points to their original position or to a slow response of the muscle to go back to a relaxed state.

Figure 5.13 (b) shows the mean strain distribution for the SS test at intensities 3, 6 and 11 which correspond to a torque equal to that exerted during the voluntary test. Also in this case positive strain is observed in the middle portion of the muscle. In contrast to the voluntary task, a wider area of the muscle is affected by positive strain and the values of the strain are higher. Positive strain is also observed across all the depths. Strain increases with intensity across depths with the maximum strain being observed around depths 6 to 8. Positive strain is observed also at the end of the stimulation (after time 15 seconds).

In appendix **??**, Figure B.4 (c) shows the regional strain distribution averaged across subjects when different current intensities are applied through the nerve. Similarly to the results obtained for the SS, positive strain is observed during the task (5 to 15 seconds) and after the end of the task (time 15 seconds at all depths. The area of positive strain increases with intensity involving mainly the middle and superficial regions. High strain is observed at superficial zones of the muscle, i.e. at depth 1, even at low intensities.

The result for the full set of intensities for both SS and NS are shown in Appendix **??** Figure B.3 and B.4.

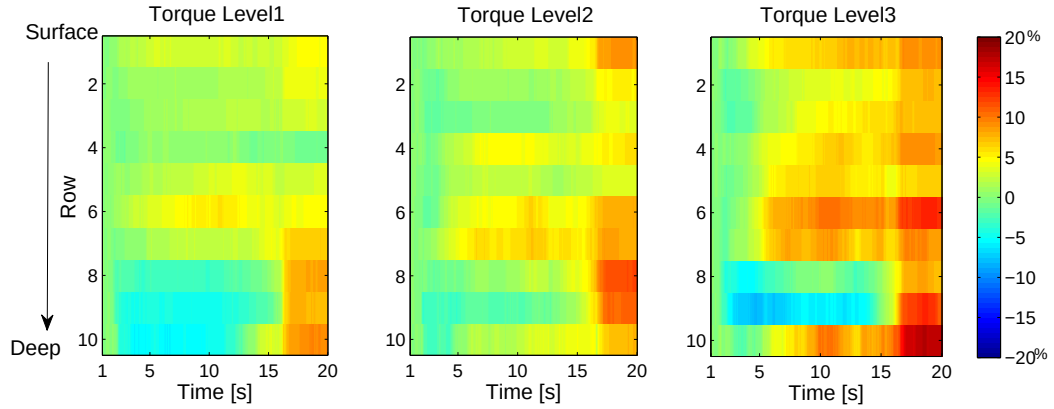

(a) Vertical Strain distribution Voluntary

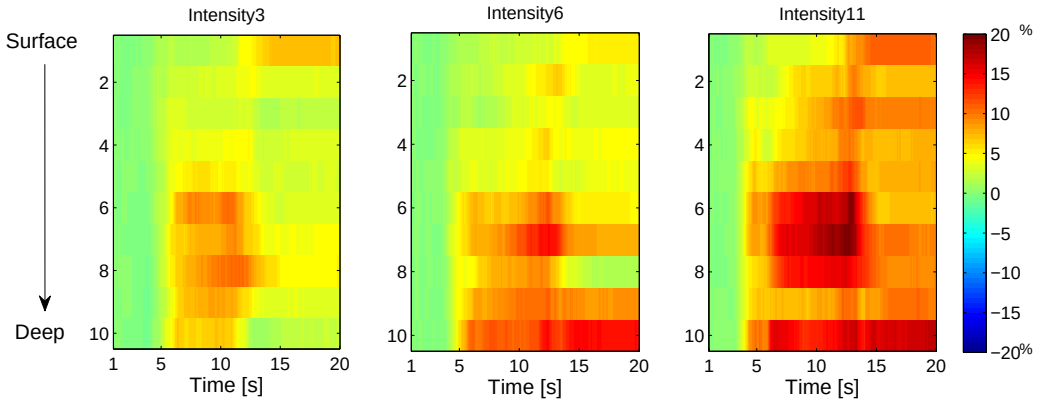

(b) Vertical Strain distribution SS

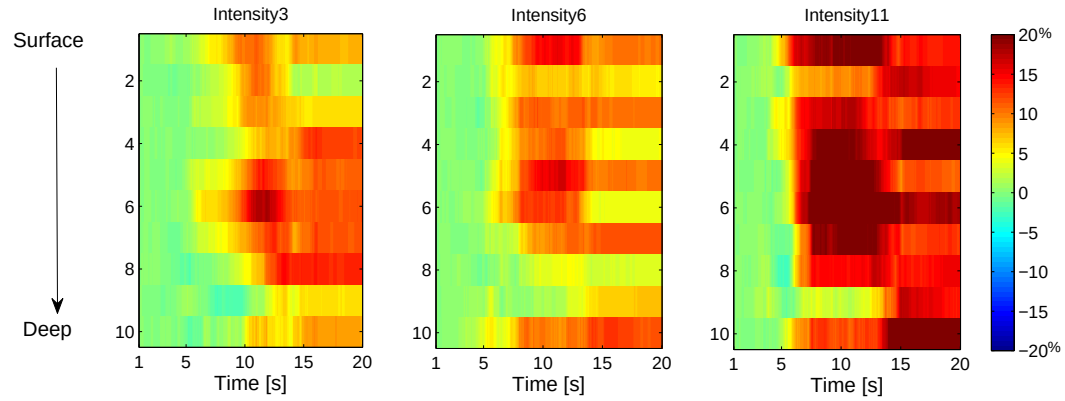

(c) Regional Vertical Strain distribution NS

Figure 5.13: In figure the average strain at each depth across subjects and during the voluntary (a) test when applying the stimulation at intensity 3, 6 and 11 for SS (b) and NS (c) tasks is shown. The y axis indicates the depth and the x axis the time of the task.

Figures 5.14 (a) to (c) show the horizontal strain across different depths.

Figure 5.14 (a) refers to the horizontal strain averaged across subjects for the voluntary test of session 1. Negative strain is observed during the contraction time 2 to 15 . For torque level 1, negative strain of about 20% is observed at depth 10 and positive strain of 5% at depth 8. The

strain is estimated to be slightly negative in some middle areas and slightly positive at depth 8 ($\varepsilon = 5\%$). At torque level 2 and 3 negative strain interests the deeper regions of the muscle mainly from depth 6 to depth 10. The strain increases with torque.

The average horizontal strain for the SS test is shown in Figure 5.14 (b). The graph referring to Intensity 3 has very similar behaviour to the graph obtained for torque level 1 in the voluntary task shown in the previous figure. Negative strain in middle areas is observed at Intensities 6 and 11. Intensity 6 has positive strain at depth 3 and depth 9 however this behaviour is not present at other depths where only negative strain is observed, cf. Appendix C. Negative strain characterises Intensity 11 in the middle portions (depths 6 to 8) while positive strain is seen at depth 10.

Similarly, Figure 5.14 (c) shows the average horizontal strain for the NS test. Middle regions and deep regions are the most affected, however a wider area has negative strain compared to the voluntary and the SS test. Also in this case the strain becomes more negative with increasing intensity.

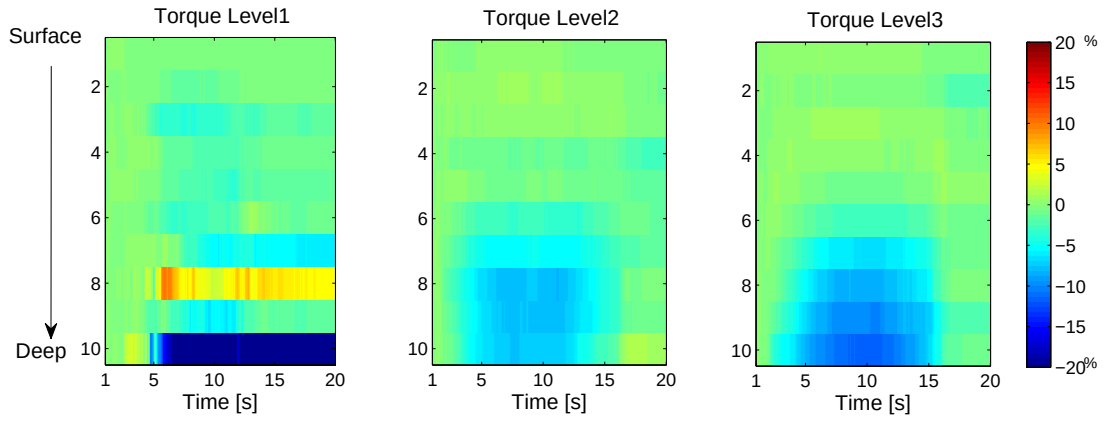

(a) Regional Horizontal Strain distribution Vol

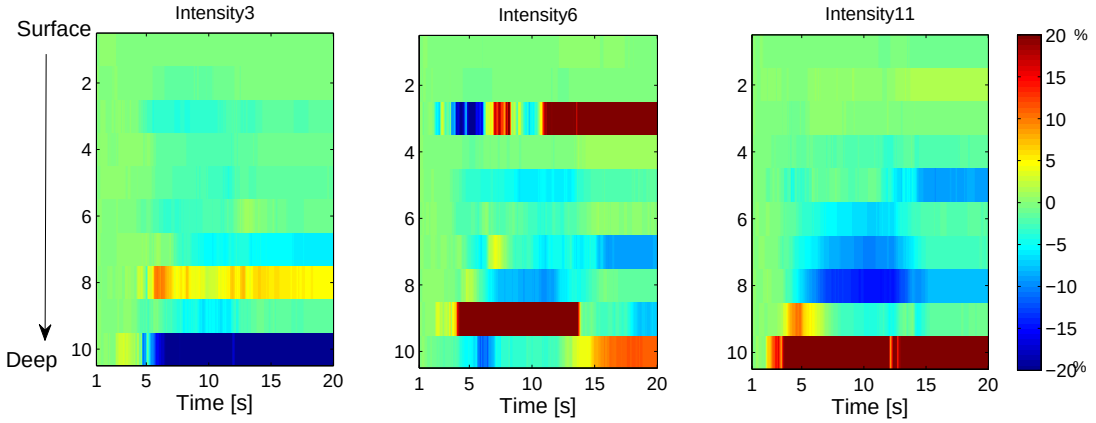

(b) Regional Horizontal Strain distribution NS

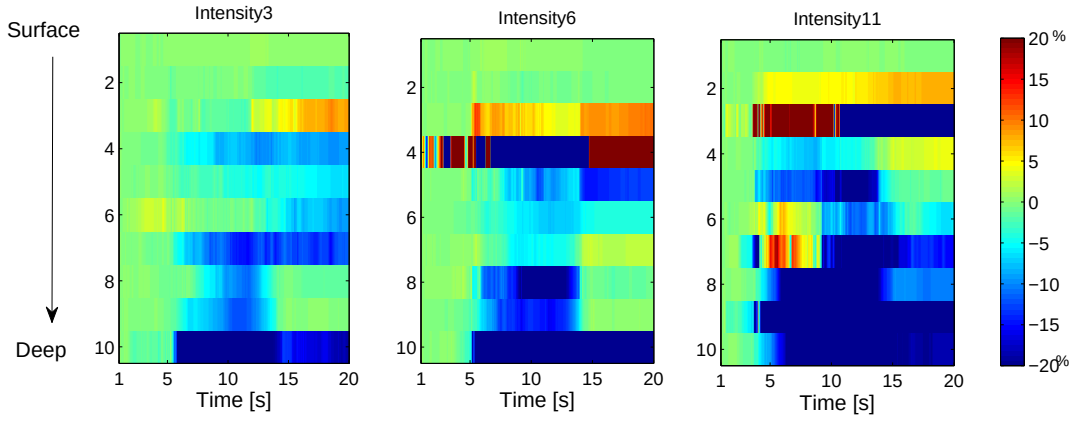

(c) Regional Horizontal Strain distribution NS

Figure 5.14: In figure the average strain at each depth across subjects and during each of the three trials of the voluntary (a) and when applying the stimulation at intensity 3, 6 and 11 for SS (b) and NS (c) tasks are shown. The y axis indicates the depth and the x axis the time of the task.

5.4.2.3 Stain rate time-frequency

In previous paragraphs it was shown that the strain is related to changes in muscle shape. The next question to answer is how fast do these changes happen? The velocity of the changes in strain is represented by the strain rate.

The strain rate averaged across subjects was estimated at each depth and for each trial (i.e. for each intensity and each torque level). Time-frequency analysis of the strain rate was performed. Some representative results are shown in Figure 5.15.

Figure 5.15 shows the time-frequency analysis results for depth 7 and for three trials of the Vol test, three of the SS and three of NS tests. In Figure 5.15 the time of the events is indicated on the x-axis; on y axis the frequency content of the information is shown. The colourmap refers to the Power Spectral Density (PSD) level, where the colour red indicates higher PSD. Increases in PSD compared to the baseline (at time 0 seconds) are identified in all cases (i.e. all depths, all trials, Vol, SS and NS) at instants in time of about 5 and 15 seconds which correspond to the starting (activation), and ending (de-activation) of the contraction.

Figure 5.15 a) shows the time-frequency results of the average Strain Rate for the three trials of the voluntary test during session 1 at depth 7. At time 15 seconds changes in the colormap indicate an increase in PSD which corresponds to an event happening. The changes in the colormap in the three subfigures of Figure 5.15 a) when reading from left to rigth (from low to high torque levels) suggest that the PSD increases with torque, thus with contraction . More frequency components are idetified at higher torque levels.

Figure 5.15 b) shows the time-frequency analysis for the SS test. In this case the main events are identified at 5 and at 15 seconds for all the three intesitties. At 5 seconds the PSD has higher values than the baseline. Similarly PSD increases at time 15 seconds where more frequency components are identified compared to the activation at time 5 seconds. The PSD increases with stimulation and more frequency components can be observed at higher stimulation intensities (i.e. the last sub-figure)

Figure 5.15 c) shows the time-frequency analysis results for the NS test. Similarly to the SS case, two events are identified at 5 and 15 seconds. More frequency components are seen at higher current intensities and at time 15 seconds.

What is shown in Figure 5.15 are representative results. However the same outcomes were obtained in the other cases.

Summarising, the time-frequency analysis suggests:

- The frequency content does not change across different depths of the muscle for Vol, SS and NS. On the other hand, the PSD changes across depths but without an apparent order.
- Peaks of PSD are identified in correspondence with the activation and the de-activation times of the contraction (time 5 and 15 seconds). Higher power is visible at the de-activation time (15 seconds).
- The voluntary task shows increase in power compared to the baseline mainly at the de-activation time. Low power and very small changes in the colour-map are visible at the activation time.
- The SS and the NS tasks have increased power at both the times of activation and de-activation, with the latter having higher PSD.
- The bandwidth has a lower limit of 0.5 Hz, the higher limit is not more than 18 Hz. However since the frame rate is 40 Hz it is not possible to reassure that no higher frequency components exist.
- Frequency components are identified within the bandwidth (0.5-18 Hz) at specific frequencies. Frequencies 2 Hz and 4 Hz are always present at the de-activation and are the first visible when peaks of power are seen at the activation time.
- More frequency components are detected at at higher stimulation intensities and at higher torque levels. Thus the frequency content increases with contraction.

.

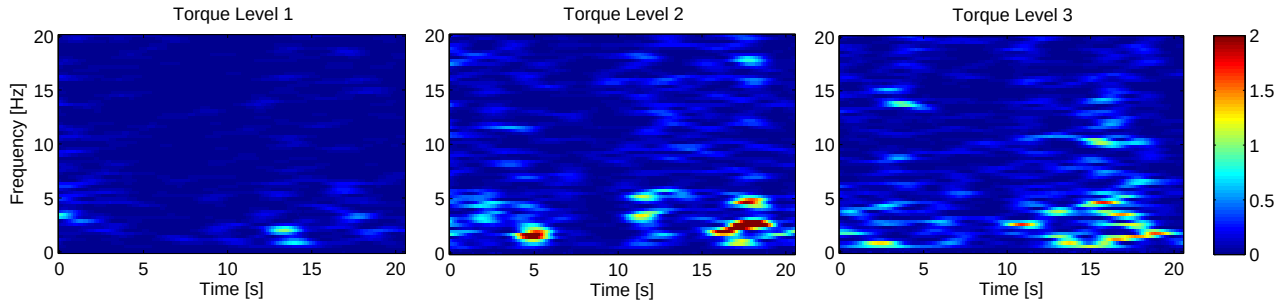

(a) Strain Rate Time-Frequency Analysis Vol

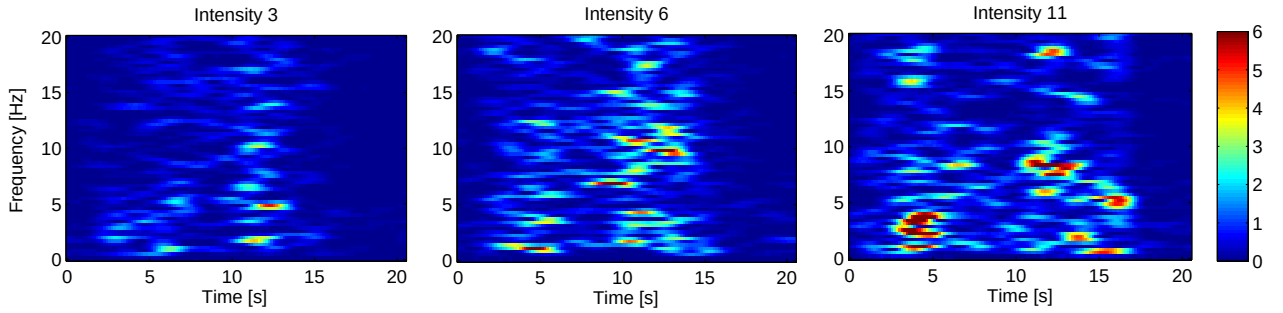

(b) Strain Rate Time-Frequency Analysis SS

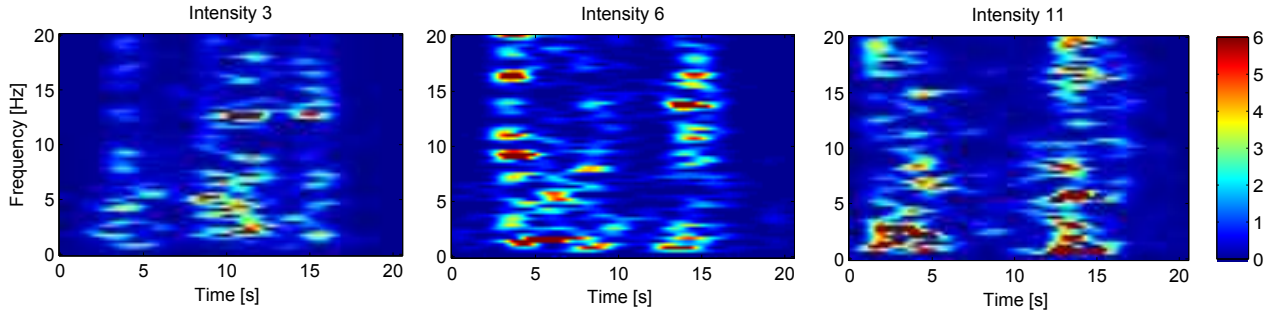

(c) Strain Rate Time-Frequency Analysis NS

Figure 5.15: Figures a), b) and c) show the time-frequency analysis at depth 7 respectively for the Voluntary test of session 1, and for Intensity 3,6 and 11 of the SS test and the NS test. The time is shown on the x-axis and the frequency is shown on the y-axis. The plots are shown as colourmap which represent the PSD of the strain rate. Lower PSD is observed during the Voluntary, therefore a different range was used.

5.5 Discussion

The aim of the study was to investigate the muscle activity during voluntary and electrically induced muscle contractions. The topic is of importance because so far, there are no studies in literature that describe the muscle activity in vivo during electrical stimulation. Previous studies used MRI images to analyse the muscle activation when electrical stimulation is applied. However, the MRI scanning does not allow real-time analysis and, in addition, the MRI represents the metabolism of the cells rather than the movement.

In this study the behaviour of a whole portion of the muscle was analysed by tracking features on the US videos recorded and allowing the mapping of muscle activation in vivo. The localisation of areas of the muscle that undergo higher mechanical activity was made possible by the technique. It is necessary to remember that the information extracted in this way represents the mechanical muscle displacement which may be caused by active contraction or represent passive movement. Parameters were identified to significantly contribute to the description of muscle activity during voluntary and electrical induced contraction. They were presented in the previous paragraphs and a discussion follows.

5.5.1 Muscle Displacement

The initial challenge was to identify what kind of biological information can be extracted from the US videos.

The first parameter recognised to be informative was the muscle displacement. The displacement was estimated by the features tracked in the US video of the gastrocnemius medialis muscle recorded while performing voluntary and electrically induced muscle contraction. The displacement of those features is directly related to the muscle contraction, in fact the muscle fibers when contracting shorten causing the muscle displacement [44].

5.5.1.1 Muscle Displacement at different depths

It was observed that superficial portions of the muscle move less than deeper portions. Similar results were obtained in previous studies where the displacement of the superficial and deeper aponeurosis was investigated [67,150]. Differences in displacement were identified and attributed to inter muscular force transmission and fascicular strain which translates into proximal - distal movement of the deep aponeurosis. Therefore, the difference in displacement between superficial and deep regions must be considered carefully because the muscle architecture and the way the forces are transmitted within the muscle make deeper portions more free to move while superficial regions are almost stationary.

A curve of sigmoidal shape was identified to be characteristic of the mean displacement at different depths during voluntary contraction. During both SS and NS tests a curve of sigmoidal shape was observed only when the stimulation resulted in effective torque. This observation was made from an a-posteriori analysis of the torque measurements. In fact the sigmoidal curve was present only when the torque exerted had values above 8% of MVC and was showing increasing torque values when increasing the intensity of the stimulations. However, since the

purpose of this study was not to identify ineffective stimulation, this assumption resulted from the examination of tasks not efficiently performed by some participants. Thus, an ad-hoc study should be prepared to confirm this hypothesis.

In this study, the muscle displacement was observed at different depths within the muscle when performing voluntary isometric contractions at different strengths and when applying different stimulation intensities through surface electrodes (SS) and through electrode placed on the nerve (NS). The quantification of the displacement showed that the displacement increased with strength during voluntary test and with intensity during electrically stimulated contraction indicating progressive muscle recruitment. In fact when increasing the current pulsewidth, more motor and sensory axons are recruited and, consequentially, more fibers [108].

5.5.1.2 Relative Muscle Displacement at different depths

Observing the increment in displacement at different depths (relative displacement), differences between voluntary and electrically induced contractions were identified. When stimulating the muscle with surface electrodes, superficial portions, just below the skin (depths 1 and 2) did not show any increment in displacement. The middle portion, from depth 3 to depth 7, moved uniformly having similar values of relative displacement. In contrast, during the voluntary contraction the increment in displacement between different depths in the muscle was more variable showing areas with larger increment, usually located at half of the muscle (depth 5). Comparing the relative displacement graphs at superficial regions (depths 1 to 4) during Voluntary and SS, a larger superficial activity was observed during SS tests.

It was generally accepted that during surface stimulation, superficial nerves are recruited, thus limiting the effect of the stimulation to fibers close to the electrodes [26,108,109,151]. However, a study by Adams et al. based on MRI images analysis indicated that deeper areas are active during surface stimulation, even at low intensities [109]. In this study the relative displacement graph during SS showed more activity at superficial areas than Voluntary and at the same time indicated activation at deeper areas. The results can be explained by considering that motor nerves, even if superficial, have spread branches which can reach deeper fibers [26].

The relative displacement observed during nerve stimulation was variable and more similar to the voluntary stimulation. However in both surface and nerve stimulation the amount of increment in displacement was comparable with the voluntary at higher current intensities. Previous studies showed that nerve stimulation and surface stimulation over the muscle belly recruit fibers through different pathways. The muscle belly surface stimulation generates contraction

by depolarising the axons beneath the stimulation electrodes and spreading within the muscle through a *peripheral* pathway. Conversely during nerve stimulation the contraction is generated through *central* pathways by the synaptic activation of motor units in the spinal cord, similarly to the voluntary contraction [106, 108]. The relative displacement graph shows indeed more similarity between the NS and voluntary rather than SS and voluntary conditions.

The fact that the relative displacement graph shows spiky behaviour during Voluntary and NS but not during SS gives rise to some hypotheses about the location of muscle innervation zones (IZ). The IZ is the site where motor neurons and their axons innervate the muscle. During NS the current spreads from the nerve to the muscle through nerve branches reaching the fibers at the neuromuscular junctions (NMJs). The relative displacement graph showed selective activation in some areas which might be related to the NMJs distribution. Localisation of IZ is a topic of interest for optimisation of electrical stimulation. It was shown in fact, that stimulation via motor point (the correspondent of the innervation zone on the skin) maximises the efficiency of the task [152]. In addition IZ is used in neurophysiology research to study the muscle morphology or, in pathological condition, such as progressive dystrophy (i.e. Amyotrophic Lateral Sclerosis), to track the alterations caused by the disease [153].

5.5.2 Strain and Strain Rate

Other parameters identified to be significant were the strain and the strain rate of the muscle which are indicative of the muscle contractile activity [136].

Previous studies analysed only the fascicle strain limiting the information to one measurement. In this study the local strain and strain rate were estimated and, thanks to a bi-dimensional colormap plot we were able to display the strain at different depths in the muscle and over time. The results obtained will be discussed in the next paragraphs.

5.5.2.1 Strain Measurement

In this study local strain was evaluated during voluntary and electrically induced muscle contractions. Local strain measurements were performed both in vertical and horizontal directions representing, respectively, changes in muscle thickness and muscle length.

During fixed-end contractions the muscle fibers shorten and tendons stretch [51]; muscle fascicle shortening is accompanied by changes in fascicle girth resulting in changes in muscle geometry [154]. In our results, the change in shape is represented by a positive strain in the vertical

direction (muscle thickness increases) and a negative strain in the horizontal direction (the muscle shortens).

A two-dimensional colourmap was used to display the muscle strain distribution over time. Positive vertical strain was observed during the tasks in both the cases of voluntary and electrically induced muscle contractions (both SS and NS). Positive vertical strain was identified in the middle portion of the muscle while negative horizontal strain was observed mainly at deeper regions during both voluntary and electrical induced (SS and NS) muscle contractions. The phenomenon can be associated with the way the force is transmitted within the muscle.

The fiber contracts as a consequence of neural stimulation which is initiated at the level of the neuromuscular junction (NMJs). NMJs are the synapses of the nerve terminal branches. In motor nerves they are usually located at the mid-point of a muscle fiber so that, when excited, they transmit action potentials on both sides traveling to the proximal and distance tendons [153, 155]. The GM muscle is characterised by *spanning* fibers which means that they span along the entire fascicle, from the tendon of origin to the tendon of insertion [52]. Therefore the NMJs should be located approximately in the middle portion of the muscle. The areas at higher vertical strain could be related to the location of the NMJs.

The horizontal strain has more negative strain at deeper regions indicating that the areas closer to the deeper aponeurosis undergo more shortening. Again the phenomenon is associated with the force transmission. The fiber contraction and rotation results in force transmission to the aponeuroses. Studies in literature documented differences between the force transmitted at the proximal and distal aponeuroses [124,127]. Therefore the differences in horizontal strain between superficial and deeper areas can be associated with the proximal-distal force differences.

The strain was observed to be higher and distributed in larger areas at higher torque levels or intensities of stimulation. To increase the power output animals recruit more motor units, increasing, as a result, the number of fibers involved [12]. The strain distribution map therefore describes the areas the areas of the muscle which undergo larger mechanical changes.

Higher positive vertical strain and more negative horizontal strain characterise the SS and NS tests at wider areas of the muscle when compared to the voluntary tests. During voluntary contraction, the soleus muscle, located just below the GM is contracted as well limiting the room for movement (and shape changes) of the gastrocnemius and contributing to the force exerted. The extension of mechanical changes (area of larger changes in strain) for SS and NS tests at low and high stimulation intensities is comparable with the area active during a voluntary contraction at high torque (torque level 3). This can be related to the inability of the

electrically induced contraction to switch across motor units (and therefore fibers) keeping the number of active motor units high.

5.5.2.2 Interpreting the Strain Rates

The strain rate was estimated directly from the derivative of the strain. Therefore high amplitude of strain rate is related to higher changes of strain. However, in this study not only the amplitude of the strain rate was estimated but also its frequency content, where the frequency components were related to the occurrence of changes in time. In other words, the power of the strain rate indicated how much change in strain is observed while the frequency indicated how often those changes happened.

A time-frequency approach was used to identify the time, frequency and power spectrum of the strain rate measurements. Four main findings were observed.

- The frequency content was uniform across all the different depths but the power spectrum showed small differences across the depths.
- Increases in power spectrum were identified in correspondence with the event of activation, when starting the task, and deactivation, when ending the task.
- Higher power spectrum and more frequency components were observed with increasing torque level or current intensity.
- Differences in frequency components and power spectrums were observed between Voluntary and electrically induced contractions.

Those findings are in agreement with the physiology of muscle fiber recruitments. Skeletal muscles are composed of two types of fibers, slow-twitch and fast twitch which have defined physiological and mechanical properties [15, 83]. It was shown that faster motor units (which recruit fast-twitch fibers) are better suited to develop force rapidly causing muscle fibers to shorten at higher strain rates. In contrast, tasks such as maintenance of posture are performed by slow-twitch fibers that shorten at low strain rates [117]. When force increases more motor units are recruited preferring faster-twitch fibers. Faster fibers are characterised by strain rate and activation-deactivation rates are two or three times higher than that of slow fibers [117].

Combing now the findings of the study with previous knowledge the following conclusions can be made. The increase in the number of motor units recruited and of fast-twitch motor units with force is related to the increase in power spectral density. The same explanation can be associated

with the increase in frequency components. In fact muscle fibers within one motor unit have similar biochemical and contractile properties [15, 156]. Therefore, increasing the number of motor units means increasing the variability in strain rate which translates into having more frequency components. Increasing power spectral density with force output is a consequence of the increasing number of motor units recruited and of fast-twitch motor units.

One main finding of this study was the difference in the power spectrum at the activation time between voluntary and electrically induced contractions. As sated previously faster motor units are activated at higher a strain rate. Our results showed higher power spectral density, and therefore higher strain rate, at the activation time during electrically induced contraction. This clearly indicates that during electrically induced contraction fast-twitch fibers are recruited at the activation time. This is not observed during voluntary contraction. The recruitment of fast motor units during FES induced contraction is a well-known phenomenon and is identified as one of the main causes of the premature muscle fatigue during FES.

5.6 Conclusions

In this chapter three main parameters were identified to give insights into the muscle activation: the displacement at different depths, the strain and the strain rate. The muscle activation was investigated under different conditions: during voluntary contraction and during electrically induced contractions obtained with electrodes placed on the muscle belly and on the nerve.

The study demonstrated that US imaging is a suitable technique to map muscle activity and mainly detects differences between voluntary and electrically induced contractions.

Major differences observed between voluntary and electrically induced contractions were related to the different recruitment pathways and to the recruitment of different motor units (slow-twitch vs fast-twitch).

In addition the study highlights that the stimulation through surface electrodes is not localised to the zones close to the electrodes but rather it spread similar to the voluntary contraction.

Detailed conclusions are summarised in the next two sections.

5.6.1 Conclusions on Muscle displacement

A sigmoidal shape characterised the muscle displacement along muscle depths during both voluntary and electrically induced contractions suggesting ongoing changes mainly in the middle

portion of the muscle. However, during electrically induced contractions a sigmoid shape was observed only when the stimulation was efficient in terms of current intensity and location of electrodes. The study suggested that a test based on the analysis of the displacement curve could be helpful for choosing electrodes location and setting of the current. However further investigation and an ad-hoc study should be performed to confirm the hypothesis.

Relative muscle displacement across depths was evaluated as well and it indicated uneven activation during voluntary and NS contractions. On the contrary uniform relative displacement was observed during SS.

The similarity observed between voluntary and NS and the difference observed in the SS suggested that different pathways are involved in the process, respectively a central and a peripheral mechanism. In addition the uneven relative displacement observed in both voluntary and NS could potentially be indicative of the location of innervation zones within the muscle.

5.6.2 Conclusions on Strain and Strain Rate

Strain measurement was used to map the activation of the muscle during contraction. Positive vertical strain and negative horizontal strain were observed during contraction. Middle portions of the muscle were the most affected by changes in vertical strain while deeper regions were affected by changes in horizontal strain, suggesting that during contraction the muscle increases its thickness and shortens at deeper regions. When increasing the strength of the contraction, either voluntary or artificially by using electrical stimulation, the strain measured increased and was affecting a wider area of the muscle. Similar patterns were observed during voluntary and electrically induced muscle contractions.

The strain rate was evaluated using time-frequency analysis which allowed a description of time, frequency and power of the events. The events were identified at the activation and de-activation times. The voluntary contraction was characterised by lower power spectral density compared to the SS and NS tests. In all the cases (Voluntary, SS and NS) the power spectral density was increasing with the strength of contraction. A similar behaviour was observed with the frequency components. More frequency components were observed for contractions at higher strength. The increase in both the PSD and frequency components was related to the increase in the number of motor units and therefore in fibers, when increasing the strength of the contraction.

The main difference between voluntary and electrically induced contraction (both SS and NS) were observed at the activation time. During SS and NS an increase in PSD was observed at both the activation and de-activation time, i.e. when the task was starting or ending. In

contrast during voluntary contraction only very small increase in PSD at the activation time were observed. This suggests that during electrically induced contraction the fibers are recruited at a faster rate. Since the rate of activation depends on the mechanical properties of the fiber, during electrically induced contraction fast fibers are recruited early compared to the voluntary task. This phenomenon may explain the early fatigue during electrical stimulation.

Chapter 6

Evaluation of muscle displacement in relation torque exerted

6.1 Summary

This chapter describes the results obtained when using polynomial fitting to estimate the relationship between the torque exerted and muscle displacement obtained from the ultrasound images.

The relationship between torque and muscle morphological changes was previously investigated using ultrasound imaging, showing that pennation angle and cross-sectional area correlate with the force exerted [57,157]. In our study we introduce a new approach for the definition of a model that describes the relationship torque-muscle displacement based on the analysis the features tracked on the portion of the muscle visualised on the ultrasound video.

A total of eleven subjects were recruited for the study and voluntary and electrically induced isometric contractions were performed while the torque exerted and ultrasound videos were recorded. To analyse the relationship between the torque exerted and the ultrasound information, surface and curve polynomial fittings were implemented. Using these techniques it was possible to derive the torque-displacement relationship.

6.2 Introduction

We use polynomial fitting to investigate the relationship between features tracked in US videos and the torque exerted during a task. The initial aim of the study was to evaluate the polynomial that describes the muscle activation in healthy muscles. However, during the analysis, we understood that the data could have also been used to estimate the torque exerted by a muscle. The latter is a topic of intensive research and was not previously investigated with the US method we are proposing.

Considering the physiological significance of the matter, we decided to include both these analyses in this chapter. Sections 6.2.1 and 6.2.2 introduce briefly the significance and the problems related to both aspects.

6.2.1 Modelling muscle displacement in healthy muscles

FES of paralysed muscles is a method used in rehabilitation centres to assist patients in executing functional movements, however different problems such as muscle fatigue or atrophy following spinal cord injury make its use is still not widespread.

In some diseases or conditions such as spinal cord injury, paralysed muscles undergo atrophy which is characterised by reduction in the size and/or the number of muscle fibers and in the amount of force produced [92]. In addition after spinal cord injury, a fiber type transformation occurs which substantially affects the capacity of paralysed muscles to sustain contractions, appearing as/resulting in increasing fatigability of muscles [73, 158]. Thus both atrophy and muscle fatigue influence directly the way the muscle contracts and the force it exerts.

Knowledge of the pathway of muscle contraction and its relation to the force in healthy and diseased muscle can facilitate the design of optimal FES stimulation protocols. This means that the relationship between muscle contraction and force exerted during voluntary and FES induced contraction should be identified.

To define a relationship between two variables (in our case the muscle displacement and the torque measured) mathematical modeling techniques can be used. A range of ways to define a model exist; among these polynomial models are used to estimate and predict the shape of the static relationship of a variable over a range of input values.

As a first step, in our study we want to investigate the relationship between the GM muscle's behaviour in healthy subjects and the torque exerted. Specifically, using polynomial fitting between the movement of features tracked on US images and the torque exerted during tasks, we aim to define the polynomial which predicts the amount of displacement occurring at different depths in the muscle from the measured torque. This relationship might be different when comparing healthy and spinal cord injured people because of atrophied fibers and fiber type alteration. Furthermore, since in SCI the contraction might not be achievable voluntarily but it is usually possible with FES, we want to investigate the displacement-torque relationship during voluntary and the FES induced contractions. The results presented here are obtained with healthy subjects with the aim to form the basis for a future study where the results from healthy subjects will be compared with spinal cord injured subjects.

6.2.2 Estimation of the torque exerted by a muscle from USI

The relationship between muscle activity and torque exerted can give insights into the muscle contraction mechanism or into the quantification of the torque generated by an activated muscle. This has relevance both in biomechanics and in clinical applications.

The analysis of literature shows many attempts to quantify the torque exerted by a muscle. The biological signal most commonly used to correlate the muscle's activity and the torque produced is surface electromyography (sEMG). The sEMG reflects the degree of activation of

the skeletal muscle and indicates a high correlation with the torque generated mainly during isometric contraction [159, 160]. Mechanomyography (MMG) and Ultrasound video analysis have also shown a correlation with the torque [9, 161]. The use of US for studying the muscle function is gaining interest because it allows the investigation of deep muscles and, differently from the sEMG, it is not affected by the cross-talk of adjacent muscles. In addition the sEMG reflects the muscle electrical activity of the area covered by the electrodes while the US allows the visualisation of the whole portion of the muscle covered by the US probe. However the interpretations of US data should be made with caution since the information extracted from the US represents the mechanical consequence of the contraction [73], and can therefore include both active contraction and passive movement of tissue.

The torque exerted by a muscle has been estimated using different techniques such as artificial neural networks, support vector machines or polynomial regression [159, 160]. The polynomial regression is the most common way to estimate the force produced by a muscle.

Previous studies investigated the relationship between torque and architectural parameters such as pennation angle or CSA [9, 161]. In this study we want to investigate the feasibility of estimating the torque exerted by a muscle using the information provided by the tracking of features in B-mode Ultrasound images.

In our study we want to analyse the muscle activity of an entire portion of the muscle. Three main questions are motivating the study:

(i) Is it there a correlation between muscle displacement observed in the US video frames and torque produced ?

(ii) Do different regions of the muscle correlate in the same way with the torque produced?

(iii) Is the torque exerted the result of the contraction at different portions of the muscle?

6.3 Methodology

6.3.1 Setup and Experimental procedure

The data used for the analysis in this chapter is the same as the data used for Chapter 5. Note that only the data from Session 1 is used here. Where Session 1 consisted of a Voluntary test and a FES test where the electrodes are placed on the muscle belly. For more details about the experimental procedure, refer to Section 5.3.1.

6.3.2 Mathematical approach

The main aim of the analysis is to define a mathematical model which represents the relationship between the displacement of the muscle tracked through the US video and the torque exerted during the tasks. The relationship torque-US displacement was estimated using polynomial fitting. In particular, in our analysis we used two different approaches:

(a) a curve polynomial fitting

(b) a surface polynomial fitting.

For the theoretical explanation of the polynomial fitting refer to Section 3.6. In the next sections the two approaches are explained.

6.3.2.1 Curve fitting

The curve fitting defines the relationship of the dependent variable with the independent variable, describing how one changes as a function of the other. In our specific case, the curve fitting aimed to define the relationship between the torque and the muscle displacement at the deeper portion of the muscle, specifically at depth 9 (close to the deeper aponeurosis).

The fitting can be used either to estimate the curve that represents the displacement at a certain depth from the torque measured, or to estimate how much torque is exerted when observing the displacement at a certain depth. Basically it was implemented in a complementary way in order to estimate:

(a) the muscle displacement from torque

(b) the torque from displacement at certain depth.

In order to estimate how much displacement occurs in the muscle at a certain torque exerted, the independent variable must be the **torque (τ)**, and the dependent variable the **Displacement (δ)**. In our specific case, the dataset was composed of the torque measured during the voluntary and the FES test and the correspondent muscle displacement at depth 9 estimated form the US video recorded. One polynomial for each subject and for the voluntary and the FES tests was fitted. To find the optimal relationship, different orders of the polynomial were tested. The optimal order was chosen considering the lower error observed in the residuals; it was consistent across subjects and for both the voluntary and the FES test. The polynomial identified was of the form expressed in Equation 6.1.

$$P(\tau) = p_1\tau^2 + p_2\tau + p_3 \tag{6.1}$$

Where τ represents the torque measured and $P(\tau)$ the displacement (expressed according to its dependency from τ). The polynomial is of order 2 with a total of three coefficients (*p1*, *p2* and *p3*).

Similarly, the torque can be estimated from the displacement considering displacement δ as an independent variable, and the torque (τ) as a dependent variable. Again, only the displacement at depth 9 was considered. The polynomial fitted is a function of δ and defined as follows:

$$P(\delta) = p_1\delta^3 + p_2\delta^2 + p_3\delta + p_4 \tag{6.2}$$

Where δ represents the displacement measured and P(δ) the torque.

The polynomial is of order 3 with a total of four coefficients (p1, p2, p3 and p4). A polynomial is fitted for each subject and for the voluntary and the FES test.

6.3.2.2 Surface Fitting: Torque-displacement-depth relationship

The polynomial that describes a relationship between three variables defines the surface that best fits the data. This polynomial is composed of two independent variables and one dependent variable. The surface polynomial fitting was estimated considering torque, displacement and depth. It aimed at defining the relationship between torque and displacement taking into account the information of the depth.

To define the mathematical model that allows the muscle displacement at a certain depth to be estimated from the torque exerted, three datasets must be considered: **torque** (τ), the **depth** (w) and the **displacement** (δ). Since our purpose is to identify how the displacement changes as a function of the torque and the depth, the independent variables are τ and w and the dependent variable is δ. Therefore, the polynomial to identify is of $P(\tau, w)$ which describes how the displacement δ changes as a function of the torque τ and the depth w.

The datasets used to define the model were the data obtained during the FES test and the voluntary test per each subject. One polynomial was fitted for each subject for the voluntary and the FES test. The FES test and the voluntary test datasets were composed of eleven and three trials respectively. Different degrees of the polynomials were tested for each subject and for the FES and voluntary tests; however the best fit was obtained using the same degrees in all

the cases. The best fit polynomial estimated was of the form:

$$P(\tau, w) = p_{00} + p_{10}\tau + p_{01}w + p_{20}\tau^2 + p_{11}\tau w + p_{02}w^2 + p_{21}\tau^2 w + p_{12}\tau w^2 + p_{03}w^3 \qquad (6.3)$$

This means that an order 2 was fitted for τ and an order 3 for w for a total of 9 coefficients.

6.3.3 Model validation

To check the independence of the dataset, to avoid over-fitting and to validate the model, a cross-validation technique was used. More details about the cross-validation technique can be found in Section 3.7.

In the FES test, the dataset was devided into five groups and a *5-Fold* cross- validation was implemented. In each round of the cross-validation a polynomial was fitted considering, in rotation, four groups as *training* set and one group as *test* set. From the *5-Fold* cross-validation process a total of five polynomials were estimated. For each polynomial fitted the goodness of the fitting was evaluated using the R^2, R^2_{adj}, *RMSE* and the *NRMSE*.

The same approach was used for the voluntary test, in this case three groups were identified and a *3-Fold* cross-validation was performed. A total of three polynomials, one for each round of cross-validation, and their corresponding parameters of goodness were estimated.

6.3.4 Preliminary analysis

As explained in the setup, both the voluntary and FES tasks, consisted of a ramping isometric contraction as indicated in Figure 4.6. This means that the polynomial should be able to detect a change in the rate of curvature due to the rise, constant and fall phases. A similar polynomial is difficult to fit and would require advanced mathematical analysis. In addition, since the three phases correspond to different physiological stages of the contraction, we decided to conduct a preliminary analysis to understand how to perform the fitting with respect to the three phases. The relationship torque-displacement at the different phases of the contraction was analysed as follows:

(a) One polynomial for all the phases (the whole task)

(b) Three separate polynomials, one for the rise phase, one for the constant phase and one for the fall phase.

(c) One polynomial for the rise+constant phases

For each of these cases polynomials of different orders were tested. For the case (a) we were not able to achieve a good fitting. Case (b) offered good fitting for the rise phase; for the constant phase and the fall phase the fitting had large errors due to the starting point which is not from zero (the constant part starts where the rising part finishes, which is not zero). The case c offered a good fitting and was able to take into account the contraction from the initial recruiting of the fibers (rise phase) to the isometric part (constant phase).

Since our interest focuses on the understanding of the dynamic nature of muscle contraction and the process of fibers recruitment during voluntary and FES induced contractions we decided to only investigate in details the case (c). The following sections refer to an analysis based on the case (c), therefore the dataset is composed only of the information obtained during the rise and the constant phases.

6.4 Results

The results for the study of the relationship between displacement and torque are presented in the next sections.

6.4.1 Estimation of muscle displacement: curve fitting

The relationship between torque exerted and muscle displacement was analysed using polynomial fitting. To define how the muscle displacement changes as a function of the torque the Equation (6.1) was used. Equation (6.1) allows an estimate of the displacement when only the torque is measured.

6.4.1.1 Order of polynomial of best fit

Figure 6.1 shows the relationship torque-displacement in two participants. The fitted curve is shown for the cases of first and second order fitting. Second order fitting generally has higher coefficient of determination R^2_{adj}. The main difference between fitting with 1st and 2nd order is observed in the test dataset. The error observed across subjects in the test dataset is lower for second order fitting, however in some cases first order is also acceptable. Details about first order fitting are shown in Appendix C. The results presented in this section refer to a second order fitting as expressed in Equation (6.1).

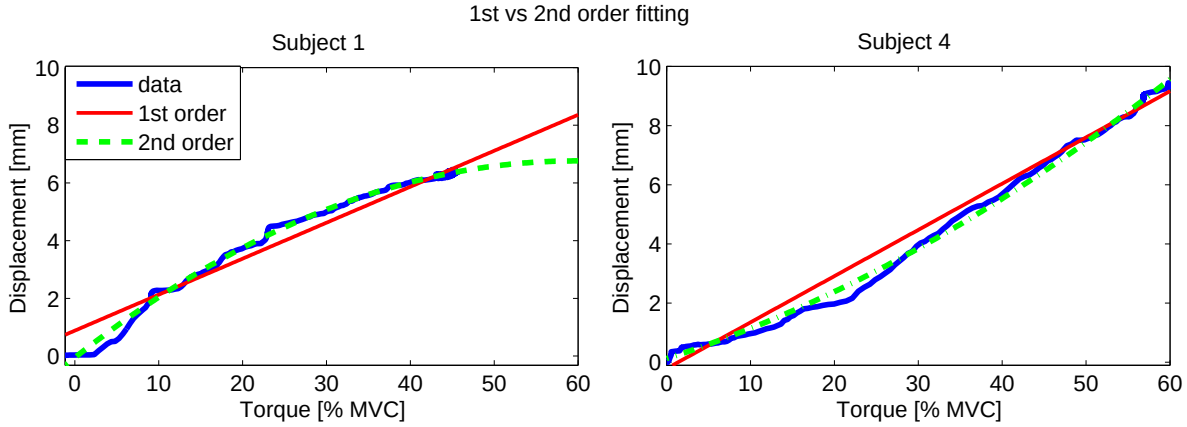

Figure 6.1: Comparison between 1st and 2nd order fitting for displacement estimation ($P(\delta)$), cases Subject 1 and Subject 2 voluntary. Subject 1 is better fitted with a second order polynomial, $R^2_{adj} = 0.74$ for 1st order and $R^2_{adj} = 0.94$ for second order fitting. Subject 4 has a good fitting with both 1st and second order, $R^2_{adj} = 0.94$ and $R^2_{adj} = 0.98$ respectively for first and second order

6.4.1.2 A case of study

An example of the results obtained for one subject during the FES test is shown in Table 6.1. In the table the values of the coefficients, the R^2_{adj} and the RMSE and the normalised root mean squared error (NRMSE) at each fold of the cross-validation for the training set and the test set are shown. The prediction ability and the repeatability of the polynomial was tested using a *5-Fold* cross-validation for the FES test and a *3-Fold* cross-validation for the voluntary test.

Table 6.1: Cross-validation results, curve fitting displacement's estimation, FES test

			Fold 1	**Fold 2**	**Fold 3**	**Fold 4**	**Fold 5**	**Avg Model**
Fitted Model	R^2_{adj}		0.933	0.936	0.944	0.935	0.934	
	RMSE		0.360	0.361	0.342	0.356	0.312	
	Coefficients	p1	0.000	0.000	0.000	0.000	-0.001	0.000
		p2	0.077	0.087	0.088	0.078	0.100	0.086
		p3	0.480	0.469	0.417	0.446	0.323	0.427
Error Training Set	R^2_{adj}		0.933	0.936	0.944	0.935	0.934	
	NRMSE		0.073	0.074	0.070	0.073	0.074	
Error Test Set	R^2_{adj}		0.864	0.925	0.853	0.935	0.854	
	NRMSE		0.133	0.093	0.126	0.083	0.112	

Table 6.1 shows the goodness of the fitting, expressed with R^2_{adj} and $NRMSE$ for each fold of the cross- validation process and for the training and test sets. The coefficients characterising the polynomial are also expressedl. The Fitted Model contains the information of the coefficients estimated at each fold. The average of the coefficients of the *5-Fold* cross-validation was also calculated and expressed in the column Avg Model. High repeatability of the results across

Folds is observed indicating that the fitted curve is independent from the dataset.

Considering Fold 1 in Table 6.1 and referring to the second order Equation (6.1), the best fit curve for this particular case can be written as:

$$P(\tau) = -0.001 \times \tau^2 + 0.077 \times \tau + 0.48 \tag{6.4}$$

Where τ is the torque measured and $P(\tau)$ is the displacement estimated through the polynomial.

From Equation 6.4 it is possible to estimate the displacement when only the torque is measured. An example of the estimation of displacement is shown in Figure 6.2 where the displacement measured and the displacement estimated are depicted for the case indicated in Equation (6.4).

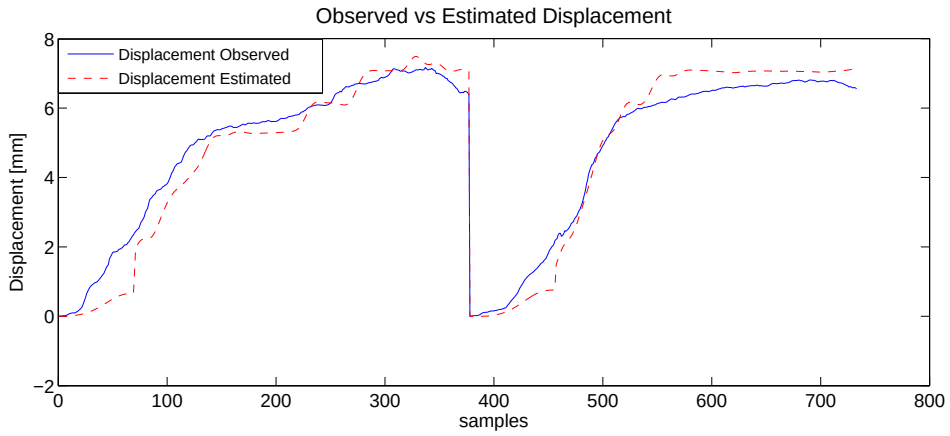

Figure 6.2: .
Observed vs Estimated displacement (respectively continuous and dashed line) for test dataset of one subject and *1 Fold* of cross-validation.

6.4.2 Coefficients distribution, analysis for all the subjects

A polynomial was fitted for each subject and for the voluntary and FES tests. The distribution of the coefficients across all the subjects for the voluntary and the FES test is shown in Figure 6.3. The coefficient $p1$ has very small values (of the order of 10^{-3}), indicating that the second order term of the fitted curve gives a small contribution. A discussion about the selection of the order of the fitting is presented in Section 6.4.1.1. The trend of the coefficients is similar for the voluntary and the FES tests but the Kruskal-Wallis statistical test was used to test for a significant difference. The statistical test indicated that the coefficients $p1$ and $p2$ for the voluntary and FES tests are statistically significant different.

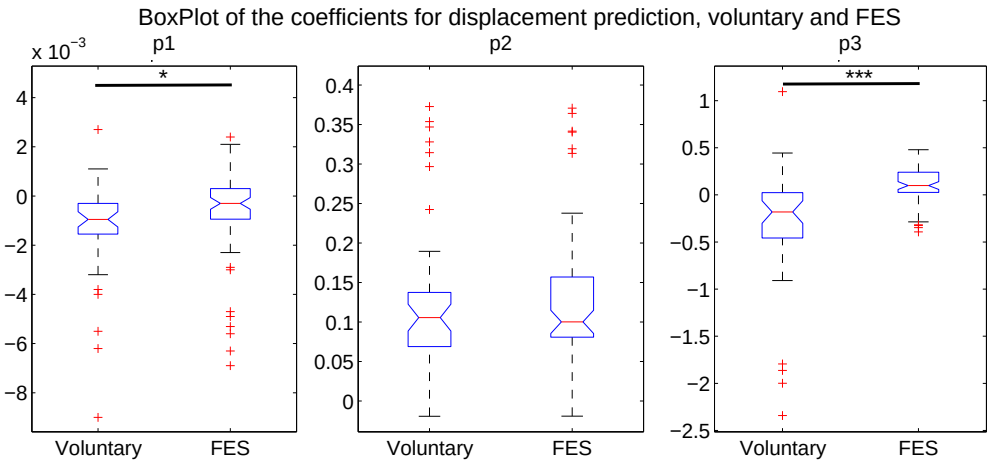

Figure 6.3: .
Boxplot of the coefficients estimated for $P(\tau)$ during voluntary and FES test. Each subplot represents the distribution of one of the coefficients of the polynomial across subjects and cross-validation Fold. Each box, within each subplot, is the results of a total 55 values (eleven subjects and 5-Fold) for the FES test and 33 values (eleven subjects and 3-Fold) for the voluntary test. A statistical analysis between the coefficients obtained for the voluntary and the FES test was performed. The significance level of the statistical analysis is indicated with no symbol if $p > 0.05$, with * if $p \leq 0.05$, with *** if $p \leq 0.001$. Where $p \leq 0.05$ rejects the null hypothesis that the values obtained for the voluntary and FES test are not different

6.4.2.1 Goodness of the fitting

The goodness of the fitting is presented in Table 6.2 for FES and Table 6.3 for voluntary. In the FES test, except for subject 7 and subject 8, the R^2_{adj} in the training set is above 0.8 having a NRMSE inferior to 15%. In the test set the goodness is lower than the training set and it changes across subjects and cross-validation folds. $R^2_{adj} > 0.8$ is observed in 7 subjects out of 11. Subjects 7, 8, 9 and 11 must be considered as unsuccessful fitting. In the voluntary test, the cross-validation for the training set showed good fitting ($R^2_{adj} > 0.8$ and $NRMSE < 15\%$) for all the subjects expect fot subject 9. On the other side, during the test set the cross-validation results were unsuccessful, offering good results only for subjects 1, 2 and 4.

Table 6.2: Goodness Prediction of Displacement curve Fitting, FES test

Subjects	**Training Set**						**Test set**					
	R^2_{adj}			*NRMSE*			R^2_{adj}			*NRMSE*		
	Meadian	*Min*	*Max*	*Meadian*	*Min*	*Max*	*Meadian*	*Min*	*Max*	*Meadian*	*Min*	*Max*
S1	0.94	0.93	0.94	7%	7%	7%	0.86	0.85	0.94	11%	8%	13%
S2	0.98	0.98	0.98	4%	4%	4%	0.98	0.98	0.98	5%	5%	9%
S3	0.95	0.94	0.96	7%	6%	7%	0.87	0.69	0.95	13%	7%	25%
S4	0.98	0.98	0.98	5%	4%	5%	0.96	0.85	0.98	7%	5%	14%
S5	0.92	0.86	0.94	8%	7%	9%	0.87	0.63	0.91	12%	9%	16%
S6	0.87	0.86	0.91	12%	10%	12%	0.86	0.48	0.93	10%	9%	23%
S7	0.47	0.39	0.51	16%	13%	18%	-0.65	-5.64	0.44	33%	25%	54%
S8	0.68	0.59	0.79	17%	13%	19%	0.53	-0.10	0.61	23%	20%	33%
S9	0.74	0.64	0.80	14%	12%	15%	0.52	0.22	0.76	21%	17%	28%
S10	0.93	0.92	0.94	9%	8%	9%	0.83	0.63	0.98	15%	6%	23%
S11	0.88	0.72	0.91	9%	8%	12%	0.38	-3.24	0.49	23%	19%	56%

Table 6.3: Goodness Prediction of Displacement curve Fitting,Voluntary test

Subjects	**Training Set**						**Test Set**					
	R^2_{adj}			*NRMSE*			R^2_{adj}			*NRMSE*		
	Meadian	*Min*	*Max*	*Meadian*	*Min*	*Max*	*Meadian*	*Min*	*Max*	*Meadian*	*Min*	*Max*
S1	0.89	0.88	0.93	11%	6%	11%	0.81	0.67	0.93	13%	7%	14%
S2	0.94	0.91	0.98	8%	6%	11%	0.90	0.83	0.96	8%	6%	11%
S3	0.93	0.90	0.96	8%	7%	9%	0.44	-2.53	0.79	16%	13%	45%
S4	0.98	0.94	0.99	4%	2%	6%	0.93	0.90	0.97	7%	6%	9%
S5	0.77	0.65	0.95	9%	8%	12%	-2.05	-3.97	-0.10	31%	27%	49%
S6	0.82	0.69	0.91	9%	7%	12%	0.19	-5.42	0.42	22%	15%	43%
S7	0.90	0.86	0.91	7%	7%	8%	0.66	0.64	0.80	12%	11%	16%
S8	0.82	0.72	0.95	13%	7%	15%	0.32	-1.78	0.41	30%	23%	46%
S9	0.69	0.63	0.82	20%	13%	20%	0.38	-1.00	0.72	26%	18%	52%
S10	0.96	0.91	0.98	7%	5%	7%	-0.51	-2.02	0.59	24%	19%	40%
S11	0.94	0.87	0.95	6%	6%	7%	0.62	-2.00	0.78	12%	10%	44%

6.4.3 Estimation of torque exerted: curve fitting

A similar process to the one described in Section 6.4.1 can be applied to estimate the torque exerted from the displacement. A third order polynomial was fitted as expressed in Equation (6.2). A total of four coefficients characterises the fitting. The fitting was tested using a 5-Fold cross-validation for the FES test and a 3-Fold cross-validation for the voluntary test.

Figure 6.4 shows the distribution of all the coefficient across subjects for both the voluntary and the FES test. A statistical analysis between the coefficients obtained during voluntary and FES tests was performed but no statistically significant difference was found using the Kruskal-Wallis test.

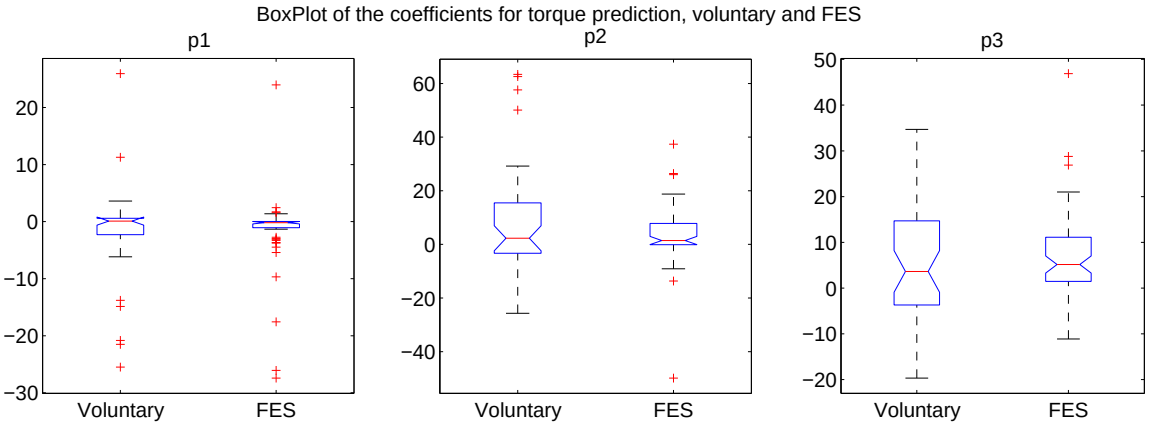

Figure 6.4: .
Boxplot of the coefficients estimated for $P(\delta)$ during voluntary and FES test. Each subplot represents the distribution of one of the coefficients of the polynomial across subjects and cross-validation Fold. Each box, within each subplot, is the result of a total 55 values (eleven subjects and 5-Fold) for the FES test and 33 values (eleven subjects and 3-Fold) for the voluntary test. A statistical analysis between the coefficients obtained for the voluntary and the FES test was performed, however no statistically significant difference was found.

The goodness of the fitting is shown in Table 6.4 for the FES test and in Table 6.5 for the voluntary test. The parameters of R^2_{adj} and $NRMSE$ obtained for the training set are indicative of good fitting ($R^2_{adj} > 0.8$ and $NRMSE < 15\%$) in 9 subjects for the FES test and 10 subjects for the voluntary test. Good fitting was observed in the training set for both the voluntary and the FES tests where the values of $R^2_{adj} > 0.8$ are obtained. The test set has values of $R^2_{adj} > 0.8$ in 5 Subjects out of 11 for the FES test and in 3 Subjects out of 11 for the voluntary test.

Table 6.4: Goodness Prediction of Torque curve Fitting, FES test

Subjects	**Training Set**						**Test Set**					
	R^2_{adj}			*NRMSE*			R^2_{adj}			*NRMSE*		
	Median	*Min*	*Max*	*Median*	*Min*	*Max*	*Median*	*Min*	*Max*	*Median*	*Min*	*Max*
S1	0.96	0.94	0.96	7%	6%	7%	0.91	0.88	0.95	11%	8%	13%
S2	0.98	0.98	0.98	5%	4%	5%	0.98	0.98	0.98	7%	5%	8%
S3	0.96	0.95	0.96	8%	7%	8%	0.75	-1.56	0.93	17%	7%	42%
S4	0.99	0.98	0.99	3%	3%	4%	0.98	0.87	0.99	4%	4%	12%
S5	0.94	0.90	0.97	8%	7%	11%	0.68	0.60	0.93	19%	10%	23%
S6	0.83	0.35	0.88	13%	11%	32%	0.83	0.35	0.88	13%	11%	32%
S7	0.41	0.34	0.54	30%	20%	33%	-0.78	-4.77	-0.39	43%	36%	65%
S8	0.71	0.66	0.82	14%	12%	17%	0.46	-0.42	0.77	20%	18%	38%
S9	0.75	0.71	0.80	15%	13%	16%	0.22	-2.02	0.70	27%	18%	55%
S10	0.94	0.93	0.95	8%	7%	8%	0.73	-0.76	0.99	18%	4%	37%
S11	0.88	0.76	0.92	10%	8%	19%	-0.41	-27.59	0.65	36%	19%	170%

Table 6.5: Goodness Prediction of Torque curve Fitting, Voluntary test

Subjects	**Training Dataset**						**Test Dataset**					
	R^2_{adj}			*NRMSE*			R^2_{adj}			*NRMSE*		
	Median	*Min*	*Max*	*Median*	*Min*	*Max*	*Median*	*Min*	*Max*	*Median*	*Min*	*Max*
S1	0.81	0.78	0.89	11%	8%	12%	0.81	0.67	0.93	13%	7%	14%
S2	0.97	0.94	0.98	7%	5%	8%	0.90	0.83	0.96	8%	6%	11%
S3	0.92	0.91	0.97	7%	6%	8%	0.44	-2.53	0.79	16%	13%	45%
S4	0.98	0.95	0.99	4%	2%	6%	0.93	0.90	0.97	7%	6%	9%
S5	0.70	0.68	0.95	10%	8%	13%	-2.05	-3.97	-0.10	31%	27%	49%
S6	0.87	0.83	0.97	9%	5%	10%	0.19	-5.42	0.42	22%	15%	43%
S7	0.90	0.87	0.91	7%	6%	7%	0.66	0.64	0.80	12%	11%	16%
S8	0.93	0.85	0.96	7%	5%	10%	0.32	-1.78	0.41	30%	23%	46%
S9	0.68	0.60	0.84	14%	9%	16%	0.38	-1.00	0.72	26%	18%	52%
S10	0.99	0.93	0.99	4%	4%	7%	-0.51	-2.02	0.59	24%	19%	40%
S11	0.95	0.88	0.97	6%	6%	7%	0.62	-2.00	0.78	12%	10%	44%

6.4.4 Estimation of muscle displacement: surface fitting

If we want to define the relationship between torque exerted and the whole muscle displacement, the information of depth must be taken into consideration as well. A tri-dimensional fitting is able evaluate the surface which best fits the data. The relationship between torque, displacement and depth was defined using the Equation (6.3) for both the voluntary and FES test.

An example of surface fitting is presented for one subject and for the FES test is shown in Figure 6.5.

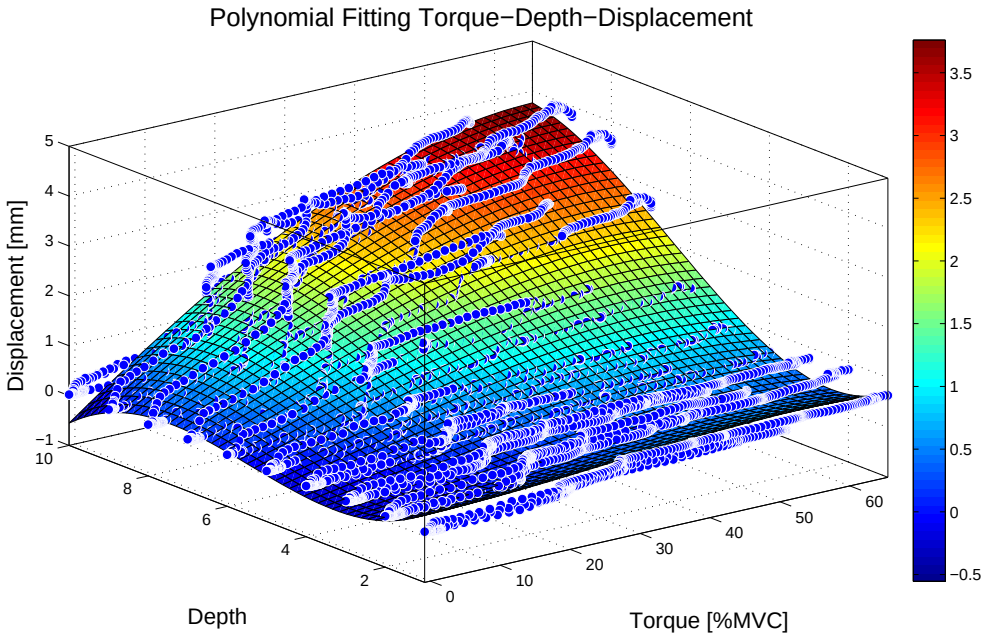

Figure 6.5: Example of surface fitting obtained for one subject during the voluntary task. The surface is the illustration of the polynomial fitted from the data torque-depth-displacement. The polynomial is of the kind shown in Equation 6.3 where the torque, depth and displacement are respresented on each axis. The surface is presented as color-map where the red is associated to higher and the blue to lower values of the vertical axis as shown in the bar on the right of the figure. The blue dots surrounding the fitted surface are the real data.

The results follow in the next sections

6.4.4.1 A case of study

Figure 6.5 represents a characteristic curve that describes the relationship between torque exerted, muscle displacement and depth. A similar curve was observed in each subject. The amount of displacement at superficial areas (depth 1 to 4) does not change across different levels of torque. On the other side, deeper zones have higher displacement at higher torques. The graph indicates that it is unlucky that the relationship torque-displacement can be studied evaluating the superficial aponeurosis and suggests that the deeper aponeurosis is probably more suitable.

Table 6.6: Cross-Validation for prediction of displacement from torque. The graph refers to one FES test of one subject. The coefficients and the parameters of goodness are shown for each Fold of the cross-validation and for the model obtained by averaging the coefficients obtained for the *5-Fold*

			Fold 1	**Fold 2**	**Fold 3**	**Fold 4**	**Fold 5**	**Avg Model**
Fitted Model	R^2_{adj}		0.949	0.948	0.957	0.951	0.935	
	RMSE		0.314	0.314	0.284	0.297	0.288	
	Coefficients	p00	0.462	0.415	0.344	0.500	0.412	0.426
		p10	0.007	0.005	0.000	0.000	-0.006	0.001
		p01	-0.358	-0.310	-0.220	-0.386	-0.288	-0.312
		p20	0.000	0.000	0.000	0.000	0.000	0.000
		p11	0.003	0.003	0.004	0.004	0.006	0.004
		p02	0.079	0.065	0.043	0.080	0.057	0.065
		p21	0.000	0.000	0.000	0.000	0.000	0.000
		p12	0.001	0.001	0.001	0.001	0.001	0.001
		p03	-0.004	-0.003	-0.002	-0.004	-0.003	-0.003
Error Training Set	R^2_{adj}		0.928	0.932	0.932	0.937	0.937	
	NRMSE		0.076	0.076	0.076	0.073	0.073	
Error Test Set	R^2_{adj}		0.868	0.923	0.926	0.900	0.947	
	NRMSE		0.132	0.089	0.094	0.095	0.072	

In Table 6.6 we can observe the results of *5-Folds* cross-validation, three sections are considered:

- the Fitted Model: indicates the results obtained for the whole dataset (all the depths)
- the Error Training Set : indicates the results obtained for the *training set*
- the Error Test Set: indicates the results obtained for the *test set*

The Fitted Model contains the information about the coefficients estimated at each fold. The average of the coefficients of the *5-Fold* cross-validation was also calculated and expressed in the column Avg Model. The parameters of goodness R^2_{adj} and RMSE of the fitted model are expressed as well and they are estimated on all the datasets (all the depths).

The goodness of the fitting estimated for both the *training* and *test* dataset was expressed by the NRMSE, the R^2_{adj} and is also shown in Table 6.6. The error calculated as difference between the observed values and the values estimated is not consistent across different depths. If the goodness is evaluated for each depth, superficial regions have lower R^2_{adj} and higher NRMSE than deeper portions of the muscle. An *Optimal Depth* can be identified as the depth with minimum NRMSE.

Considering Fold 1 in Table 6.6 and referring to the Equation (6.3), the surface that best fits the data can be written as:

$$P(\tau, w) = 0.462 + 0.007\tau - 0.358w + 9.1 \times 10^{-5}\tau^2 + 0.003\tau w + 0.079w^2 + \\ -3.5 \times 10^{-5}\tau^2 w + 0.001\tau w^2 - 0.004w^3 \tag{6.5}$$

Where τ is the torque measured, w is a weight that changes according to the depth information and $P(\tau, w)$ represents the displacement information estimated for the depth indicated in w and assumes values 1 to 10 respectively for depth 1 to depth 10. Equation (6.5) represents the surface fitted in Figure 6.5.

Assigning the values of τ and w to Equation (6.5), the estimated values of the displacement at depth w are obtained. Figure 6.6 illustrates the measured vs the estimated values of displacement across different depths.

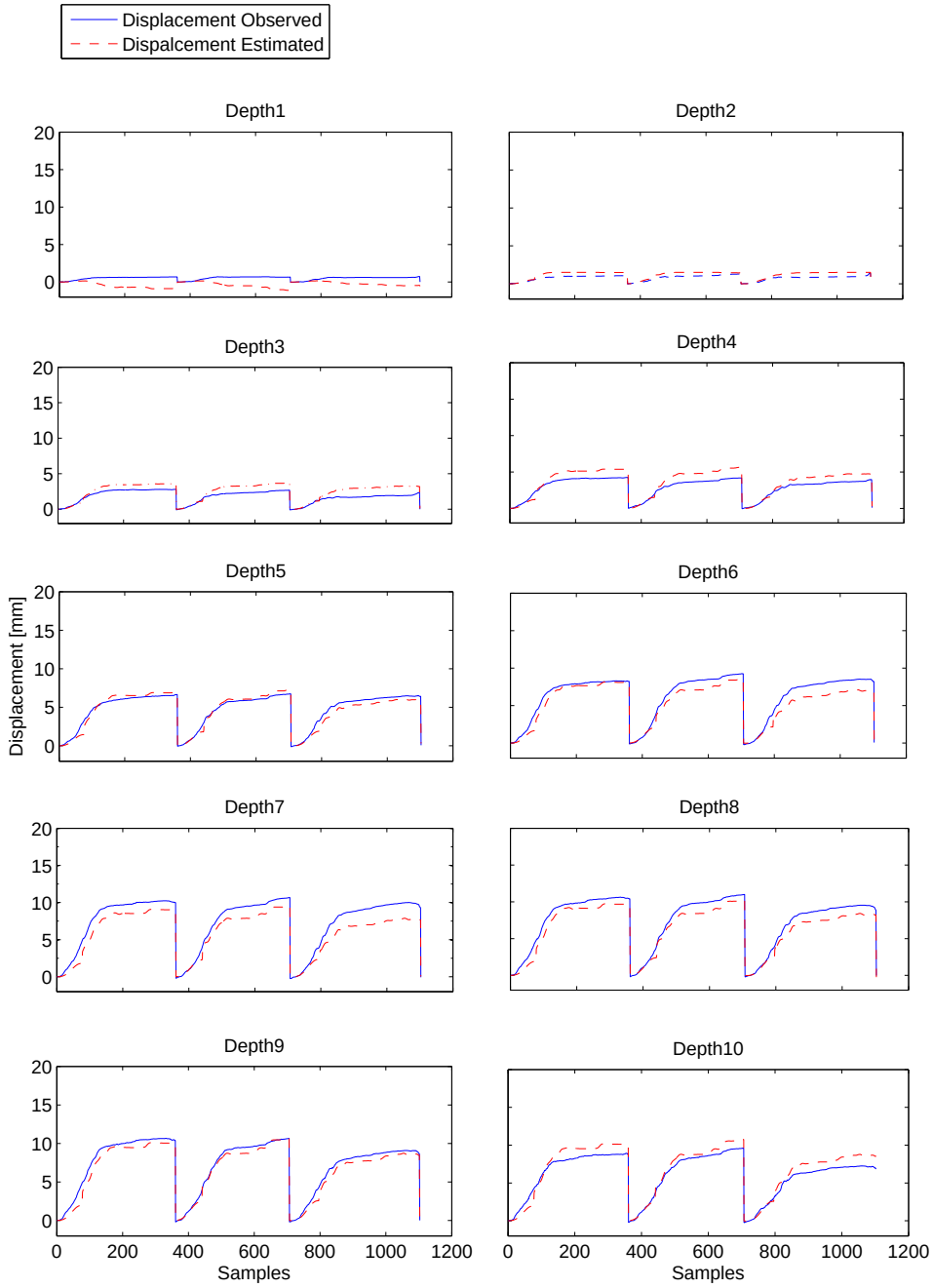

Figure 6.6: .
Observed vs Estimated displacement (respectively continuous and dashed line) for test dataset of one subject and *1 Fold* of cross-validation. We can observe a higher error (larger difference between the two lines) at superficial parts of the muscle (e.g: Depth 1 and Depth 2). The estimation improves going deeper in the muscle (e.g. after Depth 5)

In Figure 6.6 it is possible to observe that not all the depths offer the same goodness of fitting, in particular the superficial parts of the muscle have less ability to estimate the displacement. From depths five to ten the fitting improves. Similar results were observed in all the subjects.

If the fitted data is evaluated against the measured data it is possible to estimate the RMSE, the NRMSE and the R^2_{adj}. These values are indicative of the goodness of the fitting evaluated on the *test* dataset.

A high repeatability of the estimated values among different folds of the cross-validation was observed. An example is shown in Figure 6.7 where the observed values and the estimated values at one depth are plotted for each cross-validation fold.

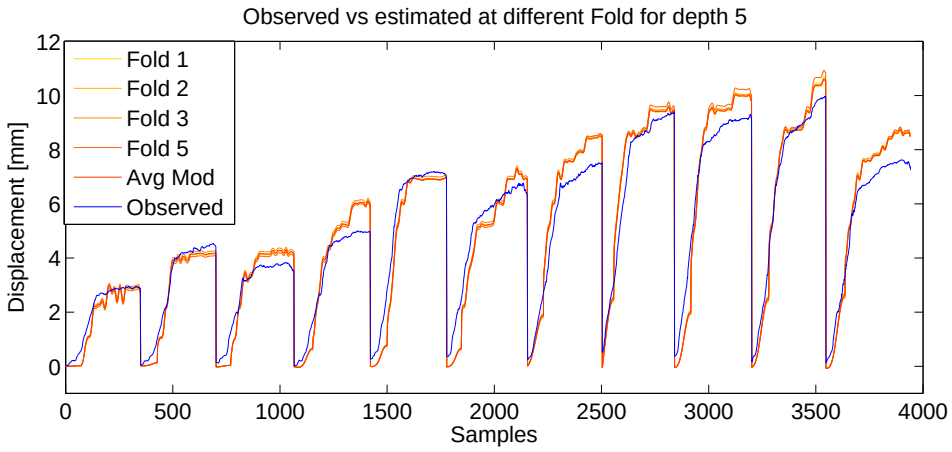

Figure 6.7: Observed vs Estimated values of the *5-Folds* cross-validation at only Depth 5 and for all the trials (11 stimulations) during the FES test of one subject. The lines in shades of red correspond to the polynomial fitted at different *Folds* of the cross-validation. The blue line represents the measured values of the displacement. We can observe a high repeatability of the estimated values among different *Folds* of the cross-validation

.

The same approach was used for evaluating the voluntary test. For each subject a different polynomial was fitted, the order of the polynomial was fixed across the subjects and the equation that represents it is Equation 6.3.

6.4.4.2 Coefficients distribution, analysis for all the subjects

The polynomials estimated for the voluntary and the FES test, both have 9 coefficients. Their trend is shown in Figure 6.8 where one subplot for each coefficient is shown for both the voluntary and the FES test. Each subplot represents the distribution of one of the coefficients across subjects and cross-validation Folds for both the voluntary and the FES test. In particular each box, within each subplot, is the result of a total 55 values (eleven subjects and 5-Fold) for the FES test and 33 (eleven subjects and 3-Fold) for the voluntary test. Each subplot shows the trend of the correspondent coefficient for the voluntary and the FES. A statistical analysis between the coefficients obtained for the voluntary and the FES test was performed. The data was not

normally distributed thus a Kruskal-Wallis statistical test was used. The level of significance was fixed at 5% ($\alpha = 0.05$) and the null hypothesis was formulated as: *the values of the coefficients for the voluntary and FES test are not different.* It is possible to observe a similar range of coefficients obtained for the voluntary and the FES. However statistical significance difference was obtained for the coefficients: *p00*, *p01*, *p20*, *p02*, *p21*, *p12*, *p03* where their correspondent **p values** obtained were $p = 0.014, p = 0.990, p = 0.029, p = 0.003, p = 0.084, p = 0.021, p = 0.024, p = 0.013, p = 0.027$.

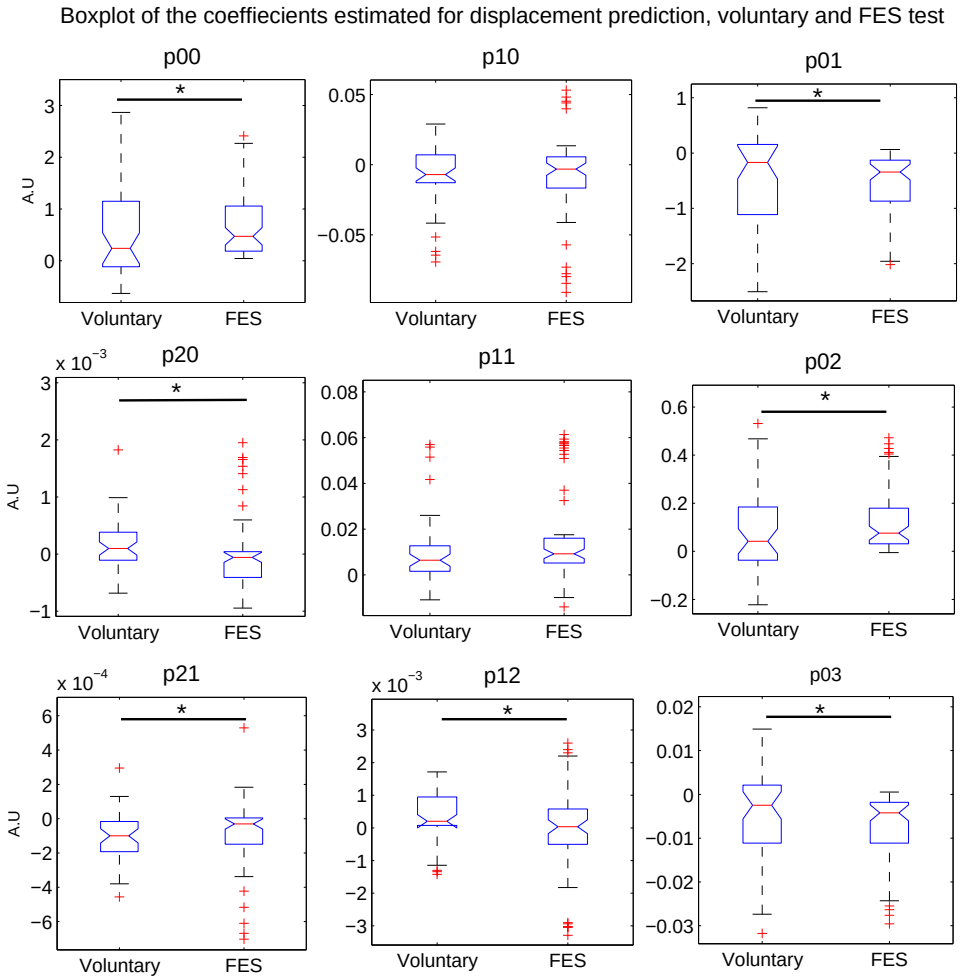

Figure 6.8: Boxplots of the coefficients estimated for $P(\tau, w)$ during voluntary and FES test. Each subplot represents the distribution of one of the coefficients of the polynomial across subjects and cross-validation Fold. Each box, within each subplot, is the result of a total 55 values (eleven subjects and 5-Fold) for the FES test and 33 values (eleven subjects and 3-Fold) for the voluntary test. A statistical analysis between the coefficients obtained for the voluntary and the FES test was performed. The significance level of the statistical analysis is indicated with no symbol if $p > 0.05$, with * if $p \leq 0.05$. Where $p \leq 0.05$ rejects the null hypothesis that the values obtained for the voluntary and FES test are not different.

6.4.5 Goodness of the fitting

An overview of the goodness obtained when evaluating the polynomial for the voluntary and the FES tests during the *training* and the *test* dataset is shown in Table 6.7 and Table 6.8 In the tables, for each subject, the minimum, the maximum and the median values of the R^2_{adj} and the *NRMSE* across different folds of the cross-validation for the *training set* and *test set* are given. The results obtained in the *training* dataset showed good fitting ($R^2_{adj} > 0.8$) in both the voluntary and the FES tasks suggesting that the polynomial successfully approximates the relationship muscle displacement-torque-depth. The ability of the polynomial to estimate a new set of data is shown in the *test* set where for the FES test 6 subjects out of 11 had values of $R^2_{adj} > 0.8$ and $NRMSE < 12\%$. For subjects 7 and 8 the polynomial does not offer a good fitting, probably because the parameters (current, pulsewidth or electrodes position) for the electrical stimulation were not set correctly and the output torque was inefficient (in 3 trials it was less than 5% of the MVC). The goodness of the polynomials estimated for the voluntary tests are shown in Table 6.8 where values of $R^2_{adj} > 0.8$ are observed in 7 subjects out of 11.

As previously stated,the goodness of the fitting changes across depths therefore better results are obtained at the *Optimal Depth* which is always identified at deeper portions of the muscle. The most frequent value for the *Optimal Depth* was identified at depth 9.

Table 6.7: Goodness of Displacement's Estimation at all Depths, FES

Subjects	**Training Dataset**						**Test Dataset**					
	$R\hat{2}$			*NRMSE*			$R\hat{2}$			*NRMSE*		
	Median	*Min*	*Max*	*Median*	*Min*	*Max*	*Median*	*Min*	*Max*	*Median*	*Min*	*Max*
S1	0.95	0.95	0.96	5%	5%	5%	0.90	0.87	0.94	8%	7%	11%
S2	0.97	0.97	0.97	5%	5%	5%	0.94	0.84	0.95	8%	6%	12%
S3	0.93	0.93	0.93	6%	6%	6%	0.83	-0.58	0.88	11%	10%	28%
S4	0.97	0.97	0.97	4%	4%	4%	0.96	0.94	0.98	5%	4%	6%
S5	0.90	0.89	0.90	6%	6%	6%	0.76	0.61	0.88	9%	7%	16%
S6	0.94	0.93	0.94	7%	7%	8%	0.86	0.83	0.96	11%	6%	12%
S7	0.71	0.70	0.72	12%	12%	12%	0.06	-0.33	0.43	24%	20%	30%
S8	0.82	0.81	0.82	10%	9%	10%	0.67	0.36	0.71	15%	14%	18%
S9	0.81	0.80	0.85	9%	8%	9%	0.25	0.14	0.79	20%	13%	21%
S10	0.93	0.93	0.94	6%	6%	6%	0.63	-3.00	0.63	16%	13%	44%
S11	0.88	0.88	0.89	7%	7%	7%	0.79	0.66	0.81	15%	11%	17%

Table 6.8: Goodness of Displacement's Estimation at all Depths, Voluntary

Subjects	**Training Dataset**						**Test Dataset**					
	$R\hat{2}$			*NRMSE*			$R\hat{2}$			*NRMSE*		
	Median	*Min*	*Max*	*Median*	*Min*	*Max*	*Median*	*Min*	*Max*	*Median*	*Min*	*Max*
S1	0.85	0.84	0.88	11%	10%	12%	0.84	0.72	0.88	12.01%	10.78%	14.89%
S2	0.97	0.96	0.98	5%	5%	6%	0.96	0.88	0.97	6.34%	5.37%	11.28%
S3	0.94	0.91	0.96	7%	5%	9%	0.80	0.32	0.85	13.73%	13.63%	22.94%
S4	0.95	0.93	0.96	6%	5%	6%	0.84	0.80	0.86	11.41%	10.71%	13.65%
S5	0.95	0.90	0.97	5%	4%	8%	0.61	0.61	0.62	15.49%	15.25%	17.43%
S6	0.97	0.93	0.97	5%	4%	6%	0.89	0.41	0.96	9.25%	6.14%	23.92%
S7	0.96	0.96	0.98	5%	4%	5%	0.95	0.92	0.96	5.67%	5.05%	7.04%
S8	0.95	0.91	0.96	6%	5%	7%	0.82	0.69	0.86	11.12%	10.74%	14.96%
S9	0.83	0.81	0.90	12%	10%	13%	0.70	0.05	0.85	18.54%	12.44%	30.48%
S10	0.95	0.94	0.95	5%	5%	5%	0.42	-1.05	0.86	19.42%	10.49%	29.16%
S11	0.96	0.93	0.96	5%	5%	8%	0.87	-0.05	0.87	10.62%	10.35%	28.12%

6.5 Discussion

As explained in the introduction, the aim of the study was to evaluate the relationship between the muscle displacement and the force exerted. This relationship can be used to model the pathway of force transmission within the muscle (estimating the displacement at a particular force) or can be used to estimate the torque exerted by the muscle (estimation of torque from the muscle displacement).

The relationship was evaluated in two different ways, considering either only the muscle displacement near the deep aponeurosis (curve fitting) or considering the displacement of the whole muscle (surface fitting).

In our study different polynomials models are estimated for the voluntary and the FES tests in order to describe the muscle behaviour of healthy subjects in voluntary and FES induced contractions. Performing the polynomial fitting in diseased muscles might result in a different polynomial, mainly regarding its order, which can be indicative of that particular disease or

stage of the disease.

6.5.1 Muscle displacement during Voluntary and FES contractions

The muscle contraction depends on the status of the fibers as this can be altered due to disease, which compromises the pathway of the contraction and the amount of force the muscle can exerts. The aim of our study is to model the muscle displacement of GM muscles of healthy subjects during voluntary and FES induced tasks. For the scope we used polynomial fitting to model the shape of the muscle contraction. The variables used to define the polynomial were the features tracked on the US video frames and the torque measured during the tasks. Two different approaches were used, a curve and a surface fitting. A discussion of the results obtained follows in the next sections.

6.5.1.1 Polynomial Model using curve fitting

The curve fitting aims to define the relationship between the muscle displacement at deep parts of the muscle and the torque exerted. The polynomial fitted was of order 2 in all the subjects and showed a good fitting ($R^2_{adj} > 0.8$) in the training dataset for both the voluntary and the FES tasks. The ability of the polynomial to predict a new dataset is shown in the results of the test dataset where a good prediction is observed in 7 out of 11 subjects for the FES task, but only 3 out of 11 subjects for the voluntary task. The boxplot of each coefficient calculated across the subjects showed few outliers indicating that the curve does not vary much for different participants. Moreover the boxplot showed a similar range of data suggesting similarity among the curves fitted. The results showed that it is possible to define a curve which represents the relationship between muscle-displacement and torque exerted, however the curve has limited ability to predict new datasets. The order of the polynomial fitted is consistent among subjects.

6.5.1.2 Polynomial Model using surface fitting

The surface polynomial fitting allows the definition of a surface which represents the muscle activation. The polynomial fitted was of order 2 for the x axis (representing the torque τ) and 3 for the y axis (representing the depth w) in all subjects in both the voluntary and the FES tasks, showing that a specific trend characterises the activation. A different polynomial was identified for each subject and for the voluntary and the FES test. A total of 9 coefficients characterised the polynomial and the boxplot analysis, representing each coefficient obtained for all the subjects and tasks, showed that they can be grouped within the interquartile range

observing few outliers. Additionally the coefficients have similar trend and range of values in both the voluntary and FES induced contractions. However 7 coefficients out of the 9 that define the polynomial, are statistically different when comparing them in the voluntary and the FES tests. It was not possible to identify a unique polynomial which could represent the muscle behaviour in general. Furthermore, the statistical analysis of the coefficients representative of the polynomials was showing differences among subjects in both the voluntary and the FES test. This is reasonable because the muscle contraction is influenced by different factors such as the position of the neuromuscular junction and the motor units activation that are not the same among human beings. This variability becomes even higher during the FES where position of electrodes and current influence the muscle contraction. However a better analysis of the coefficients could be obtained if a larger number of participants are recruited in order to compensate for this subject-related variability.

The goodness of the fitting was tested using cross-validation. The fitting was evaluated for the whole dataset (all the depths) and at the *Optimal Depth* for both the voluntary and the FES tests. The results of the whole dataset had good values of the R^2_{adj} (> 0.8) in the training indicating that the model fitted is suitable for describing the relationship. The test set had $R^2_{adj} > 0.8$ in 6 subjects for the FES test and in 8 for the voluntary test indicating the possibility of predicting new values in some cases. Similar results were obtained at the *Optimal Depth* for both the training and the test set.

6.5.1.3 Conclusion muscle displacement estimation

In our study we investigated a new technique for modelling the muscle activation based on the polynomial fitting obtained from a dataset composed of the torque measured and the information extracted from ultrasound images during a task. Data obtained from the US was analysed against the torque exerted using surface and curve fitting, based on the fact that the force produced in the sarcomeres is transmitted to adjacent structures and to the tendon. Both the approaches showed a good ability to define a mathematical model. The degree of the polynomials estimated was consistent among subjects for both the voluntary and the FES tests. The results of the surface fitting indicated that the model does not have same goodness over different depths of the muscle and was found to be better at deeper portions. Moreover it offered better results than the curve fitting only when identifying the optimal depth where the goodness of fitting is maximised. It is necessary to notice that the surface fitting has a higher computational cost than the curve fitting but its advantage is that it models the activation of the whole muscle. This can be relevant to quantify the effect of a rehabilitation therapy or to evaluate the condition of

diseased muscle.

6.5.2 Estimation of torque exerted by the GM muscle

The aim of the study is to verify whether a relationship between muscle displacement estimated from the tracking of persistent features in the ultrasound video frames and force exerted can be defined.

It is well known that the force is generated in the sarcomeres which are arranged in series along the fiber; their contraction causes the fiber shortening and fiber rotation that contribute to the muscle displacement and shortening [44]. Thus, the tracking of features in US videos recorded during isometric contraction can be indicative of the force exerted by the muscle.

6.5.2.1 Estimation of torque exerted using curve fitting

The curve fitting is based on the fact that the force produced by the sarcomeres is transmitted along the muscles line of action to the tendons or the aponeuroses (longitudinal force transmission). The muscles line of action is defined as the direction of the resultant muscle force running between the attachment sites on both ends of the muscle.

In order to verify whether the muscle displacement in the region close to the deeper aponeurosis correlates with the torque produced, the relationship between the displacement at depth 9 and the torque was investigated. The polynomial fitted was of order 3 for all the subjects for both the voluntary and the FES induced contraction. A statistical analysis was used to test the consistency of the coefficients of the polynomials fitted among the participants. It showed good regularity in the voluntary test but high variability in the FES test, suggesting that during the FES induced contraction the activation of the muscle is more inconsistent and subject dependent. This can be explained considering that the way the muscle is activated during FES strongly depends on factors such as current, pulsewidth and position of electrodes. Even if an effort was made to set those parameters in a comparable way among the partecipants and careful tests were performed to choose them, the fiber recruitment process cannot be controlled. This is most likely the reason for the variability of the polynomials fitted among different subjects.

To test the goodness of the polynomial, a cross-validation was used and the values of the R^2_{adj} and NRMSE were calculated for both the training and test dataset. The values obtained represent, for the training dataset, the goodness of the relationship found and, for the test dataset, how well the polynomial estimated predicts a new set of data. The results obtained for the FES

test show high values of coefficient of determination ($R^2_{adj} > 0.8$) in 7 out of 11 subjects in the training dataset but only 5 out of 11 achieved a value > 0.8 in the test dataset. Better results are obtained for the training dataset of the voluntary test where only 1 subject shows a low goodness of the fitting. On the contrary, the test dataset shows good fitting in 3 subjects out of 11. The low number of subjects at which the outcomes in the test dataset are good suggests that the polynomials estimated do not have sufficient prediction power on new datasets. The difference in goodness between the training and test dataset, in both the voluntary and FES tests, can be attributed to an over-fitting of the data. However different orders of the polynomial did not offer a better outcome. These results suggest that when modeling the muscle function the whole muscle should be considered and that focusing on a portion of the muscle is not enough to evaluate the muscle contraction.

6.5.2.2 Conclusion of torque estimation

The ability to predict the torque produced by the muscle from the muscle displacement estimated by the tracking of feature in the US video frames was tested using polynomial curve fitting. The polynomial was estimated from the information of the US displacement at only one depth (i.e. depth 9) close to the deeper aponeurosis based on the fact that the force is transmitted to the tendons along the muscle's fiber. The results obtained showed that in both the voluntary and the FES induced contractions the polynomials are able to describe the relationship ($R^2_{adj} > 0.8$) well in the training dataset but they are not able to predict new set of data ($R^2_{adj} < 0.8$) in the test dataset. The outcome of the study indicates that the tracking of features in US video images recorded during muscle contraction correlates with the torque exerted.

Chapter 7

Discussion

7.1 Summary

This PhD project aimed to gives further insight into the way muscle contracts during voluntary activation and when FES is applied. US muscle imaging was used as the main tool to characterise the muscle behaviour locally. The main findings of this project are summarised in this chapter.

7.2 Feasibility and effectiveness of the technique

Previous research in literature demonstrates a potential range of applications of USI in muscle, however no standard parameters have been identified to describe the muscle function. Generally, the information extracted from the US videos of the muscle are related to architectural parameters such as fiber length, pennation angle or cross sectional area. The algorithm used in this project allowed the tracking of feature displacement information from the entire portion of the muscle visualised on the US image. The advantage of this technique is based on the fact that the evaluation of regional muscle activation or movement is possible. The technique itself has not been widely investigated for clinical and physiological applications.

Chapter 4 describes the evaluation of the methodology for USI measurements and investigates the biological significance of the US information. The USI technique was tested using 3 ultrasound machines and evaluated with two software algorithms. The muscle displacement estimated with the feature tracking algorithm had comparable results across different US machines. The robustness of the tracking for the task was tested by tracking muscle contractions performed at different speeds (determined by ramp times) and with different US machines. The results suggested that the technique is able to track muscle movement performed at the three speeds tested. The software algorithm used throughout this project was developed by Darby et al. [79]. The information extracted from the features tracking of the US video was investigated and forms the basis for the analysis can be found in Chapters 5 and 6.

7.3 Muscle displacement

The displacement was estimated by the feature tracking of the US video of the gastrocnemius medialis muscle recorded while performing voluntary and electrically induced muscle contractions. The electrical stimulation was delivered with surface electrodes placed on the muscle belly and on the tibial nerve. The analysis was discussed in Chapter 4 (preliminary study) and Chapter 5 (full study).

The displacement of the features is directly related to the muscle contraction, in fact the muscle fibers when contracting shorten and rotate causing the muscle displacement. The displacement of each feature extracted from the US video analysis was evaluated in both the X and the Y directions, which correspond respectively to the proximal-distal movement and to the superficial deeper movement of each feature extracted. The main direction of movement was in X direction indicating a movement toward the knee. The result is in agreement with previous studies where the displacement of the deeper aponeuroses was observed to be in proximal direction [64, 143].

An evaluation of displacement across different depths was performed as well. It was observed that superficial portions of the muscle move less than deeper portions. The difference in the displacement between the superficial and deeper aponeuroses was previously observed and attributed to the intermuscular force transmission and fascicular strain which translates into proximal - distal movement of the deep aponeurosis [65, 73].

The muscle displacement was observed at different depths within the muscle when performing voluntary isometric contractions at different strengths and when applying different stimulation intensities. As expected, the displacement increased with strength and current stimulation applied. The muscle tissue displacement was not uniform during the contraction, instead it was larger at deeper parts of the muscle. This finding is in agreement with a previous study by Bojsen-Moller et al. that reported on the tissue displacement of the GM muscle during voluntary isometric contraction and during electrically elicited contraction [150].

In Chapter 5 the muscle displacement was observed during voluntary contraction and during electrically induced contraction when locating the electrodes for the stimulation either on the muscle belly or on the tibial nerve. In addition to the muscle displacement, the increment in displacement across different depths was evaluated. The increment was evaluated by calculating the difference in displacement between the displacement at the current depth minus the displacement at the previous depth. Differences in relative displacement between voluntary and electrically induced contractions were identified across depths (refer to Figures 5.9 (a) and (b)). When stimulating the muscle with surface electrodes, the middle portion of the muscle moved uniformly and did not show differences in relative displacement. On the contrary, during the voluntary contraction the increment in displacement between different depths in the muscle was more variable showing areas with larger increment usually located at half of the muscle. Two hypotheses were advanced to explain the difference: current dispersion within the muscle or synchronous motor unit recruitment. In order to understand the cause of the phenomenon, the increment in displacement was observed also when applying stimulation through electrodes

placed on the nerve. The increment in displacement observed during nerve stimulation was variable and more similar to the voluntary stimulation. However in both the cases of surface and nerve stimulation the amount of increment in displacement was comparable with the voluntary at higher current intensities. Following the results we concluded that the current dispersion within the muscle causes the different muscle contraction during surface electrical stimulation.

7.4 Strain and Strain Rate estimation

Further parameters identified to be significant were the strain and the strain rate of the muscle. The strain represents the change in dimension from a resting state to the one achieved following application of force, while the strain rate represents the rate of the deformation. The concept of strain in physiology was introduced in 1973 to facilitate the understanding of elastic stiffness in the heart [135]. Thus the strain represents the regional deformation of the muscle, while the strain rate is the shortening velocity per length change [136]. The strain was calculated by the differential motion between two test points in the US video at each frame and normalised to their initial separation, while the strain rate is the differential velocity between two adjoining points and corresponds to the time derivative of the strain. Also in this case, the advantage of the technique we have used is based on the fact that the distribution of the strain within the muscle can be estimated. Previous studies analysed only the fascicle strain limiting the information to one measurement. Using a two-dimensional colormap plot we were able to display the strain at different muscle depths and over time. The analysis of the strain distribution and strain rate were performed in Chapter 5 .

The strain was evaluated in both vertical and horizontal directions. Positive vertical strain was observed in the voluntary and the electrically induced muscle contractions (in both cases, of muscle belly and nerve stimulations) indicating increases in muscle thickness. As expected, the strain increases, in both value and area of distribution, with strength of contraction or intensity of the stimulation. Recurrently, higher values of strain were observed at the middle portion of the muscle. During surface stimulation at the muscle belly, at lower intensities, the deeper portions of the muscle undergo higher strain, increasing the intensity at which the strain increases and covers a wider area of the muscle. During stimulation through the tibial nerve, higher strain characterises both the middle and surface portions of the muscle. The phenomenon can be related the axons distribution; nerve trunk stimulation is more likely to recruit sensory axons which terminate at superficial parts of the muscle (cf. Section 2.3.4) [114].

The vertical strain is indicative of the regional muscle activation. During muscle belly surface

stimulation, larger changes in strain are observed in the middle portion of the muscle suggesting that the current spreads within the muscle and stimulates the nerve branches which causes the fiber contraction. Thus the fiber contraction is not caused by direct effect of the current. For a long time it has been assumed that the FES (transcutaneous stimulation applied on the muscle belly) activates primarily the superficial areas of the muscle since they are closer to the electrodes where the electric field is generated [162]. Nevertheless studies based on images of the muscle from magnetic resonance (MRI) showed that the pattern of stimulation is not exclusively superficial but rather dispersed and variable among subjects, suggesting that stimulation of a given region of the muscle cannot be taken for granted [109, 110]. Hillegass and Dudley investigated the muscle activation territory of the quadriceps in both healthy and spinal cord injured subjects demonstrating in both cases the spatial dependency of activation on electrodes placement and current intensity [110]. Adams, Hillegas and Dudley were the first to attempt the mapping of muscle activation by extracting information from MRI images obtained just after voluntary and electrically induced contractions [109, 110]. Their work was pioneering in giving insights into the regional muscle activity, however it should be clear that MRI does not measure neither the electrical activity nor the mechanical function of the muscle; but rather it depicts the muscle cell metabolism and fluid uptake that results in changes in contrast in MRI images. In addition, the images are typically acquired several minutes after the task [112]. The comparison of strain distribution between voluntary and electrically induced contractions suggests that during electrical stimulation the muscle undergoes higher vertical strain. A possible explanation can be associated with the fact that during electrical stimulation only one muscle is active and, therefore, has more space to enlarge. In contrast, during voluntary contraction other muscles (i.e. the soleus) are active limiting the muscle expansion.

Negative horizontal strain was observed at deeper areas indicating a reduction in muscle length. Horizontal strain becomes more negative and involves a wider area of the muscle at higher voluntary contractions and at higher current intensities applied. The localisation of changes in strain at deeper areas can be related to the muscle fiber rotation which results in muscle shortening near the deep aponeurosis.

The strain rate was evaluated in the time-frequency domain. Higher Power Spectral Density (PSD) characterises contractions at higher strength or stimulation intensity at the time of muscle activation and deactivation. The number of frequency components observed is lower for the voluntary contraction than for the electrically induced contraction. The voluntary test is generally characterised by lower PSD and fewer frequency components at the activation time than at the de-activation time. During electrically induced contractions (both for the muscle belly and nerve trunk stimulation) comparable PSD and frequency components are observed at both the

activation and deactivation times, mainly at higher current intensities. The phenomenon might suggest that during voluntary contraction the motor units of the same type, which fire at the same rate, are recruited. By increasing the strength of the voluntary contraction, more motor units are recruited, introducing more variability in the firing rate which is observed in the appearance of more frequency components. On the contrary, during electrical stimulation similar frequency components are observed across different intensities which might suggest a repeatable recruitment of the same motor units.

7.5 Muscle displacement in relation to torque exerted

The torque-displacement relationship was studied in Chapter 4 and Chapter 6.

Figure 4.15 of Chapter 4 shows the relationship between torque exerted and muscle displacement observed on the ultrasound. The relationship was characterised by a hysteretic curve when considering a task which involves muscle activation and de-activation. Hysteresis was previously observed on M-mode ultrasound images [84] of the biceps brachi. To evaluate the torque-displacement relationship, each phase of the contraction (activation, isometric contraction and de-activation) were studied separately. A linear relationship between torque and muscle displacement was observed for the recruitment for both the voluntary and FES contractions. Linear relationship was observed during the constant stimulation phase during FES induced contractions. Two explanations can be given, i) the tendon becomes less stiff and allows more force to be transmitted, ii) a reflex pathway is involved which recruits the sensory nerves allowing a central contribution to the contraction [114] . For the the de-activation phase a linear relationship between the square root of the torque and the displacement was observed in the voluntary test.

In Chapter 6 the relationship torque-displacement was evaluated during the activation and constant part of the contraction. A polynomial of order 2 was identified to describe the relationship torque-displacement at deeper portions of the muscle in both the voluntary and the FES cases. The best fit polynomial estimated had high values (> 0.8) of the coefficient of determination in both the voluntary and the FES test. The ability of estimating the muscle displacement from the torque exerted when a new dataset (test set) is given was also evaluated. Satisfactory results were obtained when evaluating the test set in 3 participants during the voluntary and in 5 during the FES tests. The whole muscle displacement was related to the torque exerted using a surface fitting. The surface fitting relates the displacement at each muscle depth to the torque exerted. The order of the polynomial estimated was 2 (for the torque) and 3 (for the depth)

and was consistent across subjects suggesting that a characteristic surface might represent the relationship torque-muscle displacement. A cross-validation was implemented to evaluate the ability of estimating the displacement from a new dataset. Satisfactory results were obtained in most of the subjects in both the voluntary and the FES test.

7.6 Limitations

Some limitations were identified and are discussed below.

The USI technique used throughout this project is able to track the movement of features in the video. The outcome of the analysis can be directly related to the mechanical activation of the muscle. However, the mechanical movement of the muscle depends on both the contraction resulting from the neural stimulation and passive movement of the muscle caused by the joint movement or contraction of neighbouring muscles. In this project it was assumed that the passive movement determined by joint movement was not contributing to the muscle displacement because the subject was performing isometric contractions and the foot was secured to a rigid platform. This problem could, partially, be addressed by correlating the ultrasound information with the surface electromyography (sEMG) which represents exclusively the electrical muscle activation. Although this solution would solve the problem during voluntary contraction, during electrical stimulation the sEMG is affected by stimulation artifacts that cause saturation in the electronic making it difficult to record the sEMG itself.

Another limitation is related to the way in which the voluntary and FES tasks were performed. The voluntary task consisted of pushing the foot against the forceplate while following a target torque profile, while the FES task consisted of applying an equivalent electrical stimulation profile. Considering this, during FES the stimulation intensity was adjusted according to the target pattern, but this didn't necessarily correlate with the measures torque (e.g. the torque kept increasing during the "constant" phase). In contrast, during voluntary contraction, the torque was controlled directly (by the subject). This could have been addressed by either making the subject follow a prescribed EMG pattern during voluntary contraction, or by automatically adjusting the FES intensity so that the corresponding torque follows the target pattern during FES contraction.

The FES allows the contraction of the target muscle. In this study the muscle considered was the Gastrocnemius Medialis (GM). During muscle activation more than one muscle contributes to the task, i.e. in our task the soleus is active during voluntary plantarflexion. The analysis could consider also the activation of the soleus, which is however difficult to access with surface

electrical stimulation.

Previous studies investigating the changes in architectural parameters of human muscles showed that small changes of muscle activity (strength of contraction) are associated with relatively large changes in muscle architecture, while at higher levels of contraction, the muscle architecture changes relatively little [51]. In our case, the contraction performed was never higher than 60% of Maximum Voluntary Contraction (MVC). However a possible approach would be the investigation of the muscle function for a small range of percentage of the MVC.

Chapter 8

Conclusions and Future Work

8.1 Conclusions

The aim of the PhD project was to investigate the muscle characteristics during voluntary and electrically induced muscle contractions using USI imaging. During the project we developed the methodology for identifying information from features extracted from US video frames. Parameters such as displacement of features, strain and strain rate of the muscle were recognised as significant for describing the muscle contraction during voluntary and electrically induced contraction.

The comparison between voluntary and the electrically induced contractions resulted in the following findings:

- Muscle displacement depends on the amount of torque exerted during voluntary contraction and on the intensity of the current applied during electrically induced contraction.
- The increment in displacement at different depths is uniform when stimulating with surface electrodes and variable when stimulating through nerve or during voluntary contraction.
- Strain distribution indicates that some areas of the muscle undergo higher changes in strain. Middle regions of the muscle show higher vertical strain while deeper regions are the most affected by horizontal strain. Higher vertical strain and more negative horizontal strain is observed at stronger contractions in both the case of voluntary and electrically induced contractions.
- Strain rate was analysed in the time-frequency domain and related to muscle contractility. Frequency components were identified at the onset and offset of the voluntary and the electrically induced muscle contractions, however more frequency components were observed during the electrically induced contractions. Higher power spectral density charactersises voluntary tasks at higher torque exerted and electrical stimulated contraction at higher current intensity applied.
- The feasibility of using USI to estimate the muscle displacement from the torque exerted during a task was investigated suggesting a correlation between torque exerted and muscle movement.

In conclusion a number of techniques were developed which can be used to investigate the muscle function under normal conditions or when external factors alter or modify the status of the muscle.

8.2 Future Work

The work carried out during this PhD provides the basis for investigating muscle function with an aim to develop the methodological techniques and identify biological significant information in USI.

A follow-on project can expand the work started and presented in this thesis. Two main topics should be addressed:

- Dependency of muscle activation on the FES settings
- Clinical evaluation in patients with neuromuscular impairment

8.2.1 Dependency of muscle activation on the FES settings

The strain distribution was observed to be dependent on the parameters of the stimulation, i.e. higher strain is observed when higher current is applied. The strain distribution would be evaluated when changing the setting of the stimulation such as current, pulsewidth, frequency and location of electrodes. The strain distribution would then be associated with the analysis of muscle fatigue in order to define a relationship between parameter settings, muscle activation and fatigue resistance. At the same time the strain rate will be analysed in time-frequency domain and the frequency components can be correlated with the time to fatigue.

8.2.2 Clinical evaluation

The major continuation of the current work would be regarding clinical trials. Future work should test the feasibility of using the USI in clinical trials involving patients with neuromuscular impairments, such as spinal cord injury (SCI).

Ultrasound Imaging (USI) is a potential tool that could provide objective measures of functional status of the muscle and its changes during and after acute rehabilitation for individuals with SCI. USI provides the possibility to measure static and dynamic parameters of the muscle. Static parameters are related to muscle morphology, such as muscle size, shape (e.g. thickness and length) and structure (e.g. organisation of muscle fascicles). Automatic analysis of an US video recorded during muscle activity using image analysis software allows dynamic measurements of muscle parameters such as changes in fascicle length, pennation angle, shape, and provide an indication of muscle activity (e.g. muscle lengthening or shortening).

USI in SCI can quantify parameters such as muscle size and shape, range of movement (ROM) of the muscle and small muscle twitches. Furthermore, the investigation using USI has the advantages of being reliable, feasible for clinical tests and sensitive to the magnitude of changes.

The clinical trials study can be aimed at describing the functional status of the muscle and its changes during and after acute rehabilitation in individuals with SCI. In particular aims can be synthesised as follow:

i) In vivo investigation and quantification of muscle properties and functions in SCI population at different stages post-injury.

ii) Feasibility study of prediction of recovery from the initial condition of the muscle state

iii) Investigation of USI as a technique for clinical tests for the quantification of the severity of injury.

iv) Optimisation of FES training protocols.

Possible objectives are:

- Description and quantification of muscle morphology (i.e. fascicle length, pennation angle, muscle thickness) and function (i.e: muscle displacement) during a task or attempted task at different stages post-injury.
- Polynomial fitting analysis for estimation of force exerted by a muscle in SCI at different stages post-injury.
- Identification of FES stimulation conditions which lead to movements of muscle structures which are as similar as possible to those observed during voluntary contraction, and to define and test corresponding novel stimulation protocols (e.g. number and position of electrodes, amplitude and pulsewidth of the current).

The approaches described in this thesis would provide the basis for the analysis techniques required for the proposed clinical application. This may lead to new developments in characterising changes in muscle function in patients with neuromuscular impairment, allowing improved targeting of interventions.

Bibliography

[1] V. Chan and A. Perlas, *Atlas of Ultrasound-Guided Procedures in Interventional Pain Management*. New York, NY: Springer New York, 2011.

[2] K. G. Baker, V. J. Robertson, and F. a. Duck, "A review of therapeutic ultrasound: biophysical effects.," *Phys. Ther.*, vol. 81, pp. 1351–8, July 2001.

[3] R. W. Coatney, "Ultrasound imaging: principles and applications in rodent research.," *ILAR J.*, vol. 42, pp. 233–47, Jan. 2001.

[4] J. D. Bronzino, *The Biomedical Engineering Handbook, Volume I*. CRC Prress, 1999.

[5] F. Walker and M. S. Cartwright, *Neuromuscular Ultrasound*. Elsevier, 2011.

[6] J. Z. Heckmatt, V. Dubowitz, and S. Leeman, "Detection of pathological change in dystrophic muscle with B-scan ultrasound imaging.," *Lancet*, vol. 1, pp. 1389–90, June 1980.

[7] S. Pillen, I. M. P. Arts, and M. J. Zwarts, "Muscle ultrasound in neuromuscular disorders.," *Muscle Nerve*, vol. 37, pp. 679–93, June 2008.

[8] M. Ito, Y. Kawakami, Y. Ichinose, S. Fukashiro, and T. Fukunaga, "Nonisometric behavior of fascicles during isometric contractions of a human muscle.," *J.Appl Phys.*, vol. 85, pp. 1230–5, Oct. 1998.

[9] M. V. Narici, T. Binzoni, E. Hiltbrand, J. Fasel, F. Terrier, and P. Cerretelli, "In vivo human gastrocnemius architecture with changing joint angle at rest and during graded isometric contraction.," *J. Physiol.*, vol. 496 (Pt 1, pp. 287–97, Oct. 1996.

[10] V. L. K. William D. McArdle ,Frank I. Katch, *Exercise Physiology: Energy, Nutrition, and Human Performance*. Lippincott Williams & Wilkins, 2001.

[11] S. D.U., *Human Physiology: An Integrated Approach*. Pearson, 2006.

[12] A. J. Vander;J.H. Sherman; D.S. Luciano, *Human Physiology: The Mechanisms of Body Function*. McGraw-Hill, 2004.

[13] E. D. Adrian and D. W. Bronk, "The discharge of impulses in motor nerve fibres: Part II. The frequency of discharge in reflex and voluntary contractions.," *J. Physiol.*, vol. 67, pp. i3–151, Mar. 1929.

[14] E. Henneman, G. Somjen, and D. O. Carpenter, "Functional significance of cell size in spinal motoneurons.," *J. Neurophysiol*, vol. 28, pp. 560–80, May 1965.

[15] E. F. Hodson-Tole and J. M. Wakeling, "Motor unit recruitment patterns 2: the influence of myoelectric intensity and muscle fascicle strain rate.," *J Exp Biol.*, vol. 211, pp. 1893–1902, June 2008.

[16] R. L. Lieber and J. Fridén, "Functional and clinical significance of skeletal muscle architecture.," *Muscle Nerve*, vol. 23, pp. 1647–66, Nov. 2000.

[17] R. L. Lieber and J. Fridén, "Clinical significance of skeletal muscle architecture.," *Clin. Orthop. Relat R.*, pp. 140–51, Feb. 2001.

[18] R. L. Lieber and S. C. Bodine-Fowler, "Skeletal muscle mechanics: implications for rehabilitation.," *Phys. Ther.*, vol. 73, pp. 844–56, Dec. 1993.

[19] H. H and H. H, "Changes in the cross-striations of muscle during contraction and stretch and their structural interpretation.," *Nature*, vol. 173, pp. 973–6, May 1954.

[20] E. Hultman, H. Sjöholm, I. Jäderholm-Ek, and J. Krynicki, "Evaluation of methods for electrical stimulation of human skeletal muscle in situ.," *Pflugers Arch.*, vol. 398, pp. 139–41, July 1983.

[21] N. A. Maffiuletti, "Physiological and methodological considerations for the use of neuromuscular electrical stimulation.," *Eur J Appl Physiol.*, vol. 110, pp. 223–34, Sept. 2010.

[22] R. Martin, C. Sadowsky, K. Obst, B. Meyer, and J. McDonald, "Functional electrical stimulation in spinal cord injury:: from theory to practice.," *Top Spinal Cord Inj Rehabil.*, vol. 18, pp. 28–33, Jan. 2012.

[23] L. W. T, H. J. Holmquest, D. Scot, and M. Dow, "Functional electrotherapy: stimulation of the peroneal nerve synchronized with the swing phase of the gait of hemiplegic patients.," *Arch Phys Med Rehabil.*, vol. 42, pp. 101–5, Feb. 1961.

[24] M. Vanderthommen and J. Duchateau, "Electrical stimulation as a modality to improve performance of the neuromuscular system.," *Exerc Sport Sci Rev.*, vol. 35, pp. 180–5, Oct. 2007.

[25] B. Reed, "The Physiology of Neuromuscular Electrical Stimulation.," *Pediatr Phys Ther*, vol. 9, pp. 96–102, 1997.

[26] C. M. Gregory and C. S. Bickel, "Recruitment patterns in human skeletal muscle during electrical stimulation.," *Phys Ther*, vol. 85, pp. 358–64, Apr. 2005.

[27] C. S. Bickel, C. M. Gregory, and J. C. Dean, "Motor unit recruitment during neuromuscular electrical stimulation: a critical appraisal.," *Eur J Appl Physiol.*, vol. 111, pp. 2399–407, Oct. 2011.

[28] L. R. Sheffler and J. Chae, "Neuromuscular electrical stimulation in neurorehabilitation.," *Muscle Nerve*, vol. 35, pp. 562–90, May 2007.

[29] J. S. Knutson, G. G. Naples, P. H. Peckham, and M. W. Keith, "Electrode fracture rates and occurrences of infection and granuloma associated with percutaneous intramuscular electrodes in upper-limb functional electrical stimulation applications.," *J Rehabil Res Dev.*, vol. 39, no. 6, pp. 671–83.

[30] D. N. Rushton, "Functional electrical stimulation.," *Physiol Meas.*, vol. 18, pp. 241–75, Nov. 1997.

[31] B. M. Doucet, A. Lam, and L. Griffin, "Neuromuscular electrical stimulation for skeletal muscle function.," *Yale J Biol Med.*, vol. 85, pp. 201–15, June 2012.

[32] D. I, J. Macvicar, and T. G. Brown, "Investigation of abdominal masses by pulsed ultrasound.," *Lancet (London, England)*, vol. 1, pp. 1188–95, June 1958.

[33] K. T. Dussik, D. J. Fritch, M. Kyriazidou, and R. S. Sear, "Measurements of articular tissues with Ultrasound," *Am J Phys Med*, vol. 37, pp. 160–165, June 1958.

[34] D. Kane, W. Grassi, R. Sturrock, and P. V. Balint, "A brief history of musculoskeletal ultrasound: 'From bats and ships to babies and hips'.," *Rheumatology (Oxford)*, vol. 43, pp. 931–3, July 2004.

[35] D. G. McDonald and G. R. Leopold, "Ultrasound B-scanning in the differentiation of Baker's cyst and thrombophlebitis.," *Br J Radiol*, vol. 45, pp. 729–32, Oct. 1972.

[36] A. Young, I. Hughes, P. Russell, M. J. Parkers, and P. J. Nichols, "Measurement of quadriceps muscle wasting by ultrasonography.," *Rheumatol Rehabil*, vol. 19, pp. 141–8, Aug. 1980.

[37] A. Young, M. Stokes, and M. Crowe, "Size and strength of the quadriceps muscles of old and young women.," *Eur J Clin Invest.*, vol. 14, pp. 282–7, Aug. 1984.

[38] A. Young, M. Stokes, J. M. Round, and R. H. Edwards, "The effect of high-resistance training on the strength and cross-sectional area of the human quadriceps.," *Eur J Clin Invest*, vol. 13, pp. 411–7, Oct. 1983.

[39] J. L. Whittaker, D. S. Teyhen, J. M. Elliott, K. Cook, H. M. Langevin, H. H. Dahl, and M. Stokes, "Rehabilitative ultrasound imaging: understanding the technology and its applications.," *J. Orthop. Sport. Phys.*, vol. 37, pp. 434–49, Aug. 2007.

[40] W. Grassi, E. Filippucci, and P. Busilacchi, "Musculoskeletal ultrasound.," *Best Pract Res Clin Rheumatol.*, vol. 18, pp. 813–26, Dec. 2004.

[41] F. O. Walker, M. S. Cartwright, E. R. Wiesler, and J. Caress, "Ultrasound of nerve and muscle.," *Clin Neurophysiol.*, vol. 115, pp. 495–507, Mar. 2004.

[42] N. D. Reeves and M. V. Narici, "Behavior of human muscle fascicles during shortening and lengthening contractions in vivo.," *Journal of applied physiology (Bethesda, Md. : 1985)*, vol. 95, pp. 1090–6, Sept. 2003.

[43] D. Teyhen, "Rehabilitative Ultrasound Imaging Symposium San Antonio, TX, May 8-10, 2006.," *J. Orthop. Sport. Phys.*, vol. 36, pp. A1–3, Aug. 2006.

[44] E. Azizi, E. L. Brainerd, and T. J. Roberts, "Variable gearing in pennate muscles.," *Proc Natl Acad Sci U S A.*, vol. 105, pp. 1745–50, Feb. 2008.

[45] C. Gans and A. S. Gaunt, "Muscle architecture in relation to function.," *J Biomech*, vol. 24 Suppl 1, pp. 53–65, Jan. 1991.

[46] C. Gans and W. J. Bock, "The functional significance of muscle architecture–a theoretical analysis.," *Ergeb Anat Entwicklungsgesch.*, vol. 38, pp. 115–42, Jan. 1965.

[47] C. Gans and F. de Vree, "Functional bases of fiber length and angulation in muscle.," *J Morphol.*, vol. 192, pp. 63–85, Apr. 1987.

[48] T. Muramatsu, T. Muraoka, D. Takeshita, Y. Kawakami, Y. Hirano, and T. Fukunaga, "Mechanical properties of tendon and aponeurosis of human gastrocnemius muscle in vivo," pp. 1671–1678, 2001.

[49] C. N. Maganaris, "Force-length characteristics of the in vivo human gastrocnemius muscle.," *Clin Anat (New York, N.Y.)*, vol. 16, pp. 215–23, May 2003.

[50] C. N. Maganaris, V. Baltzopoulos, and A. J. Sargeant, "In vivo measurements of the triceps surae complex architecture in man: implications for muscle function.," *J Physiol*, vol. 512 (Pt 2, pp. 603–14, Oct. 1998.

[51] P. W. Hodges, L. H. M. Pengel, R. D. Herbert, and S. C. Gandevia, "Measurement of muscle contraction with ultrasound imaging.," *Muscle Nerve*, vol. 27, pp. 682–92, June 2003.

[52] P. B. Zatsiorsky V, *Biomechanics of Skeletal Muscles*. 2012.

[53] L. R., *Skeletal Muscle Structure, Function, and Plasticity*. Lippincott Williams & Wilkins, 2002.

[54] T. Fukunaga, Y. Ichinose, M. Ito, Y. Kawakami, and S. Fukashiro, "Determination of fascicle length and pennation in a contracting human muscle in vivo.," *J Appl Physiol (1985)*, vol. 82, pp. 354–8, Jan. 1997.

[55] R. L. Lieber, G. J. Loren, and J. Fridén, "In vivo measurement of human wrist extensor muscle sarcomere length changes.," *J Neurophysiol.*, vol. 71, pp. 874–81, Mar. 1994.

[56] Y. Kawakami, Y. Ichinose, and T. Fukunaga, "Architectural and functional features of human triceps surae muscles during contraction.," *J. Appl . Physiol. (1985)*, vol. 85, pp. 398–404, Aug. 1998.

[57] T. Fukunaga, Y. Kawakami, S. Kuno, K. Funato, and S. Fukashiro, "Muscle architecture and function in humans.," *J Biomech.*, vol. 30, pp. 457–63, May 1997.

[58] J. Z. Heckmatt, N. Pier, and V. Dubowitz, "Measurement of quadriceps muscle thickness and subcutaneous tissue thickness in normal children by real-time ultrasound imaging.," *J Clin Ultrasound.*, vol. 16, no. 3, pp. 171–6, 1988.

[59] S. Pillen and N. van Alfen, "Skeletal muscle ultrasound.," *Neurol Res.*, vol. 33, pp. 1016–24, Dec. 2011.

[60] S. Pillen, R. O. Tak, M. J. Zwarts, M. M. Y. Lammens, K. N. Verrijp, I. M. P. Arts, J. A. van der Laak, P. M. Hoogerbrugge, B. G. M. van Engelen, and A. Verrips, "Skeletal muscle ultrasound: correlation between fibrous tissue and echo intensity.," *Ultrasound Med Biol.*, vol. 35, pp. 443–6, Mar. 2009.

[61] S. Pillen, M. van Keimpema, R. A. J. Nievelstein, A. Verrips, W. van Kruijsbergen-Raijmann, and M. J. Zwarts, "Skeletal muscle ultrasonography: Visual versus quantitative evaluation.," *Ultrasound Med Biol.*, vol. 32, pp. 1315–21, Sept. 2006.

[62] P. Liu, Y. Wang, H. Hu, Y. Mao, D. Huang, and L. Li, "Change of muscle architecture following body weight support treadmill training for persons after subacute stroke: evidence from ultrasonography.," *Biomed Res Int.*, vol. 2014, p. 270676, Jan. 2014.

[63] A. Kaya, M. Kara, T. Tiftik, M. Tezcan, S. Ozel, M. Ersöz, B. Göker, S. Haznedarolu, and L. Ozçakar, "Ultrasonographic evaluation of the muscle architecture in patients with systemic lupus erythematosus.," *Clin Rheumatol.*, vol. 32, pp. 1155–60, Aug. 2013.

[64] I. Loram, C. N. Maganaris, and M. Lakie, "Use of ultrasound to make noninvasive in vivo measurement of continuous changes in human muscle contractile length.," *J. Appl . Physiol.*, vol. 100, pp. 1311–23, Apr. 2006.

[65] D. D. Shin, J. A. Hodgson, V. R. Edgerton, and S. Sinha, "In vivo intramuscular fascicle-aponeuroses dynamics of the human medial gastrocnemius during plantarflexion and dorsiflexion of the foot.," *J.Appl Phys.*, vol. 107, pp. 1276–84, Oct. 2009.

[66] J. Bojsen-Moller, S. Schwartz, K. K. Kalliokoski, T. Finni, and S. P. Magnusson, "Intermuscular force transmission between human plantarflexor muscles in vivo.," *J Appl Physiol*, vol. 109, pp. 1608–18, Dec. 2010.

[67] D. D. Shin, J. a. Hodgson, V. R. Edgerton, and S. Sinha, "In vivo intramuscular fascicle-aponeuroses dynamics of the human medial gastrocnemius during plantarflexion and dorsiflexion of the foot.," *Journal of applied physiology (Bethesda, Md. : 1985)*, vol. 107, pp. 1276–84, Oct. 2009.

[68] R. Kinugasa, Y. Kawakami, S. Sinha, and T. Fukunaga, "Unique spatial distribution of in vivo human muscle activation.," *Exp. Physiol.*, vol. 96, pp. 938–48, Sept. 2011.

[69] S. P. Magnusson, P. Hansen, P. Aagaard, J. Brond, P. Dyhre-Poulsen, J. Bojsen-Moller, and M. Kjaer, "Differential strain patterns of the human gastrocnemius aponeurosis and free tendon, in vivo.," *Acta Physiol Scand.*, vol. 177, pp. 185–95, Feb. 2003.

[70] J. Gillett, R. S. Barrett, and G. Lichtwark, "Reliability and accuracy of an automated tracking algorithm to measure controlled passive and active muscle fascicle length changes from ultrasound.," *Comput. Method. Biomech. Biomed. Engin.*, pp. 37–41, Jan. 2012.

[71] S. Kawamoto, I. G. Student, N. Imamoglu, J. D. Gomez-tames, and K. Kita, "Ultrasound Imaging and Semi-Automatic Analysis of Active Muscle Features in Electrical Stimulation by Optical Flow," in *Conf Proc IEEE Eng Med Biol Soc. 2014*, vol. 2609, pp. 250–253, 2014.

[72] N. J. Cronin, C. P. Carty, R. S. Barrett, and G. Lichtwark, "Automatic tracking of medial gastrocnemius fascicle length during human locomotion.," *J Appl Physiol (1985)*, vol. 111, pp. 1491–6, Nov. 2011.

[73] J. Bojsen-Mø ller, S. Schwartz, K. K. Kalliokoski, T. Finni, and S. P. Magnusson, "Intermuscular force transmission between human plantarflexor muscles in vivo.," *J Appl Physiol (1985).*, vol. 109, pp. 1608–18, Dec. 2010.

[74] R. I. Griffiths, "Shortening of muscle fibres during stretch of the active cat medial gastrocnemius muscle: the role of tendon compliance.," *J. Physiol.*, vol. 436, pp. 219–36, May 1991.

[75] D. F. Hoyt, S. J. Wickler, A. A. Biewener, E. A. Cogger, and K. L. De La Paz, "In vivo muscle function vs speed. I. Muscle strain in relation to length change of the muscle-tendon unit.," *J Exp Biol.*, vol. 208, pp. 1175–90, Mar. 2005.

[76] S. L. Wolf, R. L. Segal, and A. W. English, "Task-oriented EMG activity recorded from partitions in human lateral gastrocnemius muscle.," *J Electromyogr Kinesiol.*, vol. 3, pp. 87–94, Jan. 1993.

[77] E. F. Hodson-Tole, I. D. Loram, and T. M. M. Vieira, "Myoelectric activity along human gastrocnemius medialis: different spatial distributions of postural and electrically elicited surface potentials.," *Journal of electromyography and kinesiology : official journal of the International Society of Electrophysiological Kinesiology*, vol. 23, pp. 43–50, Feb. 2013.

[78] D. Kernell, "Muscle regionalization.," *Can J Appl Physiol.*, vol. 23, pp. 1–22, Feb. 1998.

[79] J. Darby, E. F. Hodson-Tole, N. Costen, and I. D. Loram, "Automated regional analysis of B-mode ultrasound images of skeletal muscle movement.," *Journal of applied physiology (Bethesda, Md. : 1985)*, vol. 112, pp. 313–27, Jan. 2012.

[80] O. A. Smiseth and H. Ihlen, "Strain rate imaging: why do we need it?," *J Am Coll Cardiol.*, vol. 42, pp. 1584–6, Nov. 2003.

[81] N. L. Greenberg, M. S. Firstenberg, P. L. Castro, M. Main, A. Travaglini, J. Odabashian, J. K. Drinko, L. L. Rodriguez, J. D. Thomas, and M. J. Garcia, "Doppler-derived myocardial systolic strain rate is a strong index of left ventricular contractility.," *Circulation*, vol. 105, pp. 99–105, Jan. 2002.

[82] J. M. Wakeling, K. Uehli, and A. I. Rozitis, "Muscle fibre recruitment can respond to the mechanics of the muscle contraction.," *J R Soc Interface*, vol. 3, pp. 533–44, Aug. 2006.

[83] S. S. M. Lee, M. Miara, A. S. Allison, A. A. Biewener, and J. M. Wakeling, "Recruitment of faster motor units is associated with greater rates of fascicle strain and rapid changes in muscle force during locomotion.," *J Exp Biol.*, vol. 216, pp. 198–207, Jan. 2013.

[84] F. Lindberg, F. Ohberg, L. A. Brodin, and C. Grönlund, "Assessment of intramuscular activation patterns using ultrasound M-mode strain.," *J Electromyogr Kinesiol.*, vol. 23, pp. 879–85, Aug. 2013.

[85] T. Deffieux, J.-L. Gennisson, M. Tanter, and M. Fink, "2J-5 Ultrafast Ultrasonic Imaging of In Vivo Muscle Contraction," *2006 IEEE Ultrasonics Symposium*, pp. 1001–1004, 2006.

[86] S. Kim, H. Park, and S. Y. Lee, "Usefulness of strain elastography of the musculoskeletal system.," *Ultrasonography*, vol. 35, pp. 104–9, Apr. 2016.

[87] P. Lalitha, M. C. Reddy, and K. J. Reddy, "Musculoskeletal applications of elastography: a pictorial essay of our initial experience.," *Korean J Radiol*, vol. 12, no. 3, pp. 365–75, 2011.

[88] R. T. Abresch, J. J. Han, and G. T. Carter, "Rehabilitation management of neuromuscular disease: the role of exercise training.," *J. Clin. Neuromusc. Dis.*, vol. 11, pp. 7–21, Sept. 2009.

[89] N. B. Voet, E. L. Van der Kooi, I. I. Riphagen, E. Lindeman, B. G. van Engelen, and A. C. Geurts, "Strength training and aerobic exercise training for muscle disease.," *Cochrane Db. Syst. Rev.*, p. CD003907, Jan. 2010.

[90] R. L. Rahl, *Physical Activity and Health Guidelines*. Human Kinetics, 2010.

[91] P. L. Jacobs and M. Nash, "Exercise recommendations for individuals with spinal cord injury.," *Sports Med.*, vol. 34, pp. 727–51, Jan. 2004.

[92] T. Gordon and J. Mao, "Muscle atrophy and procedures for training after spinal cord injury.," *Phys Ther.*, vol. 74, pp. 50–60, Jan. 1994.

[93] S. Binder-Macleod and T. Kesar, "Catchlike property of skeletal muscle: recent findings and clinical implications.," *Muscle Nerve*, vol. 31, pp. 681–93, June 2005.

[94] C. M. Gregory and C. S. Bickel, "Recruitment Patterns in Human Skeletal Muscle During Electrical," pp. 358–364, 2005.

[95] A. Carty, K. McCormack, G. F. Coughlan, L. Crowe, and B. Caulfield, "Increased aerobic fitness after neuromuscular electrical stimulation training in adults with spinal cord injury.," *Arch Phys Med Rehabil. 2*, vol. 93, pp. 790–5, May 2012.

[96] J. S. Petrofsky and R. Stacy, "The effect of training on endurance and the cardiovascular responses of individuals with paraplegia during dynamic exercise induced by functional electrical stimulation.," *Eur. J. Appl. Physiol.*, vol. 64, pp. 487–92, Jan. 1992.

[97] L. Griffin, M. J. Decker, J. Y. Hwang, B. Wang, K. Kitchen, Z. Ding, and J. L. Ivy, "Functional electrical stimulation cycling improves body composition, metabolic and neural factors in persons with spinal cord injury.," *J.Electromyogr. Kines.*, vol. 19, pp. 614–22, Aug. 2009.

[98] N. K. Vø llestad, "Measurement of human muscle fatigue," *J. Neurosci Meth.*, vol. 74, no. 2, pp. 219–27, 1997.

[99] M. J. Decker, L. Griffin, L. D. Abraham, and L. Brandt, "Alternating stimulation of synergistic muscles during functional electrical stimulation cycling improves endurance in persons with spinal cord injury.," *J.Electromyogr. Kines.*, vol. 20, pp. 1163–9, Dec. 2010.

[100] C. K. Kim, J. Bangsbo, S. Strange, J. Karpakka, and B. Saltin, "Metabolic response and muscle glycogen depletion pattern during prolonged electrically induced dynamic exercise in man.," *Scand J Rehabil Med.*, vol. 27, pp. 51–8, Mar. 1995.

[101] P. Feiereisen, J. Duchateau, and K. Hainaut, "Motor unit recruitment order during voluntary and electrically induced contractions in the tibialis anterior.," *Exp Brain Res.*, vol. 114, pp. 117–23, Mar. 1997.

[102] M. Knaflitz, R. Merletti, and C. J. De Luca, "Inference of motor unit recruitment order in voluntary and electrically elicited contractions.," *J Appl Physiol (1985).*, vol. 68, pp. 1657–67, Apr. 1990.

[103] W. B. Scott, S. C. K. Lee, T. E. Johnston, and S. Binder-Macleod, "Switching stimulation patterns improves performance of paralyzed human quadriceps muscle.," *Muscle Nerve*, vol. 31, pp. 581–8, May 2005.

[104] S. A. Binder-Macleod and W. A. McLaughlin, "Effects of asynchronous stimulation on the human quadriceps femoris muscle.," *Arch. Phys. Med. Rehab.*, vol. 78, pp. 294–7, Mar. 1997.

[105] L. Z. Popovic and N. M. Malesevic, "Muscle fatigue of quadriceps in paraplegics: comparison between single vs. multi-pad electrode surface stimulation.," in *Conf Proc IEEE Eng Med Biol Soc. 2009*, vol. 2009, pp. 6785–8, Jan. 2009.

[106] A. J. Bergquist, J. M. Clair, and D. F. Collins, "Motor unit recruitment when neuromuscular electrical stimulation is applied over a nerve trunk compared with a muscle belly: triceps surae.," *J Appl Physiol (1985)*, vol. 110, pp. 627–37, Mar. 2011.

[107] D. F. Collins, "Central contributions to contractions evoked by tetanic neuromuscular electrical stimulation.," *Exerc Sport Sci Rev.*, vol. 35, pp. 102–9, July 2007.

[108] A. J. Bergquist, J. M. Clair, O. Lagerquist, C. S. Mang, Y. Okuma, and D. F. Collins, "Neuromuscular electrical stimulation: implications of the electrically evoked sensory volley.," *Eur J Appl Physiol.*, vol. 111, pp. 2409–26, Oct. 2011.

[109] G. R. Adams, R. T. Harris, D. Woodard, and G. A. Dudley, "Mapping of electrical muscle stimulation using MRI.," *J Appl Physiol (1985).*, vol. 74, pp. 532–7, Feb. 1993.

[110] E. A. Hillegass and G. A. Dudley, "Surface electrical stimulation of skeletal muscle after spinal cord injury.," *Spinal cord*, vol. 37, pp. 251–7, Apr. 1999.

[111] M. Knaflitz, R. Merletti, and C. J. De Luca, "Inference of motor unit recruitment order in voluntary and electrically elicited contractions.," *J. Appl . Physiol.*, vol. 68, pp. 1657–67, Apr. 1990.

[112] R. A. Meyer and B. M. Prior, "Functional magnetic resonance imaging of muscle.," *Exerc Sport Sci Rev*, vol. 28, pp. 89–92, Apr. 2000.

[113] B. M. Damon, E. A. Louie, and O. A. Sanchez, "Physiological basis of muscle functional MRI.," *J Gravit Physiol.*, vol. 14, pp. P85–8, July 2007.

[114] A. J. Bergquist, M. J. Wiest, and D. F. Collins, "Motor unit recruitment when neuromuscular electrical stimulation is applied over a nerve trunk compared with a muscle belly: quadriceps femoris.," *J. Appl . Physiol. (1985)*, vol. 113, pp. 78–89, July 2012.

[115] C. J. Heckman and R. M. Enoka, *Clinical Neurophysiology of Motor Neuron Diseases*, vol. 4 of *Handbook of Clinical Neurophysiology*. Elsevier, 2004.

[116] I. R. E. Burke, D. N. Levine, P. Tsairis, and F. E. Zajac, "Physiological types and histochemical profiles in motor units of the cat gastrocnemius," *J Physiol.*, vol. 234, pp. 723–748, 1973.

[117] Z. H. He, R. Bottinelli, M. A. Pellegrino, M. A. Ferenczi, and C. Reggiani, "ATP consumption and efficiency of human single muscle fibers with different myosin isoform composition.," *Biophys J*, vol. 79, pp. 945–61, Aug. 2000.

[118] G. Rau, C. Disselhorst-Klug, and J. Silny, "Noninvasive approach to motor unit characterization: muscle structure, membrane dynamics and neuronal control.," *J. Biomech.*, vol. 30, pp. 441–6, May 1997.

[119] A. Holtermann, K. Roeleveld, and J. S. Karlsson, "Inhomogeneities in muscle activation reveal motor unit recruitment.," *J Electromyogr Kinesiol.*, vol. 15, pp. 131–7, Apr. 2005.

[120] A. Turrina, M. A. Martínez-González, and C. Stecco, "The muscular force transmission system: role of the intramuscular connective tissue.," *J Body Mov Ther.*, vol. 17, pp. 95–102, Jan. 2013.

[121] J. A. Hodgson, T. Finni, A. M. Lai, V. R. Edgerton, and S. Sinha, "Influence of structure on the tissue dynamics of the human soleus muscle observed in MRI studies during isometric contractions.," *J Morphol.*, vol. 267, pp. 584–601, May 2006.

[122] R. J. Monti, R. R. Roy, J. A. Hodgson, and V. R. Edgerton, "Transmission of forces within mammalian skeletal muscles.," *J Biomech*, vol. 32, pp. 371–80, Apr. 1999.

[123] T. Finni, J. A. Hodgson, A. M. Lai, V. R. Edgerton, and S. Sinha, "Mapping of movement in the isometrically contracting human soleus muscle reveals details of its structural and functional complexity.," *J Appl Physiol (1985).*, vol. 95, pp. 2128–33, Nov. 2003.

[124] H. Maas and T. G. Sandercock, "Force transmission between synergistic skeletal muscles through connective tissue linkages.," *J Biomed Biotechnol.*, vol. 2010, p. 575672, Jan. 2010.

[125] P. a. Huijing, "Epimuscular myofascial force transmission: a historical review and implications for new research. International Society of Biomechanics Muybridge Award Lecture, Taipei, 2007.," *J Biomech*, vol. 42, pp. 9–21, Jan. 2009.

[126] H. Maas and T. G. Sandercock, "Are skeletal muscles independent actuators? Force transmission from soleus muscle in the cat.," *J Appl Physiol (1985).*, vol. 104, pp. 1557–67, June 2008.

[127] C. a. Yucesoy, H. Maas, B. H. F. J. M. Koopman, H. J. Grootenboer, and P. a. Huijing, "Mechanisms causing effects of muscle position on proximo-distal muscle force differences in extra-muscular myofascial force transmission.," *Med Eng Phys*, vol. 28, pp. 214–26, Apr. 2006.

[128] B. P. V. Zatsiorsky, *Biomechanics of Skeletal Muscles*. 2012.

[129] J. Darby, E. F. Hodson-Tole, N. Costen, and I. D. Loram, "Automated regional analysis of B-mode ultrasound images of skeletal muscle movement.," *Journal of applied physiology (Bethesda, Md. : 1985)*, vol. 112, pp. 313–27, Jan. 2012.

[130] R. Cunningham, *The application of B-Mode Ultrasonography for analysis of human skeletal muscle*. PhD thesis, 2015.

[131] T. C. Cootes T.F., "Active Shape Models. Their training and application," *Comput. Vis. Image Undage Und*, pp. 38–59, 1995.

[132] T. C. Shi J, "Good features to track.," in *Computer Vision and Pattern Recognition.*, pp. 593–600, 1994.

[133] J. Darby, E. F. Hodson-Tole, N. Costen, and I. D. Loram, "Automated regional analysis of B-mode ultrasound images of skeletal muscle movement.," *J. Appl . Physiol.*, vol. 112, pp. 313–27, Jan. 2012.

[134] P. C. P.K., Nag, Tripathi K, *Basic Mechanical Engineering.* Tata McGraw-Hill Education, 2009.

[135] I. Mirsky and W. W. Parmley, "Assessment of passive elastic stiffness for isolated heart muscle and the intact heart.," *Circ Res*, vol. 33, pp. 233–43, Aug. 1973.

[136] T. P. Abraham and R. A. Nishimura, "Myocardial strain: can we finally measure contractility?," *J Am Coll Cardiol*, vol. 37, pp. 731–4, Mar. 2001.

[137] S. M. H. Newsom, J., R. N. Jones, *Longitudinal data analysis.* Routledge, 2011.

[138] J. Jiang, *Linear and Generalized Linear Mixed Models and Their Applications.* Springer, 2007.

[139] C. B. Moler, "Least Squares," in *Numerical Computing with MATLAB: Revised Reprint* (S. I. Mathematics and Applied, eds.), ch. 5, 2004.

[140] L. H. Refaeilzadeh P, Tang L, "Cross-Validation," in *Encyclopedia of Database Systems* (L. LIU and M. T. ÖZSU, eds.), pp. 532–538, Boston, MA: Springer US, 2009.

[141] J. Li, Y. Zhou, K. Ivanov, and Y. Zheng, "Estimation and visualization of longitudinal muscle motion using ultrasonography: a feasibility study.," *Ultrasonics*, vol. 54, pp. 779–88, Mar. 2014.

[142] N. J. Cronin, C. P. Carty, R. S. Barrett, and G. Lichtwark, "Automatic tracking of medial gastrocnemius fascicle length during human locomotion.," *Journal of applied physiology (Bethesda, Md. : 1985)*, vol. 111, pp. 1491–6, Nov. 2011.

[143] M. Ito, Y. Kawakami, Y. Ichinose, S. Fukashiro, and T. Fukunaga, "Nonisometric behavior of fascicles during isometric contractions of a human muscle.," *J. Appl . Physiol.*, vol. 85, pp. 1230–5, Oct. 1998.

[144] E. Azizi and T. J. Roberts, "Biaxial strain and variable stiffness in aponeuroses.," *J. Physiol.*, vol. 587, pp. 4309–18, Sept. 2009.

[145] R. S. Gupta, R., "Hysteresis of the diary cow's teat as affected by vacuum level rates of change," *Can. Agric. Eng.*, vol. 28, pp. 149–153, 1985.

[146] T. Ruch and Patton H.D, *Physiology and biophysics*. Philadelphia, Saunders, 1965.

[147] C. Levy and A. Landesberg, "Hystereses in the force-length relation and regulation of cross-bridge recruitment in tetanized rat trabeculae.," *Am J Physiol Heart Circ Physiol.*, vol. 286, pp. H434–41, Jan. 2004.

[148] S. Walcott and S. X. Sun, "Hysteresis in cross-bridge models of muscle.," *Phys Chem Chem Phys.*, vol. 11, pp. 4871–81, June 2009.

[149] J. M. Wakeling, O. M. Blake, I. Wong, M. Rana, and S. S. M. Lee, "Movement mechanics as a determinate of muscle structure, recruitment and coordination.," *Philos Trans R Soc Lond B Biol Sci*, vol. 366, pp. 1554–1564, May 2011.

[150] J. Bojsen-Moller, S. Schwartz, K. K. Kalliokoski, T. Finni, and S. P. Magnusson, "Intermuscular force transmission between human plantarflexor muscles in vivo.," *J Appl Physiol*, vol. 109, pp. 1608–1618, Dec. 2010.

[151] C. S. Bickel, C. M. Gregory, and J. C. Dean, "Motor unit recruitment during neuromuscular electrical stimulation: a critical appraisal.," *Eur. J. Appl. Physiol.*, vol. 111, pp. 2399–407, Oct. 2011.

[152] M. Gobbo, N. a. Maffiuletti, C. Orizio, and M. a. Minetto, "Muscle motor point identification is essential for optimizing neuromuscular electrical stimulation use.," *Journal of neuroengineering and rehabilitation*, vol. 11, p. 17, Jan. 2014.

[153] F. Jahanmiri-Nezhad, P. Barkhaus, W. Z. Rymer, and P. Zhou, "Innervation zones of fasciculating motor units: observations by a linear electrode array.," *Front Hum Neurosci.*, vol. 9, p. 239, Jan. 2015.

[154] E. Otten, "Concepts and models of functional architecture in skeletal muscle.," *Exerc Sport Sci Rev.*, vol. 16, pp. 89–137, Jan. 1988.

[155] R. E. M. Bowden and E. Zaimis, *Neuromuscular Junction*. Berlin, Heidelberg: Springer Berlin Heidelberg, 1976.

[156] R. E. Burke and W. Z. Rymer, "Relative strength of synaptic input from short-latency pathways to motor units of defined type in cat medial gastrocnemius.," *J Neurophysiol.*, vol. 39, pp. 447–58, May 1976.

[157] T. Fukunaga, M. Miyatani, M. Tachi, M. Kouzaki, Y. Kawakami, and H. Kanehisa, "Muscle volume is a major determinant of joint torque in humans.," *Acta Physiol Scand.*, vol. 172, pp. 249–55, Aug. 2001.

[158] R. Burnham, T. Martin, R. Stein, G. Bell, I. MacLean, and R. Steadward, "Skeletal muscle fibre type transformation following spinal cord injury.," *Spinal cord*, vol. 35, pp. 86–91, Feb. 1997.

[159] W. Youn and J. Kim, "Feasibility of using an artificial neural network model to estimate the elbow flexion force from mechanomyography.," *J Neurosci Methods.*, vol. 194, pp. 386–93, Jan. 2011.

[160] L. L. Menegaldo, L. F. de Oliveira, and K. K. Minato, "EMGD-FE: an open source graphical user interface for estimating isometric muscle forces in the lower limb using an EMG-driven model.," *Biomedical engineering online*, vol. 13, p. 37, Jan. 2014.

[161] X. Chen, Y. Zheng, J. Guo, Z. Zhu, S.-C. Chan, and Z. Zhang, "Sonomyographic responses during voluntary isometric ramp contraction of the human rectus femoris muscle.," *Eur. J. Appl. Physiol.*, vol. 112, pp. 2603–14, July 2012.

[162] M. Knaflitz, R. Merletti, and C. J. De Luca, "Inference of motor unit recruitment order in voluntary and electrically elicited contractions.," *J Appl Physiol (1985).*, vol. 68, pp. 1657–67, Apr. 1990.

[163] L. C., *Signal Processing of Random Physiological Signals.* Morgan & Claypool, 2006.

Appendices

Appendix A

Biomedical Signal processing

Definitions of signal processing and main mathematical approaches for processing are presented in the next sections.

A.1 Definition of Signal

A *signal* is a phenomenon that conveys information. It is generally represented in a mathematical format as a function of time and its abstract notation is given as $x(t)$ or $y(t)$ [4, 163]. Signals that refer to the information of biological systems are called *biomedical signals*. The process of information extraction can vary form the estimation of the heart rate to the structure of internal soft tissues during a CT scan. The mere acquisition of the signal is not always sufficient and, mainly in biomedical applications, a processing aiming at extracting the hidden information is necessary. The signal processing aims at filtering and at enhancing the relevant information not visible. The enhancing process generally requires some transformation.

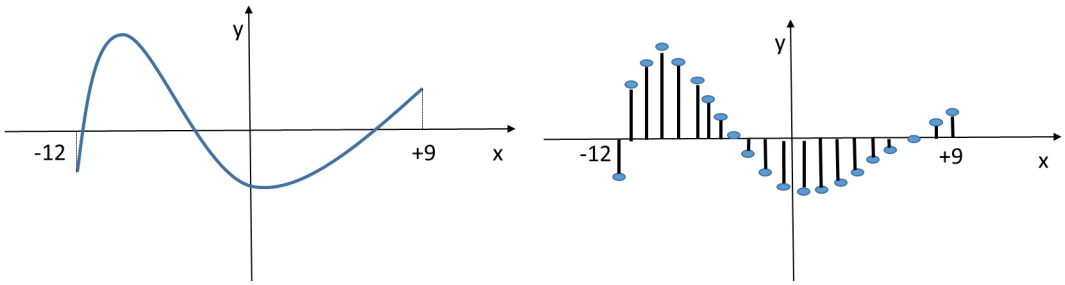

(a) Continuous Signal defined in -12, 9 (b) Discrete Signal defined in -12, 9

Figure A.1: Continuous vs Discrete Signal

The signals are classified as continuous or discrete according to the function that describes them. Most of the biomedical signals are continuous, however the technology available allows only a discrete acquisition. The process of recording a signal using discrete time is known as *sampling*. A given signal $s(t)$, is sampled into the sequence $s(m)$

$$s(m) = s(t)|_{t=m_s T_s} \tag{A.1}$$

Where T_s is the sampling interval which correspond to the **sampling frequency** $f_s = 2\pi/T_s$.

A.2 Deterministic and Stochastic Signals

Signals can be classified as *deterministic* or *stochastic*. A deterministic signal can be completely described at a given time. For example a periodic signal is a deterministic. When the signal is random it is called *stochastic* and it is usually described by a *probability function* $f_x(t)$.

Stochastic signals are described usually described by their statistics characteristics such as the moments and variance. The 1st moment is defined as the average value of the signal, it is known

also as *expected value* and is expressed as:

$$\bar{x}(t) = \int_{-\infty}^{+\infty} x f_x(x) dt = \bar{x} \quad Expected \quad value \tag{A.2}$$

Similarly, the variance of the signal is defined as

$$\sigma^2 = \int_{-\infty}^{+\infty} \left[x - \bar{x(t)}\right]^2 f_x(t) dt \quad Variance \tag{A.3}$$

The variance and the expected value are known as statistic of first order and they are defined independently from the time (time invariant).

On the contrary, the statistics of second order associated with the variables $X(t_1)$ and $X(t_2)$ are dependent on the time differences define as $\tau = |t_1 - t_2|$. Second order statistics are *auto-correlation function* and *covariance*:

$$R_{xx}(\tau) = \int x(t)x(t+\tau)d\tau \quad Autocorrelation \quad function \tag{A.4}$$

$$I_{xx} = [x(t) - x]\,[x(t-\tau) - \bar{x}] \quad Covariance \tag{A.5}$$

A signal whose statistics do not change over time is called *stationary*.

A.3 Energy and Power of a signal

The terms signal energy and signal power are used to characterise a signal. Given a signal $x(t)$, the *Energy* of the signal is defined as:

$$E = \int_{-\infty}^{+\infty} x^2(t) dt < \infty \tag{A.6}$$

While the power is defined as 'the average energy in an interval of time' ad is expressed as:

$$P = \frac{1}{t_2 - t_1} \int_{-t_1}^{t_2} x^2(t) dt \tag{A.7}$$

In the discrete-time, for the signal $x(n)$ the definitions are:

$$E = \sum_{-\infty}^{+\infty} x^2(t)dt < \infty \quad \text{And} \quad P = \frac{1}{t_2 - t_1} \sum_{-t_1}^{t_2} x^2(t)dt \tag{A.8}$$

A.3.1 Time and Frequency Domains

So far, the signal was described in it *time domain* representation. This means that the signal is described according to its values on the time axis.

However it is possible to describe a signal using another representation: the *frequency domain*. The frequency representation describes the signal by sine waves of different amplitudes and phases. This representation holds on the transformation proposed by Fourier and known as *Fourier Transform (FT)*.

$$X(f) = \int_{-\infty}^{+\infty} s(t)e^{-j\omega t}dt = F\{s(t)\} \tag{A.9}$$

Where the frequency is defined $f = 2\pi/\omega$, being ω the angular frequency. The range of frequencies within which the majority of the energy lies is defined as *bandwidth* of the signal.

A.3.1.1 The Power Spectrum and Power Spectral Density (PSD)

The square of the absolute value of the Fourier Transform of a signal is defined as *Power Spectrum*.

$$S_{xx} = |X(f)|^2 \tag{A.10}$$

The power spectrum of a signal describes the distribution of the signals power on the frequency axis.

The Fourier Transform of the autocorrelation function is called *power spectral density function* (PSD).

$$PSD = F\{r_{xx}(\tau)\} = \int_{-\infty}^{+\infty} r_{xx}(\tau)e^{-j\omega t}d\tau \tag{A.11}$$

The PSD is used to describe stochastic signals; it describes the density of power on the frequency axis.

In biomedical signal processing, the PSD is a powerful tool for getting hidden information of the signal. For example, the PSD of EEG signal changes according to physiological and psychological

states of the subject. Therefore it is used for the recognition of such states.

A.3.2 Short Time Fourier Transform (STFT)

The Fourier Transform as expressed in Equation A.9 assumes that the signal is stationary. Unfortunately most of the signals are nonstationary. A way to deal with this problem is to divide the signal into short segments. The segments are chosen in such a way that each of them con be considered as windowed sample of a stationary process. The length of the window can be defined either by a priori knowledge or my examining the local characteristics.

The representation of the Fourier Transform of each of the segments is defined as *short time Fourier transform*(STFT).

$$STFT_x(f,\tau) = F\{x(t)w(t-\tau)\} = \int_{-\infty}^{+\infty} s(t)w(t-\tau)e^{-j\omega t}dt \tag{A.12}$$

Where w is the window shifted on the time axis $t = \tau$ so that the FT is performed on a windowed segment $\tau - (T/2) \leq t \leq \tau + (T/2)$, with T the duration of the window. The STFT describes the PSD of the segment around $t = \tau$. The resolution of the STFT depend on the window duration's T, the smaller is the duration, the higher is the resolution.

A common way of presenting the STFT is by mean of a spectrogram which allows a *time-frequency* analysis. In the spectrogram, the time and the frequency axes are plotted. The PSD estimated using the STFT is given with a colormap. An example of spectrogram is given in Figure A.2.

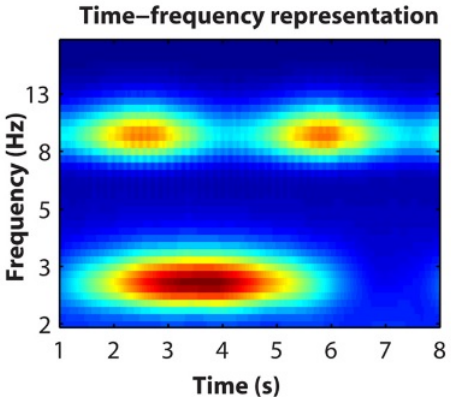

Figure A.2: Example of a Time-Frequency representation. The figure shows three main events. The first happens at time 1.5 to 6 seconds and has frequency of about 2.5 Hz. The other two have frequency of about 10 Hz and they happen respectively at time 2 to 4 seconds and 5 to 7 seconds

Appendix B

Starin

Average strain distribution across trials and subjects for SS and NS tests are presented.

B.1 Strain distribution

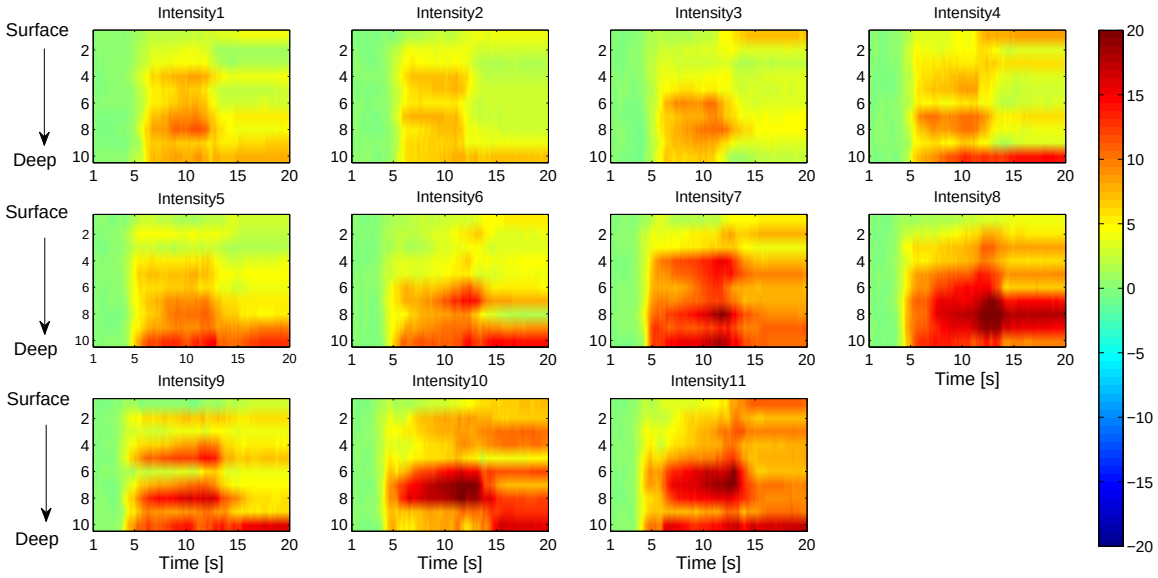

Figure B.1: In figure is shown the average strain at each depth over subjects and during each of the eleven trials (at eleven different stimulation intensities) of the SS task. On the y axis it is indicated the depth and on the x axis the time of the task. The scale of the map is from blue, negative strain, to red, positive strain. The green indicates zero strain

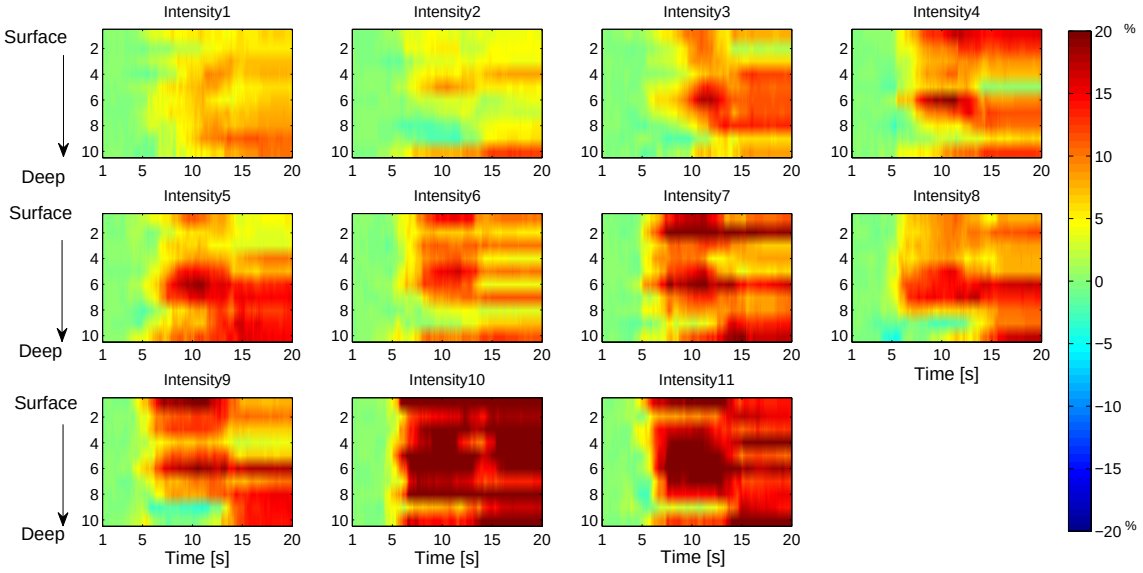

Figure B.2: In figure is shown the average strain at each depth over subjects and during each of the eleven trials (at eleven different stimulation intensities) of the NS task. On the y axis it is indicated the depth and on the x axis the time of the task.

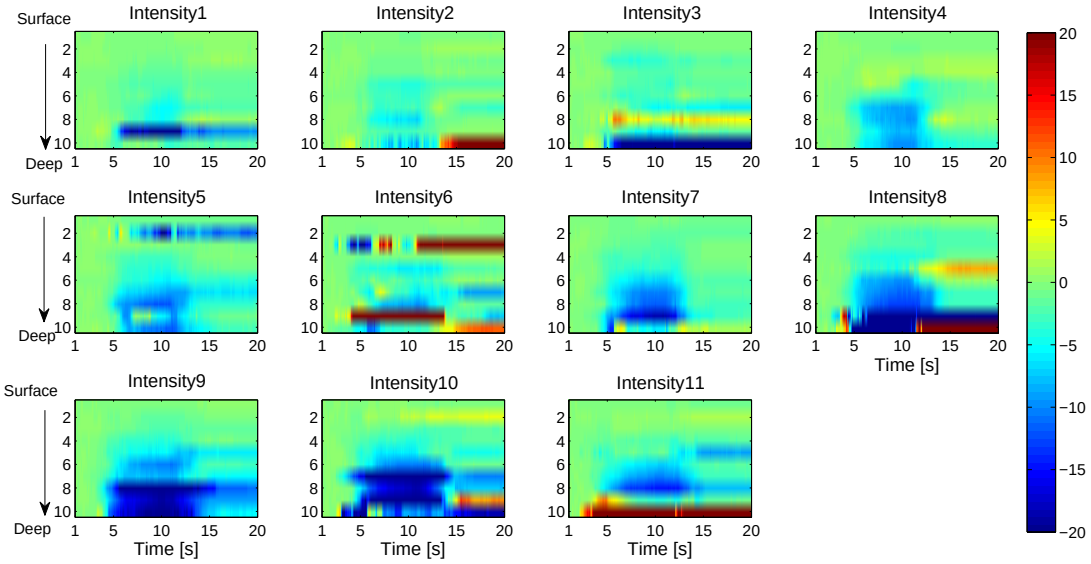

Figure B.3: In figure is shown the average strain at each depth over subjects and during each of the eleven trials (at eleven different stimulation intensities) of the SS task. On the y axis it is indicated the depth and on the x axis the time of the task. The scale of the map is from blue, negative strain, to red, positive strain. The green indicates zero strain

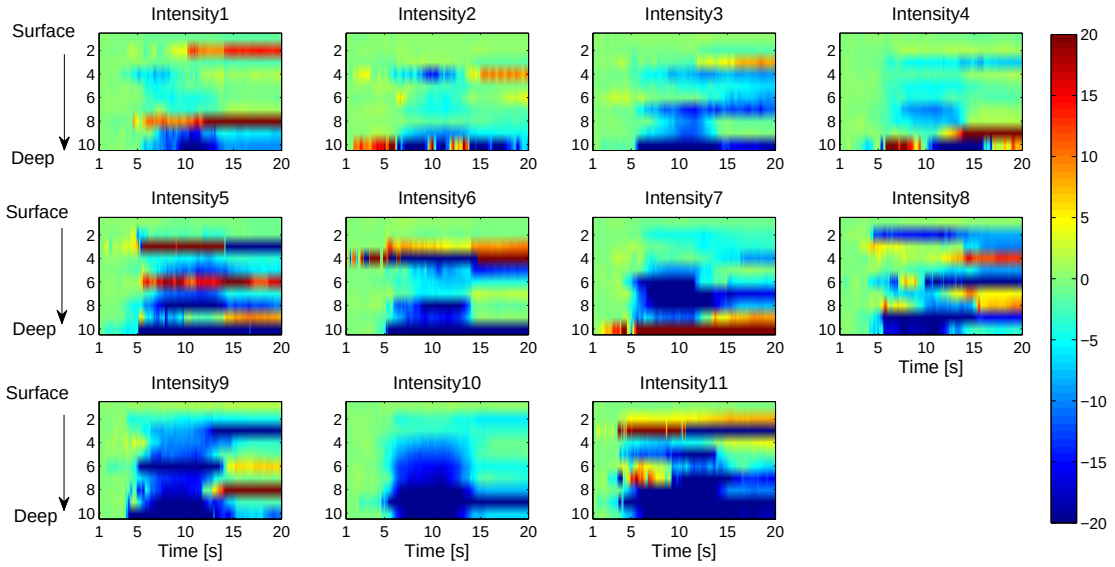

Figure B.4: In figure is shown the average strain at each depth over subjects and during each of the eleven trials (at eleven different stimulation intensities) of the NS task. On the y axis it is indicated the depth and on the x axis the time of the task.

Appendix C

Displacement-Torque: 1st order fitting

First and second order fitting were used to define the displacement- torque relationship. In this appendix the results for the first order fitting are reported.

First order fitting was used to estimate the relationship torque- displacement. Equation C.1 refers to a first order fitting where the displacement is estimated from the torque.

$$P(\tau) = p_1\tau + p_2 \tag{C.1}$$

Where τ represents the torque measured and $P(\tau)$ the displacement (expressed according to its dependency from τ). The polynomial is of order 1 with a total of two coefficients ($p1$, $p2$)

Equation C.2 refers to a first order fitting where the torque is estimated from the displacement.

$$P(\delta) = p_1\delta + p_2 \tag{C.2}$$

The distribution of the coefficients for the estimation of displacement, $P(\tau)$ for both voluntary and FES test is shown in FigureC.1.

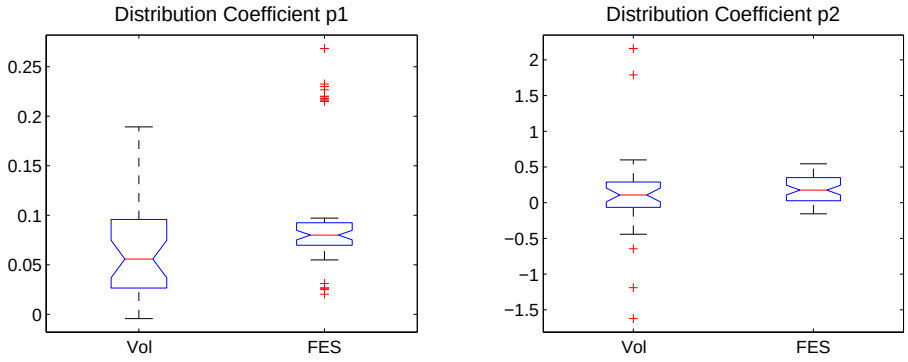

Figure C.1: .
Boxplot of the coefficients estimated for $P(\tau)$ during voluntary and FES test when first order fitting is used. Each subplot represents the distribution of one of the coefficient of the polynomial across subjects and cross-validation Fold. Each box, within each subplot, is the results of a total 55 values (eleven subjects and 5-Fold) for the FES test and 33 values (eleven subjects and 3-Fold) for the voluntary test.

The distribution of the coefficients for the estimation of torque, $P(\delta)$ for both voluntary and FES test is shown in FigureC.2.

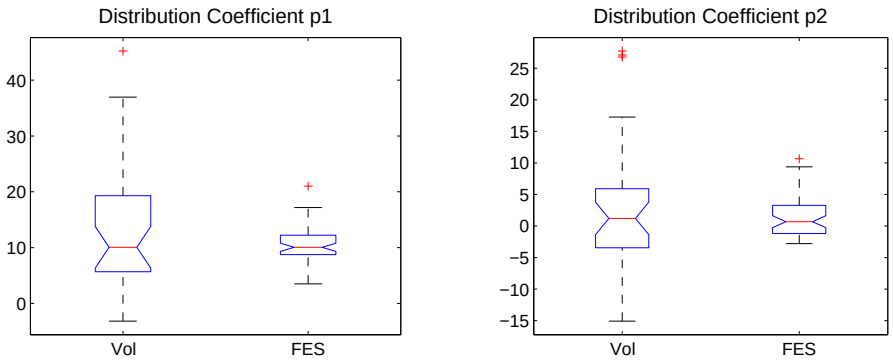

Figure C.2: .
Boxplot of the coefficients estimated for $P(\delta)$ during voluntary and FES test when first order fitting is used. Each subplot represents the distribution of one of the coefficient of the polynomial across subjects and cross-validation Fold. Each box, within each subplot, is the results of a total 55 values (eleven subjects and 5-Fold) for the FES test and 33 values (eleven subjects and 3-Fold) for the voluntary test.

Table C.1: Goodness 1st order curve Fitting displacement's estimation, FES test

Subjects	Whole model						Test Dataset					
	R^2_{adj}			**NRMSE**			R^2_{adj}			**NRMSE**		
	Meadian	**Min**	**Max**	**Meadian**	**Min**	**Max**	**Meadian**	**Min**	**Max**	**Meadian**	**Min**	**Max**
S1	0.96	0.95	0.97	6%	5%	7%	0.95	0.90	0.97	7%	6%	11%
S2	0.86	0.79	0.94	11%	8%	15%	0.77	0.62	0.90	17%	10%	21%
S3	0.94	0.93	0.95	7%	7%	8%	0.91	0.26	0.92	11%	8%	34%
S4	0.97	0.97	0.97	6%	5%	6%	0.98	0.94	0.99	5%	4%	9%
S5	0.78	0.68	0.84	13%	12%	14%	0.74	-4.92	0.87	16%	11%	66%
S6	0.80	0.74	0.85	13%	11%	14%	0.85	0.56	0.91	12%	10%	26%
S7	0.32	0.17	0.53	20%	17%	23%	-1.11	-5.15	0.45	37%	23%	55%
S8	0.71	0.49	0.75	16%	14%	19%	0.36	-0.01	0.86	24%	13%	32%
S9	0.66	0.46	0.71	17%	15%	21%	0.32	0.20	0.51	27%	25%	28%
S10	0.92	0.92	0.94	9%	8%	9%	0.81	-0.91	0.99	16%	5%	44%
S11	0.76	0.26	0.80	11%	11%	22%	0.31	-0.18	0.67	24%	15%	33%

Table C.2: Goodness 1st order curve Fitting displacement's estimation, Vol test

	R^2_{adj}			**NRMSE**			R^2_{adj}			**NRMSE**		
	Meadian	**Min**	**Max**	**Meadian**	**Min**	**Max**	**Meadian**	**Min**	**Max**	**Meadian**	**Min**	**Max**
S1	0.74	0.73	0.96	12%	11%	18%	0.50	-1.68	0.61	20%	17%	41%
S2	0.42	0.37	0.79	27%	12%	43%	-2.21	-2.48	-0.16	45%	26%	47%
S3	0.94	0.86	0.95	8%	7%	9%	0.46	-0.11	0.59	22%	18%	24%
S4	0.93	0.87	0.98	7%	6%	9%	0.62	0.53	0.78	13%	12%	22%
S5	0.76	0.34	0.84	13%	12%	19%	-4.20	-5.83	-0.04	40%	26%	52%
S6	0.85	0.84	0.95	11%	9%	13%	-1.11	-3.53	0.13	23%	22%	42%
S7	0.85	0.84	0.86	10%	9%	9%	0.48	-0.49	0.88	13%	9%	32%
S8	0.90	0.72	0.91	11%	10%	12%	0.90	-0.91	0.92	10%	9%	45%
S9	0.74	0.61	0.79	17%	16%	29%	0.53	-1.61	0.73	22%	19%	59%
S10	0.94	0.85	0.94	4%	4%	5%	-4.95	-9.37	0.97	58%	6%	63%
S11	0.92	0.67	0.94	13%	7%	29%	0.07	-1.58	0.53	19%	17%	38%

Table C.3: Goodness 1st order curve Fitting torque's estimation, FES test

Subjects	Whole model						Test Dataset					
	R^2_{adj}			**NRMSE**			R^2_{adj}			**NRMSE**		
	Meadian	**Min**	**Max**	**Meadian**	**Min**	**Max**	**Meadian**	**Min**	**Max**	**Meadian**	**Min**	**Max**
S1	0.97	0.96	0.98	5%	5%	7%	0.96	0.91	0.97	6%	5%	9%
S2	0.91	0.87	0.95	11%	6%	14%	0.84	0.78	0.94	13%	8%	18%
S3	0.94	0.91	0.94	8%	6%	9%	0.92	-2.87	0.95	13%	7%	42%
S4	0.97	0.96	0.97	6%	5%	7%	0.98	0.93	0.98	6%	4%	7%
S5	0.85	0.80	0.88	11%	9%	13%	0.68	-70.16	0.85	19%	10%	70%
S6	0.84	0.81	0.88	11%	10%	12%	0.78	0.44	0.94	18%	13%	30%
S7	-0.12	-0.32	0.43	35%	25%	57%	-0.24	-3.48	-0.01	43%	27%	57%
S8	0.59	0.47	0.66	20%	15%	21%	0.40	0.14	0.79	28%	16%	38%
S9	0.57	0.29	0.70	19%	17%	21%	0.33	-0.24	0.94	19%	7%	39%
S10	0.91	0.91	0.93	10%	7%	10%	0.79	-0.50	0.97	16%	5%	44%
S11	0.85	0.68	0.86	9%	16%	14%	0.49	-4.81	0.79	27%	18%	39%

Table C.4: Goodness 1st order curve Fitting torque's estimation, Vol test

Subjects	Whole model						Test Dataset					
	R^2_{adj}			**NRMSE**			R^2_{adj}			**NRMSE**		
	Meadian	**Min**	**Max**	**Meadian**	**Min**	**Max**	**Meadian**	**Min**	**Max**	**Meadian**	**Min**	**Max**
S1	0.74	0.73	0.96	17%	6%	17%	0.93	-10.19	0.95	8%	6%	67%
S2	0.42	0.37	0.79	16%	15%	36%	0.62	0.05	0.83	16%	11%	28%
S3	0.94	0.86	0.95	7%	6%	13%	-0.18	-2.20	0.85	26%	11%	46%
S4	0.93	0.87	0.98	10%	7%	11%	0.74	0.56	0.77	17%	13%	19%
S5	0.76	0.34	0.84	20%	11%	46%	0.75	-2.58	0.93	9%	6%	47%
S6	0.85	0.84	0.95	8%	7%	9%	0.76	0.09	0.77	12%	10%	15%
S7	0.85	0.84	0.86	9%	8%	11%	0.23	-0.02	0.69	19%	14%	22%
S8	0.90	0.72	0.91	8%	7%	18%	0.34	-0.44	0.78	24%	11%	35%
S9	0.74	0.61	0.79	19%	18%	31%	-0.99	-1.82	0.30	34%	20%	48%
S10	0.94	0.85	0.94	8%	6%	9%	0.29	-32.84	0.89	19%	10%	92%
S11	0.92	0.67	0.94	13%	7%	34%	0.42	-1.75	0.87	23%	7%	35%